The Pennsylvania State University

The Graduate School

UNIFORMITY OF SIMULTANEOUS DEPOSITION OF POWDER IN MULTIPLE DIES: MEASUREMENTS AND MODELING

A Thesis in

Agricultural and Biological Engineering

by

Xinsheng Xie

Submitted in Partial Fulfillment
of the Requirements
for the Degree of

Doctor of Philosophy

May 2006

The thesis of Xinsheng Xie was reviewed and approved* by the following:

Virendra M. Puri
Professor of Agricultural Engineering
Thesis Advisor
Chair of Committee

Michael A. Adewumi
Professor and Quentin E. and Louise L. Wood Faculty Fellow in Petroleum and Natural Gas Engineering

Abraham S. Grader
Professor and Victor and Anna Mae Beghini Faculty Fellow in Petroleum and Natural Gas Engineering

Harvey B. Manbeck
Distinguished Professor Emeritus of Agricultural Engineering

Roy E. Young
Professor of Agricultural Engineering
Head of the Department of Agricultural and Biological Engineering

*Signatures are on file in the Graduate School

ABSTRACT

This research aimed at testing, evaluating, analyzing, and modeling the deposition process and uniformity of powder fill in multiple dies. The second generation pressure deposition tester (PDT-II) was developed to investigate the effects of some factors (die geometry and size, die configuration and location of the die, powder characteristics, and feed shoe speed) on the deposition process and final pressure distribution. A battery powder mixture and an alumina powder were used to fill three parallel-oriented dies. Cylindrical, toroidal, and E-shaped dies were investigated. For the cylindrical and toroidal dies, feed shoe speeds of 20, 100, 200 (for the alumina powder), and 500 mm/s (for the battery powder mixture) were tested. For the E-shaped dies, 20 mm/s was used. A computed tomography (CT) scanner was employed to obtain fill density distribution for the cylindrical and toroidal dies filled with the two powders.

PDT-II satisfactorily generates a real-time pressure profile of the process and final pressures at multiple locations. For the cylindrical dies filled with the battery powder mixture: 1) at 20 and 100 mm/s feed shoe speeds, the half circle close to the leeward end had higher final pressures; 2) at 500 mm/s, the final pressure distribution was more uniform; 3) the final pressure distribution was not always symmetrical about the center line. Final pressure decreased with increasing radial distance for low feed shoe speeds. The distribution was not always regular for high speed; 4) the three parallel dies did not always have similar pressure distributions; 5) the 500 mm/s feed shoe speed resulted in higher ($P < 0.05$) final pressures (774.5 to 1424.5 Pa) than at lower speeds (235.2 to 1136.0 Pa) at most locations; 6) at 20 and 100 mm/s feed shoe speeds, the right die tended to have higher ($P < 0.05$) final pressures (393.8 to 1136.0 Pa) than the center die (235.2 to 726.0 Pa). At 500 mm/s, the quantitative differences between the center (774.5 to 1246.1 Pa) and right dies (897.3 to 1424.5 Pa) were reduced (most locations $P > 0.05$); 7) most powder (≥ 90%) was deposited in the forward stroke.

Results of the toroidal dies filled with the battery powder mixture showed: 1) the 0° orientation area had the highest pressures (1186.7 to 2498.0 Pa). The average pressures of the remaining area were 353.7 to 648.0 Pa; 2) the pressure distribution was symmetrical; 3) the 500 mm/s feed shoe speed led to the most nonuniform and the densest filling; 4) Higher feed shoe speed did not always result in higher final pressures ; 5) the right die tended to have higher ($P < 0.05$) final pressures (215.0 to 2498.0 Pa) than the center die (95.4 to 2052.5 Pa).

Results of the E-shaped dies indicated that: 1) the final pressures of the middle leg (308.9 to 760.7 Pa for the battery powder, and 41.9 to 130.7 Pa for the alumina) were higher ($P < 0.05$)

than those of the left and right legs (148.9 to 530.3 Pa for the battery powder, and 26.1 to 79.6 Pa for the alumina); 2) for the battery powder, the area along the back side had the highest final pressures (1054.6 to 1303.8 Pa); 3) the pressure distribution was symmetrical about the center line; 4) neither the center die, nor the right die always had higher pressures than the other one; 5) for the alumina powder, the area of the highest final pressures (126.4 to 152.3 Pa) was in the vicinity of the junction of the middle leg and the back.

For the cylindrical dies filled with the alumina powder: 1) at 20 and 100 mm/s feed shoe speeds, final pressure distribution was symmetrical. The center zone had the highest pressures ($P < 0.05$), and final pressures decreased with increasing radii; 2) at 200 mm/s, final pressure distribution was irregular and varied more than at lower feed shoe speeds; 3) no consistent shoe speed effect was discovered; 4) at 20 and 100 mm/s, the right die tended to have higher ($P < 0.05$) final pressures (49.5 to 288.8 Pa) than the center die (68.9 to 167.0 Pa). At 500 mm/s, the center (58.7 to 213.6 Pa) and the right (126.7 to 208.9) dies had similar final pressures ($P > 0.05$).

Neither of the cylindrical and toroidal dies led to consistently higher final pressures for the battery powder mixture ($P > 0.05$). For the alumina powder, no consistent trend and no large differences were observed between cylindrical and toroidal dies ($P > 0.05$).

CT scanner data of the cylindrical dies demonstrated: 1) CT number vs. bulk density did not have a strong linear correlation for the two powders ($R^2 \leq 0.625$); 2) the final bulk density distribution obtained by CT scanning was uniform within each die and among the three dies, based on the linear correlation with $R^2 \leq 0.625$ of CT number vs. bulk density; 3) CT scanner and PDT-II measured two different attributes (distribution of bulk densities and distribution of pressure values at the die bottom, respectively); 4) CT data and PDT-II data revealed that the half circle close to the leeward end had relatively high final mass (pressure) values.

For cylindrical dies filled with the battery powder mixture at 20 mm/s feed shoe speed, the entire pressure profile was divided into 10 stages, which were modeled by an overall rate equation. The overall rate equation was: $dP_p/d\tau = \alpha P_p F(\tau) + \beta$, where P_p is prorated pressure, τ is normalized time, α, β are coefficients, and $F(\tau)$ is a stage specific deposition rate function. The average root mean square error (RMSE) and the mean value of average relative difference (ARD) of the model for totally 17 locations in the vicinity of the center ($r \leq 4$ mm) of the center die were 0.13 and 0.07 (or 7%), respectively. Stage 1, a very short period in the beginning of the forward stroke, deposited most of the total powder filled during the entire filling cycle. Rate equation for stage 1 was: $dP_p/d\tau = \alpha P_p/(e^{b\tau} -1)$, where α and b are deposition rate related coefficients. The model can serve as a qualitative tool for further investigation of the multiple die filling process.

TABLE OF CONTENTS

LIST OF FIGURES

LIST OF TABLES

ACKNOWLEDGEMENTS

At the moment of completion of this dissertation, I would like to express my sincere and deep appreciation to my prestigious advisor, Dr. Virendra M. Puri, for his invaluable and unparalleled guidance throughout the course of my Ph.D. study over the last four and half years. My sincere gratitude is extended to Dr. Abraham S. Grader, one of my committee members, for his great support and guidance in the research and CT data collection, processing, and analysis. I would also like to thank the other two committee members, Dr. Michael A. Adewumi and Dr. Harvey B. Manbeck, for their insightful discussions and critical comments that assisted in improving the quality of this research.

Special thanks go to the Particulate Materials Center and its industry advisory board membership for securing financial aid during my graduate study. I am particularly thankful to Dr. Paula J. Hughes (Energizer Battery Manufacturing, Inc.), Dr. Kathy Lu (formerly with Energizer Battery Manufacturing, Inc.), and Dr. Kevin G. Ewsuk (Sandia National Laboratories) for providing me with test materials and constructive feedback on the various aspects of my research.

I am also thankful to Dr. Roy E. Young, Head of the Department of Agricultural and Biological Engineering, for providing me with the resources that were valuable for this research. Thanks to Randall G. Bock and Roderick S. Thomas for their technical support in design and fabrication of the PDT-II.

I am extremely thankful to my loving wife, Chen Si, for her perennial support and encouragement. I am also thankful to my parents, my brothers and sister, and all my friends that have positively influenced my life.

CHAPTER 1 INTRODUCTION

Powder plays a very important role in numerous industries. The food industry produces wheat flour, milk powder, and many different powder products. In the pharmaceutical industry, many medicines are produced as tablets by compression of powders. The ceramics industry forms and sinters powder products for many different applications, such as electronics, advanced structural materials, chemical processing components, and domestic products. The automotive industry uses powder for coating, making engine components, and fabricating transmission parts. Particle manufacture, packaging, and sale all represent significantly large businesses that continue to grow. For example, about 70% of DuPont's products are in the form of a powder, or involve powders during the manufacturing process (Levy and Kalman, 2001). Also, a typical U. S. car contains more than 17 kg of powder metallurgy parts (White, 2002). Products made from particles appear to be relatively easy to make, dry, separate, move, store, mix, and package than any other solid forms (Davies, 2001). Furthermore in 1988, the value of products that had gone through particle enlargement processes amounted to almost £5,000 million (about US $7.5 billion) in the UK (Geldart, 1990).

The production of powder based tablets, compacts or briquettes can be carried out by a number of techniques, the purpose of which is usually to form the powder into a more or less well defined shape. When a particulate solid is placed into a die and pressure is applied, a reduction in volume will occur and this manufacturing technique is referred as compaction (Pietsch, 1997). In order to demonstrate the procedure more clearly, the process of tableting in the pharmaceutical industry is summarized here as an example (Figure 1.1). Compressed tablets are the most common pharmaceutical dosage form. The reasons for this are: (1) they are convenient, compact, easy to carry and ship, and (2) they are usually more chemically stable than other dosage forms, since most drugs decompose by hydrolysis (Carstensen, 1984). The process of tableting is one in which (Figure 1.1) a powder is: (1) transported into the cylindrical cavity in a die, (2) retained there by a lower punch, (3) compressed by the lowering of an upper punch, and (4) ejected by the raising of both punches. One type of tablet machine, i.e., press, used for this is a single-punch machine as shown in Figure 1.1. In this press, powder flows from the feed shoe into the die in position 1. The shoe then swings away, and the upper punch is lowered to compress the powder (position 2). Both punches then are raised (position 3) lifting the tablet out of the die, and the feed shoe then comes back into its original position (and knocks the ejected tablet onto the discharge chute). The powder level in the shoe is maintained by gravity feed from a hopper. During this

process, large pores should be eliminated and the product should have a uniform density and adequate strength to survive ejection and handling (Reed, 1995).

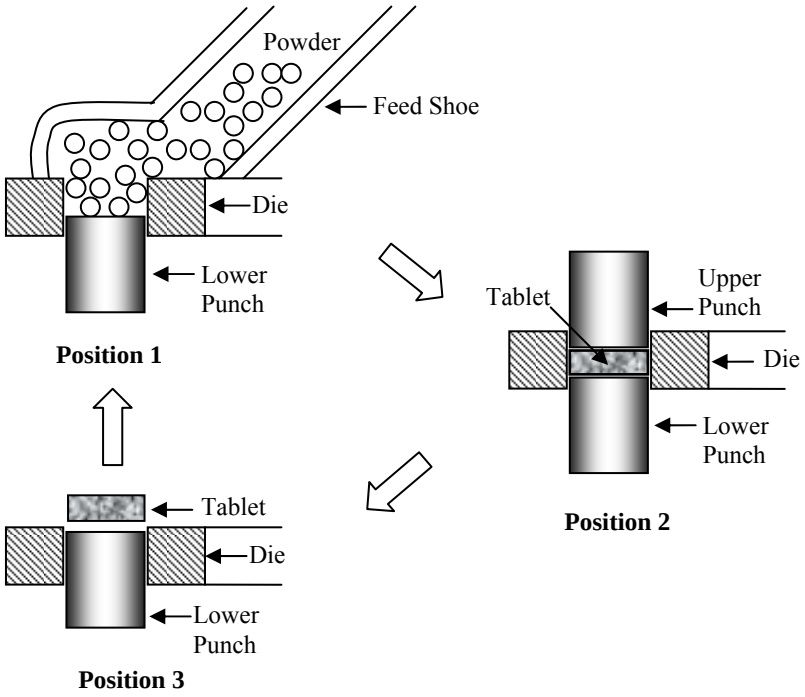

Figure 1.1 Steps in the formation of a tablet on a single punch machine (Carstensen, 1984)

Granular materials or powders are everywhere, and yet the understanding of such systems is quite limited. As a result, facilities handling granular materials waste as much as 40% of their production capacity just grappling with the unwieldy stuff (Kestenbaum, 1997). So, it is evident that in all of the operations for processing or handling powders, accurate knowledge of behavior of powders is required. For example, powders are often pressed into tablets or compacts, and although compacts should be homogeneous, in fact, they are not. The inhomogeneity is attributed, at least partly, to the deposition process. Before powders can be pressed into certain shapes and certain volume (or mass) that is needed, they have to be filled into dies of a certain shape and size. During the filling process, inhomogeneity is created, due to non-uniform bulk density distribution at different locations.

This inhomogeneity might lead to many quality problems for powder products. For instance, inhomogeneous powder assembly might show different strengths at different locations or in different directions, which might induce distortion, lamination, cracking, low strength, and shrinkage. Density gradients in the pressed parts may also lead to nonuniform shrinkage on sintering (Reed, 1995), and they may also contribute to nonuniformity in some other properties of

the product that affect normal function and performance, such as magnetic and chemical properties.

Higher fill density is also generally desirable for die filling and the following pressing process. Pressing problems are reduced when the bulk density of the powder in the die, i.e., the fill density, is high. A higher fill density reduces both the content of air in the powder and the punch travel (Reed, 1995).

To avoid these quality problems and enhance the economics of tablet, pellet, and compact formation, ensuring a uniform pre-compaction particle deposition in dies is an effective first step, since manufacturing processes have a tendency to magnify variation (Mittal and Puri, 1999b). According to previous studies (Dhanoa and Puri, 1997; Dhanoa and Puri, 1998; and Mittal and Puri, 2001), deposition uniformity is related to the filling process (including filling method, filling rate, and filling direction), die geometric characteristics, powder characteristics (such as size, size distribution, shape, and bulk density) and other factors (such as ambient conditions). Although die filling has been investigated by many researchers as corroborated by the literature review, it is still the least understood step of the entire manufacturing process.

A patented Real-Time Cumulative Mass Deposition Tester, a convenient, inexpensive, and effective tool to measure the uniformity of powder deposition in complex-shaped dies, has been reported in literature (Puri and Dhanoa, 2000, U. S. Patent Number 6,089,100). These researchers have investigated also the uniformity of deposition of different powders in a single die by using the Real-Time Cumulative Mass Deposition Tester (MDT).

With the advent of multi-station filling presses to speed up production, it has become more and more important to obtain uniform powder deposition in multiple dies. But this problem has not yet been systematically investigated or considered. In other words, no measurement, evaluation, or modeling techniques are available to guide the simultaneous powder deposition in multiple die filling stations, so as to maintain a uniform distribution of powder filled in dies.

In order to investigate the deposition process and uniformity of simultaneous powder fill in multiple dies, the second generation pressure deposition tester, or PDT-II, was designed and fabricated. The reason for using “pressure”, instead of “mass,” for the name of the device was that basically the device measured pressure distribution at the bottom of the dies. A battery powder mixture and an alumina powder were used to fill three parallel-oriented dies. Based on industrial importance, three die shapes, cylindrical, toroidal, and E-shaped, were tested. A computed tomography (CT) scanner was employed to obtain data about absolute bulk density distribution for selected cases. The CT data were correlated with the data of PDT-II, and a model to simulate the deposition process was developed and verified.

CHAPTER 2 LITERATURE REVIEW

This section describes the currently available published articles or information related to the process or uniformity of powder deposition in dies or other containers. The first part serves as introduction with some general discussion about the filling process. The second part focuses on literature related to powder flow from feed shoe, including powder flow properties and powder discharge rate through an orifice. Deposition of powder into a die or dies is discussed in the third part. Effect of powder properties, feed shoe features, die characteristics, and select factors on powder fill is reviewed. Methods or devices for testing powder deposition are especially separated as a subsection in the third part. The fourth part gives a review of related mathematical and numerical models describing the filling process or flow behavior.

2.1 General Review of Die Filling by Feed Shoe

Two common die filling methods using feed shoe were reviewed by Wu and Cocks (2004). The conventional method is gravity filling, in which powder flows into a die under gravity when the feed shoe moves across the die opening. The motion of the shoe can be linear, or contain complex patterns, such as shaking or vibration, so as to assist flow of powder. For some powders with low flowability, die filling is still difficult even with these complex patterns. So modified feed shoe systems, such as fluidized filling or agitated filling, are used to aid the flow of the powder into the die. The other common die filling method is suction filling, which uses movable punches inside a die and these punches move downwards when the shoe moves across the die opening. The motion of the punches creates negative (i.e., suction) pressure that draws the powder into the die. In this research, the emphasis will be the gravity filling.

Cocks et al. (2001) and Wu et al. (2003a) developed a model feed shoe filling system to simulate the commercial die filling process. The system consisted of transparent rectangular shoe, driven by pneumatic driving unit, and transparent die. In their experiments, the initial acceleration of the feed shoe was varied over the range of 0.1–100 m/s^2, and the steady state velocity of the feed shoe was varied over the range of 0.05–1 m/s. They noticed that during the forward stroke of feed shoe movement, the granular material was caused to move to the back of the feed shoe due to inertia when the feed shoe accelerated from rest. If the height of the powder in the feed shoe was not too high, a void was created at the front of the feed shoe, and the powder adopted a nose-shaped profile, as shown in Figure 2.1. When the shoe moved over the die cavity, powder flowed from two regions of the nose, one was from the tip and the other from the bottom of the powder

mass. The former was referred as “nose flow”, and the latter as “bulk flow.” Nose flow reached the cavity first and fed the powder into the die. As the feed shoe moved further there was a contribution from bulk flow, until the tip of the nose completely translated over the die, after which only bulk flow could occur. The authors stated that under all conditions examined, nose flow dominated the filling process.

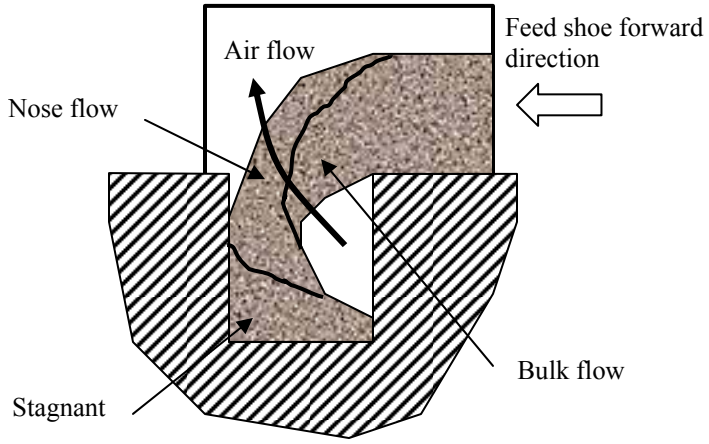

Figure 2.1 General features of die filling process (Cocks et al., 2001)

Once the tip of the nose moved past the end of the cavity, the overall flow rate of powder from the feed shoe decreased noticeably. Cocks et al. (2001) and Wu et al. (2003a) proposed two possible major reasons. The first was that when the tip of the nose moved over the cavity, the cavity was fully covered and the air in the cavity could only escape by permeating through the powder. This was more difficult for the air to escape than before the tip of the nose reached the end of the cavity, when the air could escape from the gap ahead of the nose. When the cavity was fully covered, the air trying to permeate through powder generated a back pressure that opposed the flow of the powder into the die. The second contribution came from interlocking of the particles. Particles on the surface of the nose rolled down the surface freely and were deposited into the cavity. Particles in the bulk of the powder mass, however, tended to interlock with each other, and this was reinforced by inertia effect which forced the powder to move to the back of the feed shoe when the feed shoe accelerated. It was relatively difficult for the particles to detach from the bulk and fill into the cavity. So the flow rate from the bulk was smaller than from the tip of the nose. The same experiments repeated in vacuum chamber proved that the dominant reasons of the two appeared to be the second, i.e., interlocking of the particles.

Cocks et al. (2001) then pointed out that conditions which promote nose flow are therefore likely to lead to more efficient filling than conditions beneficial to bulk flow. They illustrated this by two sets of additional experiments. An alternative strategy proposed was to

loosen the powder in the bulk, particularly at the bottom of the shoe, so as to reduce the interlocking effect of the particles in the bulk region. These included shaking the feed shoe when it was over the die cavity, vibrating the powder in the feed shoe, or using powder fluidization techniques.

Wu et al. (2003a) indicated that die filling rate slightly decreased as the feed shoe speed increased. They attributed this to the fact that nose flow was limited as the feed shoe speed increased (from 200 mm/s to 400 mm/s) , and the cohesion or interlocking of the powder was increased by a longer period of acceleration at higher feed shoe speed.

The movement of air in the die plays a significant role in the filling process (Cocks et al., 2001), especially for fine and low density particles. Sometimes a small quantity of air can be trapped in the die, particularly in a complex shaped cavity, which might result in areas of low density. The filling techniques that promoted the evacuation of air from the die should have the potential to improve die filling process and the quality of final products.

According to Guillot et al. (2002), the factors that may affect the variations in powder feeding and die filling are numerous, and they can be grouped as follows:

- Powder feeding design
  - hopper size, slope angle, …
  - tube size, number, length, …
  - feed shoe size, geometry, tube location in feed shoe, …
- Operating conditions
  - feed shoe motion during filling (e.g., shaking)
  - time for feed shoe to be over the cavity
  - tool motion during filling (e.g., suction filling)
  - powder level in feed shoe
  - powder level in hopper
- Die geometry
  - feature size
  - complexity in geometry
  - angular orientation of these features
- Powder characteristics
  - flowability
  - particle size and shape
  - internal friction
  - apparent density

- initial mixing and handling conditions

- Environment conditions
  - relative humidity
  - temperature

Hjortsberg and Bergquist (2002) listed different factors expected to influence die filling as shown in Table 2.1. These factors were prioritized based on their likely effect on filling powder density, as shown by the numbers in the table. The larger the number, the greater is the effect. Sawayama and Seki (1999) proposed the factors that affect powder filling into dies: equipment (such as the shape and motion of die or feed shoe), powder characteristics, and environment (temperature and humidity). Bruff and Jenike (1967) reported that the temperature of anthracite and the temperature of the ambient air affected flow behavior of anthracite in a silo.

Table 2.1 Factors expected to influence die filling (Hjortsberg and Bergquist, 2002)

Property	Expected importance
Feed shoe speed	9
Feed shoe acceleration	9
Feed shoe vibration	9
Number of additional filling cycles over a filled cavity	9
Cavity geometry	9
Cavity vibrations	9
Apparent density of powder	9
Powder flow	9
Powder level of feed shoe	3
The time the shoe spends stationary in the filling position	3
Suction or gravity filling	3
Particle size distribution	3
Powder tap density	3
Fill table levelness	3
Powder and machine temperature	1
Component density in powder mix	1
Method to fill feed shoe	1

Powder die deposition is increasingly becoming of great interest to scientists and engineers in various fields. The deposition process, which involves a variety of factors, is extremely complex, and it is far from being sufficiently understood. Some of the major factors, grouped in powder flow from the feed shoe and powder deposition into the dies, are discussed in detail in the following sections.

2.2 Flow of Powder from Feed Shoe

As the first step of die filling using feed shoe, flow of powder from a feed shoe requires consistent and rapid flow of powder. In order to achieve this goal, powder flow properties, its

effect on flow from feed shoe, powder discharge rate through an orifice, and effect of feed shoe features are all of prime concern. Most of these factors are discussed in this section, except feed shoe features, which is reviewed in the next section.

2.2.1 Powder flow properties

In order to design reliable and efficient filling devices, knowledge of their flow properties and the relationship between flow properties and flow behavior are of great importance. Such an understanding can help to identify the factors influencing filling efficiency and uniformity, so corresponding measures or changes can be made to improve filling process. There are many different apparatuses and tests available for measuring the flow properties of powders. In this section, the major related properties and experimental devices or methods to quantify the properties are presented.

For a rigid-plastic Coulomb solid, there is a linear yield locus that defines the limiting shear strength under any normal stress. The angle between the yield locus and the axis of normal stress is angle of internal friction (ϕ). Fine and dry powders have lower values of angle of internal friction, and coarse and wet solids and cohesive powders have higher values (Thomson, 1997). Angle of internal friction can be measured by many apparatus, such as Jenike shear cell (Jenike, 1961), ring shear cell (Walker, 1967), triaxial cell (Bishop and Henkel, 1957), and true triaxial tester (Kamath and Puri, 1990). A problem about these shear testers, as pointed out by Wu and Cocks (2004), is that the information gained from them is only accurate when predicting the behavior of powder in steady state flow. It is not clear if they can be used for transient or dynamical flow, or aerated and fluidized states, even though dynamic stress-strain properties of soils have been investigated by triaxial shear tests (Chen and Baladi, 1985). Ladipo and Puri (1997) used a computer controlled shear cell to determine a dynamic yield locus from a single test. But the prefix “dynamic” was used there to differentiate between static normal load used in the Jenike shear cell and the continuously changing strain controlled normal load in the computer controlled shear cell. The normal load and shear stress did not change as rapidly as in the process of transient flow.

The angle of internal friction can sometimes be approximated by the angle of repose for cohesionless materials. The angle of repose is stated as the angle formed between a horizontal plane and the slope lines extending along the surface of a heap formed by the powder on the horizontal plane. Angle of repose has limited usefulness. This property cannot be stated as a unique single value for a particular material, but must be defined in terms of the method by which the heap is formed. At least eight different methods or terms are commonly used for angle of

repose (Thomson, 1984), and each of them might give different results. Angle of repose is a reasonable approximation only when the cohesive strength of the powder is believed to be negligible (Seville et al., 1997).

Unconfined yield strength is another common index of powder flowability. At the free surface formed at the bottom of an arch that has been created near the outlet of a hopper, the minor consolidating stress acting normal to the surface is zero, and the major stress is tangent to the surface. The largest stress (due to above powder weight and other exerted force) that the powder can withstand at this free and unsupported surface is defined as unconfined yield strength (Thomson, 1984). The magnitude can be determined by Mohr circle. A Mohr circle that passes through the origin and tangent to the yield locus has an intersection (apart from the origin) with the axis of normal stress. The stress at this point is the unconfined yield strength (f_c in Figure 2.2). For different values of consolidating stress (σ_1 in Figure 2.2), there are different values of unconfined yield strength.

The flow function, sometimes called the failure function, characterizes the "flowability" of a bulk solid (Thomson, 1997). The unconfined yield strength is a function of the major consolidating stress σ_1 and for a value of σ_1 the corresponding value of unconfined yield strength f_c can be found from the yield locus. If a family of yield loci is constructed as shown in Figure 2.2, the corresponding values for σ_1 and f_c for each family member can be obtained as:

$$FF = \frac{\sigma_1}{f_c} \tag{2.10}$$

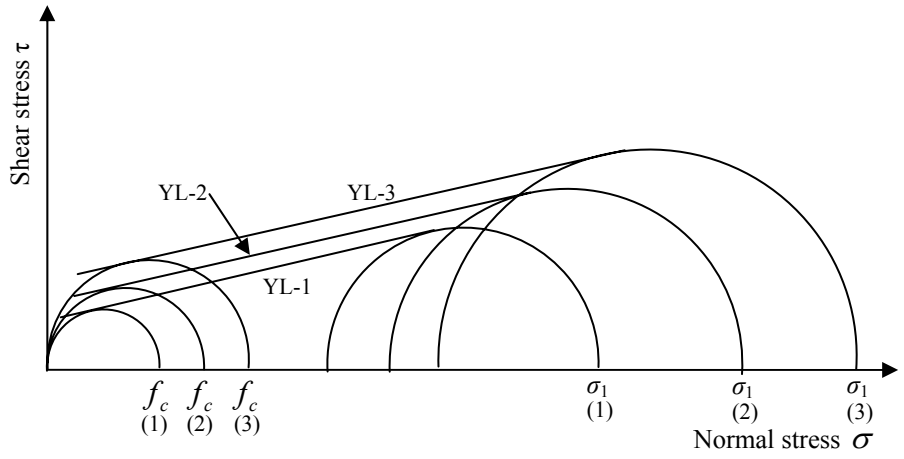

Figure 2.2 Yield loci at different normal stresses

The Hall Flowmeter has been widely used to measure flowability of metal powders. The time required to discharge 50 g of powder through a funnel is determined to be flow rate of the powder (ASTM B213-03). Although the Hall Flowmeter can be used to assess a powder, the flow rate obtained cannot be used to predict either the limiting feed shoe speed in die deposition or the flow rate through a feed hopper (Wu and Cocks, 2004). The results of the test are also affected by several interrelated powder attributes, such as particle shape, particle size, and the permeability of the powder. It is difficult for the user to differentiate between these factors with the single time measurement obtained (Bell, 1993).

Volumetric flow rate of powders can be tested by the Arnold Density Meter and the Hall Funnel (ASTM B 855-94 (Reapproved 1999)). The test method consisted of slowly sliding a bushing partially filled with powder over a 20 cm^3 hole in a hardened steel block. The volume of the powder obtained upon removal of the steel block was transferred to a Hall Flowmeter and the flow rate reported in seconds per 20 cm^3. Originated in the 1940s, the Arnold Density Meter was designed to determine the apparent density and flow characterization of powders under conditions that closely simulate the flow of powder from a feed shoe into a die cavity. Peterson and Small (1994) compared the Arnold Density Meter and the Hall Flowmeter, and found that the Arnold Meter is more sensitive to small changes in apparent density and give results more representative of flow in industrial die filling operations. They also indicated that the Hall Flowmeter has more sensitivity to powder surface smoothness. The Hall Flowmeter Funnel is also a standard device for testing apparent density of free-flowing metal powders (ASTM B212-99)

Suzuki et al. (1997) investigated a flowability testing method, which consisted of a square shoe moved by an air cylinder in the speed range of 10 to 200 mm/s. The size of the feed shoe was 80 × 80 × 70 mm, and the size of the die cavity could be changed. The principle of the test was to measure the amount of powder filled into the applied volume of the die cavity at certain shoe speed. It was confirmed that powders having better flowability (obtained by this method) had decreased part-to-part weight variation in an actual powder metallurgy application. This die flowability test device could be utilized to predict the weight variation of the actual powder metallurgy parts.

Larsson and Vidarsson (2000) created an equipment simulating filling of die cavities of different sizes, and used it to evaluate the filling characteristics of three iron powder mixes. The equipment consisted of eight rectangular cross section cavities with width varying from 1 to 20 mm. Length and depth were both 30 mm for all cavities. The feed shoe was moved automatically at different speeds.

Freeman (2001) recently developed a powder rheometer to predict powder flow behavior. This apparatus had a rotating blade that moved down through a column of powder. By measuring the torque to rotate the blade, the work exerted during the test cycle could be calculated, and the amount of work was used to evaluate the flow properties of the test powder. The disadvantage of this method was that the connection of the test data with actual application was not straightforward and it provided very limited information about the flow behavior for hopper flow or die filling (Wu and Cocks, 2004).

Rice and Tengzelius (1986) reported the findings of an ISO working group set up to examine the suitability for international standardization of procedures for determining the die filling characteristics of metal powders. They concluded that it was unlikely to have a single apparatus and method emulating die filling which is suitable for a wide range of metal powder mixes. Rice and Tengzelius (1986) investigated the Morganite flow meter (Morganite Electrical Carbon Ltd., Swansea, UK), which consisted of a hopper, 20 mm in diameter and 25 mm in depth, and four cylinder cavities. The four cylinder cavities were 25 mm in depth and 11, 7, 5, and 3 mm in diameter, respectively. The method of operation was to fill the hopper with test powder, and switch on the electric motor that rotated the hopper at four revolutions per minute. The number of revolutions of the hopper required to fill each cavity was noted and considered to represent the flowability of the test powder. They concluded that the Morganite flow meter was good for fine and unlubricated mixes of copper and graphite but was not able to differentiate between lubricated mixes used for ferrous and bronze parts manufacture.

Rice and Tengzelius (1986) also studied the Oakley flow meter (Manganese Bronze Ltd., Ipswich, UK). This apparatus consisted of a feed shoe along a block containing a recessed hole. Any one of a series of cups, some with, some without, a core rod, could be fitted into the recessed hole and filled with the test powder by traversing the feed shoe. Then the filling density was determined by weighing the powder in the cup. This apparatus was designed for investigating the change in powder bulk density when filling a constant diameter die with an increasing diameter core rod. The capacity of the feed shoe was such that not more than 20% of its content was filled into the largest of the series of cups, so as not to make the head of powder in the feed shoe change greatly during the filling operation. By plotting the cup filling densities against cup diameters, a critical diameter was found. By this apparatus it was not possible to differentiate between powders which were able to flow through a Hall Flowmeter funnel, all producing the same critical diameters of 3 or 4 mm.

A die filling apparatus was developed by an ISO working group (Rice and Tengzelius, 1986). It had a block containing a series of die cavities and a feed shoe to traverse the block.

There were 11 die cavities with diameters ranging from 1 to 32 mm, the diameters of adjacent holes being in the ratio of $\sqrt{2}$, and the depth of the holes was 25 mm. The holes were arranged axially along the block. Their results indicated that the critical diameter obtained from the device could be a useful complementary powder property to the Hall Flowmeter flow time, and gave better information when evaluating powders that are to be used for parts of thin sections. But this method failed completely to differentiate between powders which were free flowing and not free flowing in a Hall Flowmeter. The results also showed that the apparatus was operator dependent.

Wu et al. (2003b) introduced a concept of critical velocity, below which complete filling of a standard rectangular die using a feed shoe was achieved. A higher value of the critical velocity indicated an easier flowing powder. Critical velocity provided a measure of the flowability of a powder, especially for designing the shoe kinematics for a practical die filling process. It could also be used to estimate the influence of airflow and air pressure on the filling process.

Schulze (1998) reviewed some of known measuring techniques and equipment for the evaluation of the flowability of bulk solids, which are simple, applicable and used in practice. Sixteen different measuring techniques or equipments were compared, including the Jenike shear tester, the ring shear tester, and the torsional shear tester, which is considered the most favorite by the author of all the sixteen techniques.

Abdullah and Geldart (1999) investigated the relationship between bulk density of powders and the flowability of porous and non-porous powders in which particle size distribution was changed by controlling the percentage of fine components in the mixtures. Their results showed that the flowability of powder increased as particle size increased, and there appeared to be a critical size range above which flowability did not show any improvement.

Binders are additives that are commonly used in powder processing to improve the strength of the as-formed product for easy handling. Binders become stickier when the temperature approaches the melting point or exceeds the glass transition temperature of the binder system, and control of the concentration of the binder system and plasticizer (and temperature) is important for controlled flow. Relative humidity of the ambient environment may also influence the flowability of granules through water-soluble binders contained in the granules (Reed, 1995).

To summarize this section, a variety of apparatuses, devices, and methods are available for measuring different flow properties of powders, but few of them can serve as universal tests to directly evaluate powders' performance during die deposition due to the complexity of the die filling process and their own limitations. Devices suitable for evaluating the behavior of powder die deposition need to be more specific in regard to simulating the filling process, and also be

more general or versatile with respect to embracing different filling related parameters, such as die dimension and feed shoe speed. The devices should also be able to provide quantitative information about the filling efficiency or filling quality, not only qualitative description.

2.2.2 Discharge rate through orifices

Even though the problem of discharge rate of a granular material from a hole at the bottom of a silo or some containers has been investigated for a long time, it continues to remain a challenge (Sundaresan, 2001). As for predicting powder flow rate from a moving feed shoe, the problem was much more complex than hopper flow. At present, there are very few published studies available to predict powder flow rate from a feed shoe, except some studies that tried to simplify feed shoe flow and take advantage of theories and equations of hopper flow (such as Wu et al., 2003b). Undeniably, hopper flow can provide useful background knowledge to understand powder flow from a feed shoe and help to identify major factors that affect the process and flow rate. Some major experimental and theoretical investigations about hopper flow rate are discussed in the following subsections.

2.2.2.1 Experimental investigation of the discharge rate through orifices

Nedderman et al. (1982) reviewed discharge rates of granular materials from hoppers. The discharge of granular materials through orifices is best described in terms of the typical cylindrical and conical hoppers shown in Figure 2.3. The effect of the quantity of material in the hopper as typified by the height H, on the flow rate has long been realized to be slight (Nedderman et al., 1982). Most workers have reported no dependence of the mass flow rate, W, on H, though Newton et al. (1945) reported that W is proportional to $H^{0.04}$. Additional results indicated that W was independent of H provided H exceeded some critical value. Hinchley (1926) gave the critical value as 2.5 D and Brown and Richards (1959) reported that during batch discharge W remained constant until the material head in the hopper was less than the hopper diameter, i.e., $H < D$.

At these low values of H, the top surface of the material almost always showed a central depression (Nedderman et al., 1982), and Rose and Tanaka (1959) and Myers and Sellers (1978) reported that W was constant provided that H at the center line was greater than the orifice diameter D_0. Thus there seemed to be substantial agreement that W was independent of H until the hopper was almost empty though the precise value of the critical height was not clear (Nedderman et al., 1982).

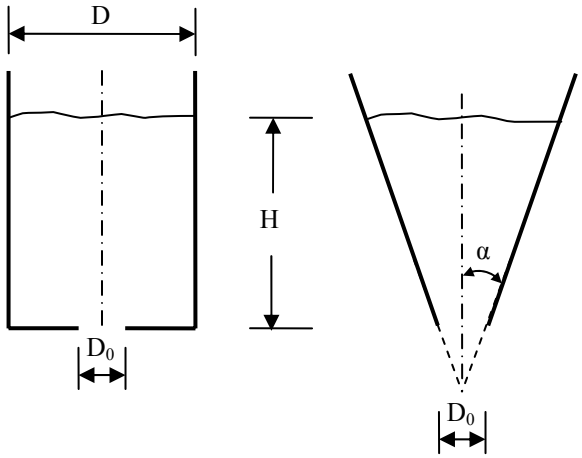

Figure 2.3 Schematic diagram defining the notation in cylindrical and conical hoppers (Nedderman et al., 1982)

Similarly, there seemed to be general agreement that the mass flow rate of particles was independent of the vessel diameter D provided this was not too small (Nedderman et al., 1982). Both Ketchum (1929) and Brown and Richards (1960) reported that W was constant provided $D > 2.5D_0$ and the latter gave correction factors for smaller values of D. Franklin and Johanson (1955) on the other hand, gave the criterion as $D-D_0>30d$ where d is the particle diameter. For smaller values of D, larger flow rates were found and in the limit as $D \rightarrow D_0$, the whole mass of material accelerated indefinitely under gravity.

Beverloo et al. (1961) found the following equation by correlating his experimental results:

$$W = C\rho\sqrt{g}(D_0 - kd)^{\frac{5}{2}} \qquad (2.1)$$

where W = mass discharge rate,

C = Beverloo coefficient,

ρ = bulk density,

g = acceleration due to gravity,

D_0 = orifice diameter,

k = dimensionless constant,

d = particle diameter.

For spherical particles, k was about 1.5 but somewhat larger values were found for angular particles. In the latter case, the value of k depended predominantly on the choice of typical dimension of the particle. The constant k was a function solely of the particle shape and no dependence on other properties could be found. Myers and Sellers (1978) found that k depended on the wall slope.

Wieghardt (1952) also gave $W \propto (D_0 - kd)^{\frac{5}{2}}$, and Brown and Richards (1960) devoted considerable attention to the concept of the "empty annulus." No particle center can approach within a distance of d/2 of the orifice edge, and, therefore, all particle centers must pass through a circle of diameter (D - d). This did not in itself explain why k > 1, but Brown and Richards (1960) also found that there was a decrease in the number of particles flowing per unit time in the zone adjacent to the orifice edge. Huntington and Rooney (1971) also found their results could be correlated well by Equation (2.1), but C and k were found to be the same for all the materials studied.

The Beverloo equation (Equation (2.1)) breaks down for fine materials, such as those with d < 500 μm (Nedderman et al., 1982). According to Crewdson et al. (1977), this is due to the effects of interstitial pressure gradients, which is discussed in greater detail below. The internal stresses in a bunker containing a flowing material increase from zero on a surcharge-free top surface to some maximum value at greater depths and subsequently fall to zero again at the so-called "free-fall arch." The interstitial voidage passed through a minimum part way down the bin. Thus near the top, the material was being compressed and air was expelled whereas somewhat above the orifice, air was drawn into the dilating material. Positive pressure developed in the upper part of the hopper, whereas the pressure in the interstitial fluid was below atmospheric immediately above the orifice. Thus the material approaching the orifice was subjected to an adverse pressure gradient (Nedderman et al., 1982). Fickie et al. (1989) recorded densities in the vicinity of the orifice some 30% less than those in the upper parts of the hopper. Interstitial pressure effects were more significant with fine powders.

Verghese and Nedderman (1995) carried out a series of experiments on fine and coarse sands with particle sizes in the range of 150-2,500 μm, and they found that the flow rate can be adjusted by a coefficient of $\sqrt{1+\frac{\lambda}{d^2}}$, where λ is a function of the compressibility and density of the material, and its best fitted value is -1.46×10^{-8} m^2. This result implied that the mass flow rate is zero for particle sizes less than 120 μm.

For orifices that are less than about 6 particle diameters across, the flow was intermittent and irreproducible (Nedderman et al., 1982). Equation (2.1) should, therefore, not be used if $D_0 <$ 6d nor may it be assumed that putting the group (D_0 - kd) equal to zero correctly predicts the orifice to particle diameter ratio at which flow ceases. This was given by Brown and Richards (1959) as 2.5 for slots and 4.0 for circular orifices. However, for fine powders, a different

mechanism known as arching was found. A stable arch could be formed over orifices of considerable size and this prevented flow from taking place.

Clearly, the Beverloo correlation requires a density for dimensional consistency but there is disagreement as to the appropriate value to use since the density within a hopper varies with respect to both time and position (Nedderman et al., 1982). Beverloo's original paper (1961) specified the use of the initial density, ρ_i, as achieved during the filling process. However, Huntington and Rooney (1971) showed that different degrees of compaction during filling had little effect on the flow rate. They argued that on initiation of flow the material dilated to some voidage characteristic of the flowing material. They observed that for more compacted beds there was a longer period between the initiation of flow and the time at which the top surface started to descend. They defined a "flowing density", ρ_f, as the ratio of the mass flow rate to the volumetric flow rate calculated from the observed rate of descent of the top surface. This value of ρ_f was found to be substantially independent of the initial voidage or the mass flow rate. Using this density in the Beverloo correlation they found a much smaller range of values of C. In the original formulation

$$W = C\rho_i \sqrt{g}(D_0 - kd)^{\frac{5}{2}} \tag{2.2}$$

C was in the range $0.55 < C < 0.65$. In the updated formulation

$$W = C'\rho_f \sqrt{g}(D_0 - kd)^{\frac{5}{2}} \tag{2.3}$$

C' was in the range $0.575 < C' < 0.595$.

The effects of the angle of internal friction ϕ and the particle shape on the flow rate were investigated by Franklin and Johanson (1955), Harmens (1963), and more recently by Kotchanova (1970). The effects however seemed to be small. Rose and Tanaka (1959) recommended the inclusion of a multiplication factor of $\exp(-7.7\times10^{-6}c/d^3\rho g^{1/2})$ to account for the effects of cohesion, c. However, c was a strong function of the voidage, and it was not specified at which voidage or stress level c should be measured. It should also be noted that this group was not dimensionally consistent (Nedderman et al., 1982).

Orifice shape was clearly an important parameter and was studied by Fowler and Glastonbury (1959). They reported that:

$$W \propto A\sqrt{D_h}\left(\frac{D_h}{d}\right)^{0.185} \tag{2.4}$$

where A = the area of the orifice,

D_h = the hydraulic mean diameter.

This correlation preceded that of Beverloo and contained no allowance for the empty annulus. Following the Beverloo approach it would seem reasonable to work in terms of the area A^* and hydraulic mean diameter D_h^* of the space remaining after a zone of width $\frac{1}{2}kd$ have been removed from the perimeter of the orifice. The Beverloo correlation can be expressed in these terms as (Nedderman et al., 1982):

$$W = \frac{4C}{\pi}\rho A^* \sqrt{gD_h^*} \tag{2.5}$$

where $\frac{4C}{\pi} \approx 0.75$.

Myers and Sellers (1978) worked with rectangular orifice of size $b \times l$ where $b << l$, and hence $D_h = 2b$. They correlated their results with an expression that was consistent with the modified Beverloo expression ($\frac{4C}{\pi} \approx 0.75$).

Most investigations have been concerned with centrally placed orifices, but Kotchanova (1970) also considered eccentrically placed orifices. In view of the increase in mass flow rate caused by the close proximity of a vertical wall, it was hardly surprising that increased flows were obtained for eccentrically placed orifices, compared to centrally placed orifices. A 10 to 20% increase in flow rate was found for an orifice adjacent to a wall, and up to 35% increase for an orifice in the corner of a rectangular hopper.

Zhang and Rudolph (1991) proposed a model to predict the flow rate of particulate solids through an orifice based on force and momentum balances at the stress-free surface, i.e., free-fall arch. It was shown that shear friction between flowing and nonflowing particles around edges of the bottom orifice was an important factor. The authors indicated that shear friction operating on the perimeter of the stress-free surface might be considered a wall effect, and for large ratios of D_0/d this wall effect would have only a small influence on flow, but for smaller value of D_0/d, the shear friction would have more effect on solid flow rate. They added a term $\sqrt{c_\tau}$ to Beverloo's equation for shear friction correction and included an effective orifice diameter $(D_0 - d)$, and

$$c_\tau = \left(\frac{3}{2} - \frac{2}{\tan\beta_w}\right) + \left(\frac{2}{\tan\beta_w} - \frac{1}{2}\right)\frac{D_0/d}{(D_0/d)_{\lim}} \tag{2.6}$$

where β_w = the angle of slide between flowing and nonflowing particles at the orifice edges (rad),

$(D_0 / d)_{\lim}$ = the limiting value of (D_0 / d) on c_τ (probably about 64).

Verghese and Nedderman (1995) found that the flow rate of coarse materials confirmed the established models of Beverloo et al. (1961) and Rose and Tanaka (1959). Material of diameter less than about 600 μm discharged at rates considerably less than those predicted by the above correlations. They measured the interstitial pressure gradients, and the gradient near the orifice was similar in magnitude to that required to give the observed reduction in flow rate. Precise agreement was not obtained and this was thought to be due to pressure variation across the hopper. The measured pressure gradients were independent of orifice size and inversely proportional to the particle diameter squared as would be expected for materials of similar compressibility but differing size. The mass flow rate was proportional to the orifice diameter to the power 5/2 for all the materials (kale seed and sands of different diameters), with the constant of proportionality being a strong function of particle diameter. A notable feature of the results was that flow rate of fine materials was affected less by hopper angle than for coarser materials.

Chang et al. (1984) evaluated the flow rate of corn through round and square horizontal orifices and found moisture content, which ranged from 12.3-22.3% (w.b.), had a significant effect on both volume and mass flow rates. For the same size of orifice, the flow rate of corn increased as the moisture content decreased. But Chang and Converse (1988) observed that the volume flow rate of sorghum increased as the moisture content increased within 11.2 to17.7% (w.b.), while the volume flow rate of wheat was not significantly affected by the moisture content, which was between 12.9 to 15.1% (w.b.).

Chang et al. (1991) tested the flow rate of wheat, corn, sorghum, and soybeans through six different horizontal orifices, which were circular, equilateral, and four rectangular with aspect ratios of 1.0, 1.5, 2.0, and 2.5. They found that for the same hydraulic diameter, differences in volume flow rate per unit orifice area were significant among the six different orifices, and the volume flow rate per unit orifice area increased as the orifice hydraulic diameter increased for all grains. They also indicated that orifice shape had more effect on the flow rate for orifices with small hydraulic diameter than for orifices with large hydraulic diameter.

For mass flow situations, according to ASAE standard (ASAE D274.1, 2003), the rate of flow of grain and oilseeds through a horizontal or vertical orifice can be predicted by the following equation:

$$W_v = C_0 A D_h^{\,n} \tag{2.7}$$

where W_v = volume flow rate, m^3/h,

A = area of the orifice, cm^2,

D_h = hydraulic diameter of the orifice, cm,

C_0 = coefficient,

n = exponent with a value between 0.5 and 1.0.

Table 2.2 shows values of C_0 and n for predicting flow rate of some grains and seeds through horizontal orifices for mass flow situations. This equation has been validated for square and circular orifices in both horizontal and vertical orientations. In the case of rectangular orifices, the equation has been validated only for horizontal orifices with aspect ratios from 1.33 to 2.67. It was also suggested that an orifice in the floor of a bin adjacent to a smooth vertical wall would discharge approximately 15% more grain than an orifice in the center of the bin floor.

Table 2.2 Coefficients and exponents for equation predicting flow of grains and seeds through horizontal orifices (ASAE D274.1, 2003)

Grain	Moisture content (% w.b.)	Orifice hydraulic diameter tested (cm)	C_0	n
Corn	12-15	13-25	0.028	0.82
	19-22	13-25	0.047	0.65
Wheat	13-15	10-25	0.050	0.69
Flaxseed	4-13	7-20	0.042	0.70

2.2.2.2 Theoretical predictions of flow rate

Many of the early theoretical analyses relied heavily on the concept of the "free-fall arch." This is the surface in the neighborhood of the orifice that forms the lower boundary of the packed bed. Above the free-fall arch the particles are in contact with one another and analyses appropriate to packed beds must be used. Below the free-fall arch the particles are not in contact with one another and accelerate freely under gravity unless impeded by some hydrodynamic drag from the interstitial medium. The concept of the free-fall arch has been the corner-stone of some earlier theoretical analyses and was implied in later ones by the normal stress on the free-fall arch must be zero (Nedderman et al., 1982).

Many earlier theories started from the assumption that the flow was independent of the depth, H, and was determined solely by the nature of the free-fall arch (Nedderman et al., 1982). The work of Harmens (1963) was typical of this approach. Harmens assumed a shape for the free-fall arch which was independent of scale so that the height above the orifice plane was necessarily of order D_0. Particles were assumed to detach from the arch with negligible velocity and to accelerate freely under gravity. Their velocity on passing through the plane of the orifice was, therefore, of order $\sqrt{gD_0}$, and the flow rate was thus proportional to $\sqrt{g}D_0^{\frac{5}{2}}$, whatever shape of arch was assumed. The constant of proportionality was determined by the assumed shape of the arch and the unknown rate of detachment of particles from the arch.

Brown and Richards (1965) used the "minimum energy theorem," which was likewise crucially dependent on the details of the free-fall arch, to derive the following expression for calculating the volumetric flow rate (Figure 2.4):

$$W_v = \frac{\frac{\pi}{6}\sqrt{g}D_0^{\frac{5}{2}}(1-\cos^{\frac{3}{2}}\beta)}{\sin^{\frac{5}{2}}\beta} \tag{2.8}$$

where D_0 = orifice diameter.

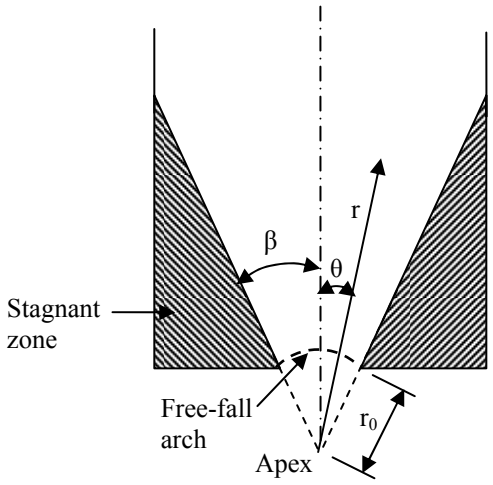

Figure 2.4 "Minimum energy theorem" of Brown and Richards (1965)

This theory provided a reasonable prediction of the mass flow rate, commonly over-predicting it by a factor of about two. Like all the other theories considered here, the Brown and Richards analysis was based on continuum mechanics and can, therefore, give no information on the effect of particle diameter (Nedderman et al., 1982).

Three very similar analyses were presented by Savage (1965), Sullivan (1973), and Davidson and Nedderman (1973) to explain the independence of the mass flow rate on the height H. Unlike the analyses of Harmens (1963) and Brown and Richards (1965), which assumed that W was independent of H, these analyses included H and showed that it had negligible effect on the flow rate. The achievement of Davidson and Nedderman's analysis (1973) demonstrated that the flow rate was independent of H. The effect of angle of internal friction was shown to be small but this did not seem to have been tested experimentally in any satisfactory way. On the other hand, the analysis did not give any information on the effect of particle size, and the dependence on the hopper half-angle α (Figure 2.3) was not in accord with experiments. In general, this analysis over-predicted the flow rate by a factor of 1.5-2 (Nedderman et al., 1982).

As stated before, the Beverloo equation (Equation (2.1)) is applicable only for bulk solids with an average grain size larger than 0.5 mm. For smaller particles, the effect of self-generated interstitial pressure gradients on the flow of the powder became significant to be disregarded. A modified Beverloo equation for fine powders was suggested by Crewdson et al. (1977). This equation accounted for the influence of the pressure gradient by multiplying the Beverloo equation by a coefficient $\sqrt{1+\frac{1}{\rho g}\frac{dp}{dr}}$, where *dp/dr* is the interstitial pressure gradient at the orifice. Experiments were conducted to verify the new equation, but only sufficient qualitative agreement was obtained to suggest that the concepts on which the theory was based are basically correct.

Mroz and Szymanski (1971) proposed that mass discharge rate was related to a variable, which was a function of the angle of internal friction and the hopper half-angle α (Figure 2.3). This variable was normally in the range 1.7-2.7, and was considerably larger than the value of 1.03 found by Myers and Sellers (1978) for the flat bottomed case. Morrison and Richmond (1976) and Morrison (1978) carried out calculations for a steep walled hopper (α=28º), and the predicted flow rate agreed with the prediction of the Beverloo correlation for a flat bottom hopper.

Katalymov and Lukyanov (1976) considered the periodic formation and destruction of a dynamic arch which was assumed to be part of a spherical surface with center at the virtual apex defined by the extrapolation of the stagnant zone boundary. They calculated the stresses on this arch under both static and dynamic cases. The difference in these stresses was linked to the acceleration of the particles on breakup of the arch. Agreement of theory with experiment to within 15% was claimed but analysis did not seem to have been tested widely (Nedderman et al., 1982).

While many of the theories described above give predictions in general agreement with experiment, precise numerical agreement was rare. It is also noteworthy that with the exception of the work of Katalymov and Lukyanov (1976), all the theoretical analyses assumed that the stress and velocity distribution were steady. However, observations on all but the most free-flowing materials showed cyclic variations in both the stresses and the velocities (Nedderman et al., 1982).

Most of the literature discussed above dealt with flow of bulk solids from a bin or hopper. No literature has been located that investigated the discharge rate of powder from a feed shoe, not to mention from a moving feed shoe. This fact makes the research about feed shoe filling especially challenging, and at the same time, particularly rewarding.

2.3 Deposition of Powder into Dies

Deposition of powder into a die or dies requires a uniform fill density distribution, less segregation, less air entrapped, or high density for some cases. Powder properties, feed shoe features, die characteristics, and some other relevant factors are all important aspects that affect powder deposition into dies. In this section, all of them are reviewed following a review of particle packing. Tests of powder deposition process conducted by previous researchers are also included.

Rice and Tengzelius (1986) found that the slower the feed shoe speed, the greater the fill density. This group also proved that increasing the number of strokes of the feed shoe was of greatest significance when the speed of the feed shoe was fast. They suggested that an important parameter was the holding time of the feed shoe over the dies. They also indicated that vibrating the equipment influenced the filling density. In many of the results the fill density was increased by vibration, but vibrating at too high a frequency appeared to result in fluidization and hence led to low densities in certain dies.

Reed (1995) proposed that powders for dry pressing in a die filled by a sliding feed shoe should be free flowing, of a relatively high bulk density, composed of deformable granules, and stable under ambient conditions. Good powder flow is essential for reproducible volumetric filling, a uniform density of the fill, and a rapid pressing rate. Dense, nearly spherical particles or granules with smooth, nonstick surface that are coarser than about 20 μm have good flow behavior and are preferred. The presence of more than 5% of fines <20 μm in size may sometimes stop flow altogether. Also, fines may enter the annulus between the punch and die wall, which increases friction and reduces the escape of air. Extremely large granules are commonly irregular in shape, and the bridging action between coarse granules may impede flow and the achievement of a uniform bulk density when powder flows into the die. The surface of granules is smoother when composed of a finer particle size and when small granules do not adhere to larger ones.

Larsson and Vidarsson (2000) demonstrated that increased flowability of powder could improve density distribution in the die, and reduce the scatter in average size of green compact made from the powder filled in the die. A drawback of the increased flowability was that the particles were more inclined to segregate.

The filling rate decreased as the average grain size decreased (Wu et al., 2003a). Also, the filling rate decreased as the irregularity of the particle morphology increased. This was attributed to the dependence of cohesion upon the average grain size and the particle morphology.

Another reason for this was the effect of air flow from the die became more important for the more irregular powder and powders with smaller average particle size.

2.3.1 Particle packing

Particle packing is of interest to many studies dealing with particulates, such as pharmaceuticals, catalysts, minerals, metal powders, seeds, and soils. In fact, the packing of particles is a problem that has attracted the interests of mathematicians, physicists, and engineers for many centuries (Cumberland and Crawford, 1987). The variables that may affect particle packing are listed in Table 2.3 (Gray, 1968). It is possible to adjust the particles to attain high packing densities or to attain specific compact properties (German, 1989).

Table 2.3 Variables controlling the packing of particles (Gray, 1968)

Variable		Experimental observation	Theory
Particle	Shape	*	**
	Absolute size	*	*
	Size distribution	**	**
	Mass	*	*
	Elasticity	**	*
	Resilience	**	*
	Surface properties	*	*
Container	Shape	*	*
	Size	**	*
	Elasticity	●	●
	Surface properties	●	●
Deposition	Intensity of deposition	**	*
	Velocity of depositing particles	**	*
	Method	*	●
Treatment after deposition	Vibratory compaction	**	*
	Pressure compaction	**	*

● no evidence
* qualitative evidence
** quantitative evidence

Generally, there are three main packing types, i.e., ordered, random loose, and random dense. An ordered packing has periodic structure that repeats over a specific and small distance. Random loose packing is represented by particles placed randomly in a container without agitation. In contrast, a random dense packing is attained by agitating or vibrating a random loose packing to the maximum density. This corresponds to the tap density (German, 1989).

Macleod (1983) indicated when a powder was poured into a container the bulk density achieved depended on several variables. In terms of powder or granule properties, the most important variables were particle size and size distribution, particle shape and surface properties.

Reed (1995) stated that powder characteristics that retard flow may hinder packing and produce density nonuniformity in the filled die.

Reed (1995) stated that a typical fill density for a granulated powder is in the range of 25-35%. The fill density depends directly on the granule density and the packing behavior. Powders composed of granules of low density and/or granules containing large pores, donut-shaped granules, and granules with rough surfaces have a relatively lower packing density.

Mittal and Puri (2001) and Mittal et al. (2001a) developed a real-time cumulative mass deposition tester capable of quantifying the uniformity of powder deposition in complex-shaped dies by using the concept demonstrated by Dhanoa and Puri (1998). They quantified the deposition characteristics of a cohesive and a cohesionless powder. The results showed that different powders had different deposition profiles in a given container, and that the deposition profiles were dependent on various powder characteristics, such as particle shape, size, and particle density.

2.3.1.1 Particle size and size distribution

Based on literature, as particle size decreases, friction, adhesion, and other surface forces become increasingly important since the surface area to volume ratio of the material increase markedly. These factors could be expected to contribute to bridging and arching in the particle system and, consequently, to produce increasing levels of porosity with decreasing particle size (Gray, 1968).

Theoretically, the maximum bulk density of binary systems is 0.86 of true density, and this occurs at a fraction of 0.73 for the coarse particles (Cumberland and Crawford, 1987). But it was observed that the practical densities were lower than the theoretical (McGeary, 1961). This suggested that the coarse and fine granules could not be arranged in dense random packing as postulated in the theory. Each component might disturb the order of the other, depending on their diameter ratio. McGeary (1961) demonstrated that when diameter ratios exceeded 7:1 the disturbance was only slight, and this ratio was close to the critical diameter ratio of 6.5 for a smaller sphere to pass through the triangular pore formed by three larger spheres in close packing. Therefore as the size ratio decreases, the mutual disturbance of the two components increases.

Duffy and Puri (2002 and 2003) also reported the existence of a critical size ratio which determined the mechanism of percolation. This size ratio defined an initial rapid discharge for binary mixtures of spherical glass beads, and it lay between 6.4:1 and 8.7:1.

In practice, in nature, and in industries, particulate materials usually consist of several sizes, and so have certain size distributions. When two sizes of spheres are mixed, the smaller

size dominates the general structure of the mass so long as the proportion of the smaller spheres is sufficiently large. As the proportion of large spheres increases the porosity of the combination falls because volumes which would otherwise contain small particles and their attendant voids are filled with solid material. When the proportion of large spheres reaches the stage at which they touch each other, the resulting porosity depends on whether the smaller spheres are sufficiently small to penetrate the voids. If they are, the larger spheres touch each other and take over control of the structure with the smaller spheres just occupying the voids. As the proportion of larger spheres increase, the smaller spheres are no longer sufficient to fill the voids and the porosity of the combination will increase. If they are not small enough to penetrate the voids, neither size completely controls the structure of the combination until the proportion of one of them has attained 100 percent (Fraser, 1935).

Sohn and Moreland (1968) studied packing density of particle systems of Gaussian and log-normal size distributions using dense random packing of two sands with particle sizes from 0.07 to 8.0 mm. They found that packing density increased if particle size distribution was extended. Packing density was shown to be function only of size distribution represented by dimensionless standard deviation, and of particle shape; it was independent of particle size.

Wakeman (1975) investigated the packing density of spherical particles with log-normal size distributions for both dense and loose packed states. He found that the density of packing of spheres in a loose packed arrangement was not as critically dependent on the particle size range as was the case with a dense packed arrangement.

2.3.1.2 Particle shape

Angularity of particles is usually undesirable because it increases porosity by raising interparticle friction and promoting bridging. Oman and Watson (1944) measured random dense and random loose packing voidages for various particle shapes and found the voidage increased in the following order: cylinders, spheres, granules, rings, and saddles.

Shergold (1953) investigated the effect of particle shape on packing, and proposed that voidage decreased when rounded particles were added successively to a mixture containing both angular and rounded particles. Mittal et al. (2001b) also pointed out that porosity tended to increase as the sphericity of sand particles decreased. However, Wakeman (1975) reported that denser packing was possible with angular particles than with spherical particles upon vibration, since the particles can reorientate themselves to fit more snugly into the available void spaces.

The vibrated packing density of coarse angular particles of uniform size was 50-60%, in contrast to the 65% density for smooth spheres. A higher porosity was generally observed when

the aspect ratio of the particles is higher and when a higher content of fibers is added into a powder containing isometric particles (Reed, 1995).

2.3.1.3 Effects of die walls

A number of workers, including Gray (1959) and Benenati and Brosilow (1962), have measured the variation in packing density or voidage with distance from the wall directly, by impregnation of the particle bed with a liquid which then solidified and fixed the particles in position. Considering the overall trends for spherical particles the results of these workers were in good agreement. Gray (1959) examined two kinds of packings. One was pouring particles (glass beads) into the container with zero impact velocity to produce a high porosity, and the other was allowing the particles to fall on to the bed at high impact velocity and at an optimum intensity of deposition to produce low porosity packings. The former resulted in a high porosity at the wall, a slightly lower porosity in the second layer from the wall and a more or less constant value throughout the rest of the container. The high value of porosity at the wall was obviously caused by the inability of the spherical particles to pack as closely against the wall as against other particles. The latter resulted in closer packing at the wall, which in turn promoted closer packing in the succeeding layers. Until four layers from the wall, the influence of the wall was no longer apparent, and the porosity increased to the level that would occur in an infinitely extensive bed.

Benenati and Brosilow (1962) also examined the detailed variation in voidage from the wall. The common feature for monosize spherical particles is the regular damped oscillation of voidage. A minimum voidage occurred at a distance corresponding to about half a diameter from the wall, i.e., at the center of the first layer of spheres. The cyclic variation in voidage extended to a distance of about 4.5 to 5 particle diameters before it is dissipated.

Ridgway and Tarbuck (1966) examined wall effects on binary mixtures of spheres. Two broad types of mixtures were chosen: (1) that in which the smaller spheres could fill the interstices of the larger spheres and (2) that in which the smaller particles force the larger ones apart, since they were not sufficiently small to enter the interstices. The mixtures showed a more rapid decay of the cyclic variation in voidage and this would appear to indicate that mixing spheres of different sizes causes a more rapid approach to randomness.

Gray (1968) summarized the effect of container walls. Almost all packings comprise a central core undisturbed by the presence of the walls, and a disturbed region adjacent to them. It appears that, for a ratio of container diameter to particle diameter greater than approximately 50, the overall porosity, and any overall characteristic dependent upon porosity, is affected by the wall to a smaller extent than the reproducibility of the packing itself. For smaller ratios, the wall

effect becomes significant; it is always so if behavior in the vicinity of the wall is being considered. The extent of disturbance depends on the conditions under which the bed is formed, since the wall may merely act as a barrier against which the particles pack less closely than against each other, or as an ordering surface from which closer, even ordered, packing may start. If the ratio of container diameter to particle diameter is quite small it may be important to consider the detailed variation in voidage near the wall. Some other investigators found the critical value of the ratio of container diameter to particle diameter, above which the porosity was reasonably constant, should be smaller than 50, such as 10 (Carman, 1937).

2.3.1.4 Effects of deposition related factors

Graton and Fraser (1935) suggested that intensity of deposition (mass of particles per unit time per unit area) and the direction and velocity (impact velocity) of the particles as they strike the surface of the growing mass of material could influence the resultant packing, and they discussed how this might take place in the case of ideal spheres.

Kolbuszewski (1950) demonstrated, quantitatively, the influence of the intensity of deposition and velocity at impact on the packing of sand. Kolbuszewski's major conclusions were: (1) a low velocity of fall, as, for example, in water, leads to a high porosity independently of the intensity of deposition; (2) a high velocity of fall, as, for example, in air and from a height of several feet, produces a low porosity with low intensity of deposition.

Macrae and Gray (1961) also examined the influence of intensity of deposition and impact velocity of the depositing particles on packings of several kinds of particles, such as steel, glass, and polystyrene. With all the materials and over the range of height of drop used, the overall porosity decreased with increasing impact velocity at constant deposition. For each material, except lead shot, there was a critical range of intensity of deposition which produced closest packing. Intensities not only above, but also below this range resulted in higher porosities.

Wadsworth (1960) studied the distribution of coordination number of smooth hard uniform spheres using 6.35 mm diameter steel ball bearings. One of his main conclusions was that in random packing the observed porosity values was a function only of the ratio of container to sphere diameter, and was fairly insensitive to the method of stacking.

2.3.1.5 Segregation

Segregation of particles occurs when particles of different properties are distributed preferentially in different parts of a deposited bed. It takes place during deposition when large relative movements of particles of different size or density can occur close to an inclined free

surface. Tang and Puri (2004) reviewed various patterns and factors influencing segregation, as well as corresponding methods to minimize segregation. They proposed four fundamental segregation mechanisms — trajectory, sieving, fluidization, and agglomeration, based on the role of particle size in the mechanism of segregation. Universal methods used to minimize segregation mainly included improvement of material properties (i.e., narrowing size distribution spread, reducing absolute size, and avoiding irregular shaped particles), proper selection of handling equipment and operational parameters (i.e., lowering free-fall height and employing mass flow bins), and proper control of material handling environmental conditions (i.e., minimizing vibration and maintaining humidity). Three primary segregation patterns, i.e., trajectory, sieving, and fluidization, might appear during filling process. Unique methods to minimize segregation in filling or deposition process were to prevent heap from forming, or reduce the heap size and free-fall height during filling large containers. There were two possible ways to minimize fluidization segregation during filling. One was to granulate the fines using various granulation techniques, such as fluid bed granulation and spray drying. The other way was to control the air current so that entrainment velocity required for separating out the fines was not reached.

Segregation according to size is probably the most common and if this takes place the deposit tends to contain pockets of near single-sized particles, a situation characterized by high porosity (Gray, 1968). Few quantitative data on segregation have been reported but one of the ways of reducing segregation (Richards, 1966) is to deposit the bed at high intensity and from low heights (low velocity at impact), conditions that form a bed of high porosity.

Lawrence and Beddow (1969) studied powder segregation during die filling with two-component mixes of Pb particles. The test die was a 150 ml beaker (50 mm in diameter), and the powder was poured into the die via a 30° sloped tinned steel cone. Their results showed that segregation occurred by fines filtering down through the moving powder mass. This effect built up an inner mound of fines-rich material on the bottom of the die and an excess of coarse particles in the periphery of the die cavity. For a particular size of large component, reducing the size of the small component increased segregation up to the point at which the average relative size difference (difference between coarse and fine divided by coarse) was around 0.7. When the fines were smaller than this, their flow was restricted and so segregation was reduced. It was found that particle shape and density in the mixtures studied had little effect upon segregation. In their investigation, segregation increased to a maximum at 15-30% fines percentage, and it approached zero at 60% fines percentage. If the mixture contained more than 60% fines, segregation was much reduced, and an excess of fines was found in the periphery of the die

cavity. It was also reported that increasing rate of die filling decreases opportunity for segregation.

Less segregation occurs with the smaller particle sizes because of the greater interparticle friction. Size segregation was less of a problem for particle sizes below approximately 100 μm. Mean particle sizes over approximately 500 μm showed no further change in segregation tendency (Williams, 1976).

When powdered material is put into a container the arrangement of the particles (and the consequent distribution of voids between the particles) has a major influence on the subsequent behavior of the powder mass. This is particularly the case when the powder is being pressed in a die because the initial bulk density of the powder dictates how much volume change is required to produce a solid compact (Cumberland and Crawford, 1987). This raises an interesting question "Is there an ideal particle size distribution which would enable all the space in a die to be filled with particles?"

2.3.1.6 Inhibited packing

In real-particle systems, the movement of particles into the minimum porosity configuration during processing is hindered by both external and internal factors. Bridging of particles and agglomerates with rough surfaces between the walls of tooling is quite significant when the spacing between external surfaces is less than about 10 particle diameters. Bridging is especially a problem when the surfaces of particles and aggregates are rough and when friction is high at the interface between the particles and tooling (Reed, 1995).

Lubrication of all surfaces may aid in achieving a higher packing density. Mechanical vibration may momentarily reduce bridging forces and facilitate the rolling and sliding of dry particles into a denser configuration (Reed, 1995). But lubricants may cause agglomeration, while vibration may promote segregation of particles of different sizes or densities.

As stated above, many factors may affect particle packing. Among these are particle size and size distribution, particle shape, effect of die walls, and deposition intensity and velocity, which are more widely investigated than some other suspected factors. In order to obtain a denser packing, a wide spread size distribution is desirable. But this seems to promote size segregation, which in turn harms the uniformity of die filling. A balance needs to be maintained to achieve desired uniformity and preferred bulk density.

2.3.2 Effect of feed shoe features

Kondoh and Takemoto (1996) tested powder feed shoe filling into three different rectangular dies, of which the length and depth were 20 or 40 mm, while the widths were 1, 2, and 5 mm, respectively. The results indicated that the filling density slightly increased with increasing feed shoe speed (10, 30, 40, 50, and 60 mm/s). When the feed shoe speed was 10 mm/s, the run off of powder began at the place where the feed shoe projected several millimeters from the edge of the die cavity. The particles then rolled down the slope along the angle of repose with the advancement of the feed shoe, gradually filling the die cavity. When the feed shoe speed was at 60 mm/s, the particles quickly fell down into the die at the place where the tip of the feed shoe reached near the center. The air in the cavity was intensely expelled out, and the particles dropped down later were blown away to the front by the air flow. The authors also suggested dividing the particles in the die into three regions according to their behavior during the process of pullback or shaking of the feed shoe (Figure 2.5). The particles in the top region (rolling region) were dragged by the movement of the feed shoe during the backward stroke, and so they moved in the horizontal direction to some distance to their right side. The particles in the sliding region slid diagonally (to the direction of the right lower corner) with the movement of the feed shoe. In the bottom region (non-sliding region) particles did not move. The moving distances of the particles were small at both left and right sides of the die, and they were large at the center of the die.

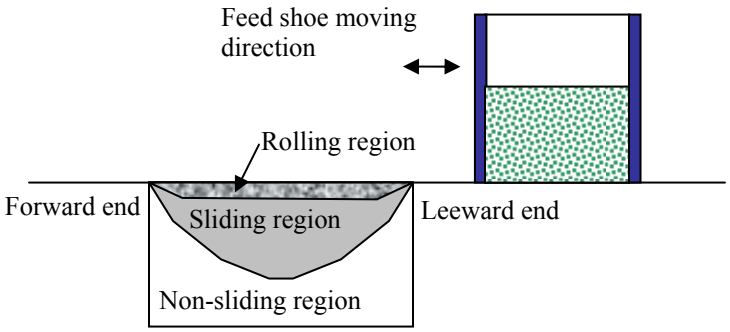

Figure 2.5 Behavior of particles during pullback or shaking of feed shoe (Kondoh and Takemoto, 1996)

Hjortsberg and Bergquist (2002) conducted die filling tests at 600 and 1400 mm/s feed shoe speeds with pure iron powder into a ring shaped cavity (inner and outer diameters were 170 and 190 mm and the height was 20 mm). Cavity density at higher speed was about 2% higher than at lower speed. But Larsson and Vidarsson (2000) pointed out that with increase of the feed shoe speed, cavities tended to be only partially filled, especially those small size cavities. The feed shoe speeds they tried ranged from 30 to 200 mm/s.

On the other hand, as Wu and Cocks (2004) stated, an increase of the feed shoe speed meant that the powder stream which fell into the die had higher horizontal kinetic energy. If this energy was sufficiently high, the oncoming particles collided with the particles already in the die, and produced higher filling density by collapsing some bridges formed, especially for a wide die.

Wu et al. (2003a) indicated that die filling rate slightly decreased as the feed shoe speed increased. They attributed this to the fact that nose flow was limited as the feed shoe speed increased, and the cohesion of the powder was increased by a longer period of acceleration at higher feed shoe speed. They also stated that high feed shoe speeds generally resulted in incomplete filling. In another paper (Wu et al., 2002), they put forward that a stationary feed shoe produced higher filling rate than a moving feed shoe, though only bulk flow occurred in this situation. They attributed this to the increased cohesion as a result of the initial acceleration when a moving feed shoe was used. But they did not mention the fact that the orifices available for the flow of powder in the feed shoe for these two situations were completely different. For stationary feed shoe, the orifice was always the die opening, while for the moving feed shoe, the orifice increased from zero to the maximum, i.e., the die opening.

Sawayama and Seki (1999) found that displacement of air in the die by filling powder was an important element in die filling, and they developed an air-replacement feed shoe. This feed shoe was an ordinary square feed shoe divided in half by a pipe diagonally to pass the air from the bottom of the feed shoe. The air-replacement feed shoe was able to improve the powder filling in the cavity. Both filling speed and parts weight variation were improved considerably by using the air-replacement feed shoe. They concluded that air replacement rather than powder friction and adhesion due to powder pressure in the feed shoe affected powder deposition into the die.

An aeration filling method was proposed to achieve uniform powder filling by improving flowability of powder in a feed shoe (Kondoh and Takemoto, 1996; Kondoh et al., 1998; Urata et al., 1998; and Nakatani et al., 1999). Small pipes were installed at the bottom of the feed shoe to carry the gas which was blown out into the powder via tiny holes on the pipes. This helped to reduce friction between particles and improved the flowability of the powder. The aeration filling method improved powder flowability and reduced particle size segregation in the filling process. It was especially effective in filling thin and complex shaped cavities uniformly and quickly, and it also decreased weight scatter and improved dimensional tolerance of powder products. Guillot et al. (2002) also indicated that their air assisted feed shoe and mixer installed feed shoe helped to reduce the standard deviation of density between parts.

Zahrah et al. (2001) developed a type of fluidized fill shoe (Figure 2.6) to increase powder flow rate and improve the uniformity of fill for complex-shaped die cavities. The new technology flowed gas from the bottom to the top of a bed powder in the feed shoe to "lubricate" powder particles, to eliminate inter-particle and wall friction, and to improve powder flow rate. A fluidized fill shoe with a custom designed delivery chute enabled the delivery of powder in a fluidized state to the die cavity. Their results demonstrated that the fluidized fill shoe added flexibility to the conventional powdered metal process by providing additional control to the user and improving production rates, while reducing the standard deviation on weight and dimensions of the products. This fluidized fill shoe could typically increase fill density for parts with a thin wall and for powders with poor flow characteristics (Zahrah and Rowland, 2002).

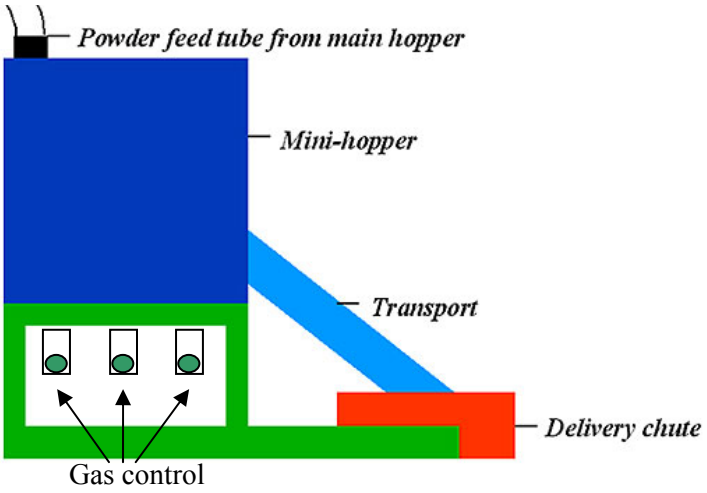

Figure 2.6 Schematic of fluidized fill shoe system (Zahrah et al., 2001))

Hashimoto et al. (2002) reported an "agitating-shoe" that could increase the filling rate by 20-80% and increase the filling density of powder in the die, and it could also decrease weight variation by 30% compared to a conventional feed shoe. The "agitating-shoe" was made by installing some rotating rods to stir powder in the feed shoe, so as to accelerate the air release from the die cavity.

Haskins and Jandeska (1998) used computed tomography (CT) technology to investigate powder flow and die filling process. They proposed that the shoe motion exerted an angled downward force due to static head pressure of extra powder in feed shoe and the horizontal velocity vector as the feed shoe was translated across powder mass in the die. The resultant downward force appeared to be better transferred through the packed bed in the lower friction powder.

Sawayama and Seki (1999) investigated the effect of shaking of feed shoe and holding (i.e., pausing) time of feed shoe over the die cavity on powder filling into dies. Holding time

was varied from 0.5 to 1 s, and shaking was done twice from 5 to 20 mm distance. The feed shoe speed varied from 65 to 200 mm/s (40 to 200 mm/s in shaking). Three ring shaped cavities with outer diameter of 30 mm and inner diameters of 10, 20, and 26 mm were used. The depth of the cavities was 30 mm. The feed shoe was 100 × 100 × 70 (h) in mm. The results indicated that for the ring dies of 20 and 26 mm inner diameter, shaking increased the amount of powder filled into the die, but holding showed no effect. As for the ring die of 10 mm inner diameter, shaking and keeping did not help in increasing the filling. Hjortsberg and Bergquist (2002) found that holding the feed shoe for two seconds increased filling density for a ring shaped cavity (inner and outer diameters were 170 and 190 mm and the height was 20 mm) filled at 200 mm/s with pure iron powder. They indicated that shaking of the feed shoe also increased powder amount in the die cavity.

Hjortsberg (2000) obtained similar results; i.e., when the number of feed shoe filling cycles (which was similar to shaking) increased, the filling density increased. But the variation of fill density within each die increased as well. Another feature was that increasing filling cycles mainly increased the filling density in the 60-150° and 210-310° sections (the forward direction of the feed shoe was 0°) of the ring cavity. Guillot et al. (2002) also proved that higher and relatively evenly distributed bulk densities were generally achieved by shaking for powder of high internal friction and poor flow properties. Wu and Cocks (2004) confirmed that filling density increased as the shaking number increased. They explained this by the relative displacement between the powder inside the feed shoe and that fed into the die cavity. Due to the relative displacement, there was a shear zone between powder inside the shoe and the die if the die cavity was totally filled before the shoe completely moved over the die. The shearing facilitated the densification of the powder inside the die.

To conclude this section, feed shoe speed, holding time of feed shoe on the die, and number of strokes of feed shoe passing the die all affect powder die filling. Many new feed shoes with different features have been proposed to improve powder flow and deposition into dies. Their common characteristic was to use flowing air or stirring rods to enhance powder flowability, so as to increase filling rate or filling density. The downside of these methods is that they make the feed shoe more complicated and may also promote segregation.

2.3.3 Effect of die characteristics

Bocchini (1987) conducted experiments to establish the influence of small die opening on the actual filling density. An apparatus, consisting of rectangular dies of various widths, was utilized with Cu and mixed elemental bronze powders. The results showed that filling densities

decreased with decreasing die opening. The angle between direction of motion in filling and main die axis also influenced the fill density through rebounds during powder fall; these rebounds played a positive role. The author attributed the changing quantity of powder entering various dies to a boundary layer, which was dependent on grain shape and size, on the die surface. The boundary layer widths related to powder type, lubricant, and the angle between filling motion and main die axis. For relatively small particles, the wall had little influence on packing efficiency. For larger particles, the influence of the die wall was important.

Rice and Tengzelius (1986) also observed that the filling density was higher for larger die cavities than small cavities. They proposed that the expansion required to permit particle rearrangement was less easily satisfied in smaller dies than in larger ones; therefore, the filling densities in small dies were lower.

Readey and Mahoney (1995) showed that die fill density decreased markedly with decreasing die diameter and aspect ratio. They investigated four die diameters: 25 mm, 12.5 mm, 6.2 mm, and 3.1 mm. For the 25 mm die, the fill density was approximately 28% of the theoretical density, while for the 6.2 mm die, the fill density decreased to nearly 21% of the theoretical density. Moreover, the magnitude of the difference was also a strong function of aspect ratio; the greatest differences in fill density occurred at the lowest aspect ratio. The results also suggested a strong correlation between initial and final compact densities. Larsson and Vidarsson (2000) also pointed out that fill density decreased with decreasing cavity width. They indicated that fill density decreased less with decreasing cavity size for more flowable powder. Wu et al. (2003a) and Guillot et al. (2002) proved that incomplete fill was often observed for narrow dies or small holes. The kinematics of the filling process was more complex when the die contained complex features, such as steps. Guillot et al. (2002) also showed that usually the larger the depth of the die, the lower was the bulk density of the powder deposited into the die.

Dhanoa and Puri (1997) evaluated the effect of die cross-section and die size (aspect ratio, the ratio of die height to depth) on the spatial fill density distribution. Their results showed that die shape and die size (aspect ratio) were important factors affecting spatial die fill density distribution.

Mittal et al. (2001a) and Mittal and Puri (2001) investigated the effect of die shape on the mass distribution in an E-shaped and a toroid die (Figure 2.7 and Figure 2.8). The numbers in the figures represented mass values detected by load cells in mg. They used a real-time cumulative MDT and investigated the deposition behavior of a free-flowing ceramic powder, manganese zinc ferrite ($Mn_{0.5}Zn_{0.5}Fe_2O_4$) (Figure 2.9). This powder consisted of spray-dried spherical granules with 150 μm median size and 5.03 g/cm^3 granule density. The results showed that container shape

affected powder deposition behavior in the E-container. High mass distribution was observed in the middle leg, which was wider than the other two legs. This trend was attributed to less influence from container wall for the middle leg. For toroid, the powder mass concentrated in the direction parallel to the direction of the feed shoe.

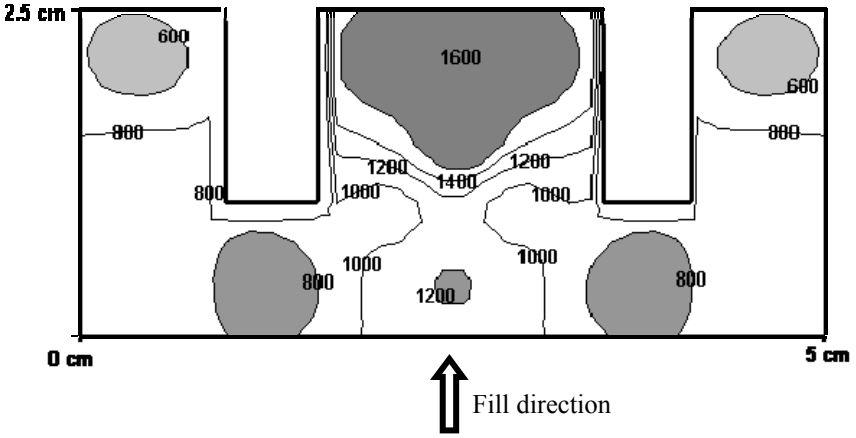

Figure 2.7 Powder's spatial mass distribution at the end of fill process in shown direction (Mittal et al., 2001a)

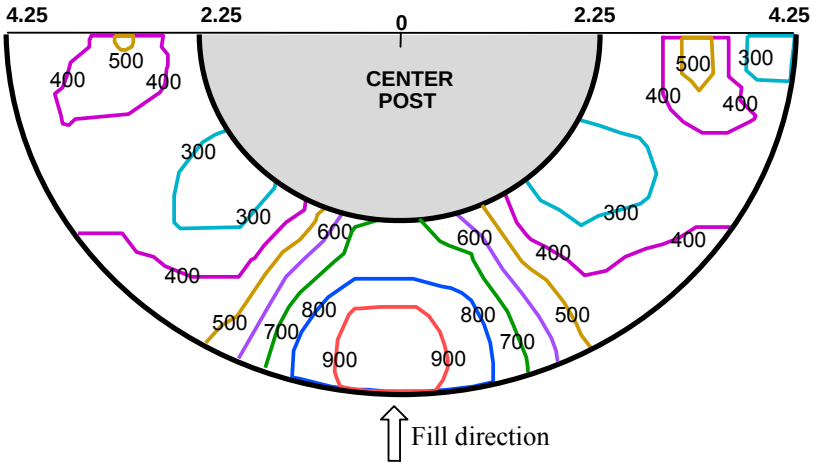

Figure 2.8 Contour plots of MZF powder distribution in toroid die (Mittal and Puri, 2001)

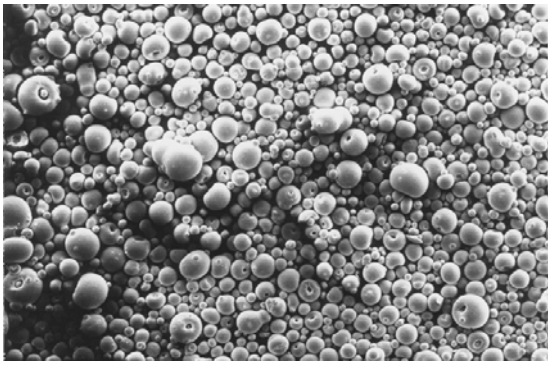

Figure 2.9 Scanning electron microscope photograph of MZF powder (Photo courtesy of Magnetics Div., Spang and Co., Butler, PA)

Vidarsson and Arvidsson (2000) investigated die fill with some rectangular dies, and the results indicated that when the feed shoe moved in a direction parallel to the cavity orientation, the fill was relatively easy. When feed shoe was in the direction perpendicular to the cavity orientation, the fill was more difficult, especially for narrow cavities. The authors proposed the reason was that when filling in parallel direction, a cavity remained open during most of the time while the feed shoe was moving across, thus allowing air to escape from the cavity until almost the whole cavity had been filled. Filling a cavity in perpendicular direction, however, caused air to be entrapped in the cavity before the fill was completed, especially when the cavity was narrow and/or when relatively high feed shoe speed was used. Upward movement of the entrapped air caused aeration, or partial fluidization of the powder remaining in the feed shoe, thus influencing the packing pattern for the powder entering the cavity during the final stage of filling.

Effect of die vibration on die filling was investigated by Lawrence and Beddow (1968). They found that vibration reduced radial segregation because the inner mound of fines tended to be leveled off and so a higher proportion of these fines was located in the peripheral zone. The effect of vibration on vertical segregation depended upon vibration amplitude and frequency. If the powder mass was bouncing or quiescent, vertical segregation was a minimum. Segregation increased with the onset of churning. The results also indicated that in the bottom zone of the die, for conditions of churning, increasing the time of vibration tended to allow some mixing to occur which caused a moderate reduction in the vertical segregation. An apparent anomaly in the vertical segregation was observed; i.e., the coarse component tended to locate in the bottom zone of the die during vibratory die filling.

Lawrence and Beddow (1969) studied powder segregation during die filing. The powder, two-component mixes of Pb particles, was poured into the die via a 30° sloped tinned steel cone. They proposed that decreasing the diameter of the die and increasing the orifice of the cone led to reduced segregation in the outer layers. The author believed that this was due to change of flow time. As the orifice diameter was increased or the die size was decreased, the die was filled more rapidly, and this effectively reduced the time available for segregation.

The literature indicates that die shape, die size, and die configuration with respect to the feed shoe motion are all factors that may influence powder die deposition, including filling rate, filling density, and density distribution. A vibration die might increase filling, but this might also raise the possibility of segregation and increase the complexity of the die filling system.

2.3.4 Effect of selected process related factors

Lawrence and Beddow (1969) found that increasing the rate of die filling decreased opportunity for segregation, and increasing the height from where the powder fell into the die caused mixing and decreased segregation. Faikin et al. (1976) did experiments to investigate the relationship between the rate of filling and powder density. The powders used were nickel, bronze, stainless steel, corundum, and carborundum powders ranging in size from 0.063 mm to 0.8 mm. The particles of the metal powders were spherical and those of the corundum and carborundum powders were irregular-shaped. In the experiments, the container for pressing the powder was a die of 40 mm outer diameter, 34 mm inner diameter, and a 250 mm long tube. The filling method was to discharge powder from a hopper mounted above the die. The intensity of filing varied by employing hoppers with different discharge orifice diameters (3, 5, 7, 11, 16, 18, and 22 mm). The results showed that with the increase of filling rate, the density of the powder fill decreased, and there was a limit beyond which the density would not decrease with the increase of filling rate. Conversely, decreasing the filling rate increased the bulk density of the powders in the die. The reason was that at higher filling rate, the powder particles had less time to rearrange and for the trapped air to escape to get a closer packing. The authors also indicated that the intensity of pouring could be increased, without adversely affecting the density of shaped parts, by applying vibrations to the die during the pouring of powder.

Macleod (1983) pointed out that when a powder was poured into a container, the bulk density attained depended on several variables. In terms of process characteristics, the governing variables were rate of deposition and the relationship between container diameter and particle diameter.

Moysey (1984) showed that method of filling had a significant effect on fill bulk density. A shear box was filled with two different filling methods, of which one was sprinkle filling and the other was stream filling. The sprinkle fill was achieved by dropping the grain from a height of 300 mm through a screen with 6 mm mesh, which was located 150 mm above the shear box. Stream fill consisted of placing the outlet of a funnel on the bottom of the shear box, filling the funnel and then raising it up slowly so that the grain flowed out in a gentle stream and produced a very loose fill. Test materials were wheat and flax seed. The results showed that not only did sprinkle fill achieve denser packing, the kernels of grain tended to arrange themselves with the long axis in horizontal directions because they were able to come to rest in a preferred orientation. In contrast, when a funnel or spout was used, the kernels slid down a sloping surface and arranged differently. Similar results were obtained by Molenda et al. (1993) and Smid et al.

(1993). Molenda et al. (1996) also found that filling method significantly ($p<0.05$) influenced the radial distribution of vertical pressure on the floor of the bin.

There are two basic modes of flow, namely mass flow and funnel flow. In mass flow, the bulk material is in motion at every point in the bin whenever material is drawn from the outlet. The material flows along the walls of the bin and hopper (that is, the tapered section of the bin) forming the flow channel. Mass flow is the ideal flow pattern and occurs when the hopper walls are sufficiently steep and smooth, and there are no abrupt transitions of inflowing valleys. Funnel flow, on the other hand, occurs when the material sloughs off the surface and discharges through a vertical channel that forms within the materials in the bin (Figure 2.10). This mode of flow occurs when the hopper walls are rough and the angle of the slope is large. In most instances, funnel flow is an undesirable flow pattern (Thomson, 1984).

Mittal and Puri (1999a) tested the influence of different deposition methods on compression response of two powders by using a medium pressure flexible boundary cubical triaxial tester (CTT). The filling methods were feed shoe, funnel, and rainy (Figure 2.11). The two powder materials were silicon nitride-based ceramic powder (KY 3500) and a microcrystalline cellulose-based pharmaceutical powder (MCC). The results showed that filling methods significantly influenced ($p<0.05$) some stress-strain related parameters of the two powders. In the case of KY 3500, shear modulus and compression index values were sensitive to deposition methods ($p<0.05$), whereas the bulk modulus and swelling index values of KY 3500 were insensitive ($p>0.05$) to deposition methods. For the MCC powder, bulk modulus, shear modulus, compression index and swelling index were sensitive to deposition methods ($p<0.05$). They also tested the compact quality, and found for KY 3500 compacts, the deposition methods had a pronounced effect on compact quality, though for MCC compacts, the deposition methods did not affect the compact quality.

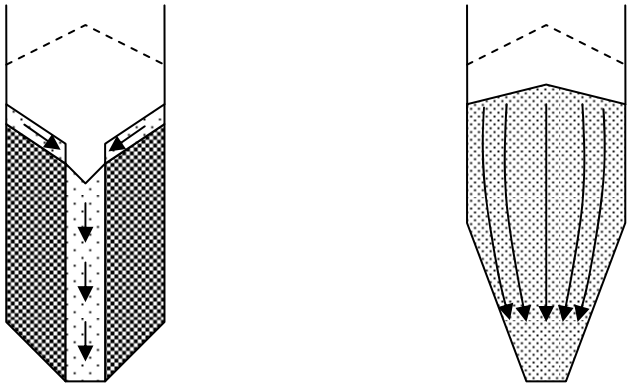

(a) Funnel flow (b) Mass flow

Figure 2.10 Bin flow characteristics (Thomson, 1984)

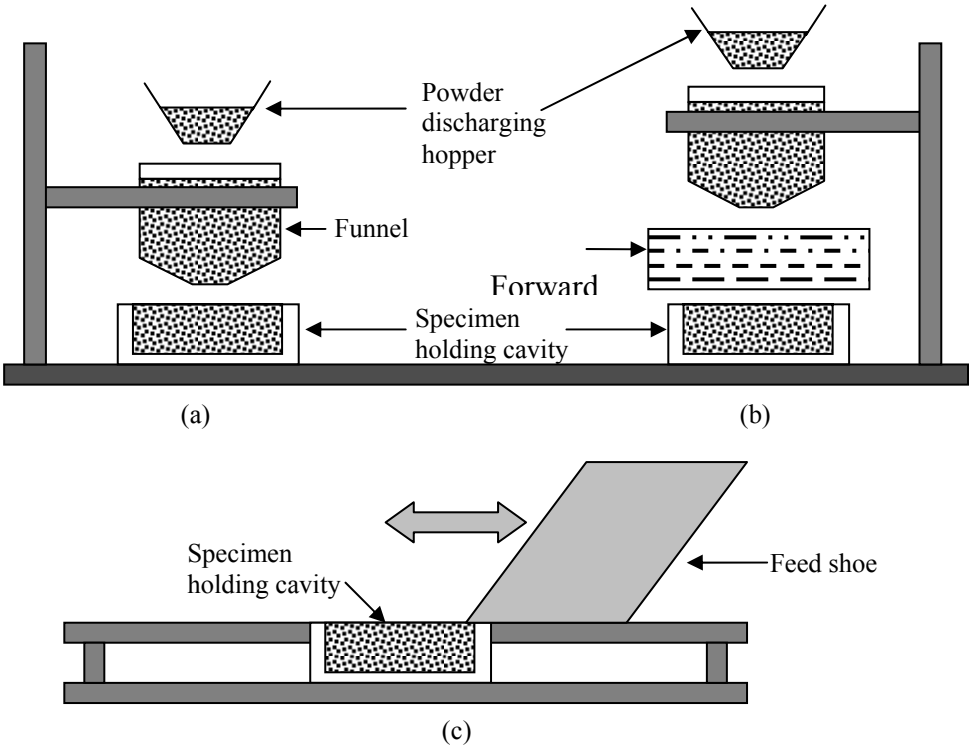

Figure 2.11 Schematic of the three powder deposition methods: (a) funnel, (b) rainy, and (c) feed shoe (Mittal and Puri, 1999a)

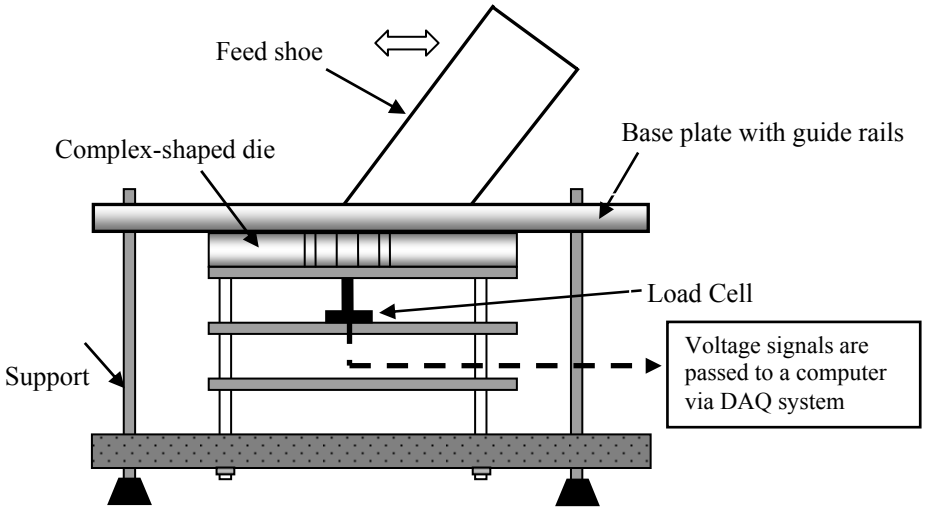

Figure 2.12 Schematic of MDT along with feed shoe deposition method (Dhanoa and Puri, 1997)

Table 2.4 Materials used and factors considered in the experiments (Dhanoa and Puri, 1997)

Filling Method	Funnel filling and Rainy (sieve) filling
Die Cross-section	Circular, square and hexagon
Aspect Ratio	1, 2 and 4
Die Filling Rate	Slow and Rapid
Powders	Wheat flour, Alumina, Silicon nitride and Micro-crystalline cellulose

Dhanoa and Puri (1997) designed and built a mass deposition tester (MDT) to evaluate the effect of filling method, rate of fill on the spatial fill density distribution (Figure 2.12). The factors and materials that were considered or used in their experiments are shown in Table 2.4. Their results showed that die fill rate was an important factor affecting spatial die fill density distribution. Dhanoa and Puri (1998) also used MDT to investigate the process of deposition of particulates into a small cylindrical die with h = 66 mm and d = 66 mm. They used funnel and sieve filling methods. Their results suggested a more uniform powder fill for the sieve filling compared to the funnel filling.

The effect of different filling directions on the mass distribution was tested by Mittal et al. (2001a) in an E-shaped die (Figure 2.7). The numbers in the figure represent mass values detected by load cells in mg. The results were that filling direction affected the powder deposition behavior in the E-container.

Sawayama and Seki (1999) investigated the effect of powder level in the feed shoe on die flowability. The feed shoe they used was 100 × 100 ×70 (h) in mm, and the maximum feed shoe speed was 500 mm/s. The amount of powder placed in the feed shoe was varied from 25% to 75% of the feed shoe height. The cavity was ring shaped with a 30 mm outer diameter, 20 mm inner diameter, and 30 mm depth. Powder filled into the cavity was weighed. The feed shoe travelled in a round trip motion returning above the center of the cavity at constant speeds (40, 75, or 100 mm/s). They found that at higher powder levels, 50% and 75%, the cavity filled fully at the lowest feed shoe speed (40 mm/s), but filled insufficiently at 75 mm/s. However, at 25% powder level, the cavity was filled completely even at the highest feed shoe speed 100 mm/s. Effects of powder level on displacement of the air in the cavity with the powder in the feed shoe, interparticle friction, and/or adhesion due to powder pressure were considered possible reasons for the results. It was also found that when the cavity was fully filled, fill density in the die depended on the powder pressure over the cavity (or powder level in the feed shoe). Fill density was lower for lower powder level in the feed shoe, and fill density also varied more when powder level was lower.

Hjortsberg and Bergquist (2002) tested the effect of feed shoe powder level on die filling at 200 mm/s feed shoe speed with pure iron powder into a ring shaped cavity (inner and outer diameters were 170 and 190 mm and the height was 20 mm). The feed shoe paused over the cavity for two seconds before returning to original position. The amount of powder in the feed shoe was changed, so the powder height in the feed shoe varied from 25 up to 150 mm. Their results showed that the density was not sensitive to the amount of powder within the feed shoe.

Wu et al. (2003b) reported there were two flow patterns in die filling process using a feed shoe. One of them was bulk flow, and the other was nose flow, which was an inherently faster filling than bulk flow. Completely filling the feed shoe might hinder the creation of a nose profile and reduce the contribution of nose flow to the filling process. This might result in a decrease in the net flow rate of powder into the die. Slow feed shoe speeds, such as speeds less than 100 mm/s favored nose flow. So the beneficial effect of nose flow must be balanced by the fact that at low feed shoe velocities, only a small portion of the available cross-sectional area of the die opening was used when the die was filled. Under these conditions, the net flow rate could be increased by creating multiple noses. This could be achieved by dividing the feed shoe into a number of compartments using transversal separating walls.

In addition to powder properties, feed shoe features, and die characteristics, some other factors might also affect powder die filling process. These factors, including filling method, filling intensity, filling direction, and height of powder in the feed shoe, have been discussed in this section. As for this research, feed shoe filling method was used, and filling intensity was controlled by changing feed shoe speed.

2.3.5 Tests of powder deposition into dies

Haskins and Jandeska (1998) used computed tomography (CT) technology to investigate powder flow and die filling process. They demonstrated that a difference in the flow characteristics between the two powders used could be detected by CT analysis, and absolute density differences were also determined with this technology. They expected that absolute density were determined to within 1% to 2% accuracy and that determination of relative density differences might be more precise. Farber et al. (2003) also used CT technology to study the porosity and morphology of granules. However, the costs involved might be very expensive, and it is simply impossible to test certain powders, ones that would cause high attenuation of incident x-rays so as to render them undetectable by a CT scanner. Furthermore, only final density or mass values can be collected by CT technology, and no real-time deposition profile can be obtained by a CT scanner, partly due to its relatively slow inspection rate (Copley et al. 1994).

Quantitative analysis of deposition into small dies is more difficult, at least partly because of lack of suitable apparatus. Dhanoa and Puri (1998) addressed the problem by developing a low-cost tester capable of acquiring real-time data for experimental analysis of the die filling process. Their tester consisted of a tiered arrangement of load cells such that the load cell load application points (top of the custom fitted buttons) were nearly flush with the uppermost plate top surface as shown in Figure 2.13. A thin plastic film was placed over the tester to isolate the

fill particulate materials from the load cells. The open-ended die was then placed over the tester. The output voltage signals from the load cells during the die filling process were recorded using a state-of-the-art data acquisition system (Model # AT-AI-16XE-10, National Instruments, Austin, TX). The resultant data captured by the data acquisition system could then be subjected to statistical analysis to determine the fill distribution. They also carried out some preliminary experiments to study the influence of filling methods on powder uniformity by using the tester. The results suggested a more uniform powder fill for the sieve filling method than the funnel filling method. The new tester was also verified as being a reliable technique to quantify the density distribution of powders in small containers.

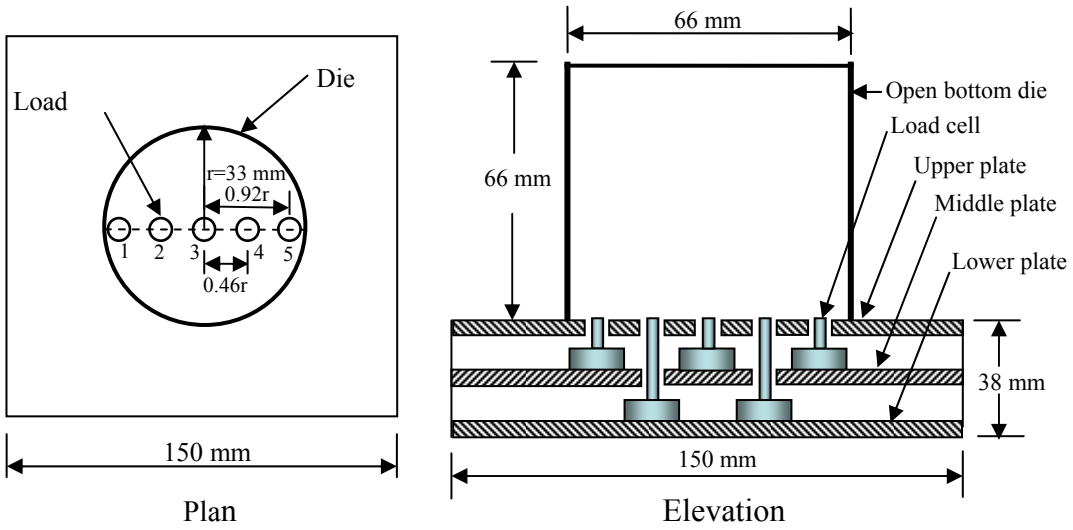

Figure 2.13 Schematic of tester (not to scale) (Dhanoa and Puri, 1998)

Demetry et al. (1998) explored a novel means of assessing density uniformity of powders in dies prior to compaction. What they employed to detect non-uniform mass distribution after the die filling process was a tactile sensor, which was located at the bottom of the die. They also measured density of different locations after applying pressure to produce a green compact. Their results demonstrated the feasibility of using tactile sensors as a quality assessment, process development tool in dry pressing operations. They showed that nonuniformity in mass distribution of the powder fill could be detected as gradients in transmitted pressure at the bottom of the molding die. A pouring device that introduced the powder mix immediately above the die opening rather than from the side of the die was shown to result in a more uniform pressure distribution.

Kondoh and Takemoto (1996) carried out a study to clarify the powder behavior in filling a die cavity by using a camera to record the state of the filled powders. The effects of the shape

of the die cavity and feed shoe speed on the filling behavior, density, and particle size segregation of filled powders were investigated for gravity filling of atomized iron powders.

Using an aeration filling method for die filling (Kondoh and Takemoto, 1996; Kondoh et al., 1998; Urata et al., 1998; and Nakatani et al., 1999), Urata et al. (1998) investigated density variation within compacted cap shaped test parts (total height was 40 mm, and the outer diameter was 70 mm). They discovered that the density varied little on the left and right side to the feed shoe movement direction, but it varied in the front to rear direction. There was a tendency for the density of the pullback end side to be higher than the advancing end side. This tendency was common for both aeration filling and common feed shoe filling.

Hjortsberg and Bergquist (2002) built a filling device that was similar to industrial filling systems to establish correlations between the density and different process variables. The authors believed this approach represented a more cost and time efficient alternative to improve the quality of powder metallurgy products. This device basically contained a feed shoe (inner dimensions are 320 × 320 × 160 mm) and a ring shaped cavity (inner and outer diameters were 170 and 190 mm and the height was 20 mm). Density variation measurement was conducted by dividing the cavity into four 90° sections by inserting four plates into the filled die. The powder of each section was then sucked out of the die and separated from the air stream with a 15 μm filter. The separated powder was then weighed to get the density of each section. The authors believed that the loss of a small amount of the finest particles had a negligible effect on the relative density variations between different sections.

Many different devices or methods, such as CT technology and camera, have been created and used for investigating die deposition. However, most of them either gave only qualitative assessments, or the method was too expensive. The methods of installing load cells at the bottom of the die (Dhanoa and Puri, 1998) or using a tactile sensor (Demetry et al. 1998) were relatively inexpensive and they could provide quantitative values for die deposition evaluation. Therefore, they are better techniques and more promising.

2.3.6 Computational models

Sundaresan (2001) reviewed the research progress about storage and discharge of granular materials in hoppers and bins. Three methods have been widely used to analyze bin discharge, and they are kinematic models, finite element simulation of continuum models, and discrete element simulation of particle assemblies. The kinematic models are limited because they need the rate of discharge to be specified as input, and then the flow patterns inside the bin can be computed. The finite element codes that are commonly used cannot simulate filling process in a

realistic manner, and hence, the initial state prior to discharge has to be specified. Challenges in this approach include exit boundary conditions and reliable constitutive models. For the discrete element method, in principle, the filling and consolidation events can be analyzed. However, it is not feasible to model large number of particles without using large fictitious particles each of which represents thousands of actual particles.

In the finite element method, the solid is represented as a continuum with an appropriate constitutive law, usually based on a semiempirical interpretation of static tests on small samples of the particulate solid. The analysis may be static or dynamic. In the discrete element method, each particle is separately represented and mechanical interactions between particles are modeled in a manner that attempts greater rigor. The analysis is always dynamic. Real solids contain a very large number of particles with varied shapes and multiple normal and frictional contacts. The detection and evaluation of these inter-particle contacts in a dynamic calculation makes DEM very demanding on computer resources. Current programs are, therefore, restricted either to a small number of particles or to particles with very simple geometries, usually in two-dimensional space only (Holst et al., 1999).

Wu et al. (2002 and 2003a) used discrete element method, which took into account the irregular particle shapes and airflow effects, to simulate the die filling process. The numerical results for the filling was obtained for both die filling in air and in vacuum, and the results were in broad agreement with the experimental observations. The experimental and numerical investigation enhanced the understanding of the mechanics of the filling process. However, their numerical investigation also had significant flaws, such as only considering 2D particles, limited particle numbers (2000–3000), and specified particle shapes (circular and polyhedral).

There are a great number of FEM and DEM models in the literature, which are relevant to silo pressure or powder discharge from silos, such as Jofriet et al. (1977), Zhang et al. (1986), Langston et al. (1995), Tejchman (1998), Kamath and Puri (1999), Matuttis et al. (2000), and Chen et al. (2001).

CHAPTER 3 GOAL AND OBJECTIVES

3.1 Goal

The goal of this research was to test, evaluate, analyze, and model the deposition process and uniformity of powder fill in multiple dies. This research also aimed to correlate the data obtained with the second generation pressure deposition tester (PDT-II) to data obtained from X-ray computed tomography (CT).

3.2 Objectives

To achieve the goal, the objectives were to:

Objective 1: Design and fabricate the second generation pressure deposition tester (PDT-II) for evaluation of simultaneous powder deposition in multiple dies.

Objective 2: Employ the PDT-II to collect mass (or pressure) distribution data of powder filled into dies and analyze the data, so as to test the effects of die configurations, fill directions, feed shoe speeds, and powder characteristics, on uniformity of powder fill in multiple dies.

Objective 3: Obtain data using a computed tomography (CT) scanner for selected test cases used in Objective 2, and correlate these data with data obtained by the PDT-II.

Objective 4: Develop and verify physics-based mathematical models to simulate the deposition process, and make recommendations for uniform filling.

CHAPTER 4 DATA COLLECTION USING PDT-II AND CT SCANNER

4.1 Evaluation of the First Generation MDT (MDT-I)

The first generation mass deposition tester (denoted as MDT-I) was developed by Dhanoa and Puri (1997 and 1998) and later modified by Mittal and Puri (2001) (Figure 2.12 and Figure 2.13). It is based on the principle that an anisotropic fill density distribution would result in an uneven particulate vertical pressure distribution on the inside face of the die bottom. Further, this uneven vertical pressure distribution can be detected by placing sensitive and high precision load cells on the inside face of the die bottom.

The main strength of MDT-I includes the novel concept for quantifying the mass of powder deposited at any location during the deposition process. The MDT-I load cells can generate real-time deposition profile as the feed shoe moves across the die cavity, in addition to the final mass values at different locations. Data collected by MDT-I can be used to study the effects of various filling related parameters, such as die shape, powder flowability, and feed shoe speed, on the deposition process and final spatial mass distribution. The quantitative information can be used to optimize the deposition process in order to obtain a uniform fill.

Compared to other published testers or methods, such as CT scanning and using a camera, MDT-I is a reliable, effective, efficient, and low-cost tester to quantitatively test and analyze uniformity of powder deposition in a single die or multiple dies. Another major advantage is that it can collect real-time deposition profile, from the start of the filling to the end of the filling. The recorded data can be used to construct real-time, dynamic mass contour plots starting from an empty die to a fully filled die. These mass contour plots can be visualized in movie form to observe and evaluate the fill pattern.

However, MDT-I also has the following major shortcomings:

(1) Manual operation – The feed shoe needs to be manually operated, so the feed shoe speed and its initial acceleration rate cannot be controlled accurately. Since one of the major objectives of this research was to evaluate the effects of feed shoe speed (at a fixed initial acceleration rate) on uniformity of powder deposition, precise and automatic control of feed shoe speed and acceleration rate are essential requirements for this tester.

(2) Time consuming to relocate load cells – The upper plate can only have certain number of holes at certain locations due the physical size of each load cell (Figure 2.13), so the load

cells have to be relocated if mass distribution at other locations is to be tested. This is a time consuming process that also requires extra care so as not to damage the load cells.

(3) Lack of flexibility – Different upper, middle, and lower plates with holes for load cells at different locations are needed for dies of different shapes and sizes. This increases the complexity of MDT-I and makes the device considerably less flexible to changes.

4.2 Design Requirements and Features of PDT-II

Given the limitations of the first generation MDT (MDT-I), the second generation MDT (denoted as PDT-II) was designed to overcome the limitations of MDT-I. The major components of PDT-II are a feed shoe, a measurement system, and a drive system. There are also some other components to support or improve the performance of the major components, including XY table, feed shoe table and guide rails, linear actuator table, base plate, vibration-damping mounts, frames supporting the tables, and die plates (Figure 4.1).

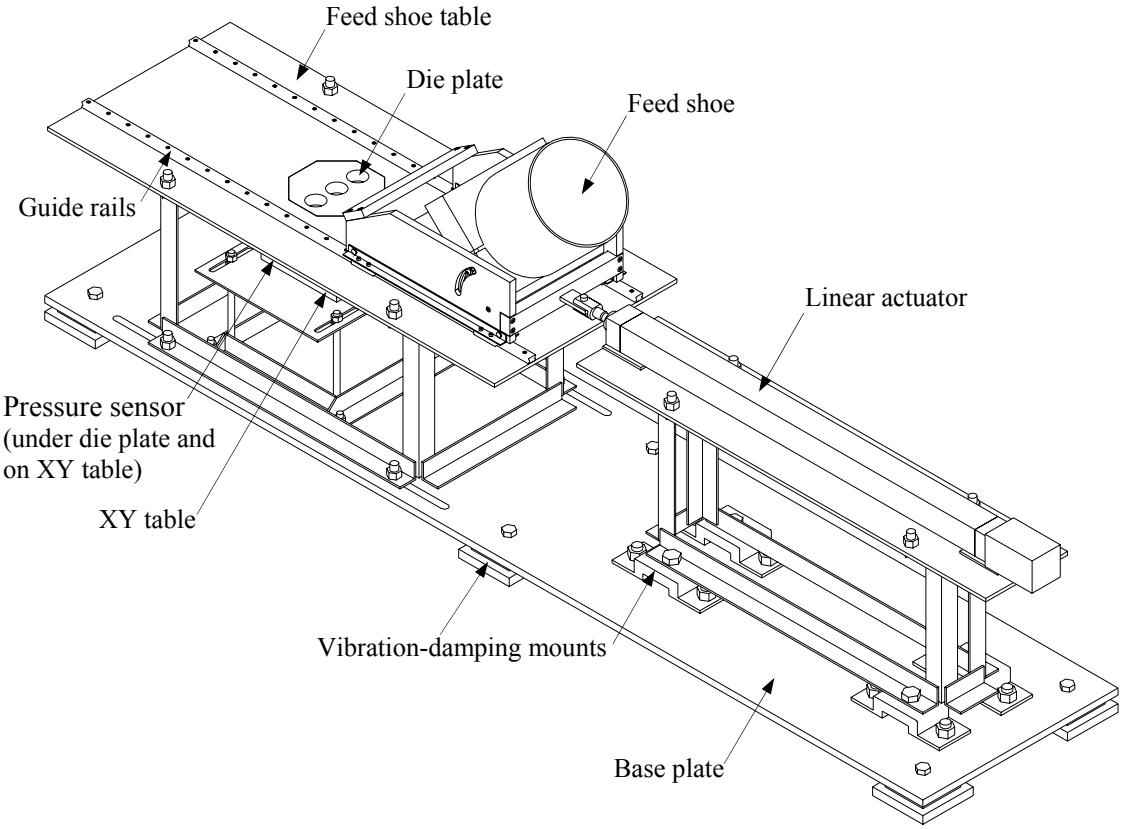

Figure 4.1 An AutoCAD drawing of the assembled PDT-II

In general, PDT-II should meet the following major performance requirements: (1) The movement of the feed shoe, including speed, acceleration, and travel distance, should be

automatically and precisely regulated and controlled. (2) The measurement system should: a) have the ability to quantify, with sufficient sensitivity and precision, the distribution of mass or pressure values across the die (or dies) through the entire deposition process; b) have the flexibility to be relocated to measure pressures at different locations of dies of different shapes and sizes. (3) The device design should permit easy adjustment and setting of various deposition-related parameters, such as feed shoe angle, feed shoe speed and acceleration, and die shape and size.

The specific design requirements and features of the components considered essential were:

- *Feed shoe* should
  i. Hold the feed shoe tube tightly
  ii. Allow the vertical angle between the feed shoe tube and the feed shoe table (denoted as feed shoe angle) to be adjustable
  iii. Minimize the gap between the bottom of the feed shoe tube and the feed shoe table
  iv. Minimize the friction between the feed shoe and the feed shoe table during the filling process
  v. Guarantee a linear motion along the feed shoe table
  vi. Provide constant and controllable speed, acceleration, and travel distance
- *Measurement system* should
  i. Be sensitive, precise, and accurate
  ii. Be able to measure multiple locations simultaneously
  iii. Be suitable for dies of different shapes and sizes
  iv. Be simple to operate and relocate
  v. Collect data automatically at high collection rates for required length of time
- *Drive system* should
  i. Produce required power, speed, acceleration, and travel distance with enough precision
  ii. Be easy to adjust speed, acceleration, and travel distance
  iii. Be easy to maintain
  iv. Be automatically controlled
  v. Generate minimum side effects, such as vibration effect on and electromagnetic interference with the measurement system and data collection process
- *XY table* should
  i. Provide precise and adjustable horizontal positions (in x- and y-directions)

ii. Provide a platform that is flat and large enough to attach the pressure sensor strip and support the die plate
iii. Be stable under motion

- *Feed shoe table and guide rails* should
  i. Provide sufficient flat space for the feed shoe motion
  ii. Guarantee a linear motion of the feed shoe
  iii. Minimize friction between the feed shoe and table during the filling process
- *Base plate* should
  i. Be strong enough to support and provide a platform for other components
  ii. Be heavy enough to reduce the influence of vibration
- *Vibration*-damping *mounts* should
  i. Be strong enough to support the upper components
  ii. Be able to reduce vibration during the filling process
- *Frames supporting the tables* should
  i. Be strong enough to support the upper components
  ii. Have enough space for the operation, such as adjusting the horizontal and vertical position of the XY table
  iii. Be stable under motion while minimizing any vibrations
- *Die plates* should
  i. Be easy to remove and replace
  ii. Have surface finish similar to that of the dies of industrial practices

4.3 Design and Fabrication of PDT-II

Based on design and fabrication requirements, and information received from industrial mentors, PDT-II was initially designed using AutoCAD® (AutoCAD 2002, Autodesk, Inc., San Rafael, CA 94903) software. Subsequent evaluation and redesign paved the way for fabrication. In the following sections, the design principles and features of each component are summarized.

4.3.1 Feed shoe

Two side plates, a front bar, and a rear bar provide a frame for holding the feed shoe tube (Figure 4.2). A shoe tube holder (denoted as *Shoe tube hold I* in Figure 4.2) was inserted between the two side plates. *Shoe tube hold I* was fastened to its position by two screws on each side, respectively. One of the screws served as a pivot, and the other could permit rotation by riding

along a curved slot (one on each side). Another shoe tube holder (denoted as *Shoe tube hold II* in Figure 4.2) was attached to *Shoe tube hold I* by four screws, and the two shoe tube holds tightly secured the feed shoe tube in its position. A tongue with a drilled hole was welded to the rear bar to connect the linear actuator with the feed shoe.

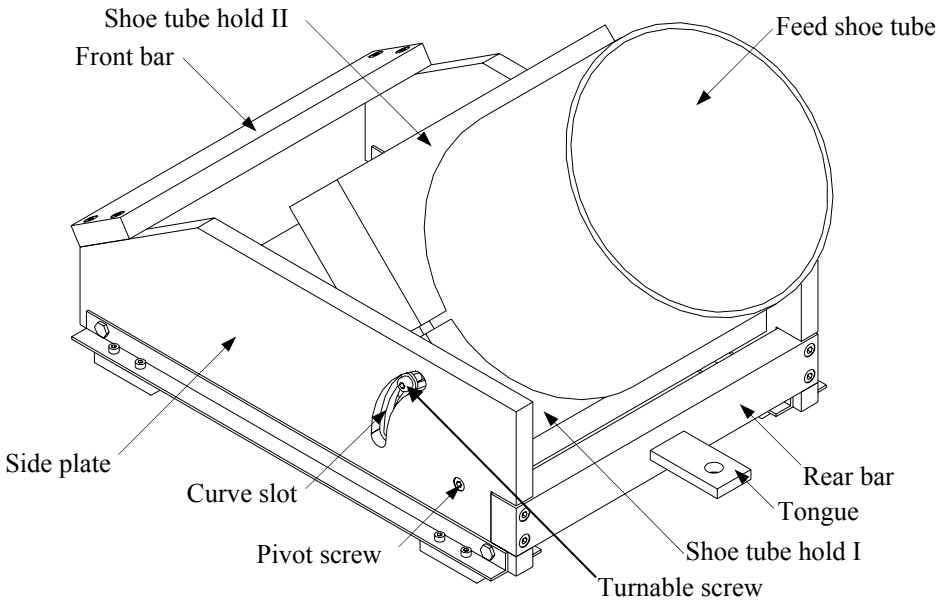

Figure 4.2 3D view of the designed feed shoe

A curved slot was made in each side plate for the turnable screw to be able to rotate around the pivot screws. If a different feed shoe angle is needed, a new feed shoe tube of specified angle can be made and used. The feed shoe angle can be changed between 30° and 90°, which was sufficiently flexible based on industrial mentor inputs for this and most of the anticipated future research projects to evaluate the effect of feed shoe angle on die filling.

The feed shoe tube was cut out from a clear cast acrylic tube, of 165.1 mm outer diameter and 158.8 mm inner diameter. The dimensions were provided by vendor and were verified to be accurate. The top end of the feed shoe tube was perpendicular to the center line, while the bottom end was cut at 45° to the center line. Figure 4.3 shows the dimensions of the feed shoe tube in two different views, side view and top view of the bottom in contact with the feed shoe table.

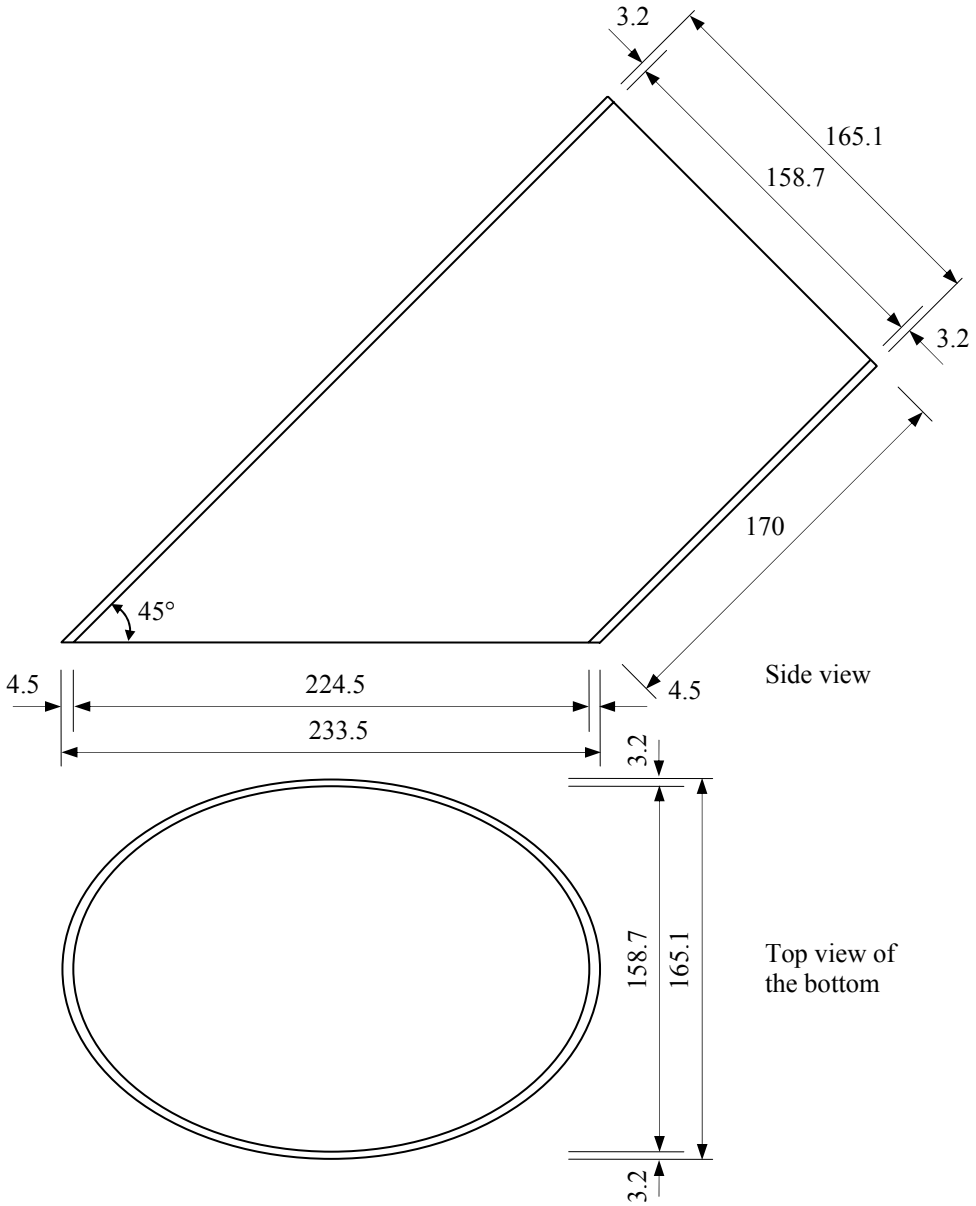

Figure 4.3 Dimensions of the feed shoe tube (in mm)

4.3.2 Feed shoe table

In order to maintain a linear motion of the feed shoe, two guide rails were installed on the top surface of the feed shoe table (Figure 4.4). On the bottom of the two side plates of the feed shoe, four guide blocks were attached, with two for each side plate. The guide blocks with roller bearings to minimize friction could slide effortlessly on the guide rails. The guide blocks and guide rails helped to reduce friction between the feed shoe and table, in addition to guaranteeing the linear motion of the feed shoe. A cavity of octagonal shape was cut in the feed shoe table to

accommodate the die plate. The reason for the selection of this shape is summarized in section 4.3.6.

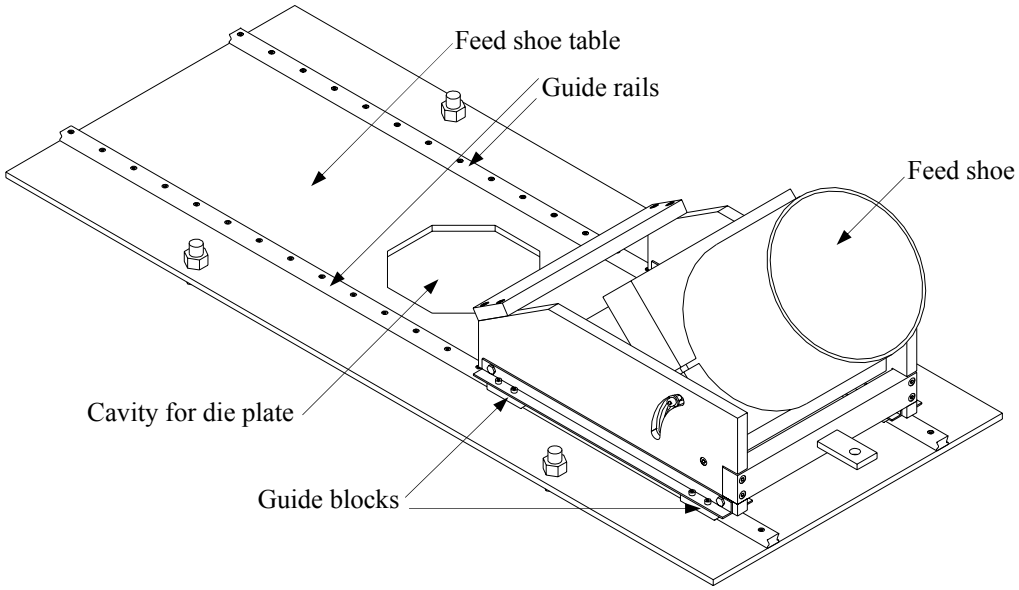

Figure 4.4 A 3D view of the feed shoe table and the feed shoe

4.3.3 Measurement system

According to the research conducted with sensors similar to those in MDT-I and sensor requirements considered essential (see section 4.2) for PDT-II, P-1500 (Pressure Profile Systems Inc., Los Angeles, CA) was the best choice available for this research. All of the other potential choices either had too low sensitivity, or too large area of sensor elements, or too low data collection rate, or could only measure one location at a time. The pressure sensor system of P-1500 was connected to a data acquisition system and data analysis software. The software was designed to display the pressure in real time on the computer screen in 2D or 3D images.

Figure 4.5 shows a schematic dimensioned drawing of the pressure sensor. There were 16 active elements in the sensor array, each 1.9 mm × 5 mm and spaced 2 mm on center. The centerlines of the sensor plate are marked in Figure 4.5 – the vertical centerline coincides between elements 8 and 9, and horizontal along the middle of elements. Four through-holes of 3 mm diameter were available for screws to secure the pressure sensor to any flat surface.

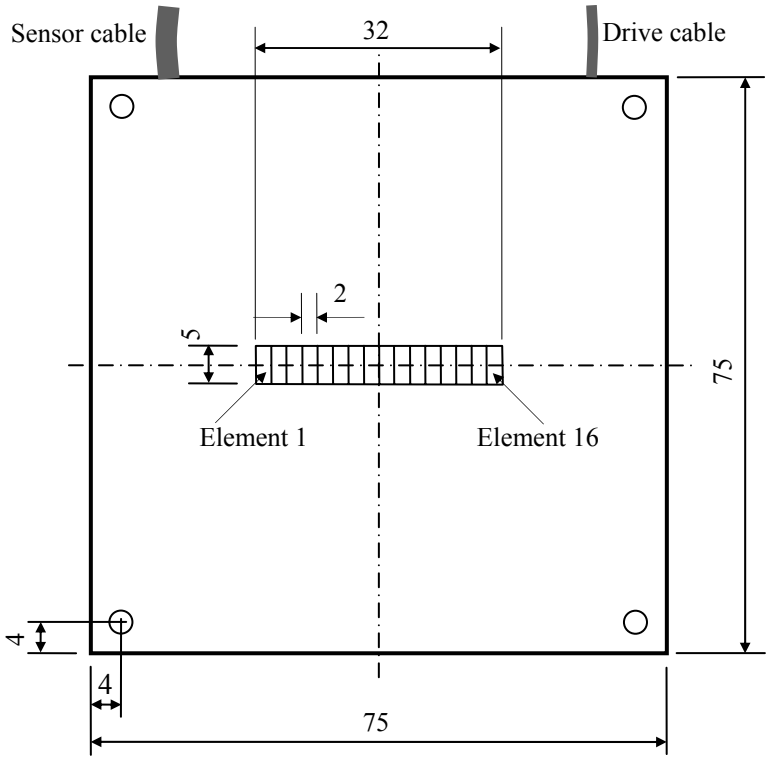

Figure 4.5 Plan view of the pressure sensor plate (the thickness was 3.2, all units in mm)

Some specifications of the pressure strip are shown in Table 4.1. The resolution of the pressure needed for this research was about 6 Pa (or 5.8 mg on an area of 1.9 mm × 5 mm), and the sensitivity of P-1500 is 0.1% of the full scale range, namely 5 Pa (or 4.8 mg on an area of 1.9 mm × 5 mm) (5 kPa or 0.73 psi full scale range times 0.1% sensitivity), so P-1500 had sufficient resolution for this research. The overpressure value was 551.6 kPa, which was high enough to protect the pressure sensor from damage caused by over loading. In addition, the spatial resolution of 2 mm × 5 mm was small enough for most of the die dimensions. The minimum time interval between two data points could be 8.84 ms, or in other words, the maximum data collection rate was 113 Hz, which was sufficient for this research. Basically, there was no limit for data collection duration.

Table 4.1 Some specifications of the P-1500 pressure strip

Specifications	Value
Full Scale Range (FSR)	5 kPa (0.73 psi)
Overpressure Value	551.6 kPa
Spatial Resolution	2 mm × 5 mm
ADC Range & Resolution	5 V, 12-bit
Non-Linearity	0.1%
Scale Factor Non-Repeatability	0.1% RMS
Bias Non-Repeatability	0.1% RMS
Baseline Temperature Stability	0.2%/10°C

4.3.4 Drive system

One of the key components of PDT-II was the drive system. A primary requirement was to move the feed shoe linearly forward and backward at different required speeds with adjustable accelerations to speed up or slow down within a certain travel distance. Another requirement of drive system was to provide sufficient force to move the feed shoe filled with powder at predetermined speeds. For this, a linear actuator (ETS50-B01LA3X-FC600-A662 Electric Cylinder, Parker Hannifin Corporation, Wadsworth, OH) was employed.

A photograph of the actuator is shown in Figure 4.6, along with the drive/controller (OEM ZL6104). Key specifications of the linear actuator are given in Table 4.2. The maximum travel distance was 600 mm, which was sufficient for this research. Based on industrial members' inputs, the maximum possible speed needed for this research was 900 mm/s, which was less than the maximum speed (1524 mm/s) provided by this selected linear actuator. The maximum acceleration was g, or 9.8 m/s^2, which was acceptable for this research. The maximum thrust of 3200 N was more than sufficient compared with the maximum thrust needed for this research, which was about 200 N.

Figure 4.7 shows the speed profile of the linear actuator that was used for this research. The linear actuator started from stationary with certain acceleration, and then reached required steady speed. At the end of the forward stroke, it decelerated at the same rate as acceleration until it reached rest position. Following a brief pause, the movement direction was reversed, and with the same acceleration, the speed reached the same steady value as in the forward stroke. The backward stroke ended at the starting point with the same deceleration. The values of the acceleration and the deceleration used for this research were 0.2g, since the feed shoe table could provide enough travel distance. By using the lower acceleration and deceleration, powder sample in the feed shoe was less likely to be compacted and hinder die filling during the filling process.

4.3.5 XY table

The pressure sensor strip could only cover limited area with an array of 16 sensor elements. In order to measure pressure values of different locations within dies of different shapes and sizes, the horizontal position of the pressure sensor strip needed to be adjustable with sufficient accuracy. An XY table was installed to provide a platform for the pressure sensor to be secured with adjustable horizontal position (Figure 4.8). The XY table, with top and bottom plate dimensions of 152.4 mm × 152.4 mm, had travel distances of 50.8 mm × 50.8 mm.

Figure 4.6 ETS50-B01LA3X-FC600-A662 Electric Cylinder and OEM ZL6104 drive/controller (Parker Hannifin Corp., Wadsworth, OH)

Table 4.2 Some specifications of ETS50-B01LA3X-FC600-A662 Electric Cylinder (Parker Hannifin Corp., Wadsworth, OH)

Parameters	Values
Max. travel (mm)	600 mm
Max. speed (mm/s)	1524
Max. thrust (N)	3200

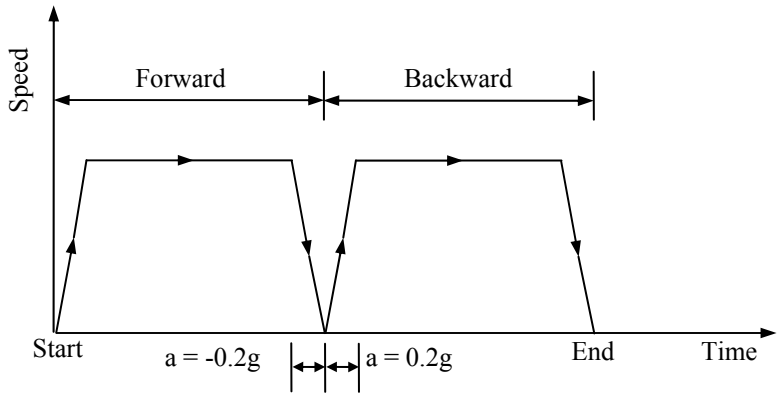

Figure 4.7 Schematic of speed profile of the linear actuator

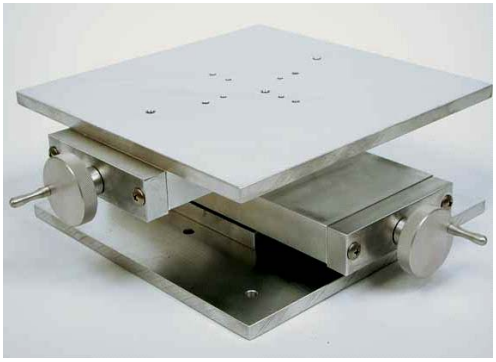

Figure 4.8 Photograph of the XY table (Model AXY4006W1, Velmex, Inc., Bloomfield, NY)

4.3.6 Die plates

Cylinder, toroid, and E-shape are common shapes in powder products, such as magnetic cores, and batteries (such as AA). So these shapes were included for this research. Three plates corresponding to the three die shapes were made (Figure 4.9, Figure 4.10, and Figure 4.11). In order to satisfy the requirement (i.e., being suitable for different die configurations with the same die plate), the die plates were cut into an octagon, and an octagonal hole was also cut in the feed shoe plate to accommodate the die plate (Figure 4.4). Figure 4.12 and Figure 4.13 show examples of the ease with which the configuration or the direction of the die plate can be changed with respect to the feed shoe movement direction.

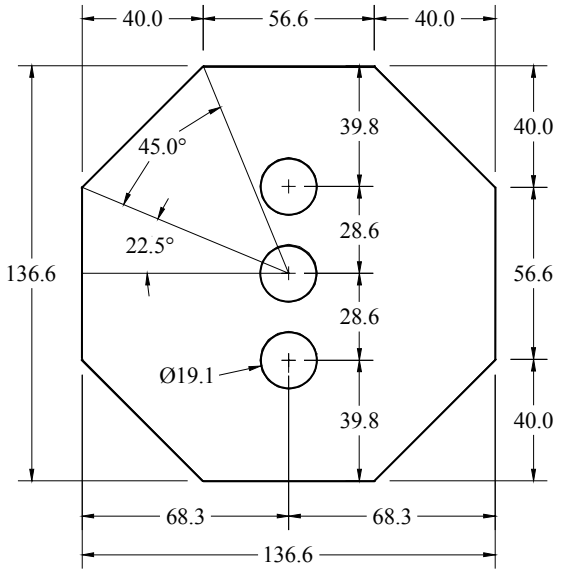

Figure 4.9 Dimension of the cylindrical dies and die plate (thickness: 19.1)(unit: mm)

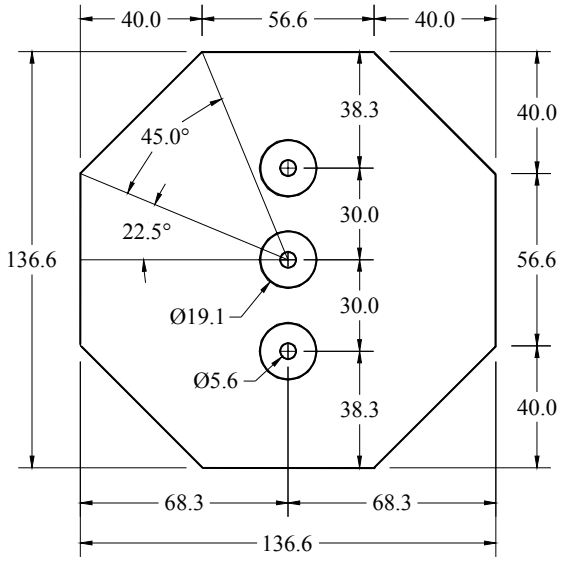

Figure 4.10 Dimension of the toroidal dies and die plate (thickness: 19.1)(unit: mm)

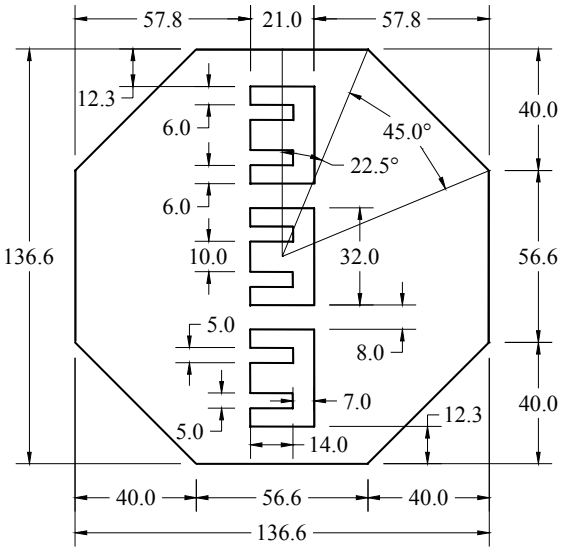

Figure 4.11 Dimension of the E-shaped dies and die plate (thickness: 19.1)(unit: mm)

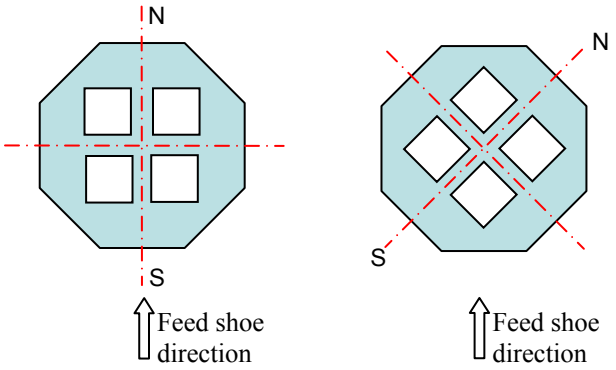

a. Along 0º b. Rotated 45º

Figure 4.12 Rotation of die plate to change filling directions (an example of four square dies)

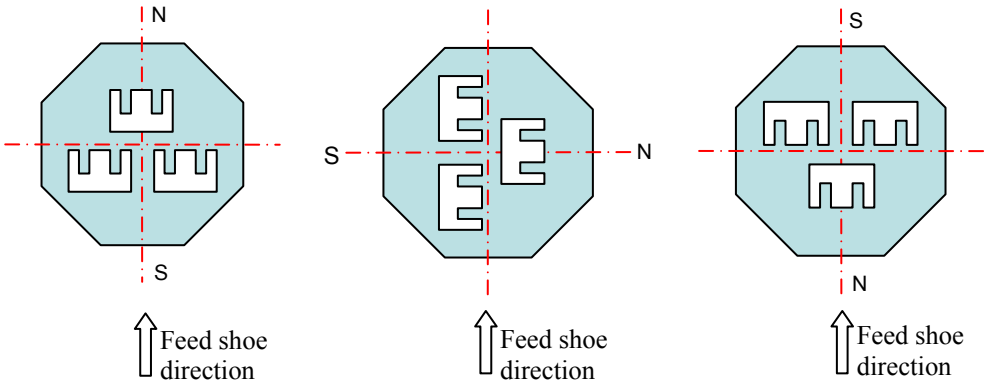

a. Along 0º b. Rotated 90º c. Rotated 180º

Figure 4.13 Rotation of die plate to change filling directions (an example of three E-shaped dies)

In order to protect the pressure sensor strip from being damaged by high pressures from the die plate in use and the impact from the feed shoe during filling process, a narrow gap was maintained between the pressure sensor and the die plate in use. The gap was of 0.23 mm. This gap was marginally larger than the clearance between the die and punch in the common industry practice. The clearance between the die and punch is about 10-25 μm when pressing micron-size powders and about 100 μm when pressing granular particles larger than 44 μm (Reed, 1995).

4.3.7 Additional features

The travel distance of the XY table was limited to 50.8 mm in either of the two horizontal directions, which was less than needed travel. To solve this problem and increase the flexibility of PDT-II to accommodate dies of different sizes, slots, instead of only holes, were cut in the plate supporting XY table and the base plate (Figure 4.14). By doing this, the plate supporting the XY table was movable in both of the two horizontal directions, and this indirectly increased the available travel distance of the XY table. Four vertical bolts were used to support the plate supporting the XY table, and two screw nuts, below and above the plate, respectively, on each vertical bolt secured the plate at its desired horizontal location. By lowering or increasing the screws on the vertical bolts, the vertical position of the plate supporting the XY table was also adjustable to meet the requirements of die plates of different thicknesses.

Similar slots were also cut in the base plate for the screws to secure the frame supporting the feed shoe table (Figure 4.1 and Figure 4.14). These slots made the feed shoe table movable in the feed shoe movement direction, and this enabled the relative position of the feed shoe table to the linear actuator to be changeable. These features permitted full advantage of the travel distance of the linear actuator for various configurations of dies of diverse shapes and sizes.

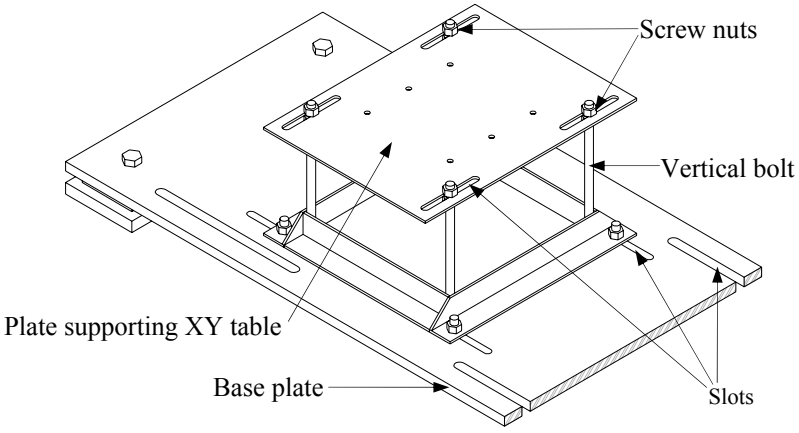

Figure 4.14 Plate supporting the XY table and the base

In order to reduce the influence of vibration from the linear actuator on powder deposition process, the feed shoe table was separated from the table installed with the linear actuator. Through vibration-damping mounts, the frame supporting actuator table was fixed to the base plate. Six other vibration-damping mounts were also installed to the base plate to reduce the vibration of the entire device. The pressure sensor was attached on the top surface of the XY table, which was fixed on a plate supported by a separate frame (Figure 4.1). The frame supporting the feed shoe table and the frame supporting the pressure sensor table were fixed to the same base plate as of the frame supporting actuator table. A photograph of the assembled PDT-II is shown in Figure 4.15.

Figure 4.15 A photograph of the fabricated and assembled PDT-II

4.4 Methodology of PDT-II Test

To ensure the performance of PDT-II, a specific test methodology was followed. The test methodology included the operation procedure and calibration of the pressure sensor strip. These are discussed in the following sections.

4.4.1 Operation procedure

Preparation-Prior to operation of the PDT-II, the pressure sensor strip and the linear actuator were warmed up for at least one-half hour. Test powder sample was then filled layer by layer into the feed shoe tube to the height of 35 mm with a scoop of 8 × 4 × 2.5 cm. After each scoop of powder was filled, the powder was leveled by the scoop. The final top surface was

leveled by a brush with minimal pressure on the powder mass in the feed shoe. The plate supporting the XY table, including the XY table, was adjusted vertically by turning the nuts on the four supporting rods to a suitable height to bring the top surface of the die plate to the same level as the top surface of the feed shoe table. Horizontally, the pressure sensor strip was moved to desired position by regulating the top plate of the XY table. The pressure sensor strip was covered with a layer of LDPE plastic film of 0.05 mm thickness for protection purpose.

Running tests-The program operating the linear actuator, Motion Architect Program (Parker Hannifin Corp., Wadsworth, OH), and the program recording the data of the pressure sensor, TactAray Visualization (Pressure Profile Systems Inc., Los Angeles, CA), were installed in two separate computers. Once all the preparation work was done, the two programs were turned on and started simultaneously to launch the die filling process and collect real-time pressure distribution profiles. The feed shoe motion included forward and backward strokes. After finishing the die filling process, the data were saved, and the dies were vacuumed by a vacuum (Shop-Vac®, # 4045, 4.5HP/12 gal). Then the next test was conducted.

4.4.2 Locations of the pressure sensor strip

The pressure sensor strip was placed at the bottom of the right and center dies for all the three die shapes (Figure 4.16, Figure 4.17, and Figure 4.18). Powder deposition was assumed to be symmetrical about the feed shoe movement direction, and the left die of the three dies was assumed to have the same powder distribution as the right die. So the powder distribution of the left die was not measured for all the three die shapes because of cost and time limitations. The assumption that the left and the right dies have symmetrical powder distribution about the feed shoe movement direction was examined or verified by data collected by a CT scanner.

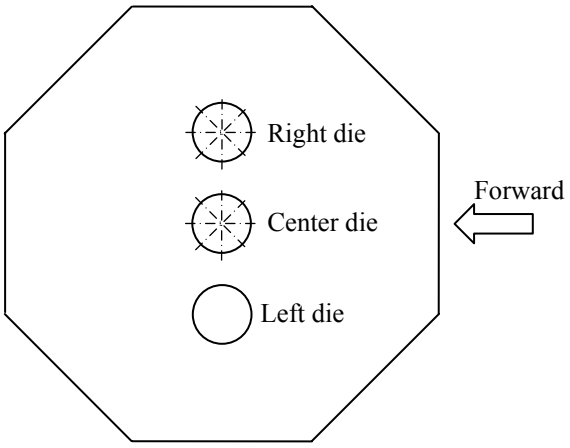

Figure 4.16 Locations of the pressure sensor strip for cylindrical dies

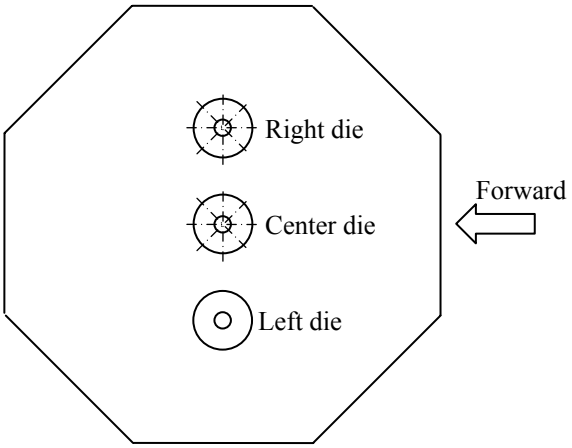

Figure 4.17 Locations of the pressure sensor strip for toroidal dies

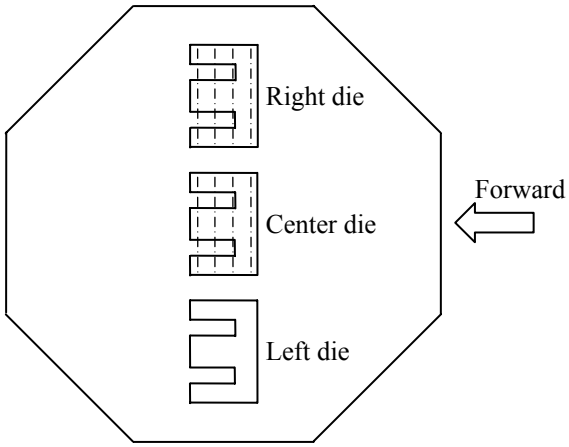

Figure 4.18 Locations of the pressure sensor strip for E-shaped dies

As shown in Figure 4.18, the feed shoe approached the E-shaped dies from the back side, since this direction results in denser packing (Mittal et al., 2001a). For cylindrical dies, the pressure sensor strip was oriented in four separate directions, i.e., 0º-180º, 45º-225º, 90º-270º, and 135º-315º, with respect to the feed shoe movement direction (Figure 4.19). For each direction, nine sensor elements were exposed to record pressure increase profiles. For toroidal dies, the pressure sensor was oriented in the same four directions, i.e., 0º-180º, 45º-225º, 90º-270º, and 135º-315º (Figure 4.20). Data were collected for all the four directions. Because of the center post, only six sensor elements were fully exposed to record pressure increase profiles. For E-shaped dies, the pressure sensor strip was placed in four locations perpendicular to the feed shoe movement direction (Figure 4.21). All the sixteen sensor elements were exposed for location L4, while only ten sensor elements were fully exposed for locations L1, L2, and L3.

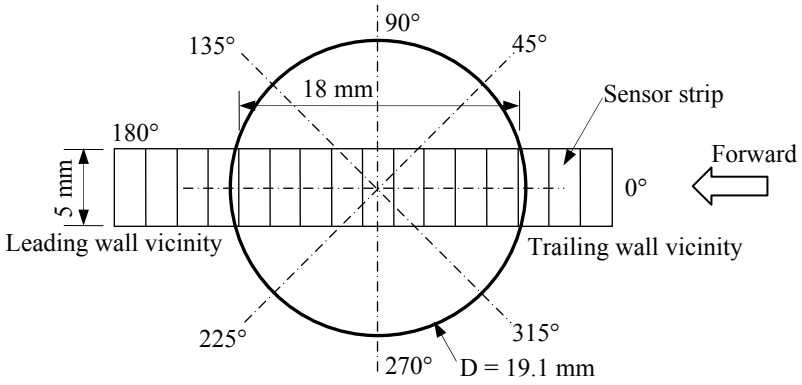

Figure 4.19 Locations of the pressure sensor strip in a cylindrical die (drawn to scale)

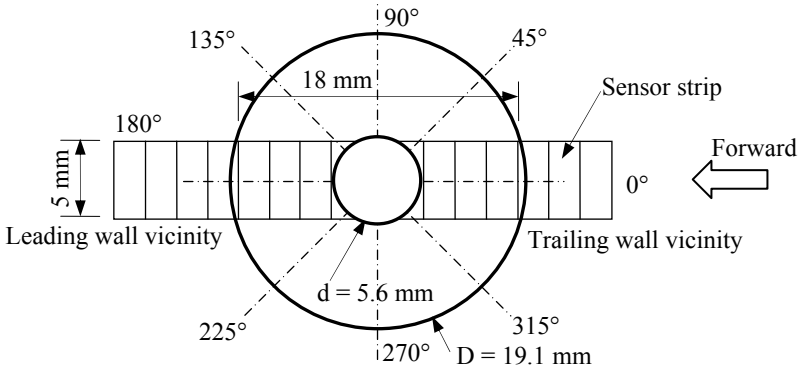

Figure 4.20 Locations of the pressure sensor strip in a toroidal die (drawn to scale)

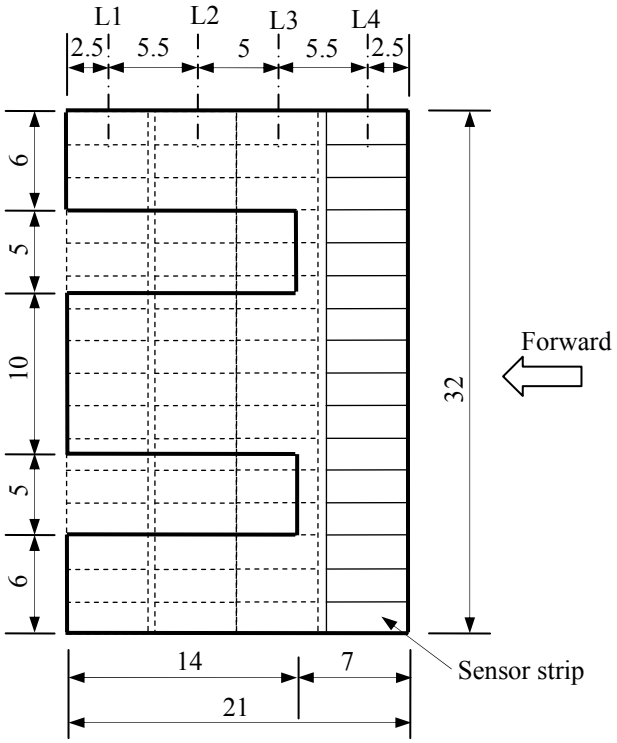

Figure 4.21 Locations of the pressure sensor strip in an E-shaped die (drawn to scale)

4.4.3 Calibration of the pressure sensor strip

Based on discussion with and input from the engineer at Pressure Profile Systems Inc., Los Angeles, CA, a water column precision calibration system was fabricated and used for pressure sensor strip (Figure 4.22). The pressure sensor was first secured to an aluminum plate by four screws, and then a layer of LDPE plastic film of 0.05 mm thickness was placed on top to protect the sensor strip. The plastic film also made the setup of the calibration consistent with PDT-II tests, since during the tests the pressure sensor was also protected by a layer of plastic film of the same thickness. An acrylic cylinder was set on the plastic film with a thin layer of petroleum jelly applied to the base of the cylinder to prevent water from leaking. Water was then filled into the cylinder to different heights to generate different pressure levels. Voltage response of each sensor element at different pressure levels was recorded. The minimum water pressure value was 0, and the maximum water pressure was 1500 Pa. The increment of water head was 10 mm, which was approximately 100 Pa. In all 16 data points were collected for a single calibration test. For each sensor element, the data, pressure vs. voltage, were regressed to obtain the best straight line passing through the origin. The slope of the line was the gain value (in Pa/V) for that sensor element. The sensor calibration was repeated every 50 PDT-II tests to account for any drift. Previous tests proved that this frequency of calibration was sufficient to ensure valid and accurate measured pressure values.

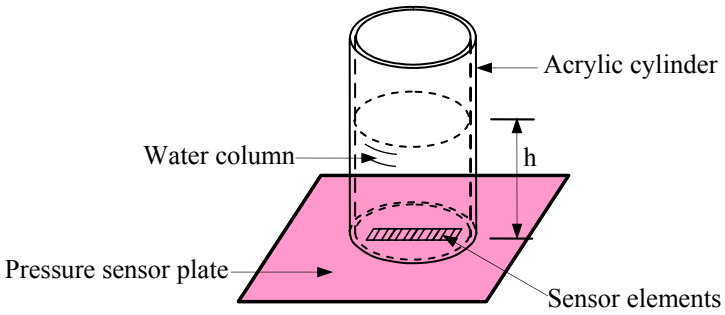

Figure 4.22 Calibration setup for pressure sensor strip P-1500

4.4.4 Comparison of mass values after forward stroke and entire filling

In order to investigate to what extent the cylindrical dies were filled after the forward stroke, compared to the entire filling process, tests shown in Table 4.3 were conducted for cylindrical dies. Only the battery powder mixture was used for these tests.

One bottom plate was made of gray PVC with thickness of 6.35 mm. It was first cut into the same shape and size as the cylindrical die plate. Then it was glued to the bottom of the cylindrical die plate. Extra care was taken to maintain a gap of about 0.23 mm between the bottom plate and dies to be consistent with PDT-II die fill experiments.

Table 4.3 Comparison of mass values of powder filled in the dies after only forward stroke with those of powder filled in the dies after the entire filling process

Feed shoe speeds, mm/s	Tested dies	Number of treatments
20	R, C, L*	6
100	R, C, L	6
500	R, C, L	6

* R, C, and L represent the right, center, and left dies, respectively.

Mass values of powder in each die after the forward stroke were first obtained. The feed shoe was stopped at the end position of the forward stroke after the forward stroke filling, the die plate, with filled powder, was weighed using a balance of 0.1 gram accuracy. Then the die plate was removed from the balance, and one of the three dies was vacuumed carefully by covering the other two dies with paper. The die plate, with only two dies filled with powder, was weighed again. This step was repeated till the powder mass of each of the three dies was obtained. Then the die plate was placed back into PDT-II, and next die filling and weighing process was conducted. Six replicates were conducted for each combination.

After the eighteen tests were done for the mass values of the forward stroke, test combinations shown in Table 4.3 were conducted again to get mass values of powder filled in the dies after the entire filling process. Similar procedures as for only forward stroke were repeated, and the only difference was that the dies were filled with both forward and backward strokes.

4.5 Collecting, Processing, Analyzing, and Interpreting PDT-II Data

4.5.1 Battery powder mixture data

A battery powder mixture was used as one of the two test materials. It was a black powder with no odor. The major components were manganese dioxide (80-93% by weight), graphite (3-13% by weight), potassium hydroxide (2-5% by weight), barium sulfate (0-5% by weight), niobium titanium dioxide (0-5% by weight), and polytetrafluoroethylene (0-5% by weight). The specific gravity of this powder was 4.7, and its bulk density was 1.65 g/cm^3. It was stable under ambient conditions. The lower and upper limits of the granule size of the battery powder mixture were supposed to be 210 and 1000 μm, respectively. However, as it was very friable, some granules crumbled into finer granules during the handling and transportation process. The actual granule size distribution just before the tests of this research is shown in Figure 4.23. The median size (d_{50}) was 600 μm. The test method used was dry sieve analysis, and the sieves were shaken by hand to avoid breaking too many granules. Figure 4.24 is a micrograph of the battery powder mixture. During the entire test procedure, the ambient environment

conditions were controlled, i.e., the ambient temperature was maintained at 23 ± 2°C, and relative humidity was 35 ± 3%.

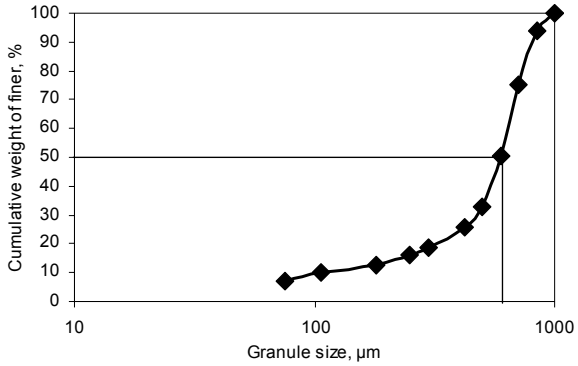

Figure 4.23 Granule size distribution of the battery powder mixture

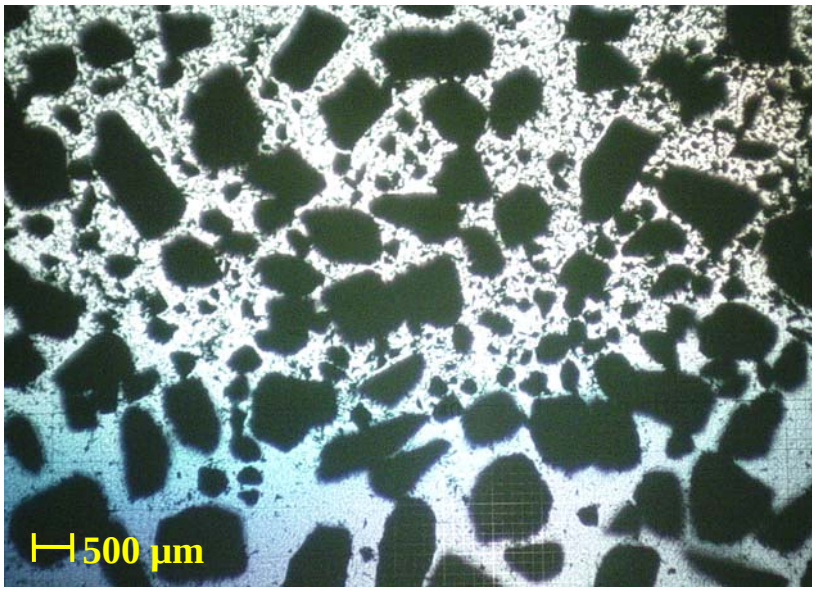

Figure 4.24 Micrograph of the battery powder mixture

Cylindrical, toroidal, and E-shaped dies were tested with the battery powder mixture, and feed shoe speeds were 20, 100, and 500 mm/s for the first two die shapes, and only 20 mm/s for the E-shaped dies because of limited time and resources. Pressure deposition profiles were collected from the right and the center dies (Figure 4.16, Figure 4.17, and Figure 4.18), with the pressure sensor strip located at four different locations for each die (Figure 4.19, Figure 4.20, and Figure 4.21). Table 4.4 shows the test combinations for the battery powder mixture. Based on previous experiences (Dhanoa. and Puri, 1998; Mittal et al., 2001a), each test combination was repeated six times. It allowed a mean value with coefficient of variation (COV) less than 15 ~ 20%, thereby indicating that the data obtained from six replications was consistent.

Table 4.4 Test combinations for the battery powder mixture

Die shape	Feed shoe speed, mm/s	Tested dies	Test locations	# of treatments
Cylinder	20, 100, 500	Right, center	0º-180º, 45º-225º, 90º-270º, 135º-315º	24
Toroid	20, 100, 500	Right, center	0º-180º, 45º-225º, 90º-270º, 135º-315º	24
E-shape	20	Right, center	Locations 1, 2, 3, and 4	8

4.5.2 Alumina powder data

An alumina powder (Sandia National Laboratories, Albuquerque, NM) was used as the second test material. Figure 4.25 shows micrographs of the alumina powder. Being a dense white powder with mild ammoniacal odor, the alumina powder consisted of aluminum oxide (non-fibrous forms) (85-95% by weight), silica (1-5% by weight), magnesium hydroxide (1-5% by weight), and calcium carbonate (1-5% by weight). It was stable under ambient conditions. Its particle density and bulk density were 3.33 and 0.83 g/cm^3, respectively. The granule size distribution is shown in Figure 4.26. The median size (d_{50}) was 87 μm, obtained by using Malvern Mastersizer S (Malvern Instruments Ltd., UK), a single lens laser diffraction system using a small helium neon laser of the order of 2 milliwatts power to measure particle size.

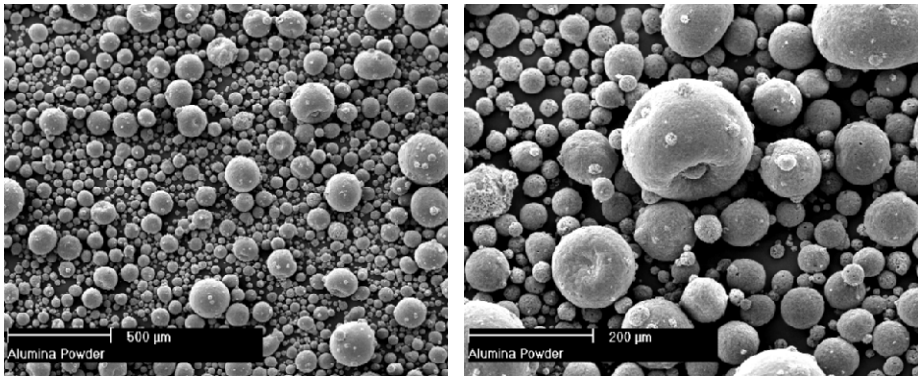

Figure 4.25 Micrographs of the alumina powder

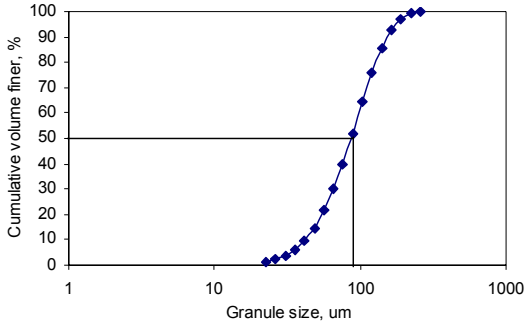

Figure 4.26 Granule size distribution of the alumina powder

Cylindrical, toroidal, and E-shaped dies were tested with the alumina powder, and feed shoe speeds used were 20, 100, and 200 mm/s for the first two die shapes, and only 20 mm/s for

the E-shaped dies because of limited time and resources. The high shoe speed of 200 mm/s, instead of 500 mm/s, was selected because the cylindrical die was not completely filled at speeds above 250 mm/s. Mass deposition profiles were collected from the right and the center dies (Figure 4.16, Figure 4.17, and Figure 4.18), with the pressure sensor strip located at four different orientations or locations for each die (Figure 4.19, Figure 4.20, and Figure 4.21). Table 4.5 shows test combinations for the alumina powder. Each test combination or treatment was repeated six times to obtain a mean value with coefficient of variation less than 20%.

Table 4.5 Test combinations for the alumina powder

Die shape	Feed shoe speed, mm/s	Tested dies	Test locations	# of treatments
Cylinder	20, 100, 200	Right, center	0º-180º, 45º-225º, 90º-270º, 135º-315º	24
Toroid	20, 100, 200	Right, center	0º-180º, 45º-225º, 90º-270º, 135º-315º	24
E-shape	20	Right, center	Locations 1, 2, 3, and 4	8

4.6 Factors Influencing Die Filling in This Research

In sections 2.1 and 2.3.1, factors that were reported or assumed to influence die filling and particle packing are discussed. Some of the factors were not applicable for this research, such as hopper size, number of additional filling cycles, and vibratory compaction. Some other factors were related to this research, but they were kept as constants or unchanged, such as powder level in the feed shoe. Feed shoe angle was also supposed to be a factor influencing die filling. However, only the angle of 45° was used due to limited time and resources for this research. The factors that were relevant and varied in this research were: die geometry and size, die wall effect (for locations within the same die), die configuration and location of the die (with respect to the feed shoe center line and feed shoe movement direction), powder characteristics (particle shape, size, size distribution, bulk density, and flowability), and feed shoe speed.

Feed shoe speed could influence powder deposition in many ways. It could also affect intensity of deposition, velocity of depositing particles, and time for the feed shoe to cover the cavity. It could as well influence the time needed for the powder in dies to release the stress induced by the feed shoe and the friction between particles and the die wall. As the pressure sensor measured the pressure distribution at the bottom of the die, the release of the stress could impact the measured values of the pressure sensor substantially.

Two other factors that can be inferred from above discussion are thickness and rigidity of the feed shoe wall. These factors were kept constant, since the same feed shoe was used throughout all the experiments. However, as these have not been considered by other researchers previously, it is worthwhile to discuss them here. Varying the thickness and rigidity of the feed shoe wall might change the pressure applied to the powder filled in the dies during backward

stroke of the filling process, and also the duration of the pressure. These in turn could compact the filled powder to different extents, and also result in different bulk density distributions.

4.7 Introduction of CT Technology

X-ray computed tomography (CT, XCT or XRCT) is a well-established and accepted technology in the field of nondestructive testing (NDT) or nondestructive evaluation (NDE). It has the advantage of revealing inner structure without the need to cut or destroy the parts. Its main applications include flaw detection and failure analysis (Copley et al., 1994; Obrist et al., 2004).

Computed tomography is distinguished from conventional radiography and radioscopy by the different orientation of the image plane, and by the nature of the data. Figure 4.27 illustrates the common mode of producing an x-ray image. In conventional radiography, the image plane is approximately normal to the x-ray beam, and the image represents total x-ray attenuation through the object. The three-dimension volume of an object is compressed, along the direction of the x-ray, to a two-dimensional image. Fundamental limitations of conventional radiograph are superposition and conspicuity due to overlapping structures (Copley et al., 1994; Jiang, 2003).

The CT method creates a digital representation of a thin slice parallel to the x-ray beam travelling through the object with no interference from adjacent planes (Figure 4.28). Because of this, CT systems require a computing procedure to calculate, locate, and display the point-by-point relative attenuation of the energy beam passing through the object. The image is reconstructed from multiple x-ray views through the object at different angles by rotating the object. The image is stored as a matrix of numbers representing local x-ray attenuation for the small volume elements (voxels) that make up the slice (Figure 4.29). The object is moved vertically and another scan performed to acquire the data for other CT planes (Copley et al., 1994; Martz et al., 2002; Obrist et al., 2004).

The intensity (I) of the photon flux (i.e., the number of photons per second per unit area) is reduced when passing through a material by scattering and photoelectric absorption. The attenuation in the intensity of a single-energy x-ray beam passing through a small length (dL) of material is described by

$$\frac{dI}{I} = -\mu dL \tag{4.1}$$

which defines the linear attenuation coefficient (μ). Integrating the above equation over a length of uniform material gives

$$I = I_0 e^{-\mu L} \tag{4.2}$$

where I_0 is the initial intensity (Copley et al., 1994).

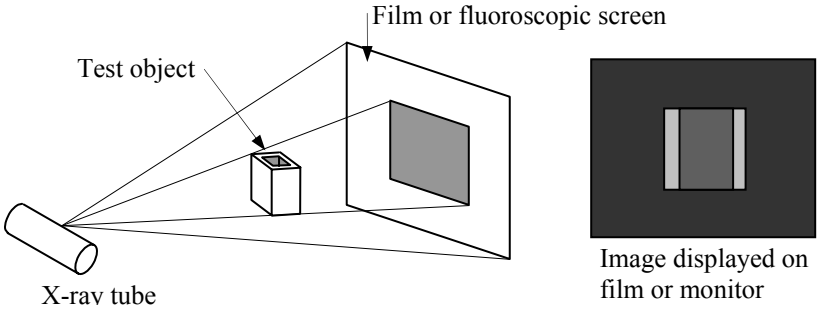

Figure 4.27 A conventional radiograph is formed by projecting an x-ray shadow image onto a plane normal to the x-ray beam (Copley et al., 1994)

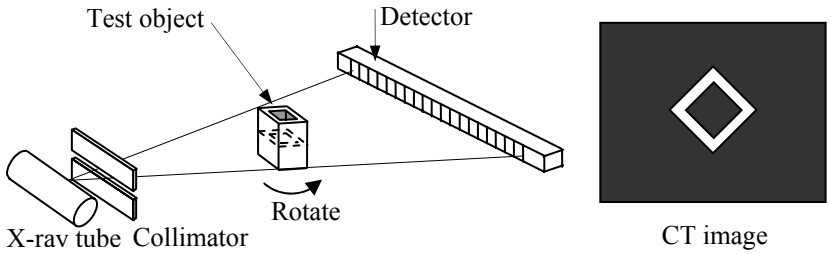

Figure 4.28 Computed tomography forms images of a cross-sectional slice parallel to a collimated x-ray fan beam (Copley et al., 1994)

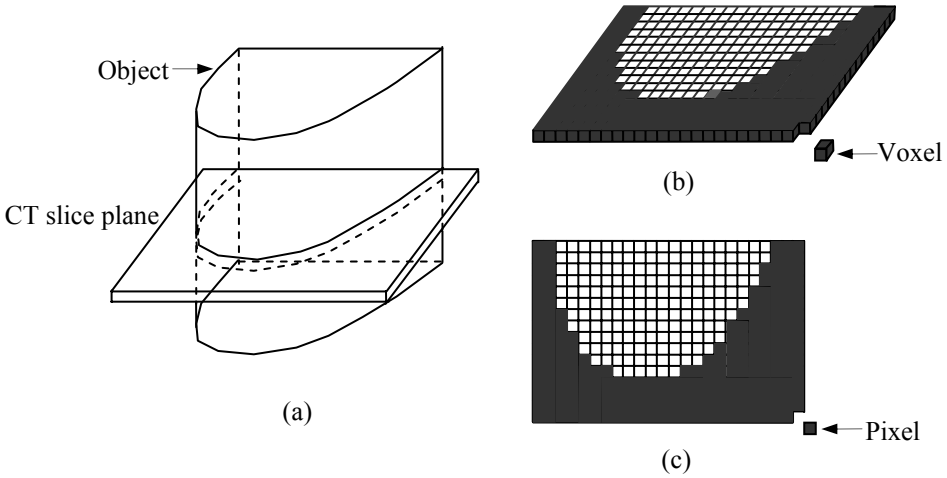

Figure 4.29 (a) A CT image represents a thin slice plane within the object; (b) The slice plane is represented as consisting of a large number of voxels; (c) The CT image consists of pixels with shading that represent the local x-ray attenuation in the corresponding voxel (Copley et al., 1994)

Film radiographs are images of the transmitted intensity, which is represented as darkness or density of the image, and which depends on the integrated value of μ along the particular path

through the object. The CT reconstruction separates out and images either the local values of μ or CT numbers related to μ (Copley et al., 1994).

The value of μ increases with material atomic number and density. It is also a function of x-ray energy. In the range where most CT is performed, x-rays with shorter wavelength (higher photo energy) are more penetrating. The selection of the x-ray energy for a particular application is usually a trade-off between good penetration (favoring high energy) and high contrast (favoring low energy) (Copley et al., 1994).

Standard CT techniques cannot separate out the effects of material density and composition. But if the composition is known and constant, density can be determined by establishing a calibration of CT number versus density, using samples of the same composition with a range of densities (Copley et al., 1994).

The digital data are usually displayed as a gray-scale image, in which high values of x-ray attenuation are represented as lighter shades. The smallest area represented on the image is one pixel, so the resolution of the image is limited by the pixel size (Copley et al., 1994).

A typical industrial CT system comprises an x-ray source, a detector, a part manipulator to rotate and move the test object relative to the source and detector, a computer system to perform the reconstruction calculations, a display to view the results, and data storage media. Typical slice thickness for industrial CT is from 0.025 to 3 mm, with pixel sizes in the range of 0.025 to 1 mm (Copley et al., 1994).

4.8 Data Collection with CT Scanner

4.8.1 Introduction of the CT scanner

The x-ray CT facility, an industrially based OMNI-X Imager, is located in the Center for Quantitative Imaging, Energy Institute, Penn State University. There were two SUN systems supporting this imaging facility for reconstruction calculation, results display, and data storage. One was a SUN Enterprise 6500 with thirty CPUs and a large storage array of 28 GB for processing and archiving. The other was a SUN Ultra 60 high-end visualization system.

The OMNI-X Industrial system had twin x-ray sources and one detector, allowing use of one source at a time. The system was mounted on a heavy optical grade table and could be rotated between the horizontal and vertical positions. The machine produced an array format of *1024×1024×number of slices*. The maximum spatial resolution of the system is 5-10 μm in 3-D. The scanner could acquire a single 2-D slice in one rotation, or up to 100 slices in one rotation.

An estimate of resolution of any given sample was 1/1000 of its diameter. Table 4.6 shows some specifications of the CT imager. Figure 4.30 is a photo of the OMNI-X Imager.

Table 4.6 Specifications of OMNI-X Imager

Parameters	Values
Large focal source	320 kV
Micro focal source	225 kV
Maximum current	5 mA
Maximum diameter	200 mm
Maximum length	1000 mm
Base resolution	1/1000 of diameter
Maximum resolution	0.005 mm
Orientation	Horizontal to vertical
Maximum weight	150 kg

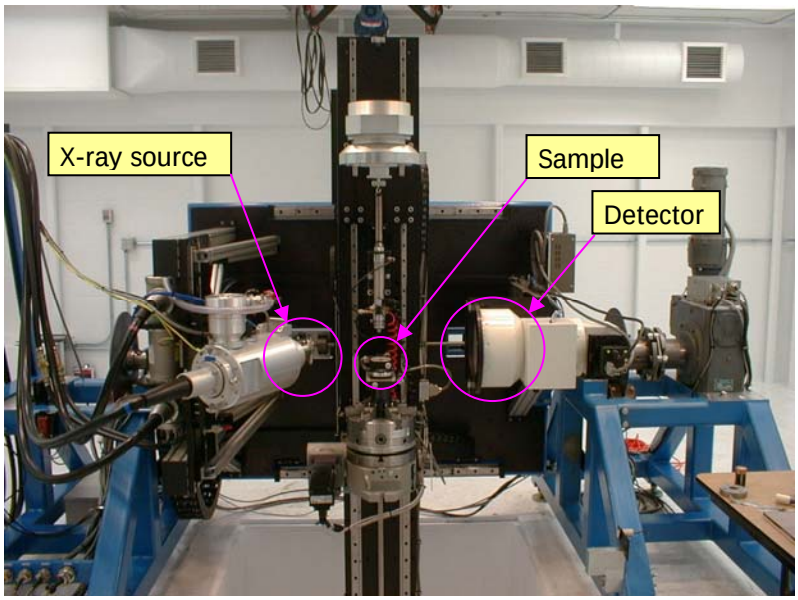

Figure 4.30 Photograph of the OMNI-X Imager

4.8.2 Selected cases for CT test

Table 4.7 shows the selected cases for CT tests. Due to cost and time considerations, E-shaped dies were not tested. In order to correlate the CT data to the PDT-II data, the same feed shoe speeds for PDT-II tests were used for CT scanning. According to the PDT-II data, there was no significant difference between die filling at 20 and 100 mm/s feed shoe speeds. So the feed shoe speed of 100 mm/s was not included. Feed shoe speeds of 20, 200 (only for the alumina powder), and 500 mm/s (only for the battery powder mixture) were used. There were eight different combinations and two replicates for each combination. Totally, sixteen tests were conducted by using the CT scanner.

Table 4.7 Selected cases for CT test

Test powders	Die shapes	Feed shoe speeds, mm/s	Tested dies	Number of treatments
Battery powder mixture	Cylinder	20	R, C, L*	2
		500	R, C, L	2
	Toroid	20	R, C, L	2
		500	R, C, L	2
Alumina	Cylinder	20	R, C, L	2
		200	R, C, L	2
	Toroid	20	R, C, L	2
		200	R, C, L	2

* R, C, and L represent the right, center, and left dies, respectively.

To collect data using CT scanner, the PDT-II was moved next to the x-ray CT facility. After filling the dies with PDT-II, the filled dies were moved slowly and carefully to the CT scanner for data collection.

4.8.3 Modification to die plates for CT test

The dies for tests using PDT-II were open-ended and not suitable for CT experiments, since the filled die plates were to be carried from PDT-II to the CT imager. Two bottom plates of the same shape and size of the die plates were made of gray PVC with thickness of 6.35 mm. They were glued to the bottom of the cylindrical and toroidal die plates. A gap of 0.23 mm was maintained between the bottom plate and dies to be consistent with PDT-II die fill experiments.

In order to make it easier to handle and carry the die plates, two holes were drilled and tapped in the cylindrical and toroidal die plates, separately (Figure 4.31 and Figure 4.32). Two machine screws of gray PVC were inserted to level the tapped holes with die surface during filling. Additionally, they served as holders for handling the filled dies when moving from PDT-II to CT scanner. The two holes were drilled to different depth to mark the orientation of the die plate and the relative locations of the three dies during the CT scanning process.

4.8.4 CT experiments

Before the CT experiments, PDT-II, including the computer to operate the linear actuator, was disassembled and transported into the same room as the CT system. There the device was reassembled and set up for CT tests.

For all the cases listed in Table 4.7, the dies were first filled using PDT-II at their required feed shoe speeds and at acceleration rate of 0.2g or 1.96 m/s^2. Then the two screws in the die plate were slowly rotated up by about 60% of its length. By using the screws as handles, the die plate, filled with powder, was carefully lifted up from the cavity of the feed shoe table. Then

the die plate was carried gently to the CT imager, and placed on the platform for the test object. The total moving distance was about four meters. Generally, no visible disturbance of the powder in the dies was observed for all of the tests.

The dimensions of each voxel of CT image were: $\Delta x = \Delta y = 0.1$ mm, and $\Delta z = 0.125$ mm. It took about 40 minutes for a die plate with three filled dies to be scanned. After scanning, the die plate, with filled powder, was weighed using a balance of 0.01 gram accuracy. Then the die plate was removed from the balance, and one of the three dies was vacuumed carefully by covering the other two dies with paper. The die plate, with only two dies filled with powder, was weighed again. This step was repeated till the powder mass of each of the three dies was obtained. Then the die plate was placed back into PDT-II, and the next die filling and scanning process was conducted.

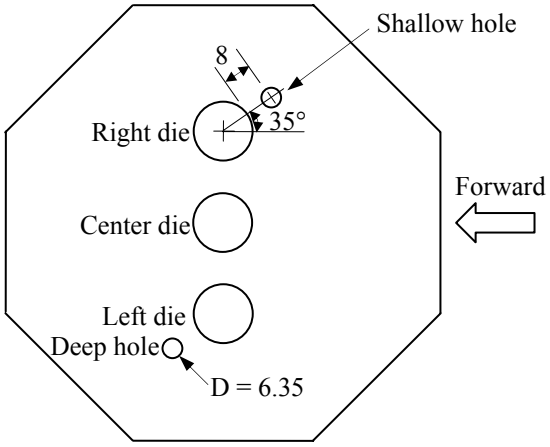

Figure 4.31 Modification to cylindrical die plate for CT test (unit: mm)

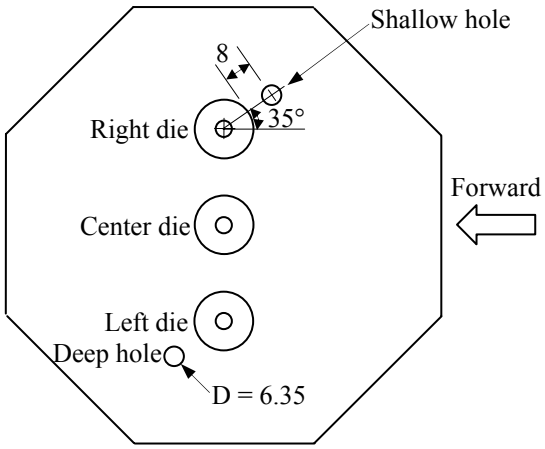

Figure 4.32 Modification to toroidal die plate for CT test (unit: mm)

CHAPTER 5 RESULTS OF PDT-II USING BATTERY POWDER MIXTURE

5.1 Cylindrical Dies

Multiple cylindrical die configuration and dimensions and the dimension of the feed shoe are shown in Figure 5.1. The feed shoe (158.7 mm I. D. inclined at 45°) cross-section in contact with the feed shoe table was an ellipse. In this study, the movement direction of the feed shoe was parallel to the long axis of the ellipse. The three parallel cylindrical dies were configured symmetrical about the long axis of the ellipse.

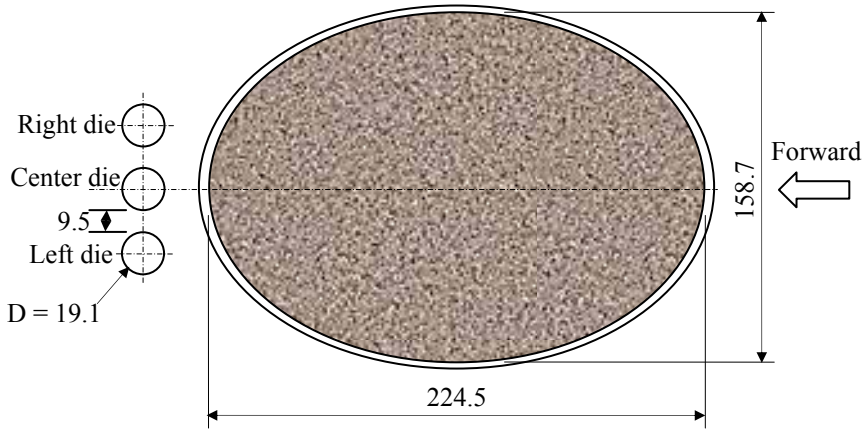

Figure 5.1 Dimensions of the cylindrical dies and the feed shoe cross-section in contact with the table surface (drawn to scale) (unit: mm)

5.1.1 Within-die comparison of the center die

In this section, data collected within each die are analyzed and compared to assess uniformity of powder deposition. Prorated final pressure ratios of the center die in 0°-180°, 45°-225°, 90°-270°, and 135°-315° orientations and 20, 100, and 500 mm/s feed shoe speeds are discussed separately. Subsequently, contour plots obtained based on the data of all the four orientations are presented and discussed.

5.1.1.1 Data prorating

Ideally, all the final pressure values collected in different replicates of a certain treatment at a given location should be identical. However, because of unavoidable experimental variations and the nature of powder behavior there was scatter of final pressure values. To minimize the

scatter, all measured pressure values may be corrected to take into account the scatter in the experiments. This statistical procedure is called prorating.

For all three cylindrical dies, the geometrical center region of the die was the common zone covered by the pressure sensor strip in all of the four orientations. Accordingly, the pressure value of the sensor element at the center location was used to obtain the prorated pressure values of all the sensor elements at different radial locations in the same orientation. The equation to prorate pressure values is shown below:

$$P_p(r) = \frac{P(r)}{P_c} \tag{5.1}$$

where *P(r)* is measured pressure value obtained by any sensor element at any location (r) with the pressure sensor strip in a certain orientation (θ fixed), P_c is the measured pressure value obtained by the sensor element at the center of the cylindrical die (r = 0) in the same test, and P_p is the prorated pressure value (or prorated pressure ratio) in this test at that location (r).

For example, when the pressure sensor strip was in the orientation of 0°-180° in a cylindrical die, nine final pressure values were obtained for nine locations with the nine sensor elements exposed to powder deposited in the die. The middle one of the nine sensor elements was at the center location. The measured final pressure values of the nine sensor elements were divided by the measured final pressure value of the center sensor element, and the results obtained were prorated final pressure values of the nine sensor elements. In the following sections, except when specified, the pressure values for cylindrical dies are all prorated pressure values.

As mentioned earlier in Chapter 4, each element of the pressure sensor strip was 1.9 mm × 5 mm. The pressure value obtained from any sensor element is the total pressure of powder above this rectangular area. By assigning the pressure value obtained by the entire sensor element to the center point of this rectangular area, an assumption was made that the pressure distribution within this area was uniform (or the pressure at the center point represented the average of the pressure across the area). Also, there was no need to divide the pressure value of any sensor element by the area of the sensor element to get the density of pressure at a point, since all the sensor elements had the same area.

For data prorating, there are at least two approaches. One approach was discussed above. The other approach takes the average of pressure values of six replicates at the center location, and uses this value to divide the pressure values of all the sensor elements of each replicate, respectively. Two major reasons led to the selection of the former. First, the major concern here was to compare the relative pressure distribution of the same orientation, which could be better

demonstrated by using the first way of prorating. Second, variations among different replicates were large that, otherwise, tended to mask the difference among different locations within the same orientation.

5.1.1.2 Statistical analysis

In order to study if different locations received different amount of filled powder, pairwise comparison, where two means of final pressure values of two locations at a time are being compared, can be used. The null hypothesis for these tests was that the two means are equal, i.e., H_0: $\mu_i = \mu_j$, where i, j start from 1 to the number of locations to be compared, and $i \neq j$. The alternative hypothesis was that the two means are not equal, i.e., H_0: $\mu_i \neq \mu_j$. These pairwise comparisons may be accomplished by using multiple comparison procedures. A large number of these procedures are available, such as Tukey's test, Fisher's least significant difference method, Bonferroni procedure, and Duncan's multiple range test (Montgomery, 2005).

A simple and effective method is Bonferroni procedure (or Bonferroni adjustment). If one's objective is to keep the experimentwise error rate to a specified level (usually $\alpha = 0.05$), a straightforward approach is to divide the acceptable α-level by the number of comparisons. Let N_{pc} denote number of pairwise comparisons to be made. If $N_{pc} = 10$ and if the overall experimentwise error rate is to be maintained at 5%, then one can evaluate each of the pairwise comparisons against 0.05 divided by 10. That is, for any one comparison to be considered significant, the obtained P-value would have to be less than 0.005 – and not 0.05. This procedure is called Bonferroni procedure (or Bonferroni adjustment). This obviously makes it harder to claim a significant result and in so doing decreases the chance of making a Type I error to very acceptable levels (Schiff and D'Agostino, 1996). In fact, some authors (e.g., Jaccard and Wan, 1996) pointed out that this method of controlling type I error becomes very conservative, perhaps too conservative, when the number of comparisons grows large. It is relatively more likely to miss an effect that is actually there.

Type I error is the error of rejecting the null hypothesis when the null hypothesis is true. The second kind of error is Type II error, which is accepting the null hypothesis when the null hypothesis is false. The probability of making a type I error is the level of significance, i.e., α (Schiff and D'Agostino, 1996).

An alternative way of using Bonferroni adjustment is to multiply the obtained P-values by the number of pairwise comparisons, i.e., N_{pc}. Then the multiplied P-values are compared with the acceptable α-level (0.05). Actually, this is the same as comparing the originally obtained P-values with the result of the acceptable α-level divided by the number of comparisons.

Jaccard and Wan (1996) suggested the use of a modified Bonferroni procedure. It is more powerful than traditional Bonferroni method but adequately maintains experimentwise error rates at the desired α-level (usually 0.05). It is applied as follows. Rank P-values obtained from multiple comparisons from smallest to largest. Tied P-values may be ordered arbitrarily. The largest difference (which has the smallest P-value) is evaluated based on an α of $0.05/ N_{pc}$, where N_{pc} denotes number of pairwise comparisons, just as in the Bonferroni procedure discussed above. If this leads to rejection of the null hypothesis, then the next largest difference is tested against $0.05/(N_{pc}-1)$, where $(N_{pc}-1)$ is the remaining number of comparisons. If this test leads to null hypothesis rejection, then the next largest difference is tested against an α level of $0.05/(N_{pc}-2)$ and so on, until a nonsignificant difference is observed.

Bonferroni procedure and modified Bonferroni procedure were used here to conduct statistical analysis. The major reason for using Bonferroni procedure and modified Bonferroni procedure is that these can be easily combined with paired *t*-test, which was also used in data analysis. Paired *t*-test is known to minimize the heterogeneousness or large scatter of final pressure values among different replicates of a treatment and reveal the difference that might not be detected by other statistical methods, such as Tukey's Test. For example, each of the six final pressure values of all the replicates at a location was lower than that of the other locations in the same replicate. But these might be not significantly different ($P > 0.05$) if multiple comparison analysis was conducted by using one-way ANOVA (Tukey's Honest Significant Difference (HSD) method). However, paired *t*-test demonstrated that they were significantly different ($P < 0.05$).

The statistical analysis was carried out in the following steps. First, paired t-test was conducted separately for all of the N_{pc} pairwise comparisons. N_{pc} was equal to $N_{loc}(N_{loc}-1)/2$, where N_{loc} was the number of locations to be compared. Second, the obtained P-values were multiplied by the number of pairwise comparisons, i.e., N_{pc}. Then, modified Bonferroni procedure was performed to the multiplied P-values of the second step. To do this, the multiplied P-values of the second step were ranked from smallest to largest. The largest difference (which has the smallest P-value) was kept unchanged. If this P-value was smaller than 0.05 and led to rejection of the null hypothesis, then the P-value of the next largest difference was multiplied by $(N_{pc}-1)/ N_{pc}$. If this P-value led to null hypothesis rejection, then the P-value of the next largest difference was multiplied by $(N_{pc}-2)/ N_{pc}$ and so on, until a nonsignificant difference was observed. The P-values modified after these three steps were compared with the acceptable α-level (0.05) to decide if significant differences exist among final pressure values of different locations.

5.1.1.3 0°-180° orientation

20 mm/s feed shoe speed: Table 5.1 shows the prorated final pressure ratios in the 0°-180° orientation of the center cylindrical die filled at feed shoe speed of 20 mm/s. Locations of each sensor element are represented by their radial distance from the center of the die and the orientations of the pressure sensor strip, in the format of (radial distance in mm, orientation in degrees), such as (6, 0°). The location of the center is (0, 0°). Figure 5.2 shows the prorated mean final pressure ratios with respect to radial distance. Because locations (8, 180°) and (8, 0°) were next to the die wall, the wall friction was expected to play an important role. Since the contribution of wall friction was not known, pressure values obtained at these locations are not included in the following discussion, especially in statistical analysis. The locations right next to the die wall in other orientations, i.e., 45°-225°, 90°-270°, and 135°-315°, are not included in discussion below, either. Another reason for not including these locations was that fine particles might get into the gap (0.23 mm) between the die plate and the pressure sensor. This made the die plate and even the feed shoe above the die plate also contribute to the pressure values collected by the pressure sensor at locations close of the die wall.

Table 5.1 Prorated final pressure ratios in 0°-180° orientation of the center cylindrical die filled at feed shoe speed of 20 mm/s

Orientation	180°				Center	0°			
Radius, mm	8	6	4	2	0	2	4	6	8
Run #1	0.21	0.68	0.85	0.81	1.00	1.54	1.02	1.02	1.24
Run #2	0.67	1.09	0.89	1.03	1.00	1.54	1.48	1.53	1.42
Run #3	0.42	0.54	0.56	0.91	1.00	0.78	1.01	1.10	0.68
Run #4	0.49	0.60	0.66	0.70	1.00	1.23	1.32	1.49	0.72
Run #5	0.32	0.46	0.55	0.66	1.00	0.89	1.43	1.35	1.10
Run #6	0.39	0.62	0.72	0.76	1.00	1.22	1.00	1.10	1.07
Mean	0.42	0.67	0.71	0.81	1.00	1.20	1.21	1.26	1.04
StDev	0.16	0.22	0.14	0.14	–	0.32	0.23	0.22	0.29
COV	37.4	33.0	20.1	17.0	–	26.5	18.7	17.5	27.8

All of the locations in 0° orientation and the center location had higher final pressure ratios than locations in 180° orientation (Figure 5.2). Table 5.2 shows the P-values of two-tailed paired *t*-tests obtained after modified Bonferroni procedure. As shown in Figure 5.2 and Table 5.2, final pressure ratio of locations (2, 0°) was significantly ($P < 0.05$) higher than those of locations (4, 180°) and (6, 180°). At location (6, 0°), the final pressure ratio was significantly higher ($P < 0.05$) than that of location (6, 180°). The possible reasons for the final pressure ratios of 0° orientation to be higher than those of 180° orientation are discussed in section 5.1.1.7.

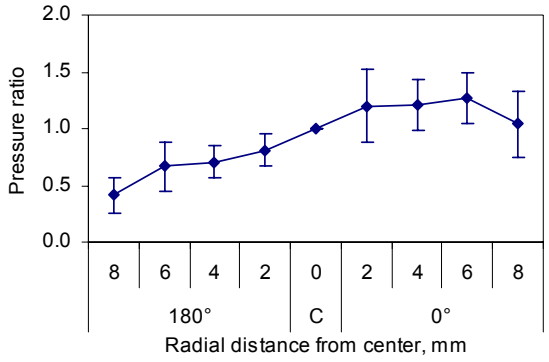

Figure 5.2 Prorated average final pressure ratios in **0°-180°** orientation of the center cylindrical die filled at feed shoe speed of **20 mm/s**

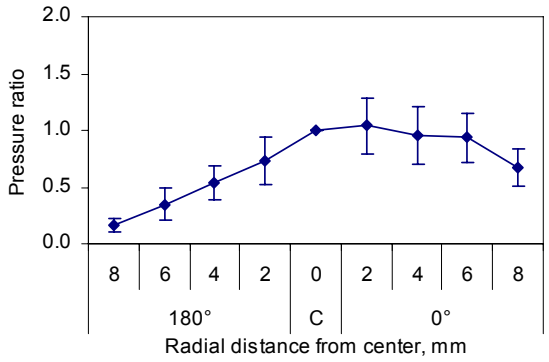

Figure 5.3 Prorated average final pressure ratios in **0°-180°** orientation of the center cylindrical die filled at feed shoe speed of **100 mm/s**

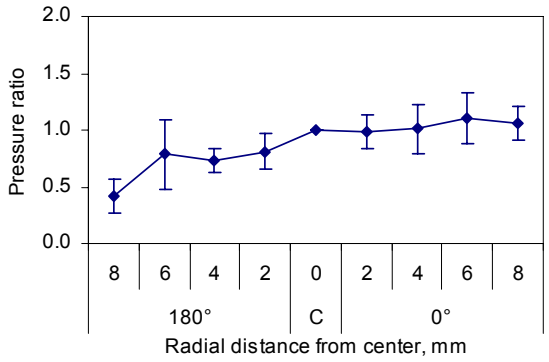

Figure 5.4 Prorated average final pressure ratios in **0°-180°** orientation of the center cylindrical die filled at feed shoe speed of **500 mm/s**

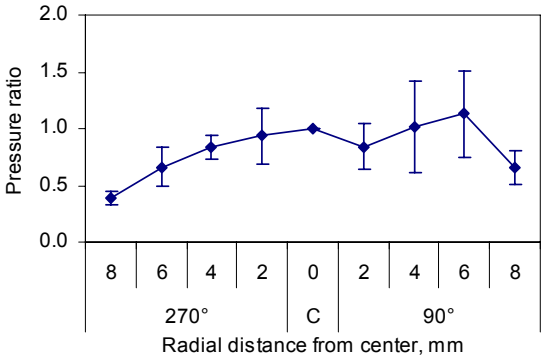

Figure 5.5 Prorated average final pressure ratios in **90°-270°** orientation of the center cylindrical die filled at feed shoe speed of **20 mm/s**

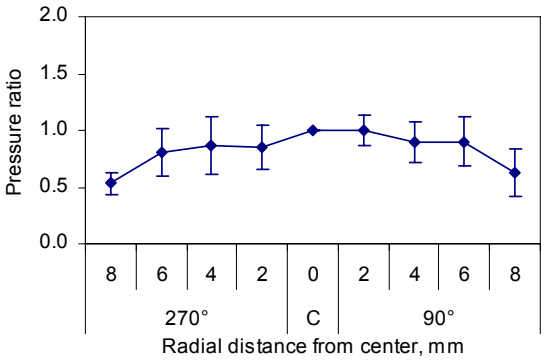

Figure 5.6 Prorated average final pressure ratios in **90°-270°** orientation of the center cylindrical die filled at feed shoe speed of **100 mm/s**

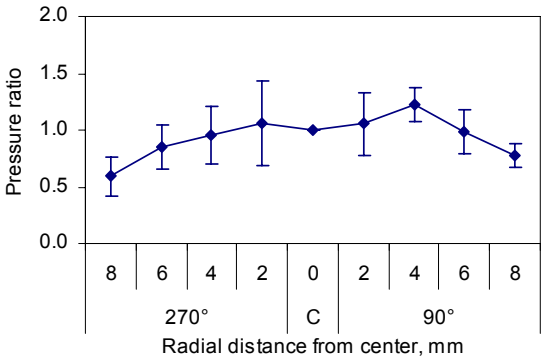

Figure 5.7 Prorated average final pressure ratios in **90°-270°** orientation of the center cylindrical die filled at feed shoe speed of **500 mm/s**

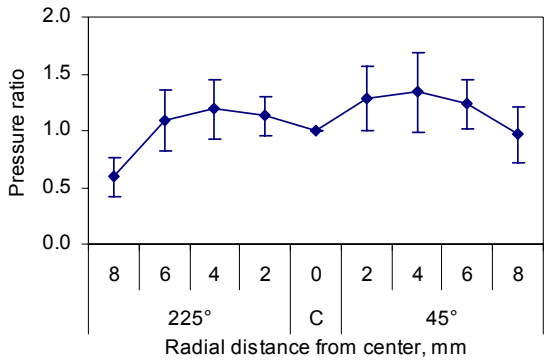

Figure 5.8 Prorated average final pressure ratios in **45°-225°** orientation of the center cylindrical die filled at feed shoe speed of **20 mm/s**

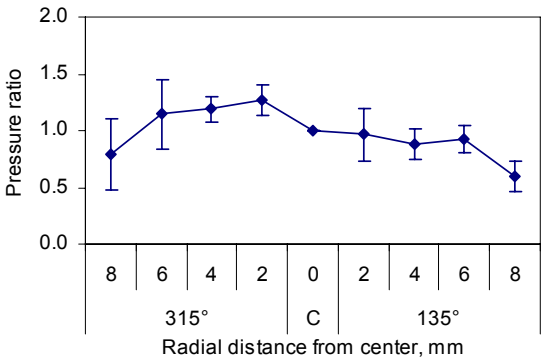

Figure 5.11 Prorated average final pressure ratios in **135°-315°** orientation of the center cylindrical die filled at feed shoe speed of **20 mm/s**

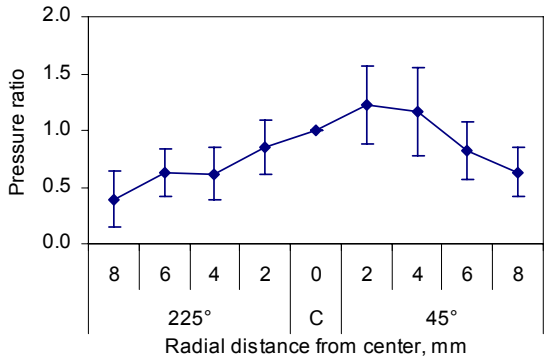

Figure 5.9 Prorated average final pressure ratios in **45°-225°** orientation of the center cylindrical die filled at feed shoe speed of **100 mm/s**

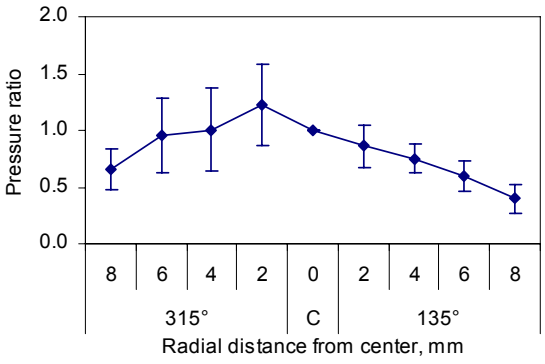

Figure 5.12 Prorated average final pressure ratios in **135°-315°** orientation of the center cylindrical die filled at feed shoe speed of **100 mm/s**

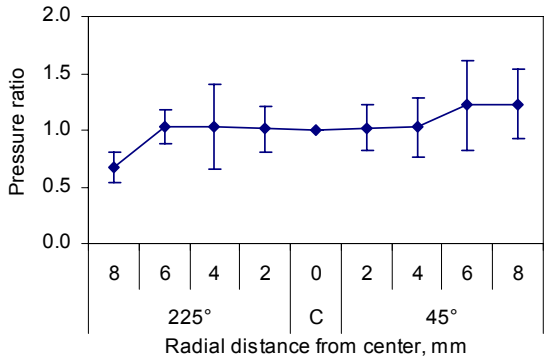

Figure 5.10 Prorated average final pressure ratios in **45°-225°** orientation of the center cylindrical die filled at feed shoe speed of **500 mm/s**

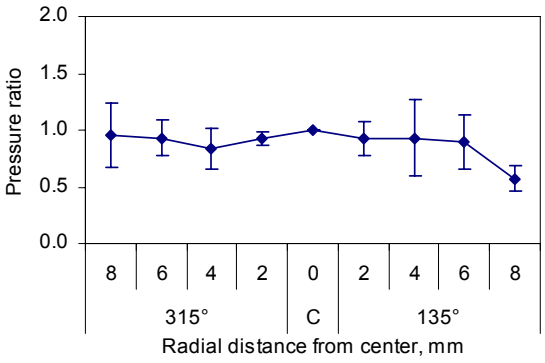

Figure 5.13 Prorated average final pressure ratios in **135°-315°** orientation of the center cylindrical die filled at feed shoe speed of **500 mm/s**

Table 5.2 P-values of paired t-test after modified Bonferroni procedure for prorated final pressure ratios in 0°-180° orientation of the center cylindrical die filled at feed shoe speed of 20 mm/s

	Orientation	180°				Center	0°			
	Radius, mm	8	6	4	2	0	2	4	6	8
180°	8	–	–	–	–	–	–	–	–	–
	6	–	–							–
	4	–	9.848							–
	2	–	1.026	2.165						–
Center	0	–	0.283	0.079	0.440					–
0°	2	–	**0.030**	**0.026**	0.520	3.909				–
	4	–	0.065	0.109	0.300	1.541	20.043			–
	6	–	**0.029**	0.053	0.149	0.691	14.122	3.644	–	–
	8	–	–	–	–	–	–	–	–	–

*Entries in bold are significantly different ($P < 0.05$)

100 mm/s feed shoe speed: Figure 5.3 shows the prorated final pressure ratios of 0°-180° orientation collected at feed shoe speed of 100 mm/s. The center location and most of the locations in 0° orientation had higher mean final pressure ratios than locations in 180° orientation. Statistical analysis indicated that final pressure ratio of location (6, 180°) was significantly lower than those of the center, locations in 0° orientation, and locations (2, 180°) and (4, 180°) ($P < 0.05$) (Table A.4 in Appendix B). Pressure ratio of location (4, 180°) was significantly ($P < 0.05$) lower than those of the center and location (2, 180°). Within 180° orientation, final pressure ratios decreased monotonically with increasing radii.

500 mm/s feed shoe speed: Figure 5.4 was plotted based on the prorated final pressure ratios of 0°-180° orientation collected at feed shoe speed of 500 mm/s. Mean final pressure ratios of 180° orientation were lower than those of 0° orientation, but there was no significant difference (Table A.6 in Appendix B). Only final pressure ratio of location (4, 180°) was significantly lower than that of the center location ($P < 0.05$). This was different from results of the same locations at feed shoe speeds of 20 and 100 mm/s. Causes behind this difference are discussed in section 5.1.1.7.

5.1.1.4 90°-270° orientation

20 mm/s feed shoe speed: Pressure distribution along 90°-270° direction was expected to be symmetrical, but this was not the case for the data collected at feed shoe of 20 mm/s. Figure 5.5 shows that the overall pressure distribution was not quite symmetrical, even though there was no significant difference among pressure ratios of different locations (Table A.8 in Appendix B). This nonsymmetrical distribution might be attributed to the complexity of the flow and deposition process. Sundaresan (2001) pointed out that the method of filling and/or small imperfections in the bins can introduce asymmetries in the stress and packing density, so a seemingly symmetrical

bin can manifest asymmetric flow patterns during discharge. It is conceivable that symmetric discharge may be unstable and give way to asymmetric discharge patterns, with the imperfection providing the necessary kick to cause the destabilization.

100 mm/s feed shoe speed: Pressure distribution along 90°-270° orientation at feed shoe speed of 100 mm/s was quite symmetrical as expected (Figure 5.6). The reason for this symmetry might be the imperfection was smoothed out at this feed shoe speed. The mean final pressure ratios were symmetrical about the center location, with an overall trend of pressure decreasing with increasing radial distance. There was no significant difference among different locations ($P > 0.05$) (Table A.10 in Appendix B).

500 mm/s feed shoe speed: Pressure distribution along 90°-270° orientation at feed shoe speed of 500 mm/s was not as symmetrical as 100 mm/s, with mean pressure ratio of location (4, 90°) higher than those of other locations (Figure 5.7). There was no significant difference observed among different locations ($P > 0.05$) (Table A.12 in Appendix B).

5.1.1.5 45°-225° orientation

20 mm/s feed shoe speed: Figure 5.8 shows the average prorated final pressure ratios of 45°-225° orientation at feed shoe speed of 20 mm/s. The distribution of final pressure ratios was quite different from that of 0°-180° orientation. It was symmetric about the center location, with the mean final pressure ratio at the center being lower than most of other locations. This type of pressure distribution along a certain orientation was not observed in any other orientation or the same orientation at any other feed shoe speeds. Although the reason for this was not entirely clear, this unusual distribution can be attributed to the complexity of the flow and deposition process. Statistical analysis showed no significant differences among final pressure ratios of different locations ($P > 0.05$) (Table A.14 in Appendix B).

100 mm/s feed shoe speed: For 45°-225° orientation at feed shoe speed of 100 mm/s, the general trend was that mean final pressure ratios increased from 225° orientation, the center, to 45° orientation (Figure 5.9). The pressure distribution profile was similar to that of 0°-180° orientation at 100 mm/s feed shoe speed (Figure 5.3). Statistical analysis indicated no significant difference among final pressure ratios of different locations ($P > 0.05$) (Table A.16 in Appendix B), even though the average final pressure ratios of locations (2, 45°) and (4, 45°) were much higher than those of many other locations. The reasons for some of the final pressure ratios of 45° orientation to be higher than those of 225° orientation are discussed in section 5.1.1.7.

500 mm/s feed shoe speed: Figure 5.10 shows the average prorated final pressure ratios of 45°-225° orientation at feed shoe speed of 500 mm/s. Unlike 45°-225° orientation at feed shoe

speed of 100 mm/s, most of the locations had similar final pressure ratios, even though the overall trend was that mean final pressure ratios increased from 225°orientation, the center, to 45° orientation. This is explained in section 5.1.1.7. Statistical analysis verified that there was no significant difference among the locations of this orientation at feed shoe speed of 500 mm/s ($P > 0.05$) (Table A.18 in Appendix B).

5.1.1.6 135°-315° orientation

20 mm/s feed shoe speed: Figure 5.11 shows the average prorated final pressure ratios of 135°-315° orientation at feed shoe speed of 20 mm/s. The overall trend was that mean final pressure ratios increased from 135° orientation, the center, to 315° orientation. The reasons are discussed in section 5.1.1.7. Final pressure ratio of location (2, 315°) was significantly ($P < 0.05$) higher than that of location (6, 135°) (Table A.20 in Appendix B).

100 mm/s feed shoe speed: At feed shoe speed of 100 mm/s, most of the locations of 315° orientation had higher final pressure ratios than locations of 135° orientation (Figure 5.12), but the differences were not significant ($P > 0.05$) (Table A.22 in Appendix B). Only the pressure ratio of the center was significantly higher than that of (6, 135°) ($P < 0.05$). Within 135° orientation, final pressure ratios decreased monotonically with increasing radii, and this trend even passed through the center and reached location (2, 315°) (Figure 5.12).

500 mm/s feed shoe speed: Figure 5.13 shows the average prorated final pressure ratios of 135°-315° orientation at feed shoe speed of 500 mm/s. Unlike at feed shoe speed of 100 mm/s, most of the locations had similar final pressure ratios. This was similar to the pressure distribution of 45°-225° orientation at 500 mm/s feed shoe speed, and it is discussed in section 5.1.1.7. No significant difference was observed among these locations (Table A.24 in Appendix B).

5.1.1.7 Comparison of within-die pressure distribution using contour plots

The previous discussion, based on the four separate orientations of the pressure sensor strip, did not provide the overall pressure distribution within the entire die. In this subsection, contour plots obtained from the prorated final pressure ratios of all the four orientations are used to discuss pressure distribution within the center die. They are presented in the order of the feed shoe speeds, i.e., 20, 100, and 500 mm/s. Some of the observations listed in preceding sections are also explained.

20 mm/s feed shoe speed: Figure 5.14 is contour plot of the center cylindrical die using the prorated final pressure ratios at feed shoe speed of 20 mm/s. Generally the half circle close to the leeward end had higher final pressure ratios than the forward half, except locations along 225°

orientation. The backward stroke of feed shoe movement cycle contributed most to this distribution pattern. As mentioned in Chapter 2, the particles in the die could be divided into three regions according to their behavior during the process of pullback of the feed shoe (Figure 2.5) (Kondoh and Takemoto, 1996). The particles in the top region, rolling region, were dragged by the movement of the feed shoe during the backward stroke, and so they moved horizontally to some distance to the leeward end. The particles in the sliding region slid diagonally (to the direction of the right lower corner) with the movement of the feed shoe. These rolling, dragging, and sliding effects were considered to be especially pronounced for battery powder mixture, since particle size was relatively large (210 – 1000 μm) and particle shape was not spherical.

100 mm/s feed shoe speed: Figure 5.15 shows the distribution of prorated average final pressure ratios in the center cylindrical die at 100 mm/s. Similar to feed shoe speed of 20 mm/s, the overall trend was that the half circle of the leeward end had higher final pressure ratios than the forward half. The highest pressure ratios occurred around the center area in 45° and 315° orientations. The lowest pressure ratios were close to the die wall in 180° orientation.

500 mm/s feed shoe speed: Figure 5.16 shows the distribution of prorated average final pressure ratios in the center cylindrical die filled at feed shoe speed of 500 mm/s. The quarter circle between 0° and 90° orientations had pressure ratios higher than other locations, except some locations in 225° orientation that had somewhat high pressure ratios. The lowest pressure ratios were in 180° orientation. Generally the pressure distribution was different from those of 20 and 100 mm/s feed shoe speeds. The major reason was that at the highest feed shoe speed (500 mm/s) the rolling, dragging, and sliding effects discussed above were not as prominent as at lower feed shoe speeds, since there was less time for particles to rearrange by these mechanisms. These effects could not reach the same depth of the powder in the die when compared with the lower feed shoe speeds.

5.1.1.8 Comparison of uniformity among the three speeds

Table 5.3 shows some statistical parameters obtained for the center cylindrical die at the three feed shoe speeds (20, 100, and 500 mm/s) using the prorated final pressure ratios. Average pressure ratios of the six replicates were first obtained for all the locations of each orientation (except the two end locations close to the die wall). Then these averages of all the orientations were used to generate the Max, Min, and Mean etc. values in Table 5.3. Based on these values, 500 mm/s feed shoe speed, which had the lowest (Max-Min)/Mean, Max/Min, StDev (standard deviation), and COV, led to the most uniform filling among the three speeds. Higher momentum possessed by particles at higher feed shoe speed might contribute to relatively uniform filling by

minimizing arching and allowing particles to locally rearrange themselves. Another possible reason was that higher rate of die filling at 500 mm/s feed shoe speed decreased opportunity for particle segregation and promoted uniform filling, as observed by Lawrence and Beddow (1969).

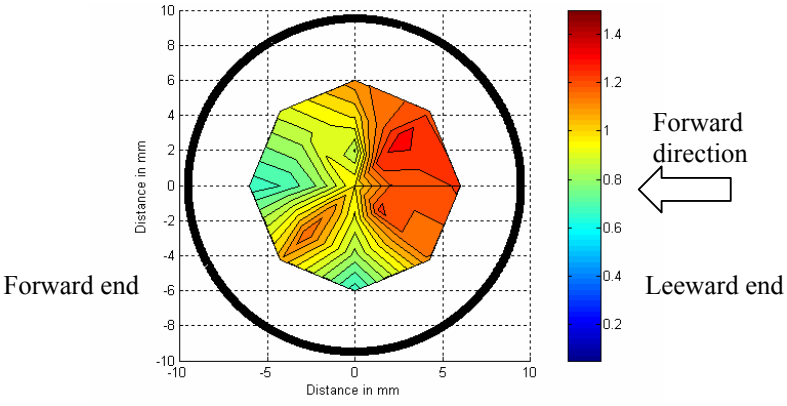

Figure 5.14 Contour plots of the distribution of prorated average final pressure ratios in the center cylindrical die filled at feed shoe speed of 20 mm/s

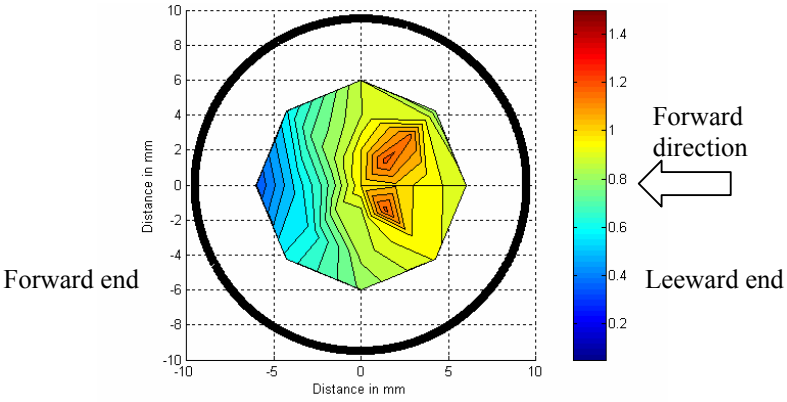

Figure 5.15 Contour plots of the distribution of prorated average final pressure ratios in the center cylindrical die filled at feed shoe speed of 100 mm/s

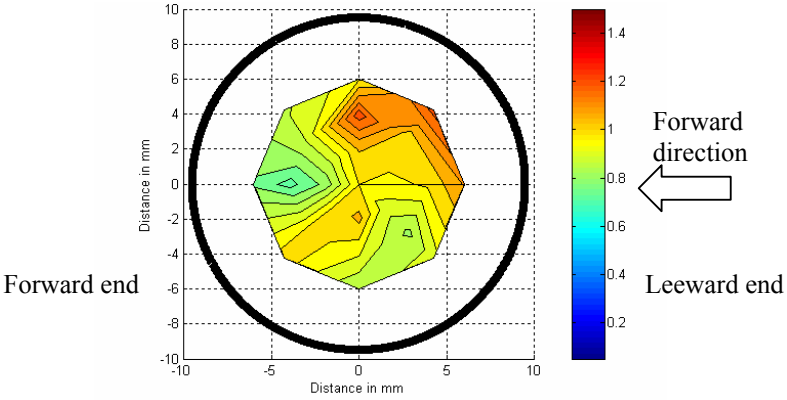

Figure 5.16 Contour plots of the distribution of prorated average final pressure ratios in the center cylindrical die filled at feed shoe speed of 500 mm/s

Table 5.3 Comparison of key statistical parameters for the center cylindrical die at the three feed shoe speeds using prorated final pressure ratios

Feed shoe speed, mm/s	Max	Min	Mean	(Max-Min)/Mean	Max/Min	StDev	COV (StDev×100/Mean)
20	1.34	0.66	1.03	0.65	2.01	0.19	18.7
100	1.22	0.35	0.88	1.00	3.51	0.20	23.1
500	1.23	0.73	0.98	0.51	1.69	0.11	11.6

5.1.2 Within-die comparison of the right die

This section analyzes data of the right cylindrical die and studies within die uniformity. Prorated final pressure ratios of the right die in 0°-180°, 45°-225°, 90°-270°, and 135°-315° orientations and 20, 100, and 500 mm/s feed shoe speeds are discussed. Contour plots of pressure distribution are presented.

5.1.2.1 0°-180° orientation

20 mm/s feed shoe speed: Figure 5.17 shows the average prorated final pressure ratios of the 0°-180° orientation at 20 mm/s. Like the center die, the average final pressure ratios of the right die along 0° orientation and the center were higher than those of the 180° orientation, though none of the differences were significant ($P > 0.05$) (Table A.26 in Appendix B).

100 mm/s feed shoe speed: As shown in Figure 5.18, pressure ratio distribution along 0°-180° orientation at 100 mm/s was somewhat symmetrical. Though some of the locations of 0° orientation had higher mean final pressure ratios than locations of 180° orientation at feed shoe speed of 100 mm/s, no significant difference was observed ($P > 0.05$) (Table A.28 in Appendix B). This was different from the general trend that final pressure ratios of 0° orientation were higher than those of 180° orientation. This demonstrated the complexity of the flow and deposition process. It also indicated that the right die might have different pressure distribution compared with the center die.

500 mm/s feed shoe speed: At feed shoe speed of 500 mm/s, all of the locations of 0° orientation had higher mean final pressure ratios than locations of 180° orientation, as shown in Figure 5.19. No differences were significant ($P > 0.05$) (Table A.30 in Appendix B). The pressure distribution was more uniform than those of 20 and 100 mm/s.

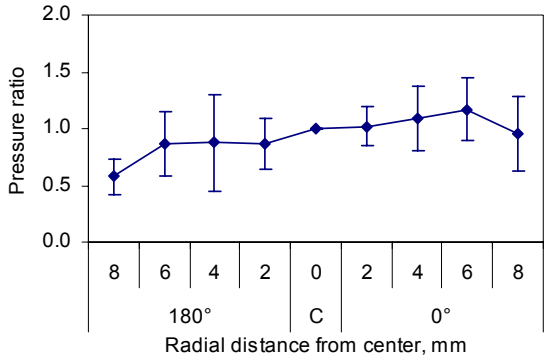

Figure 5.17 Prorated average final pressure ratios in **0°-180°** orientation of the right cylindrical die filled at feed shoe speed of **20 mm/s**

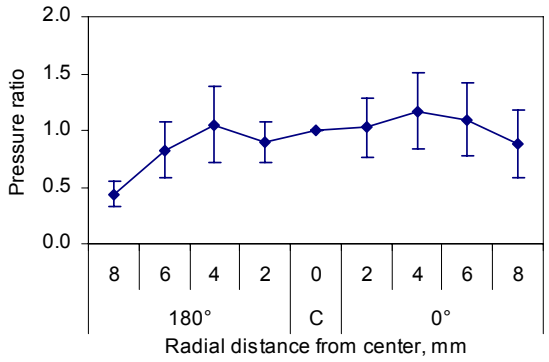

Figure 5.18 Prorated average final pressure ratios in **0°-180°** orientation of the right cylindrical die filled at feed shoe speed of **100 mm/s**

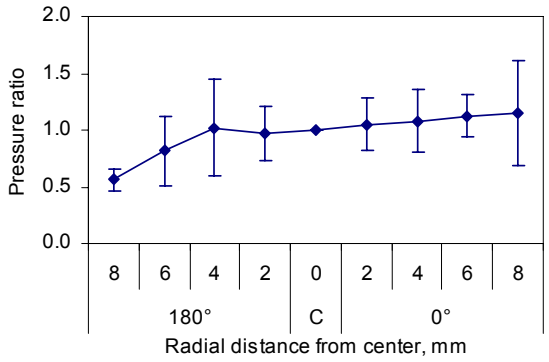

Figure 5.19 Prorated average final pressure ratios in **0°-180°** orientation of the right cylindrical die filled at feed shoe speed of **500 mm/s**

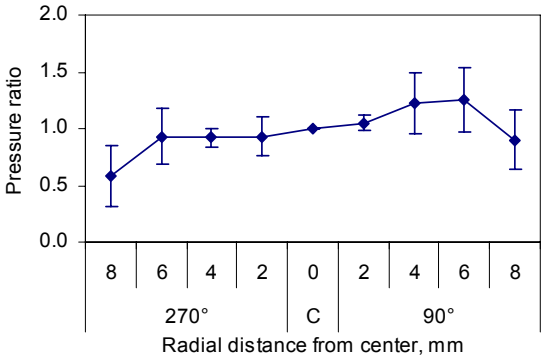

Figure 5.20 Prorated average final pressure ratios in **90°-270°** orientation of the right cylindrical die filled at feed shoe speed of **20 mm/s**

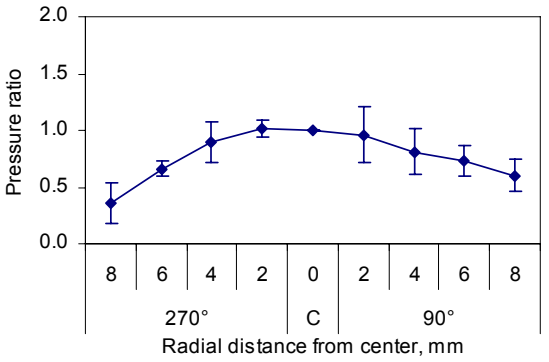

Figure 5.21 Prorated average final pressure ratios in **90°-270°** orientation of the right cylindrical die filled at feed shoe speed of **100 mm/s**

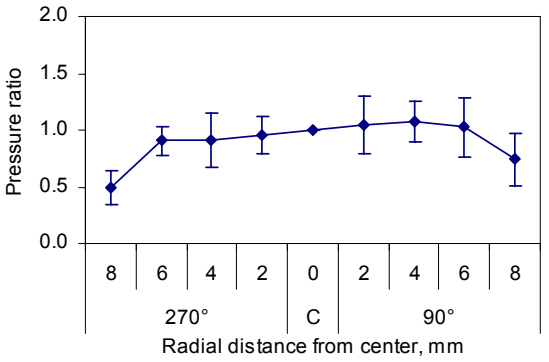

Figure 5.22 Prorated average final pressure ratios in **90°-270°** orientation of the right cylindrical die filled at feed shoe speed of **500 mm/s**

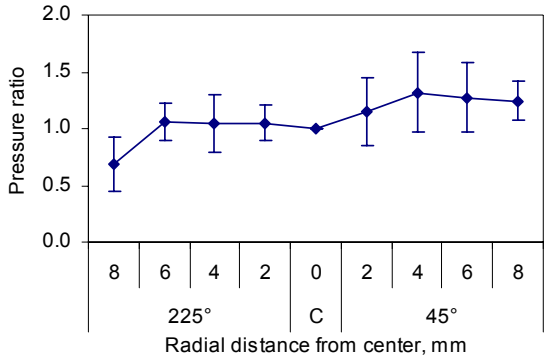

Figure 5.23 Prorated average final pressure ratios in **45°-225°** orientation of the right cylindrical die filled at feed shoe speed of **20 mm/s**

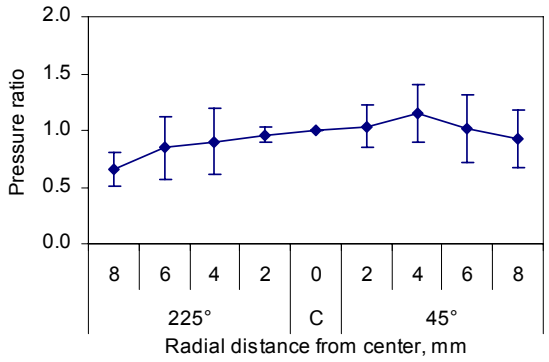

Figure 5.24 Prorated average final pressure ratios in **45°-225°** orientation of the right cylindrical die filled at feed shoe speed of **100 mm/s**

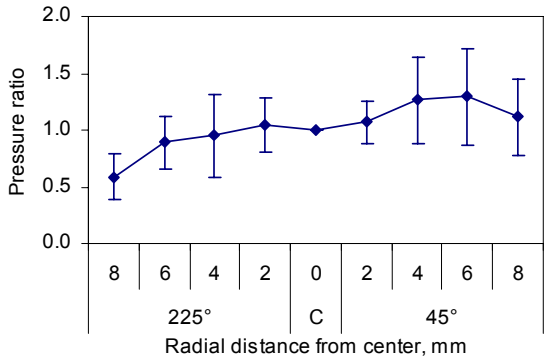

Figure 5.25 Prorated average final pressure ratios in **45°-225°** orientation of the right cylindrical die filled at feed shoe speed of **500 mm/s**

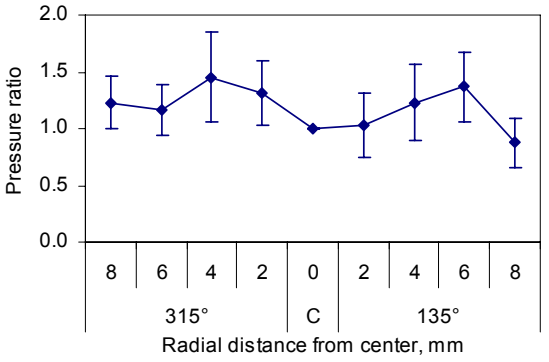

Figure 5.26 Prorated average final pressure ratios in **135°-315°** orientation of the right cylindrical die filled at feed shoe speed of **20 mm/s**

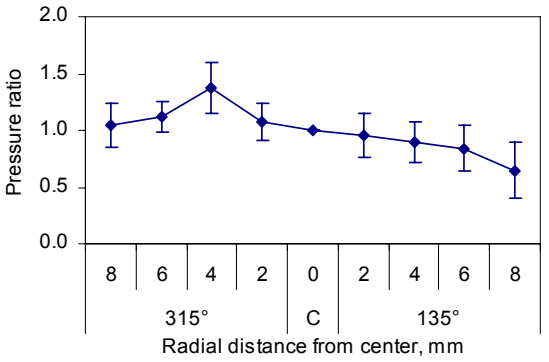

Figure 5.27 Prorated average final pressure ratios in **135°-315°** orientation of the right cylindrical die filled at feed shoe speed of **100 mm/s**

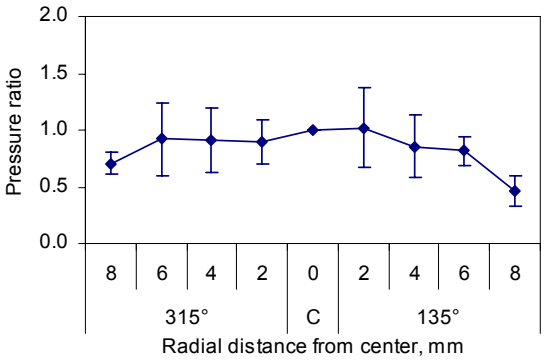

Figure 5.28 Prorated average final pressure ratios in **135°-315°** orientation of the right cylindrical die filled at feed shoe speed of **500 mm/s**

5.1.2.2 90°-270° orientation

20 mm/s feed shoe speed: Figure 5.20 shows the average prorated final pressure ratios of 90°-270° orientation at 20 mm/s feed shoe speed. They were not quite symmetrical about the center. In fact, all of the locations of 90° orientation had higher mean final pressure ratios than locations of 270° orientation, even though there was no significant difference (Table A.32 in Appendix B). Again, this nonsymmetrical distribution could be attributed to the complexity of the flow and deposition process and asymmetrical particle packing in the feed shoe. Another reason could be that 90° orientation of the right die was closer to the right side of the feed shoe wall than 270° orientation.

100 mm/s feed shoe speed: At feed shoe speed of 100 mm/s, the final pressure ratio distribution was quite symmetrical (Figure 5.21). Final pressure ratios of the center and location (2, 270°) were significantly higher than that of location (6, 270°) (Table A.34 in Appendix B).

500 mm/s feed shoe speed: Figure 5.22 shows the prorated average final pressure ratios of 90°-270° orientation at feed shoe speed of 500 mm/s. The final pressure ratio distribution was quite uniform (except the two ratios at both ends) and symmetrical about the center, even though most of the pressure ratios of 90° orientation were slightly higher than those of 270° orientation. No significant differences were observed among these locations (Table A.36 in Appendix B).

5.1.2.3 45°-225° orientation

20 mm/s feed shoe speed: As shown in Figure 5.23, all of the locations of 45° orientation had higher mean final pressure ratios than locations of 225° orientation at feed shoe speed of 20 mm/s. None of the differences were significant ($P > 0.05$) (Table A.38 in Appendix B). This again indicated that the particles in the die might be dragged to the area close to the leeward end (or the feed shoe approach direction in the forward stroke), most probably during the backward stroke.

100 mm/s feed shoe speed: Figure 5.24 shows the average prorated pressure ratios in 45°-225° orientation at 100 mm/s feed shoe speed. Most of the locations of 45° orientation had higher mean final pressure ratios than locations of 225° orientation, even though no differences were significant ($P > 0.05$) (Table A.40 in Appendix B).

500 mm/s feed shoe speed: At feed shoe speed of 500 mm/s, all of the locations of 45° orientation had higher mean final pressure ratios than locations of 225° orientation (Figure 5.25). However, no significant differences were found ($P > 0.05$) (Table A.42 in Appendix B). The only significant difference was between location (2, 225°) and location (6, 225°) ($P < 0.05$).

5.1.2.4 135°-315° orientation

20 mm/s feed shoe speed: As shown in Figure 5.26, the final pressure ratios at 20 mm/s were erratic along 135°-315° orientation. No obvious pattern, such as symmetrical or increasing from one end to the other end, was observed. No significant difference was observed among final pressure ratios of different locations (Table A.44 in Appendix B). This demonstrated how complex and random the deposition process and the pressure distribution could be even with seemingly the same deposition related parameters.

100 mm/s feed shoe speed: Figure 5.27 shows the final pressure ratios at 100 mm/s along 135°-315° orientation. All of the average final pressure ratios of 315° orientation were higher than those of 135° orientation. The highest pressure ratio was at location (4, 315°). The overall trend was that final pressure ratio values increased from the end of 135° orientation to the end of 315° orientation. Statistical analysis showed that the final pressure ratio of location (4, 315°) was significantly higher ($P < 0.05$) than that of location (6, 135°) (Table A.46 in Appendix B). Especially, high pressure ratio of (4, 315°) might be caused by the previously discussed dragging effect during the backward stroke.

500 mm/s feed shoe speed: Unlike at feed shoe speed of 100 mm/s, final pressure ratios at 500 mm/s were quite symmetrical about the center (Figure 5.28). No significant difference was observed among final pressure ratios of different locations (Table A.48 in Appendix B). Compared with 20 and 100 mm/s, the pressure ratios were more evenly distributed. This indicated that it is possible to reach more uniform distribution at higher feed shoe speed.

5.1.2.5 Comparison of within-die pressure distribution using contour plots

20 mm/s feed shoe speed: Figure 5.29 shows contour plots of the right cylindrical die made by using the prorated final pressure ratios at 20 mm/s. The half circle of the leeward end had higher final pressure ratios. Part of the forward half had relatively high final pressure ratios.

100 mm/s feed shoe speed: Figure 5.30 shows the distribution of prorated average final pressure ratios in the right cylindrical die filled at 100 mm/s. Again, the overall trend is that the half circle close to the leeward end had higher final pressure ratios than the forward half. The highest pressure ratios occurred in 315° orientation.

500 mm/s feed shoe speed: Figure 5.31 is the distribution of prorated average final pressure ratios in the right cylindrical die filled at feed shoe speed of 500 mm/s. The quarter circle between 0° and 90° orientations had pressure ratios higher than other locations.

In summary, for all the three feed shoe speeds, the half circle close to the leeward end had higher final pressure ratios than the forward half. This was similar to pressure distributions of the center die. The reasons have been discussed previously.

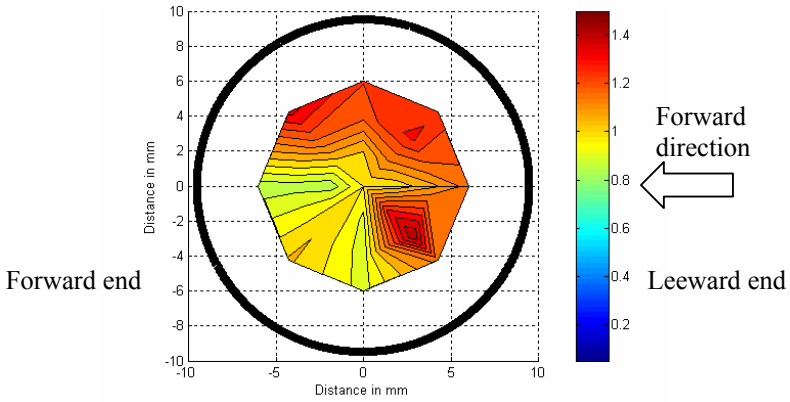

Figure 5.29 Contour plots of the distribution of prorated average final pressure ratios in the right cylindrical die filled at feed shoe speed of 20 mm/s

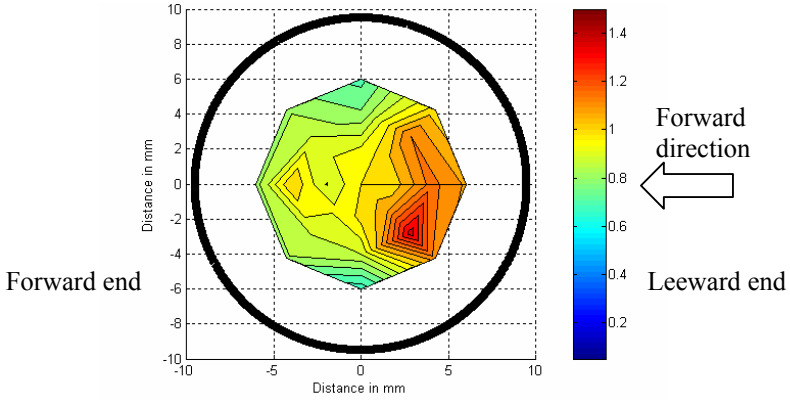

Figure 5.30 Contour plots of the distribution of prorated average final pressure ratios in the right cylindrical die filled at feed shoe speed of 100 mm/s

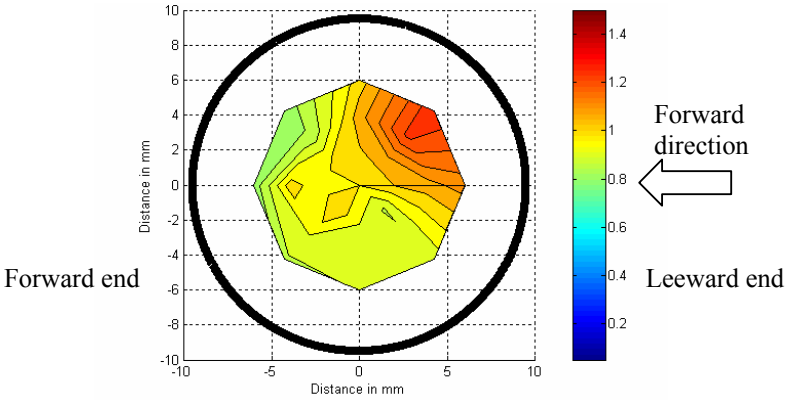

Figure 5.31 Contour plots of the distribution of prorated average final pressure ratios in the right cylindrical die filled at feed shoe speed of 500 mm/s

5.1.2.6 Comparison of uniformity among the three speeds

Table 5.4 shows some statistical parameters obtained for the right cylindrical die at 20, 100, and 500 mm/s feed shoe speeds using the prorated final pressure ratios. Having the lowest (Max-Min)/Mean, Max/Min, StDev, and COV, 500 mm/s feed shoe speed led to the most uniform filling among the three speeds. This is similar to the observation for the center cylindrical die, and possible explanations are given in section 5.1.1.8.

Table 5.4 Comparison of key statistical parameters for the right cylindrical die at the three feed shoe speeds using prorated final pressure ratios

Feed shoe speed, mm/s	Max	Min	Mean	(Max-Min)/Mean	Max/Min	StDev	COV (StDev×100/Mean)
20	1.45	0.87	1.10	0.54	1.68	0.16	14.7
100	1.38	0.66	0.98	0.73	2.08	0.14	14.8
500	1.29	0.81	1.00	0.48	1.59	0.11	11.3

5.1.3 Comparison of effects of the three feed shoe speeds

5.1.3.1 Center die

Figure 5.32 shows the comparison of average final pressure values measured at feed shoe speeds of 20 and 100 mm/s. For most locations, the final pressures were similar for the two speeds. Figure 5.33 plots the final pressure values at feed shoe speeds of 20 and 500 mm/s. For all of the locations, 500 mm/s feed shoe speed had higher final pressure values. Figure 5.34 compares final pressure values of 100 and 500 mm/s feed shoe speeds. Again, the higher feed shoe speed, 500 mm/s, resulted in higher final pressure values for all the locations.

One-way analysis of variance (ANOVA) (Tukey's method) was used to do multiple comparisons for final pressure values of the same locations at the three different feed shoe speeds. No paired t-test was conducted here, so the previously used Bonferroni and modified Bonferroni procedures were not used. The results showed that final pressures at 500 mm/s feed shoe speed were significantly higher than final pressures at 20 mm/s ($P < 0.05$). This was true for all the locations of all the orientations measured. The final pressures at 500 mm/s feed shoe speed were significantly higher also than final pressures at 100 mm/s ($P < 0.05$). For almost all of the locations, there were no significant differences between final pressures at 20 and 100 mm/s feed shoe speeds ($P > 0.05$), except the center and location (2, 0°) in 0°-180° orientation.

A plausible explanation is that the higher horizontal kinetic energy at higher feed shoe speed helped to densify the particles (by collapsing bridges and/or rearranging particles) inside the die (Wu and Cocks, 2004). Obviously, there is an upper limit, beyond which fill density will decrease with increasing feed shoe speed due to many factors, such as air escaping and minimum

time needed to fill the die. This upper limit is expected to be different for different die dimensions and/or die shapes (and some other parameters, such as particle size and particle density).

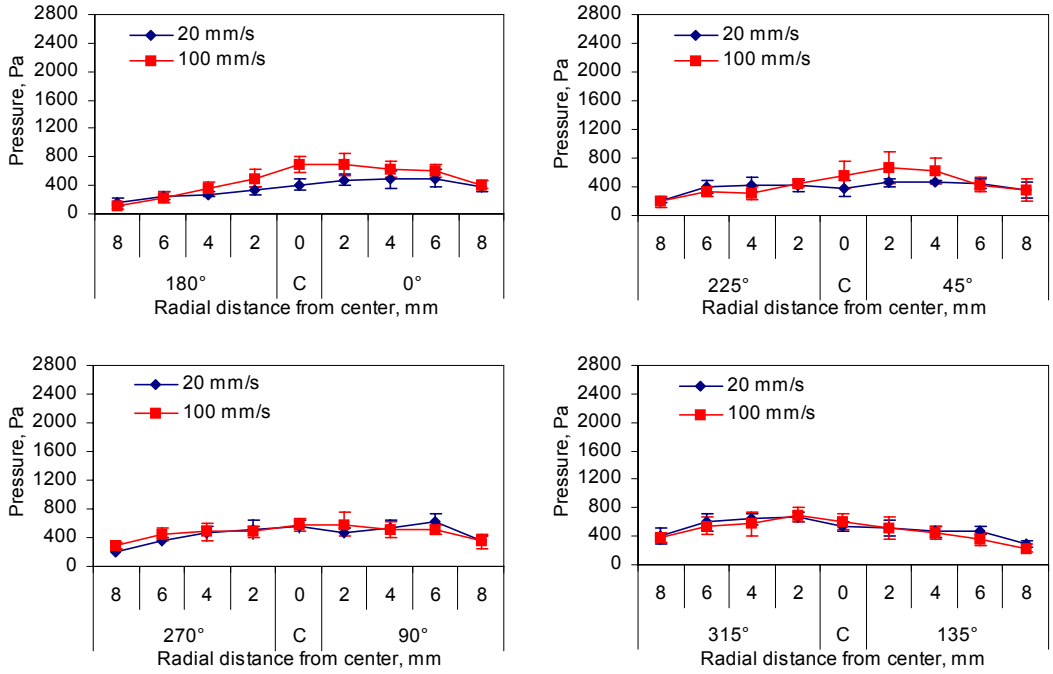

Figure 5.32 Comparison of 20 and 100 mm/s feed shoe speeds (center cylindrical die)

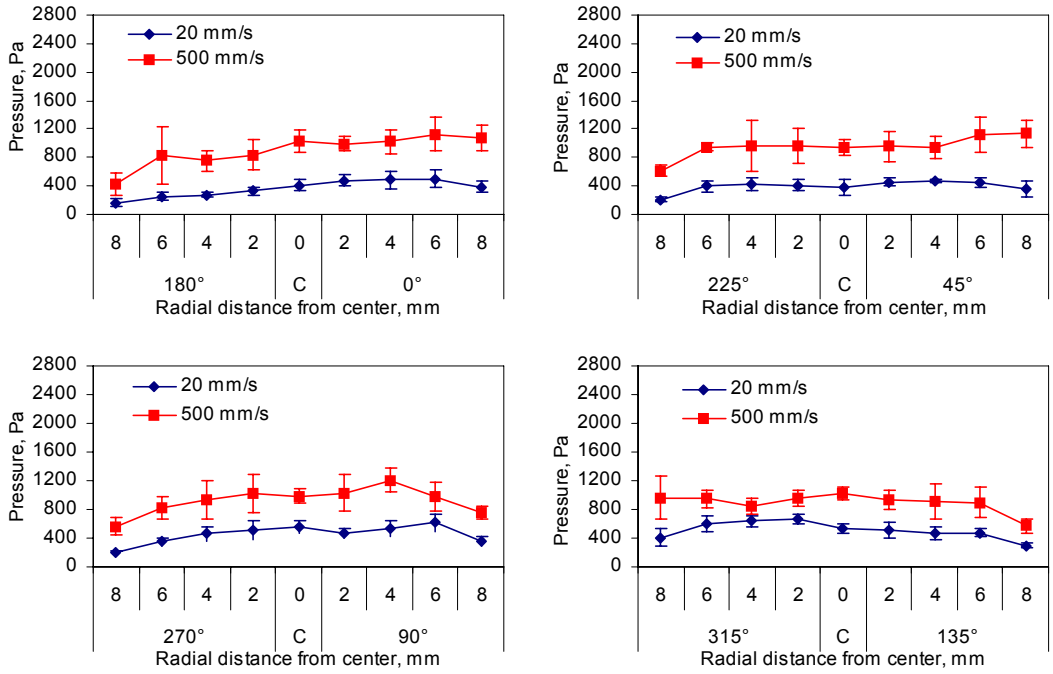

Figure 5.33 Comparison of 20 and 500 mm/s feed shoe speeds (center cylindrical die)

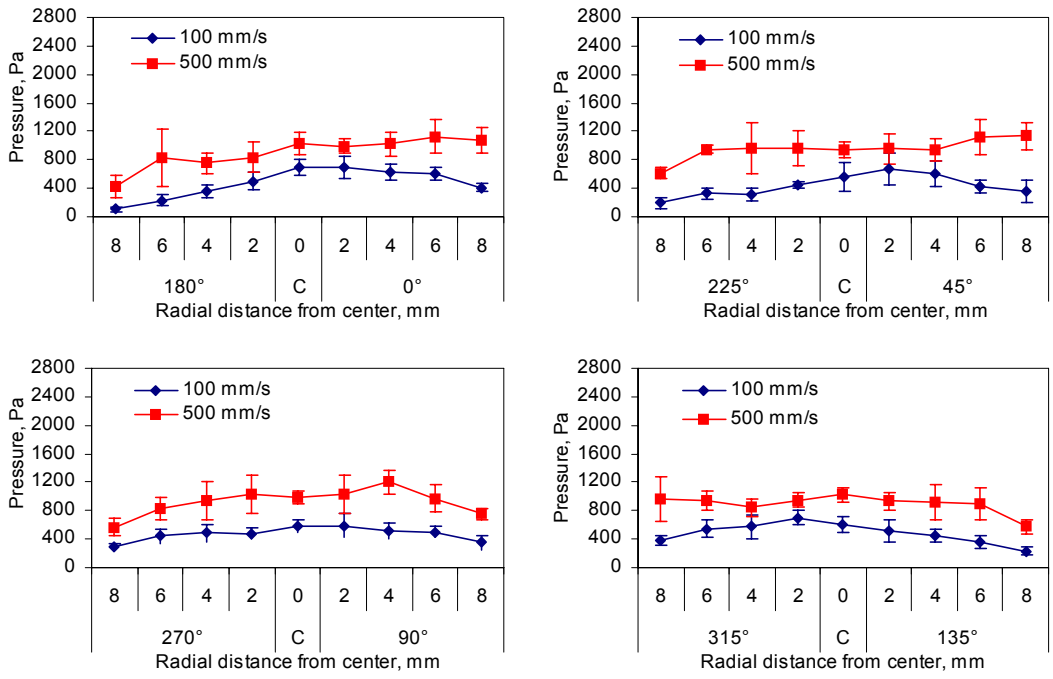

Figure 5.34 Comparison of 100 and 500 mm/s feed shoe speeds (center cylindrical die)

5.1.3.2 Right die

Figure 5.35 compares average final pressure values obtained at feed shoe speeds of 20 and 100 mm/s. For most of the locations, the final pressure values were similar for the two feed shoe speeds. Statistical analysis showed that except for one location (6, 135°), there were no significant differences between final pressure values at 20 and 100 mm/s feed shoe speeds ($P > 0.05$). Figure 5.36 shows the average final pressure values at feed shoe speeds of 20 and 500 mm/s. For almost all of the locations of 0°-180°, 45°-225°, and 90°-270° orientations, 500 mm/s feed shoe speed had significantly higher final pressure values ($P < 0.05$), except location (8, 225°). However, even though 500 mm/s had higher average final pressure values at most locations of 135°-315° orientation, only two locations (the center and (2, 135°)) showed significant differences ($P < 0.05$). Figure 5.37 shows the comparison of average final pressure values at 100 and 500 mm/s feed shoe speeds. For all the locations of 0°-180° and 90°-270° orientations, the higher feed shoe speed, 500 mm/s, resulted in significantly higher final pressure values ($P < 0.05$). For 45°-225° and 135°-315° orientations, 500 mm/s had higher average final pressure values at most of the locations, even though eight out of eighteen locations were not significantly different ($P > 0.05$). Probably, 500 mm/s, which did not yield significant differences for the right die at some locations, was already above or close to the upper limit that could result in the densest packing.

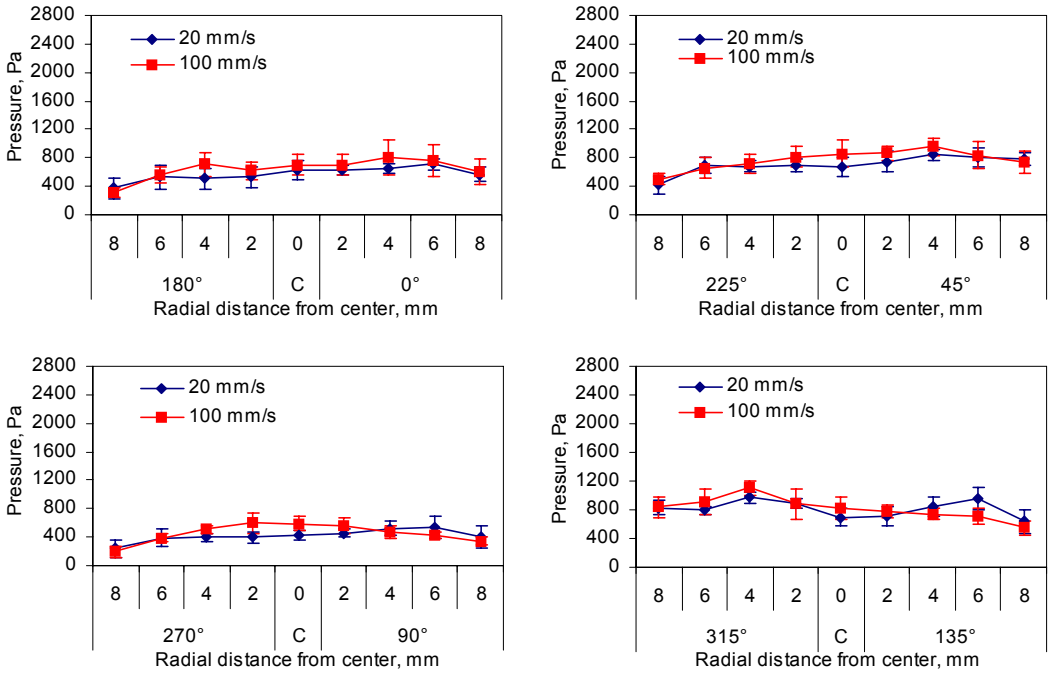

Figure 5.35 Comparison of 20 and 100 mm/s feed shoe speeds (right cylindrical die)

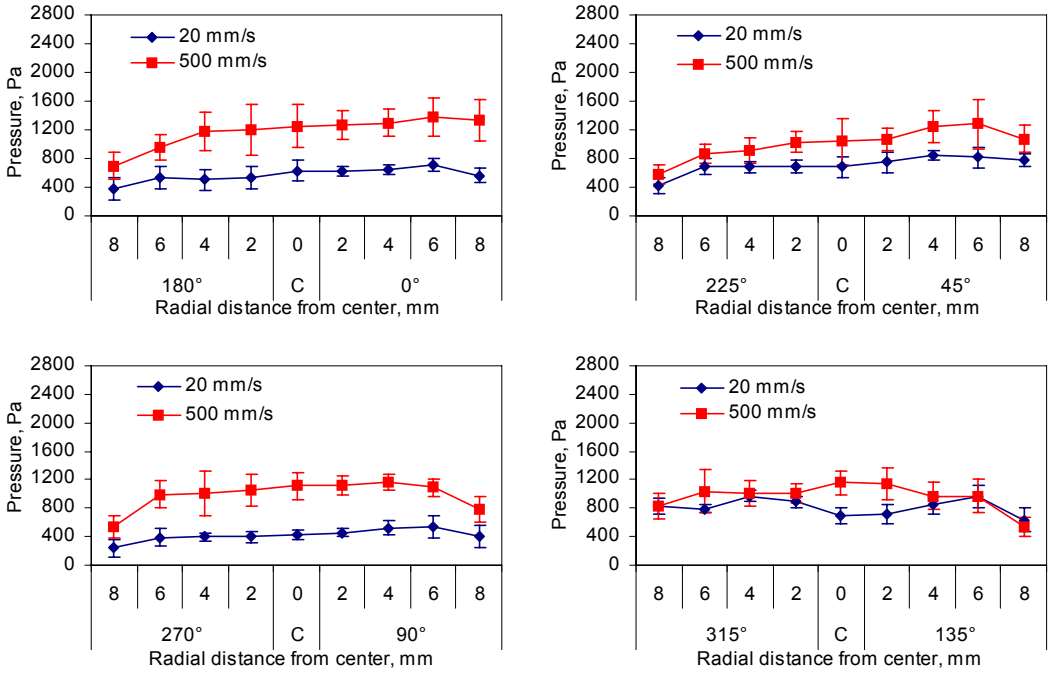

Figure 5.36 Comparison of 20 and 500 mm/s feed shoe speeds (right cylindrical die)

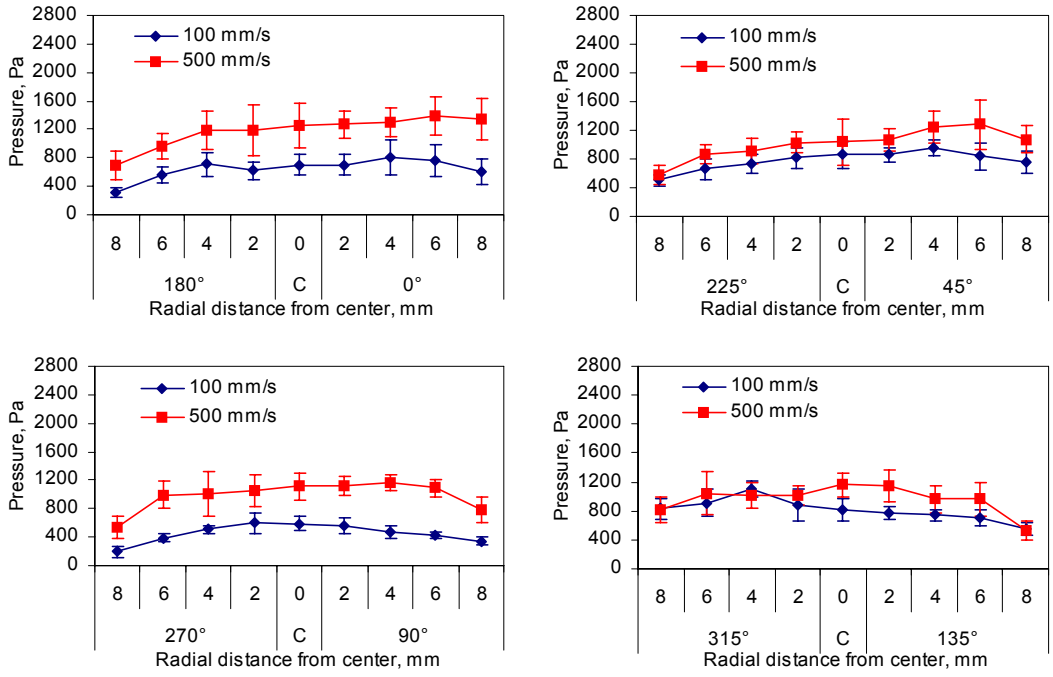

Figure 5.37 Comparison of 100 and 500 mm/s feed shoe speeds (right cylindrical die)

5.1.4 Center vs. right dies

20 mm/s feed shoe speed: For most locations, the right die had higher final pressures (Figure 5.38). Statistical analyses were conducted for corresponding locations of the center and the right dies, i.e., the same radial distances and orientations, such as location (6, 180°) of the center die vs. location (6, 180°) of the right die. For a certain location, only two samples were compared, and a paired t-test was not appropriate. Two-sample *t*-tests (assuming equal variances) were used. For all the locations of 0°-180°, 45°-225°, and 135°-315° orientations, final pressures of the right die were significantly higher than those of the center die ($P < 0.05$) (Table A.49 in Appendix B). But there were almost no differences between the two dies in the orientation of 90°-270°, which was perpendicular to the feed shoe movement direction. Only location (2, 270°) and the center of the center die were significantly different from those of the right die.

The differences of the center and right dies were attributed to the complex flow pattern within the feed shoe tube during simultaneous filling of the three dies. Because of the oval cross-section shape of the feed shoe, the powder in the feed shoe already began to flow and fill the center die before started filling the right die. This could promote powder deposition into the right die by reducing or eliminating the interparticle friction of powder in the feed shoe. In addition, the oval cross-section shape of the feed shoe influences the take-off trajectories of powder particles and pressing of powder by the die wall during the forward and backward strokes.

The major reason for the right die not to have higher final pressure values along 90°-270° orientation might be that particles along this orientation experienced the least compression induced by the feed shoe wall during the filling process. In other words, 90°-270° orientation served as a border separating particles of the half circle being densified and the half circle being loosened. During the forward stroke, the rear wall of the feed shoe tube loosened particles in the leeward half circle of cylindrical dies and densified particles in the forward half circle due to the existence of the die wall. During the backward stroke, particles in the forward half circle of cylindrical dies were loosened and those in the leeward half circle were densified. During the entire filling process, only locations of 90°-270° orientation were densified to the least degree.

100 mm/s feed shoe speed: Observations were similar to those of 20 mm/s (Figure 5.39). However, compared to 20 mm/s, fewer locations had significant differences in the orientations of 45°-225° and 135°-315°, especially the 0°-180° orientation (Table A.50 in Appendix B).

500 mm/s feed shoe speed: In the 0°-180° orientation, the mean final pressures of the right die were higher than those of the center die (Figure 5.40). There were significant ($P < 0.05$) differences between some locations of 0°-180° orientation of the two dies (Table A.51 in Appendix B). However, in other orientations, the center and right dies had similar final pressure values. This may be explained by the higher kinetic energy, which densified particle packing in both dies and reduced their difference, at higher feed shoe speed. It seems that the quantitative differences between center and right dies were reduced with increasing feed shoe speed.

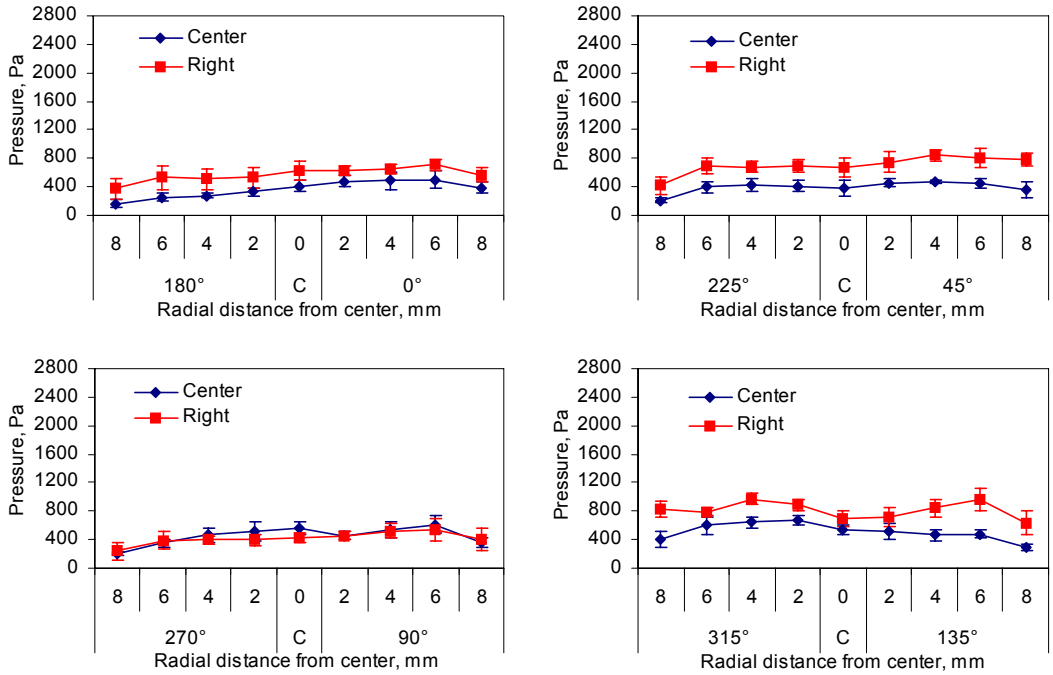

Figure 5.38 Comparison of center and right dies at 20 mm/s feed shoe speed

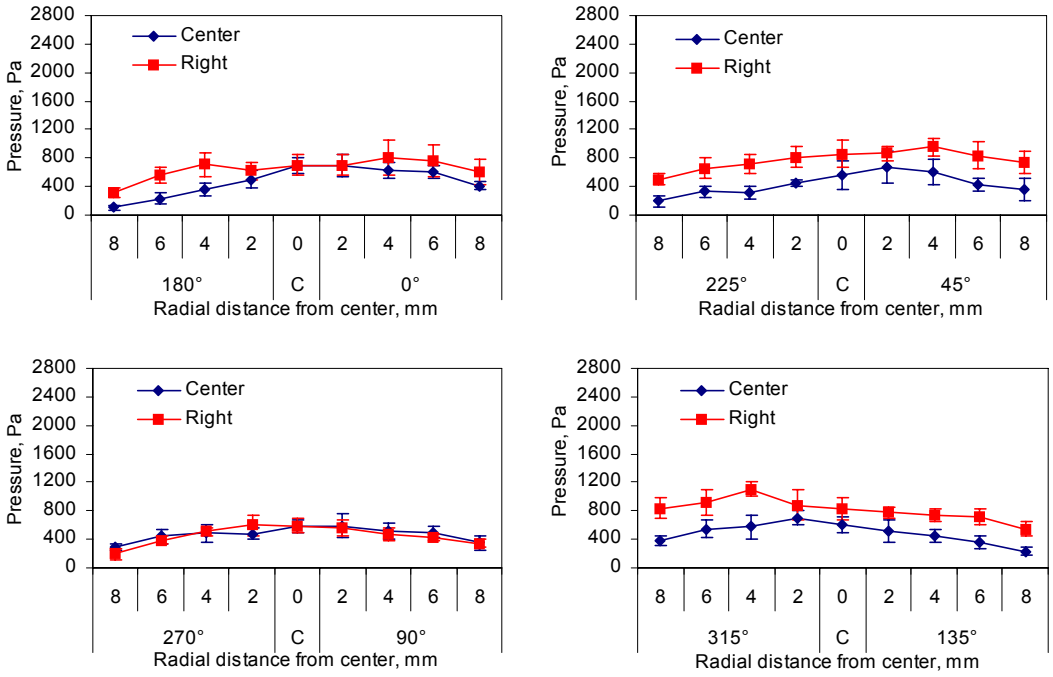

Figure 5.39 Comparison of center and right dies at 100 mm/s feed shoe speed

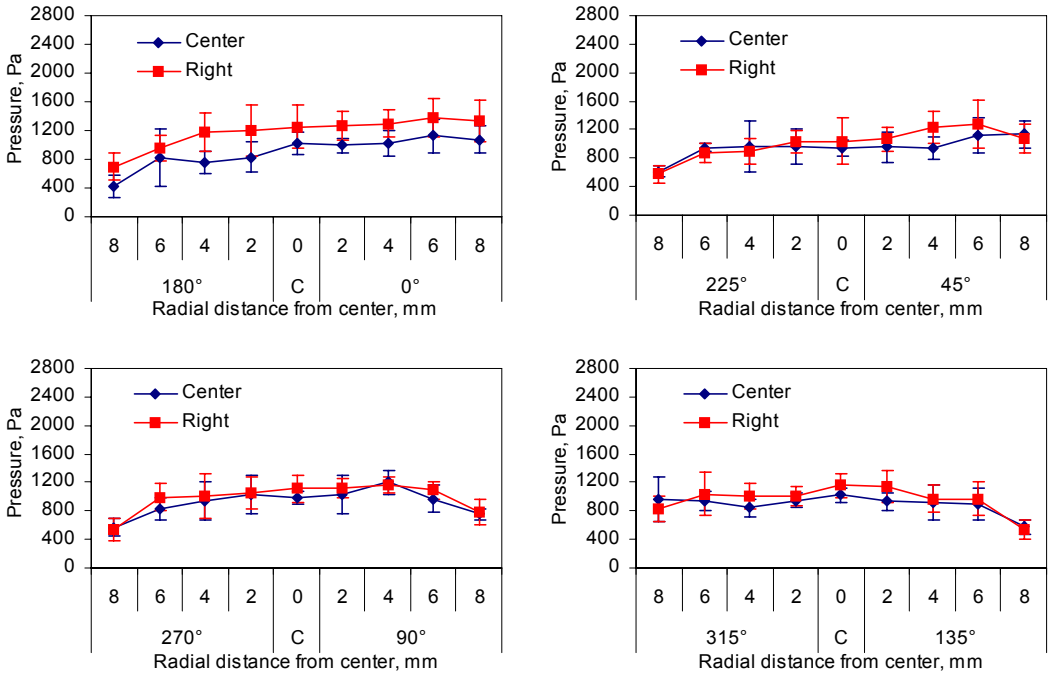

Figure 5.40 Comparison of center and right dies at 500 mm/s feed shoe speed

5.1.5 Comparison of mass values after forward stroke and entire filling

Table 5.5 shows the mass values of powder in each of the three cylindrical dies after only the forward stroke at the feed shoe speed of 20 mm/s. Table 5.6 shows the mass values of powder

in each of the three cylindrical dies after the entire filling process at the same feed shoe speed. As shown in Table 5.7, at the end of the forward stroke, the three dies were already 92.8% to 93.9% filled. The contribution from the backward stroke to the amount of powder totally filled at the end of the entire filling process was only about 6.6%.

Similar results were obtained for the feed shoe speed of 100 mm/s. Mass values of powder filled in three dies after only forward stroke at 100 mm/s feed shoe speed are shown in Table 5.8. Mass values of filled powder after the entire filling process at 100 mm/s are shown in Table 5.9. At the end of the forward stroke, the three dies were almost fully filled (95.8% to 97.6%)(Table 5.7). The backward stroke only contributed about 3.4% to the total amount of powder in the dies.

For the feed shoe speed of 500 mm/s, the backward stroke contributed about 9.5% to the total amount of powder filled in the dies (Table 5.7). The leeward ends of the dies were partially empty after the forward stroke. Table 5.10 shows the amount of powder in each of the three cylindrical dies after only the forward stroke at 500 mm/s feed shoe speed. Table 5.11 shows the amount of powder in each of the three cylindrical dies after the entire filling process at the same feed shoe speed.

The above results indicated that the backward stroke contributed only slightly to die filling. For lower feed shoe speeds, i.e., 20 and 100 mm/s, more than 92% (92.8%) of the powder was filled in the forward stroke. The backward stroke densified the powder in the dies with the pressure from the powder in the feed shoe and the feed shoe wall, and by shear friction between moving particles in the feed shoe and static particles in the dies. Also, the backward stroke added less than 8% of the total amount of powder in the dies.

For the highest feed shoe speed, 500 mm/s, more than 88% (88.2%) of the powder was filled in the forward stroke. It was less than the filled mass at 20 and 100 mm/s feed shoe speeds. The reason was that there was not sufficient time for the dies to be fully filled in the forward stroke at 500 mm/s feed shoe speed.

Table 5.5 Mass values of powder filled in three dies after only forward stroke at 20 mm/s feed shoe speed (g)

Test	Left die	Center die	Right die
#1	9.5	9.3	9.4
#2	9.4	9.5	9.6
#3	9.3	9.5	9.6
#4	9.6	9.8	9.9
#5	9.6	9.8	9.8
#6	9.6	9.8	9.7
Mean	9.5	9.6	9.7
Standard deviation	0.1	0.2	0.2

Table 5.6 Mass values of powder filled in three dies after the entire filling process at 20 mm/s feed shoe speed (g)

Test	Left die	Center die	Right die
#1	10.0	10.3	10.2
#2	10.2	10.1	10.3
#3	10.3	10.4	10.2
#4	10.3	10.3	10.4
#5	10.3	10.4	10.2
#6	10.3	10.3	10.5
Mean	10.2	10.3	10.3
Standard deviation	0.1	0.1	0.1

Table 5.7 Extent of three dies being filled after the forward stroke (%)

Feed shoe speed, mm/s	Left die	Center die	Right die	Average	Contribution from backward stroke, %
20	92.8	93.4	93.9	93.4	6.6
100	97.6	96.3	95.8	96.6	3.4
500	88.2	91.3	91.9	90.5	9.5
Mean	92.9	93.7	93.9	93.5	6.5
Standard deviation	4.7	2.5	2.0		

Table 5.8 Mass values of powder filled in three dies after only forward stroke at 100 mm/s feed shoe speed (g)

Test	Left die	Center die	Right die
#1	9.9	9.7	9.9
#2	9.7	9.6	9.6
#3	9.6	9.5	9.7
#4	9.7	9.7	9.4
#5	9.6	9.6	9.5
#6	9.6	9.8	9.6
Mean	9.7	9.6	9.6
Standard deviation	0.1	0.1	0.2

Table 5.9 Mass values of powder filled in three dies after the entire filling process at 100 mm/s feed shoe speed (g)

Test	Left die	Center die	Right die
#1	10.0	9.9	10.0
#2	9.9	9.9	9.9
#3	9.9	9.9	10.0
#4	9.7	10.1	10.0
#5	10.0	10.1	10.0
#6	10.0	10.2	10.3
Mean	9.9	10.0	10.0
Standard deviation	0.1	0.1	0.1

Table 5.10 Mass values of powder filled in three dies after only forward stroke at 500 mm/s feed shoe speed (g)

Test	Left die	Center die	Right die
#1	8.9	9.2	9.2
#2	8.9	9.1	9.2
#3	8.9	9.5	9.5
#4	9.3	9.5	9.7
#5	9.4	9.6	9.6
#6	9.4	9.6	9.7
Mean	9.1	9.4	9.5
Standard deviation	0.3	0.2	0.2

Table 5.11 Mass values of powder filled in three dies after the entire filling process at 500 mm/s feed shoe speed (g)

Test	Left die	Center die	Right die
#1	10.4	10.4	10.4
#2	10.4	10.3	10.4
#3	10.4	10.3	10.3
#4	10.3	10.4	10.3
#5	10.3	10.3	10.2
#6	10.3	10.2	10.3
Mean	10.4	10.3	10.3
Standard deviation	0.1	0.1	0.1

5.1.6 Summary

Based on above discussion, the following concluding remarks can be made for cylindrical dies filled with the battery powder mixture:

1. At low feed shoe speeds (20 and 100 mm/s), the half circle close to the leeward end had higher final pressure values than the forward half circle, and the backward stroke of feed shoe movement contributed to this distribution pattern.
2. At high feed shoe speed (500 mm/s), the final pressure distribution was more uniform than at lower feed shoe speed. Higher momentum of particles at higher feed shoe speed might contribute to this trend by minimizing arching and allowing particles to locally rearrange themselves. Another possible reason was that higher rate of die filling decreased the opportunity for particle segregation and promoted uniform filling.
3. The final within-die pressure distribution at the bottom of the dies was not always symmetrical about the center line of the feed shoe movement direction. The overall trend was that pressure decreases with increasing radial distance for lower feed shoe speeds. The distribution was not always regular for higher feed shoe speed.

4. The three parallel dies did not always have similar and symmetrical pressure distributions.
5. Higher feed shoe speed (500 mm/s) resulted in higher final pressure values (774.5 to 1424.5 Pa) than lower feed shoe speeds (20 and 100 mm/s) (235.2 to 1136.0 Pa) at most of the locations. The results suggested there is an upper limit, beyond which fill density will decrease with increasing feed shoe speed.
6. At lower feed shoe speeds (20 and 100 mm/s), the right die tended to have higher final pressure values (393.8 to 1136.0 Pa) than the center die (235.2 to 726.0 Pa). At higher feed shoe speed (500 mm/s), the quantitative differences between center (774.5 to 1246.1 Pa) and right dies (897.3 to 1424.5 Pa) were reduced. This suggested that different distances between the dies and the feed shoe wall possibly influence die filling. Dies of different interval spaces might also result in different filling features.
7. Most of the filled powder was deposited in the forward stroke (about 93% at 20 mm/s, 97% at 100 mm/s, and 90% at 500 mm/s).

5.2 Toroidal Dies

Multiple toroidal die configuration and dimensions and the dimension of the feed shoe are shown in Figure 5.41. The movement direction of the feed shoe was parallel to the long axis of the ellipse. The three parallel toroidal dies were symmetrical about the long axis of the ellipse.

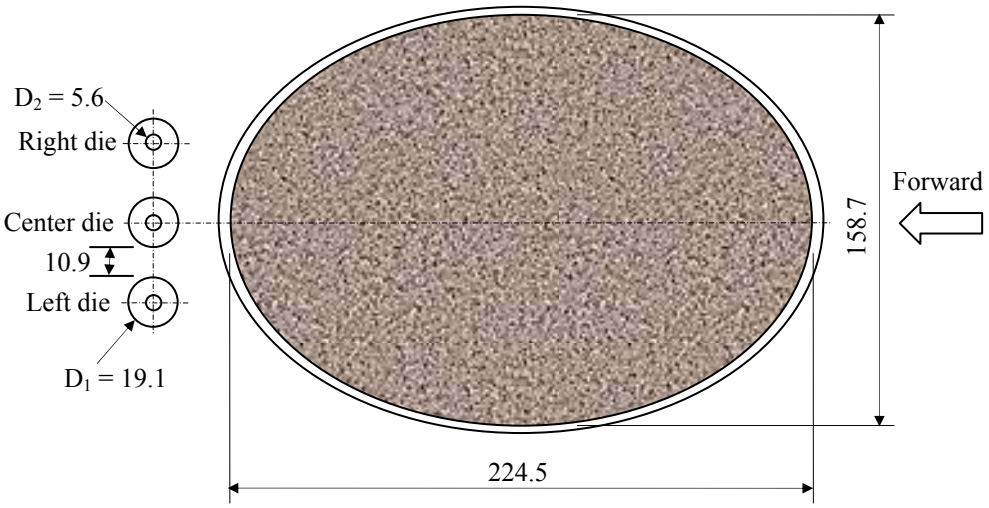

Figure 5.41 Dimensions of the toroidal dies and the feed shoe cross-section in contact with the table surface (drawn to scale) (unit: mm)

5.2.1 Within-die comparison of the center die

In this section, data collected within each die are analyzed and compared. Final pressure values of the center die in 0°-180°, 45°-225°, 90°-270°, and 135°-315° orientations and 20, 100, and 500 mm/s feed shoe speeds are discussed separately. Then contour plots obtained based on the data of all the four orientations are presented and discussed. The results of statistical analysis are listed in Appendix B.

5.2.1.1 0°-180° orientation

20 mm/s feed shoe speed: Figure 5.42 shows the average final pressure values in the 0°-180° orientation of the center toroidal die filled at feed shoe speed of 20 mm/s. Locations (4, 180°), (8, 180°), (4, 0°), (8, 0°) were next to the die wall, and the wall friction is expected to play an important role. Nevertheless, in each direction (such as 0° direction), pressure values of only three locations were measured. The pressure values of locations close to the die wall represented two thirds of all the data, therefore, these were used in analysis and comparison.

All locations of 0° orientation had higher final pressures than locations of 180° orientation. Final pressures of location (8, 180°) was significantly lower ($P < 0.05$) than those of the 0° orientation. Compared to (6, 0°) and (8, 0°), locations (6, 180°) and (4, 180°) had significantly lower ($P < 0.05$) final pressures. Possible reasons are discussed in section 5.2.1.5.

100 mm/s feed shoe speed: Figure 5.43 shows the average final pressure values of 0°-180° orientation collected at feed shoe speed of 100 mm/s. The general pattern was very similar to that of 20 mm/s feed shoe speed.

500 mm/s feed shoe speed: Figure 5.44 was plotted based on the average final pressure values of 0°-180° orientation collected at feed shoe speed of 500 mm/s. All of the final pressure values of the locations in 0° orientation were significantly higher than those of the locations in 180° orientation. All the mean final pressure values were higher than those of 20 and 100 mm/s feed shoe speeds, especially for 0° orientation. The reason for this trend could be that the higher kinetic energy at higher feed shoe speed helped to densify the particles (by collapsing bridges and/or rearranging particles) inside the die (Wu and Cocks, 2004), as with the cylindrical dies.

5.2.1.2 90°-270° orientation

20 mm/s feed shoe speed: Pressure distribution along 90°-270° direction was quite symmetrical at feed shoe of 20 mm/s (Figure 5.45). Except that final pressure value of location (8, 270°) was significantly lower ($P < 0.05$) than that of location (6, 270°), no other significant differences were observed.

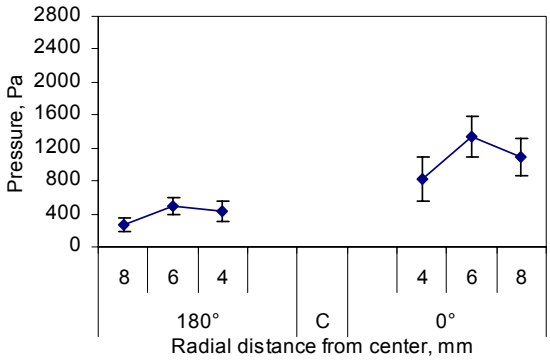

Figure 5.42 Average final pressure values in **0°-180°** orientation of the center toroidal die filled at feed shoe speed of **20 mm/s**

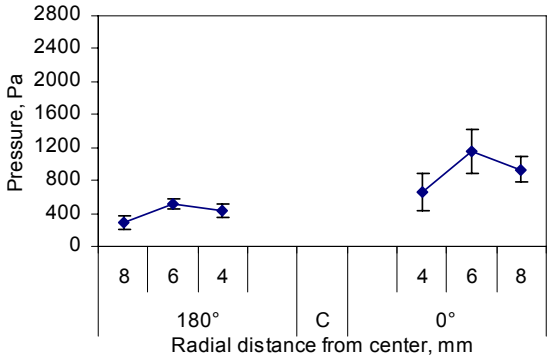

Figure 5.43 Average final pressure values in **0°-180°** orientation of the center toroidal die filled at feed shoe speed of **100 mm/s**

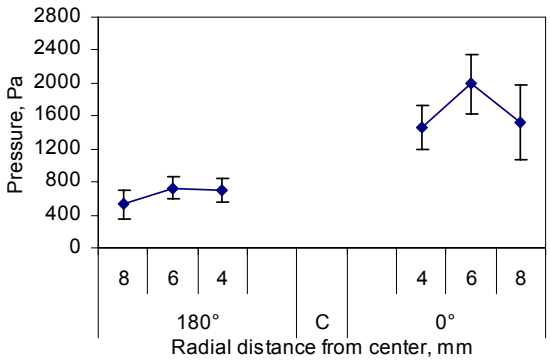

Figure 5.44 Average final pressure values in **0°-180°** orientation of the center toroidal die filled at feed shoe speed of **500 mm/s**

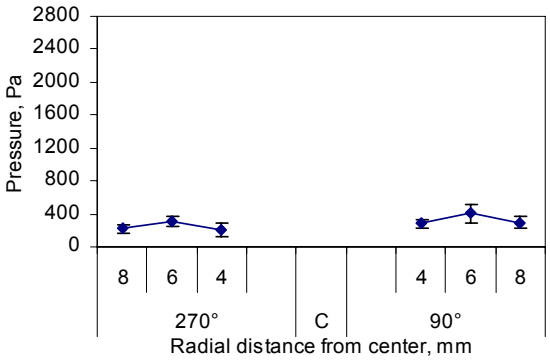

Figure 5.45 Average final pressure values in **90°-270°** orientation of the center toroidal die filled at feed shoe speed of **20 mm/s**

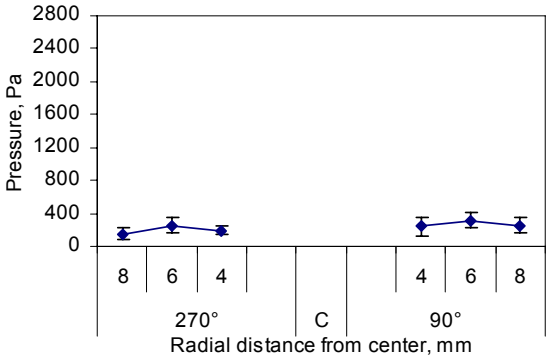

Figure 5.46 Average final pressure values in **90°-270°** orientation of the center toroidal die filled at feed shoe speed of **100 mm/s**

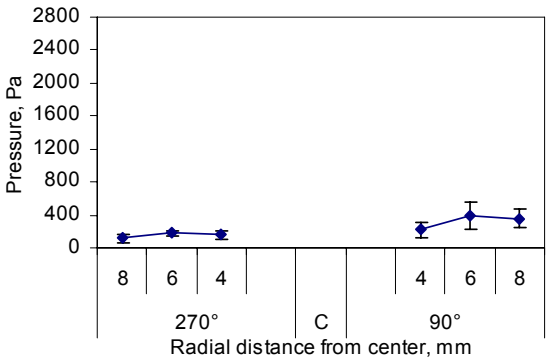

Figure 5.47 Average final pressure values in **90°-270°** orientation of the center toroidal die filled at feed shoe speed of **500 mm/s**

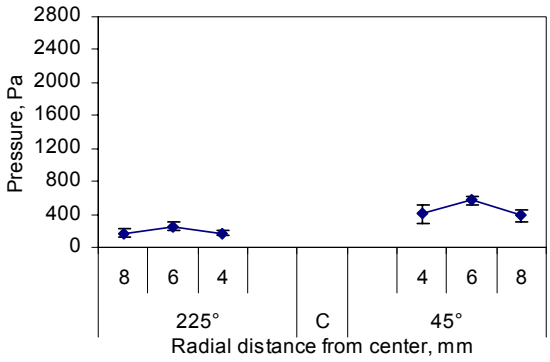

Figure 5.48 Average final pressure values in **45°-225°** orientation of the center toroidal die filled at feed shoe speed of **20 mm/s**

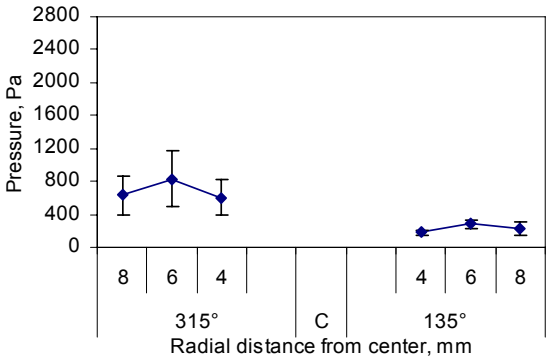

Figure 5.51 Average final pressure values in **135°-315°** orientation of the center toroidal die filled at feed shoe speed of **20 mm/s**

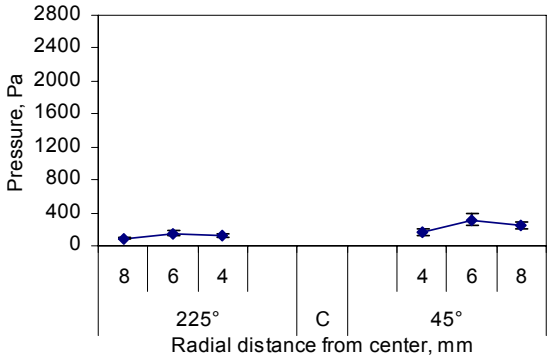

Figure 5.49 Average final pressure values in **45°-225°** orientation of the center toroidal die filled at feed shoe speed of **100 mm/s**

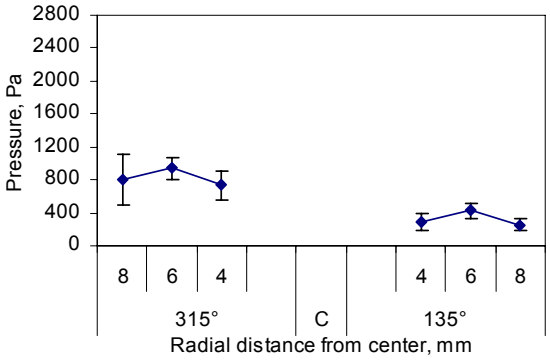

Figure 5.52 Average final pressure values in **135°-315°** orientation of the center toroidal die filled at feed shoe speed of **100 mm/s**

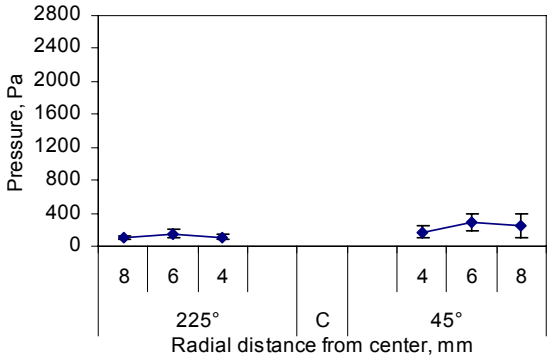

Figure 5.50 Average final pressure values in **45°-225°** orientation of the center toroidal die filled at feed shoe speed of **500 mm/s**

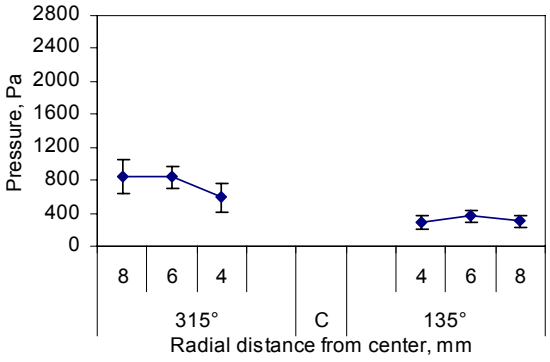

Figure 5.53 Average final pressure values in **135°-315°** orientation of the center toroidal die filled at feed shoe speed of **500 mm/s**

100 mm/s feed shoe speed: Pressure distribution along the 90°-270° orientation at 100 mm/s was quite symmetrical and similar to that of 20 mm/s (Figure 5.46). Except for one comparison, no significant differences were observed; i.e., final pressure value of location (8, 270°) was significantly lower ($P < 0.05$) than that of location (6, 270°).

500 mm/s feed shoe speed: The pressure distribution along 90°-270° orientation at feed shoe speed of 500 mm/s was nearly as symmetrical as 20 and 100 mm/s (Figure 5.47). Except for one comparison, no significant differences were observed, i.e., final pressure value of location (4, 270°) was significantly lower ($P < 0.05$) than that of location (8, 90°). One of the reasons for this significant difference was that the standard deviations of the final pressure values were low. So, even for small differences between the average values of the two locations, the difference could be significant.

5.2.1.3 45°-225° orientation

20 mm/s feed shoe speed: Figure 5.48 shows the average final pressure values of 45°-225° orientation at feed shoe speed of 20 mm/s. Almost all of the final pressure values of 45° orientation were significantly higher ($P < 0.05$) than those of 225° orientation. The reasons for this are provided in section 5.2.1.5.

100 mm/s feed shoe speed: At feed shoe speed of 100 mm/s, the pressure distribution in 45°-225° was similar to that of 20 mm/s, except the average final pressure values were slightly lower (Figure 5.49). Almost all of the final pressure values of 45° orientation were significantly higher ($P < 0.05$) than those of 225° orientation, except that final pressure value of location (4, 45°) was not significantly higher ($P > 0.05$) than that of location (6, 225°).

500 mm/s feed shoe speed: Figure 5.50 shows the average final pressure values of 45°-225° orientation at feed shoe speed of 500 mm/s. Like 45°-225° orientation at feed shoe speed of 20 and 100 mm/s, all of the locations of 45° orientation had higher average final pressure values than those of 225° orientation, even though no differences were significant ($P > 0.05$).

5.2.1.4 135°-315° orientation

20 mm/s feed shoe speed: Figure 5.51 shows the average final pressure values of 135°-315° orientation at feed shoe speed of 20 mm/s. All of the average final pressure values of 315° orientation were higher than those of 135° orientation. This trend is explained in section 5.2.1.5. No significant differences were observed.

100 mm/s feed shoe speed: At feed shoe speed of 100 mm/s, all of the locations of 315° orientation had higher final pressure values than locations of 135° orientation (Figure 5.52). Most

of these differences were statistically significant ($P < 0.05$). Only the difference between locations (8, 315°) and (4, 135°) and the difference between locations (8, 315°) and (6, 135°) were not significant ($P > 0.05$).

500 mm/s feed shoe speed: Figure 5.53 shows the average final pressure values of 135°-315° orientation at feed shoe speed of 500 mm/s. Similar to those of feed shoe speed of 20 and 100 mm/s, all of the locations in 315° orientation had higher final pressure values than 135°. Final pressure values of locations (6, 315°) and (8, 315°) were significantly higher ($P < 0.05$) than those of all of the locations in 135° orientation.

5.2.1.5 Comparison of within-die pressure distribution using contour plots

20 mm/s feed shoe speed: Figure 5.54 shows contour plots of the center toroidal die made by using the average final pressures at feed shoe speed of 20 mm/s. The pressure distribution was symmetrical about the center line parallel to the forward feed shoe movement direction. The area around 0° orientation (close to the leeward end) had the highest pressures. The area around 180° orientation (close to the forward end) had pressure values that were slightly higher than its surrounding area. This distribution pattern was mostly caused by the existence of the center post. During the forward stroke of the feed shoe motion, the center post blocked the particles from the feed shoe and bounced them back to the area near the trailing wall vicinity. So the particles were packed more densely than other locations. The center post also acted as a lower punch for the particles around 0° orientation to be compressed by the upper punch, the feed shoe wall, in the forward and reverse strokes of the feed shoe motion. Similar but less effects contributed to the slightly high pressure values of 180° orientation. For locations in orientations other than the feed shoe motion direction, the existence of the center post reduced the opening of the toroidal containers, and so decreased the amount of particles deposited in those locations. Another reason was that the particles in the top region were dragged by the movement of the feed shoe during the backward stroke, and so they moved horizontally some distance toward the leeward end.

100 mm/s feed shoe speed: At 100 mm/s feed shoe speed, the pressure distribution was very similar to that of 20 mm/s (Figure 5.55). The pressure distribution was symmetrical about the center line parallel to the forward feed shoe movement direction. The area of the highest pressure values was around 0° orientation, but offset slightly to 315° orientation.

500 mm/s feed shoe speed: Figure 5.56 shows the distribution of the average final pressure values in the center toroidal die filled at feed shoe speed of 500 mm/s. The pressure distribution was very similar to that of 20 mm/s, but the highest pressure values were higher than those of 20 mm/s. This was attributed partly to the higher momentum of filling particles at higher

feed shoe speed. The higher momentum of filling particles resulted in denser packing by reducing the chance that particles arched or bridged in the die. Another possible reason could be that at higher feed shoe speeds, the powder in the dies had less time to release the stress induced by the feed shoe and the friction between particles and the die wall.

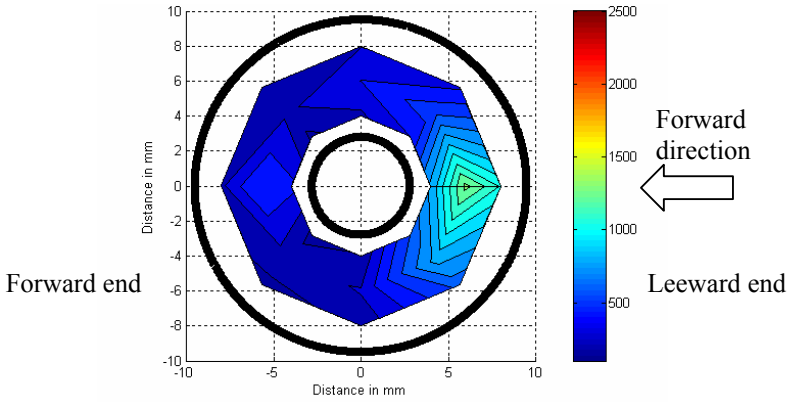

Figure 5.54 Contour plots of the average final pressure value (Pa) distribution in the center toroidal die filled at feed shoe speed of 20 mm/s

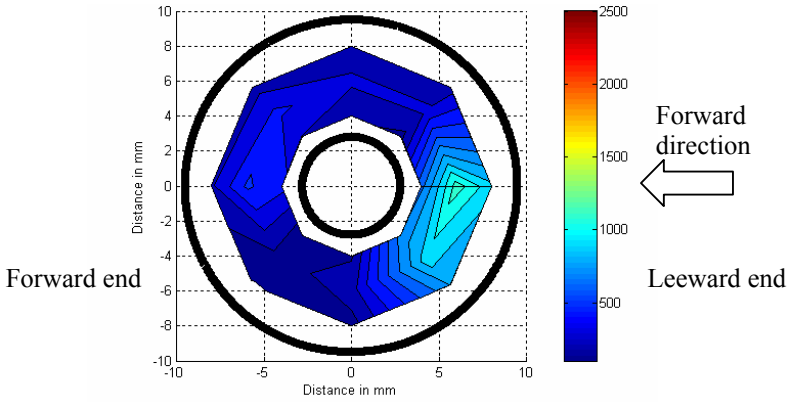

Figure 5.55 Contour plots of the average final pressure value (Pa) distribution in the center toroidal die filled at feed shoe speed of 100 mm/s

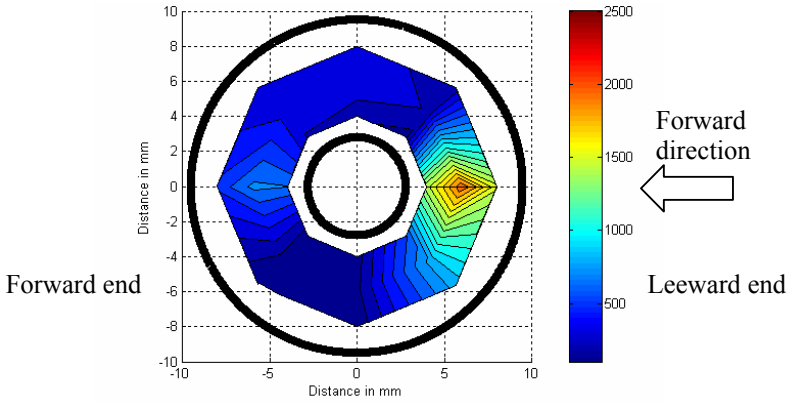

Figure 5.56 Contour plots of the average final pressure value (Pa) distribution in the center toroidal die filled at feed shoe speed of 500 mm/s

5.2.1.6 Comparison of uniformity among the three speeds

Table 5.12 shows some statistical parameters obtained for the center toroidal die at the three feed shoe speeds (20, 100, and 500 mm/s) using the final pressure values. Based on these values, 500 mm/s feed shoe speed, which had the highest (Max-Min)/Mean, Max/Min, StDev (standard deviation), and COV, was inferred to have the most nonuniform pressure distribution among the three speeds. The 500 mm/s feed shoe speed also resulted in the highest Max and Mean final pressure values. Higher momentum possessed by particles at higher feed shoe speed is expected to contribute to denser filling by minimizing arching and allowing particles to rearrange themselves. The presence of the center post contributed toward the most nonuniform filling at the highest feed shoe speed, given the fact that the highest feed shoe speed resulted in the most uniform filling for the cylindrical dies of the same outer diameter as the toroidal dies. The high COV values indicated that final pressure values varied considerably from test to test.

Table 5.12 Comparison of key statistical parameters for the center toroidal die at the three feed shoe speeds using the final pressure values (Pa)

Feed shoe speed, mm/s	Max	Min	Mean	(Max-Min)/Mean	Max/Min	StDev	COV (StDev×100/Mean)
20	1372.1	179.6	467.3	2.55	7.64	312.2	66.8
100	1186.7	95.5	427.5	2.55	12.43	306.4	71.7
500	2052.5	98.1	543.9	3.59	20.91	516.1	94.9

5.2.2 Within-die comparison of the right die

In this section, data collected within the right toroidal die are analyzed and compared for studying within-die uniformity. The final pressure values of the right die in 0°-180°, 45°-225°, 90°-270°, and 135°-315° orientations and 20, 100, and 500 mm/s feed shoe speeds are discussed separately. Then contour plots of pressure distribution are presented to discuss the filling uniformity of the entire die.

5.2.2.1 0°-180° orientation

20 mm/s feed shoe speed: Figure 5.57 shows the average final pressure values of 0°-180° orientation at feed shoe speed of 20 mm/s. Along 0° orientation, the final pressure values were all significantly higher ($P < 0.05$) than those of 180° orientation. This trend was similar to that of the center die, and the possible reasons were discussed previously.

100 mm/s feed shoe speed: As shown in Figure 5.58, pressure value distribution along 0°-180° orientation at 100 mm/s was similar to that of 20 mm/s. The final pressure values of 0° orientation were all significantly higher ($P < 0.05$) than those of 180° orientation.

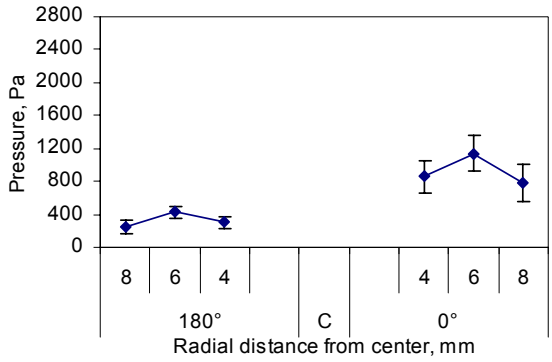

Figure 5.57 Average final pressure values in **0°-180°** orientation of the right toroidal die filled at feed shoe speed of **20 mm/s**

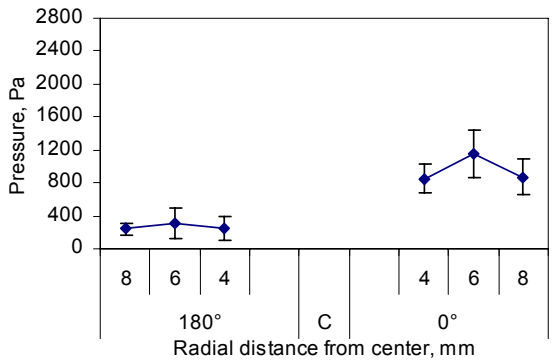

Figure 5.58 Average final pressure values in **0°-180°** orientation of the right toroidal die filled at feed shoe speed of **100 mm/s**

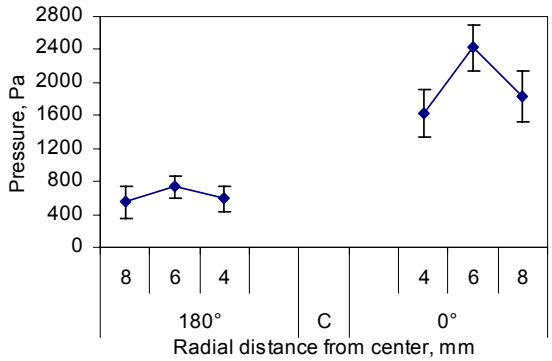

Figure 5.59 Average final pressure values in **0°-180°** orientation of the right toroidal die filled at feed shoe speed of **500 mm/s**

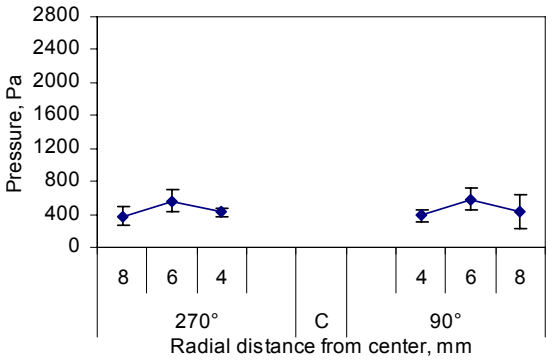

Figure 5.60 Average final pressure values in **90°-270°** orientation of the right toroidal die filled at feed shoe speed of **20 mm/s**

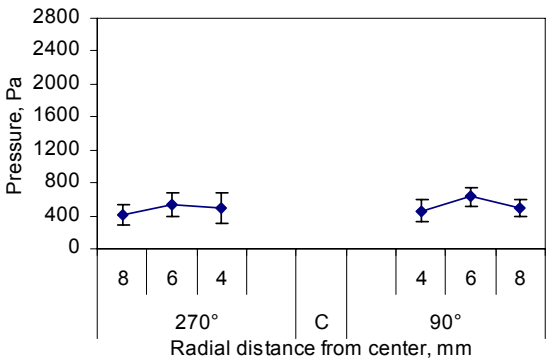

Figure 5.61 Average final pressure values in **90°-270°** orientation of the right toroidal die filled at feed shoe speed of **100 mm/s**

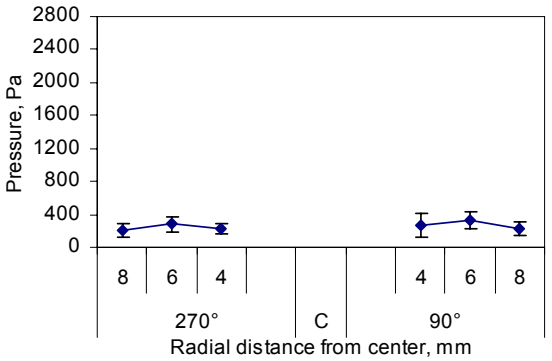

Figure 5.62 Average final pressure values in **90°-270°** orientation of the right toroidal die filled at feed shoe speed of **500 mm/s**

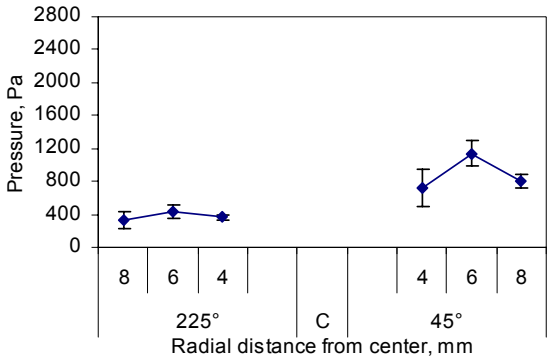

Figure 5.63 Average final pressure values in **45°-225°** orientation of the right toroidal die filled at feed shoe speed of **20 mm/s**

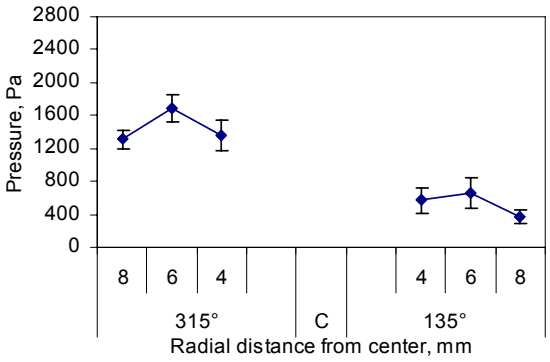

Figure 5.66 Average final pressure values in **135°-315°** orientation of the right toroidal die filled at feed shoe speed of **20 mm/s**

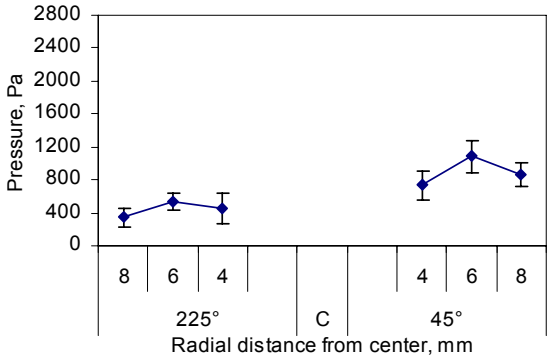

Figure 5.64 Average final pressure values in **45°-225°** orientation of the right toroidal die filled at feed shoe speed of **100 mm/s**

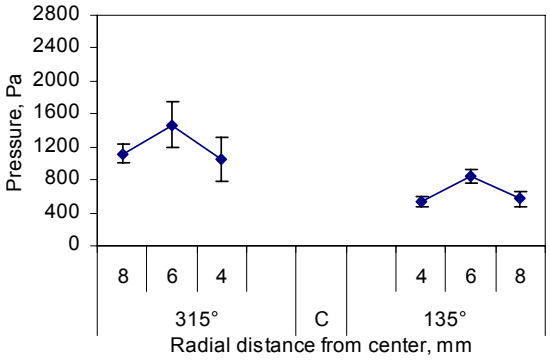

Figure 5.67 Average final pressure values in **135°-315°** orientation of the right toroidal die filled at feed shoe speed of **100 mm/s**

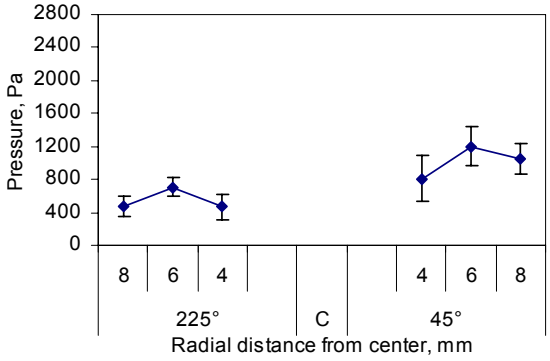

Figure 5.65 Average final pressure values in **45°-225°** orientation of the right toroidal die filled at feed shoe speed of **500 mm/s**

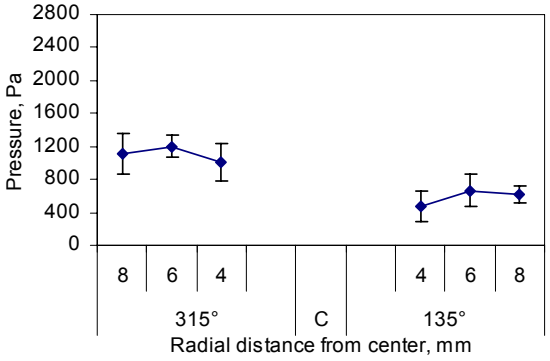

Figure 5.68 Average final pressure values in **135°-315°** orientation of the right toroidal die filled at feed shoe speed of **500 mm/s**

500 mm/s feed shoe speed: At feed shoe speed of 500 mm/s, all of the locations of 0° orientation had significantly higher ($P < 0.05$) final pressure values than locations of 180° orientation, as shown in Figure 5.59. Both 0° and 180° orientations had higher average final pressure values than those of 20 and 100 mm/s.

5.2.2.2 90°-270° orientation

20 mm/s feed shoe speed: Figure 5.60 shows the average final pressure values of 90°-270° orientation at 20 mm/s feed shoe speed. As expected, the distribution was quite symmetrical about the center. No significant difference ($P > 0.05$) was observed among the different locations.

100 mm/s feed shoe speed: At feed shoe speed of 100 mm/s, the final pressure value distribution was also quite symmetrical (Figure 5.61). Except for one comparison, no significant differences were observed, i.e., final pressure value of location (6, 90°) was significantly higher ($P < 0.05$) than that of location (8, 90°). One of the reasons for this trend might be that location (8, 90°) was close to the die wall.

500 mm/s feed shoe speed: Figure 5.62 shows the average final pressure values of 90°-270° orientation at feed shoe speed of 500 mm/s. The final pressure value distribution was symmetrical about the center. No significant difference ($P > 0.05$) was observed among these locations. The average final pressure values of both 90° and 270° orientations were somewhat lower than those of 20 and 100 mm/s.

5.2.2.3 45°-225° orientation

20 mm/s feed shoe speed: As shown in Figure 5.63, all of the locations of 45° orientation had higher average final pressure values than locations of 225° orientation at feed shoe speed of 20 mm/s. Compared to locations along 225° orientation, locations (6, 45°) and (8, 45°) had significantly higher ($P < 0.05$) final pressure values. The possible causes were discussed earlier.

100 mm/s feed shoe speed: Figure 5.64 shows the average final pressure values in 45°-225° orientation at 100 mm/s feed shoe speed. Similar to that of 20 mm/s feed shoe speed, all of the locations of 45° orientation had higher average final pressure values than locations of 225° orientation. Final pressure value of locations (8, 45°) was significantly higher ($P < 0.05$) than those of locations in 225° orientation. At location (6, 45°), final pressure value was significantly higher ($P < 0.05$) than that of (8, 225°).

500 mm/s feed shoe speed: At feed shoe speed of 500 mm/s, all of the locations of 45° orientation had higher average final pressure values than locations of 225° orientation (Figure 5.65). Final pressure values of locations (6, 45°) and (8, 45°) were significantly higher ($P < 0.05$)

than those of locations in 225° orientation. Locations (4, 45°) had final pressure value that was significantly higher ($P < 0.05$) than that of location (4, 225°).

5.2.2.4 135°-315° orientation

20 mm/s feed shoe speed: The final pressure values of 315° orientation were significantly higher ($P < 0.05$) than those of 135° orientation (Figure 5.66). As stated before, the existence of the center post might contribute to this distribution pattern. Another reason could be that the particles in the top region were dragged by the movement of the feed shoe during the backward stroke to somewhere close to the leeward end.

100 mm/s feed shoe speed: Figure 5.67 shows the final pressure values at 100 mm/s along 135°-315° orientation. Except for one comparison, final pressure values of 315° orientation were significantly higher ($P < 0.05$) than those of 135° orientation, i.e., final pressure value of location (4, 315°) was not significantly ($P > 0.05$) higher than that of location (6, 135°).

500 mm/s feed shoe speed: At 500 mm/s feed shoe speed, all the average final pressure values of 315° orientation were higher than those of 135° orientation (Figure 5.68). Some of the differences were statistically significant ($P < 0.05$), such as that final pressure values of locations (8, 315°) and (6, 315°) were significantly higher than that of location (4, 135°), and final pressure value of location (6, 315°) was significantly higher than that of location (8, 135°).

5.2.2.5 Comparison of within-die pressure distribution using contour plots

20 mm/s feed shoe speed: Figure 5.69 shows contour plots of the right toroidal die made by using the final pressures at 20 mm/s. The pressure distribution was quite symmetrical about the center line that was parallel to the feed shoe movement direction. The area close to the leeward end had higher final pressures. The highest final pressures were around 315° orientation.

100 mm/s feed shoe speed: Figure 5.70 shows the distribution of the average final pressure values in the right toroidal die filled at feed shoe speed of 100 mm/s. The overall distribution was very similar to that of 20 mm/s feed shoe speed, except that the highest pressure values were slightly lower than those of 20 mm/s.

500 mm/s feed shoe speed: At 500 mm/s feed shoe speed, the distribution of the average final pressure values in the right toroidal die was very symmetrical about the center line that was parallel to the feed shoe movement direction (Figure 5.71). The zone around 0° orientation (close to the leeward end) had the highest final pressure values, and the area of 0° orientation had higher final pressure values than its surrounding area. The highest final pressure values of 500 mm/s were much higher than those of 20 and 100 mm/s feed shoe speeds.

Generally, the final pressure distributions of the right toroidal die at the three feed shoe speeds were similar to those of the center toroidal die. Potential reasons for these observations were presented in the subsection of the center toroidal die.

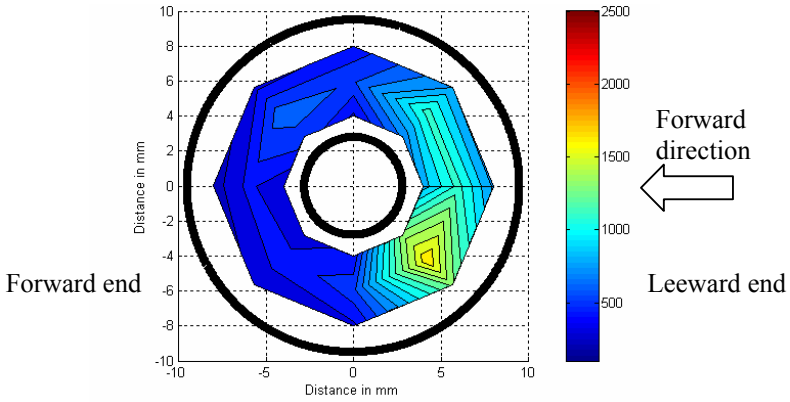

Figure 5.69 Contour plots of the average final pressure value (Pa) distribution in the right toroidal die filled at feed shoe speed of 20 mm/s

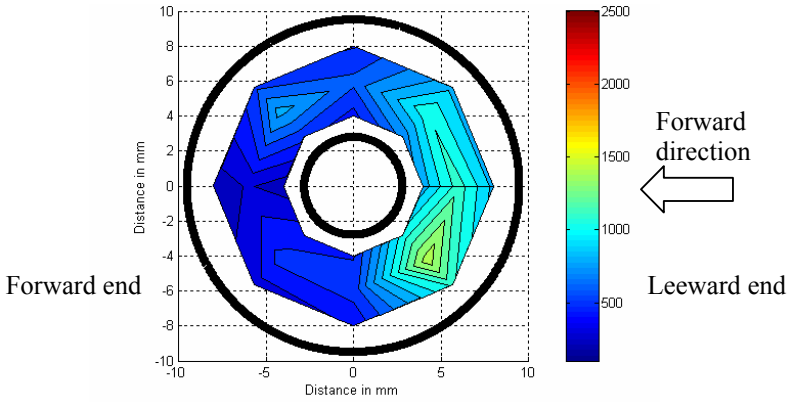

Figure 5.70 Contour plots of the average final pressure value (Pa) distribution in the right toroidal die filled at feed shoe speed of 100 mm/s

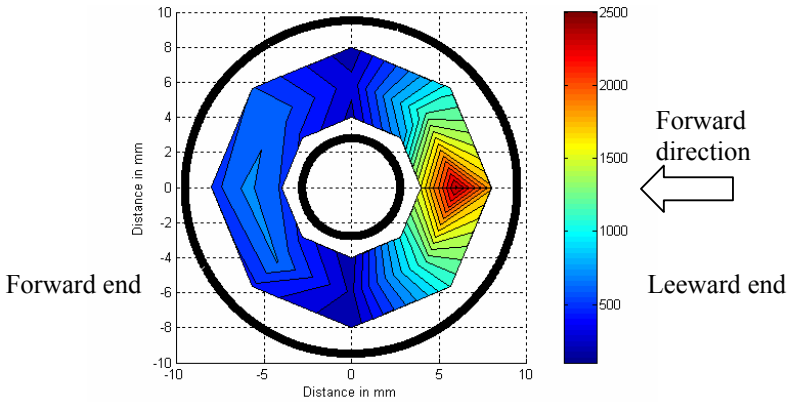

Figure 5.71 Contour plots of the average final pressure value (Pa) distribution in the right toroidal die filled at feed shoe speed of 500 mm/s

5.2.2.6 Comparison of uniformity among the three speeds

Table 5.13 shows some statistical parameters obtained for the right toroidal die at the three feed shoe speeds (20, 100, and 500 mm/s) using the final pressure values. Based on these values, 500 mm/s feed shoe speed, which had the highest (Max-Min)/Mean, Max/Min, StDev (standard deviation), and COV, was inferred to have the most nonuniform filling among the three speeds. 500 mm/s feed shoe speed also resulted in the densest filling, and its Max and Mean final pressure values were the highest. These observations were similar to those of the center toroidal die.

Table 5.13 Comparison of key statistical parameters for the right toroidal die at the three feed shoe speeds using final pressure values (Pa)

Feed shoe speed, mm/s	Max	Min	Mean	(Max-Min)/Mean	Max/Min	StDev	COV (StDev×100/Mean)
20	1739.1	254.2	698.2	2.13	6.84	401.4	57.5
100	1516.6	247.6	701.1	1.81	6.13	334.5	47.7
500	2498.0	215.0	819.3	2.79	11.62	575.9	70.3

5.2.3 Comparison of effects of the three feed shoe speeds

5.2.3.1 Center die

Figure 5.72 shows the comparison of average final pressure values measured at feed shoe speeds of 20 and 100 mm/s. For some locations, the final pressure values were similar for the two feed shoe speeds. For some locations, the lower feed shoe speed resulted in higher pressure values, while the higher feed shoe speed yielded higher pressure values for some other locations. Figure 5.73 was plotted based on the final pressure values at feed shoe speeds of 20 and 500 mm/s. Neither of the two feed shoe speeds had consistently higher or lower final pressure values at all the locations. Figure 5.74 compares final pressure values of 100 and 500 mm/s feed shoe speeds. Except the locations of 0° and 180° orientations that indicated large difference between final pressure values of the two speeds, most of the locations had similar final pressure values.

One-way analysis of variance (ANOVA) (Tukey's method) was used to do multiple comparisons for final pressure values of the same locations at the three different feed shoe speeds. No paired t-test is conducted here, so the previously used Bonferroni and modified Bonferroni procedures are not used here either. The results demonstrated that for most of the locations, there was no significant difference ($P > 0.05$) between 20 and 100 mm/s, with the exception of five locations of 45° and 225° orientations and locations (6, 135°) and (4, 135°). Even for locations having significant differences, neither of the two speeds was indicated to have consistently resulted in higher or lower final pressure values.

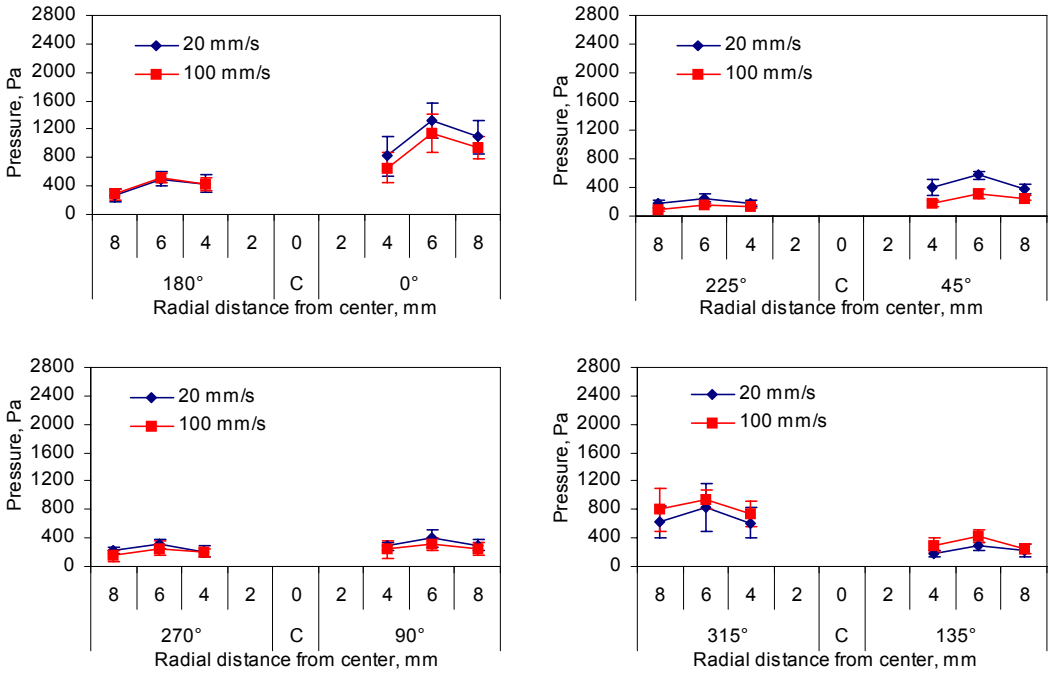

Figure 5.72 Comparison of 20 and 100 mm/s feed shoe speeds (center toroidal die)

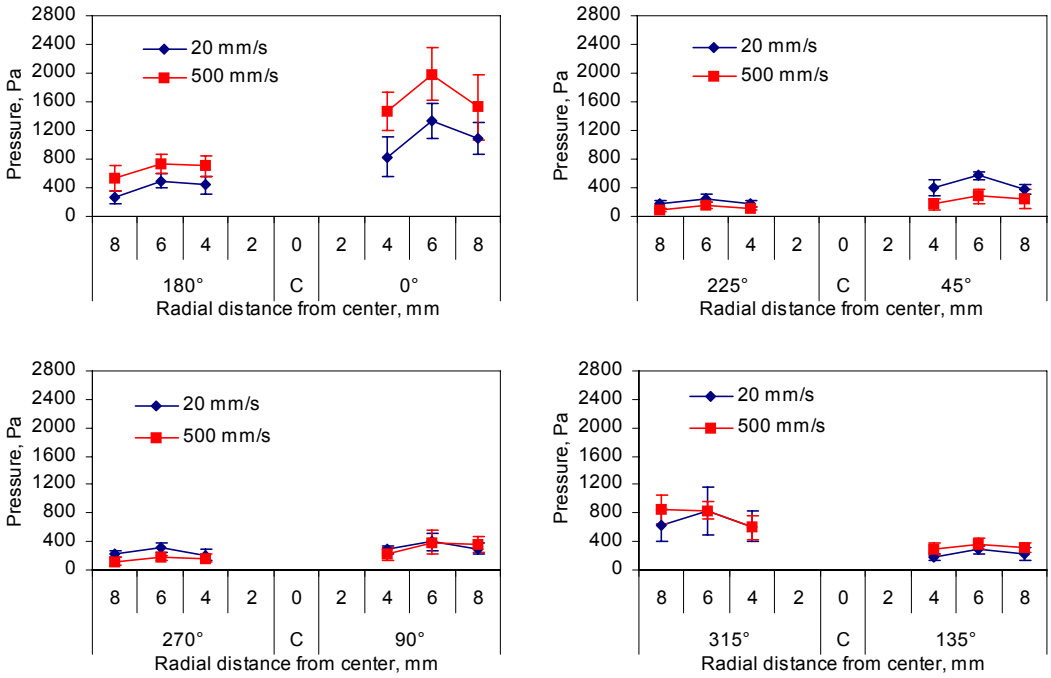

Figure 5.73 Comparison of 20 and 500 mm/s feed shoe speeds (center toroidal die)

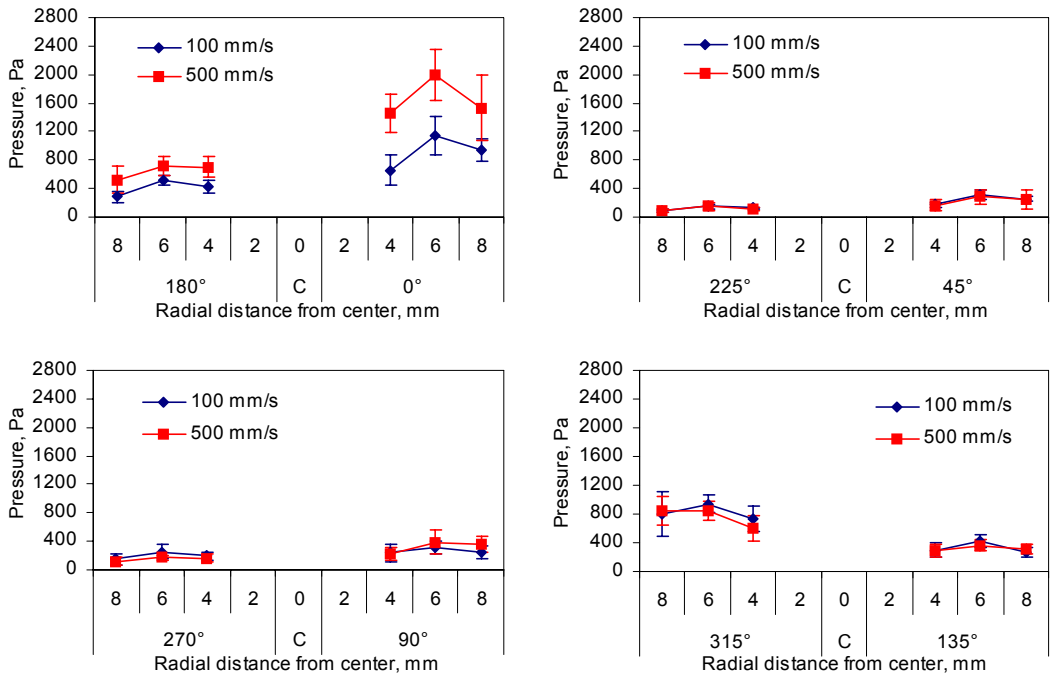

Figure 5.74 Comparison of 100 and 500 mm/s feed shoe speeds (center toroidal die)

For almost all of the locations of 0° and 180° orientations, 500 mm/s feed shoe speed had significantly higher ($P < 0.05$) final pressure values than 20 and 100 mm/s ($P < 0.05$). However, for all of the rest locations, there was no significant difference ($P < 0.05$) between 100 and 500 mm/s feed shoe speeds. More significant differences ($P < 0.05$) between 20 and 500 mm/s were observed at most locations along 45° and 225° orientations (except location (8, 45°)), and two locations along 270° orientations (at r = 6 mm and r = 8 mm).

Unlike the center cylindrical die, where 500 mm/s resulted in significantly higher ($P < 0.05$) final pressure values than 20 and 100 mm/s for all of the locations, deposition in toroidal dies showed limited effect of feed shoe speed on final pressure values at some of the measured locations. As stated before, higher kinetic energy of particles at higher feed shoe speed is expected to densify the powder mass (by collapsing bridges and/or rearranging particles) inside the die (Wu and Cocks, 2004). But the opening of the toroidal dies was much smaller than that of the cylindrical dies, so the effect of higher feed shoe speed was not as pronounced as for the cylindrical dies. For locations along certain orientations, such as 0° and 180°, the highest feed shoe speed (500 mm/s) did result in significant differences. This might be attributed to the fact that in these two orientations, the surrounding wall of the die and the center post was perpendicular to the incoming particles. This helped to bounce back particles more effectively at higher feed shoe speed and promoted denser packing around these areas.

5.2.3.2 Right die

Figure 5.75 compares average final pressure values collected at feed shoe speeds of 20 and 100 mm/s. For most of the locations, the final pressure values were similar for the two feed shoe speeds. Statistical analysis showed that except for one location (8, 135°), there was no significant difference between final pressure values at 20 and 100 mm/s feed shoe speeds ($P > 0.05$). Figure 5.76 shows the average final pressure values at feed shoe speeds of 20 and 500 mm/s. Significant differences were observed at many locations, but the effect of feed shoe speed was not consistent. For instance, the higher speed resulted in significantly higher ($P < 0.05$) final pressure values at locations of 0° and 180° orientations. For locations of 270° orientation, the lower speed caused significantly higher ($P < 0.05$) final pressure values, and it was also true for locations (6, 90°), (4, 315°), and (6, 315°). Figure 5.77 compares average final pressure values at 100 and 500 mm/s feed shoe speeds. Similar observations can be made as for the comparison between 20 and 500 mm/s feed shoe speeds.

5.2.4 Center vs. right dies

20 mm/s feed shoe speed: For most of the measured locations, the right die had higher final pressure values than the center die (Figure 5.78). The exceptions were locations of 180° and 0° orientations, where the center die had similar or even higher final pressure values than the right die. Statistical analyses were conducted to study if there were any differences between the center and the right dies. For a certain location, only two samples needed to be compared, and paired t-test was not appropriate. Thus, two-sample *t*-test (assuming equal variance) was used for corresponding locations of the center and the right dies that of the same radial distances and orientations. For almost all the locations of 45°-225°, 90°-270°, and 135°-315° orientations, final pressure values of the right die were significantly higher than those of the center die ($P < 0.05$). The only exception was location (8, 90°), where the difference was not significant ($P > 0.05$). The differences in the center and right dies might be attributed to the complex flow pattern within the feed shoe tube during simultaneous filling of multiple dies. In addition, the oval cross-section shape of the feed shoe influences the take-off trajectories of powder particles and pressing of powder by the die wall particularly during the backward stroke. This trend was probably also related to the fact that the right die was closer to the (right) side of the feed shoe wall.

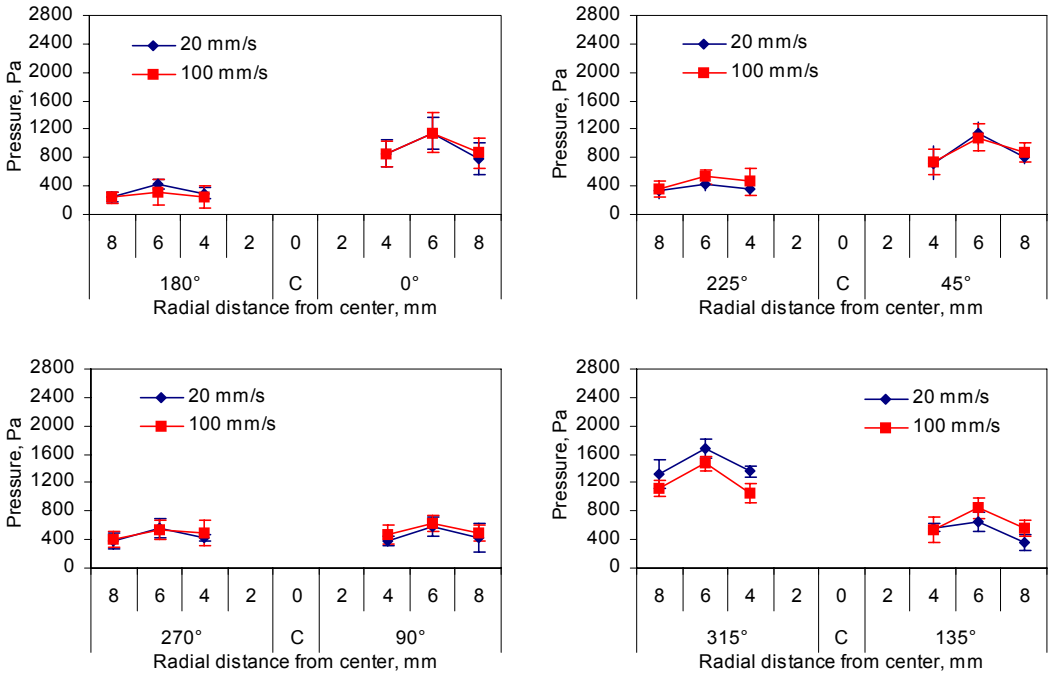

Figure 5.75 Comparison of 20 and 100 mm/s feed shoe speeds (right toroidal die)

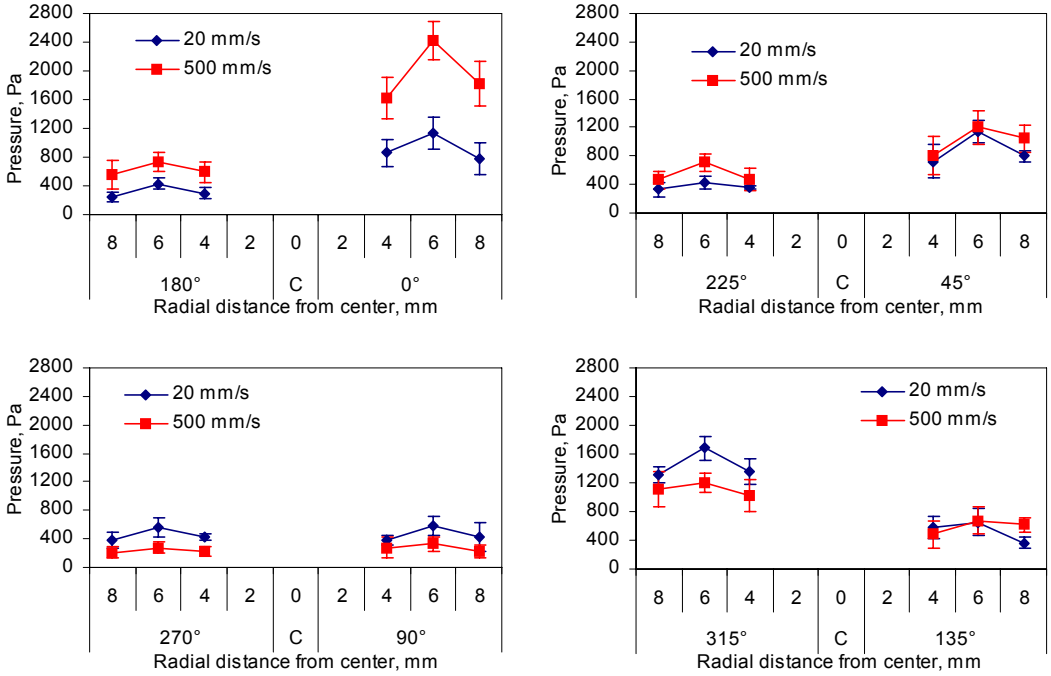

Figure 5.76 Comparison of 20 and 500 mm/s feed shoe speeds (right toroidal die)

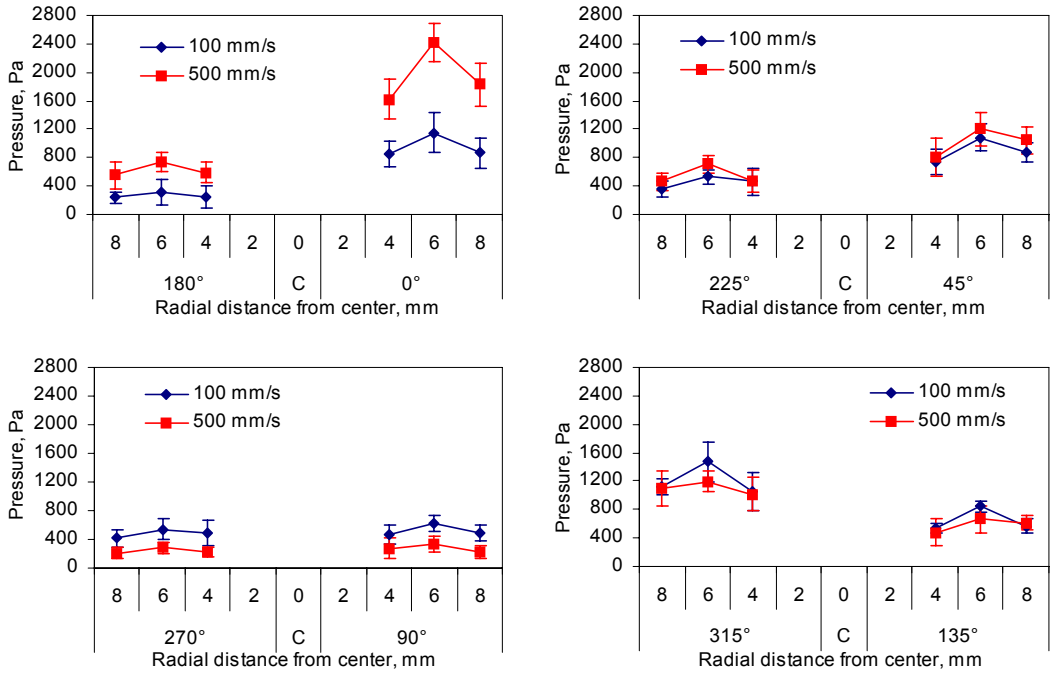

Figure 5.77 Comparison of 100 and 500 mm/s feed shoe speeds (right toroidal die)

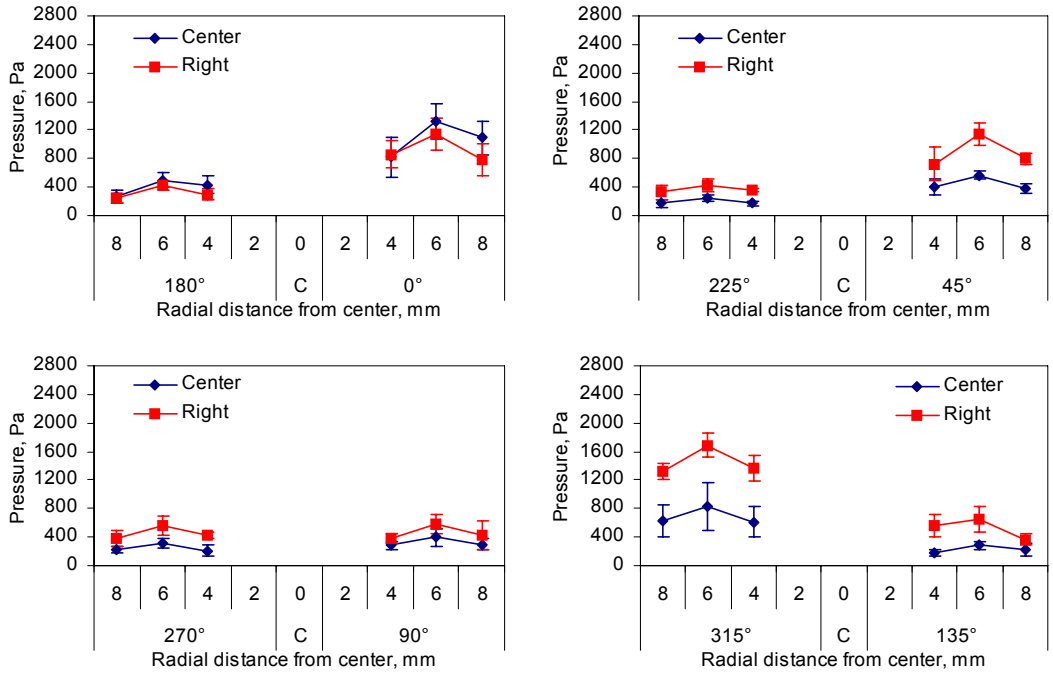

Figure 5.78 Comparison of center and right dies at 20 mm/s feed shoe speed

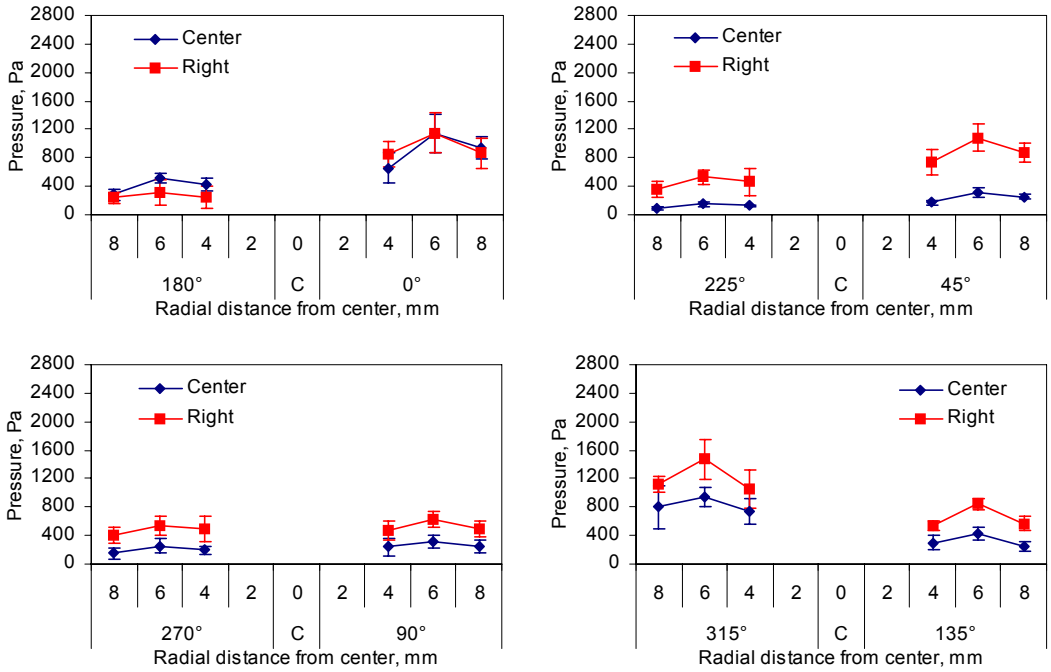

Figure 5.79 Comparison of center and right dies at 100 mm/s feed shoe speed

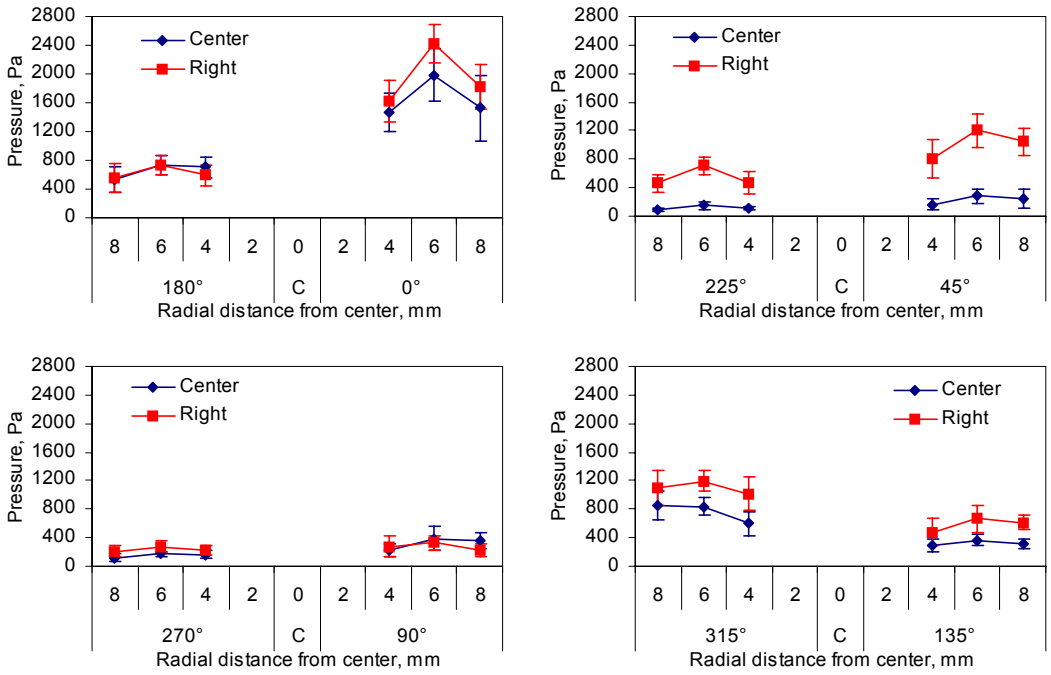

Figure 5.80 Comparison of center and right dies at 500 mm/s feed shoe speed

100 mm/s feed shoe speed: Observations similar to 20 mm/s feed shoe speed can be made (Figure 5.79). The right die had significantly higher ($P < 0.05$) final pressure values in 45°-225°,

90°-270°, and 135°-315° orientations. Only in 0°-180° orientation, the center die had similar or higher final pressure values than the right die.

500 mm/s feed shoe speed: At 500 mm/s feed shoe speed, the right die had higher average final pressure values at most locations, except some locations in 180° and 90° orientations (Figure 5.80). Most of the final pressure values of the right die were significantly higher ($P < 0.05$) than those of the center die in 270°, 45°-225°, and 135°-315° orientations. The quantitative differences between the center and the right dies were reduced with increasing feed shoe speed for the orientation of 90°-270°. But for 45°-225° and 135°-315° orientations, the amount of the differences between the center and the right dies were similar for 100 and 500 mm/s feed shoe speeds. This again demonstrated the complexity and high variation of the deposition process. This was also related to the existence of the center post, which seemed to impact 90°-270° orientation less than other orientations.

5.2.5 Summary

Based on above discussion about toroidal dies filled with the battery powder mixture, the following concluding remarks can be made:

1. The area around 0° orientation (close to the leeward end) had the highest pressure values (1186.7 to 2498.0 Pa). The average pressure values of the remaining area were 353.7 to 648.0 Pa.
2. The pressure distribution was symmetrical about the center line parallel to the feed shoe movement direction.
3. Based on PDT-II data, the highest feed shoe speed (500 mm/s) led to the most nonuniform and the densest filling among the three speeds.
4. Higher feed shoe speed did not always result in higher final pressure values.
5. The right die tended to have higher final pressure values (215.0 to 2498.0 Pa) than the center die (95.4 to 2052.5 Pa). The possible reasons for this trend were the complex powder flow pattern, the oval cross-section shape of the feed shoe, and the relative positions of the two dies to the feed shoe wall.

5.3 E-shaped Dies

Three E-shaped die configuration and dimensions and the dimension of the feed shoe are shown in Figure 5.81. Additional dimensional details of the dies are illustrated in Figure 4.11. The direction of movement of the feed shoe was parallel to the long axis of the ellipse. The three

parallel E-shaped dies were symmetrical about the long axis of the ellipse. Due to time and resource constraints, only one feed shoe speed, 20 mm/s, was used for E-shaped dies.

5.3.1 Within-die comparison of the center die using contour plots

Figure 5.82 shows contour plots of the center E-shaped die made by using the average final pressure values. The pressure distribution was symmetrical about the center line parallel to the feed shoe movement direction. The final pressure values of the middle leg were higher than those of the left and the right legs. This was attributed to the wider opening of the middle leg. The area along the back side had the highest final pressure values. This observation was consistent with the pressure distribution of cylindrical and toroidal dies for the battery powder mixture. This could be explained by the larger opening of the back and the drag effect of the backward movement of the feed shoe. The particles in the top region were dragged by the movement of the feed shoe during the backward stroke, and they moved horizontally to some distance to the back. This was assumed to be especially pronounced for battery powder mixture, with large (210 – 1000 μm) granule size of nonspherical shapes.

5.3.2 Within-die comparison of the right die using contour plots

Figure 5.83 shows the average final pressure values of the right E-shaped die. The pressure distribution was very similar to that of the center die, except that the highest pressure value of the right die were lower than that of the center die. This trend is discussed in detail in section 5.3.3.

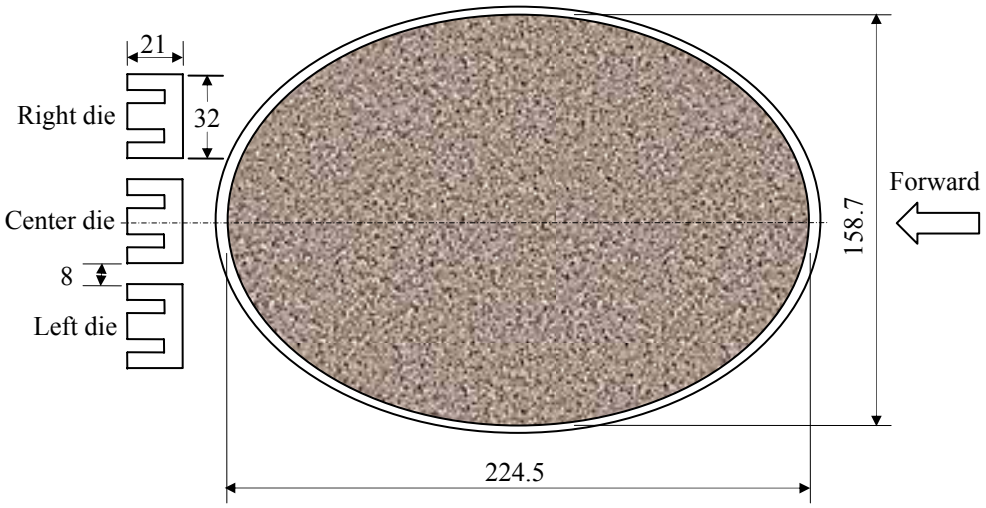

Figure 5.81 Dimensions of the E-shaped dies and the feed shoe cross-section in contact with the table surface (drawn to scale) (unit: mm)

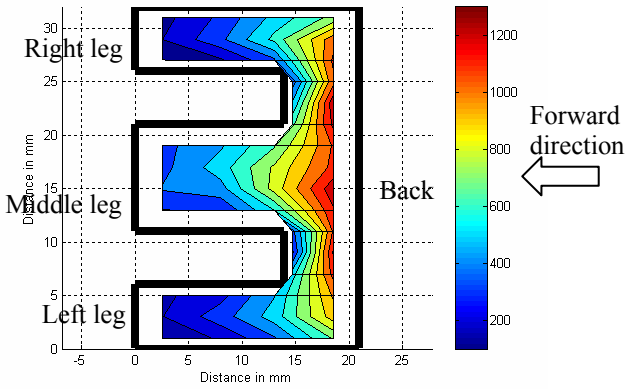

Figure 5.82 Contour plots of the average final pressure value (Pa) distribution in the center E-shaped die filled at feed shoe speed of 20 mm/s

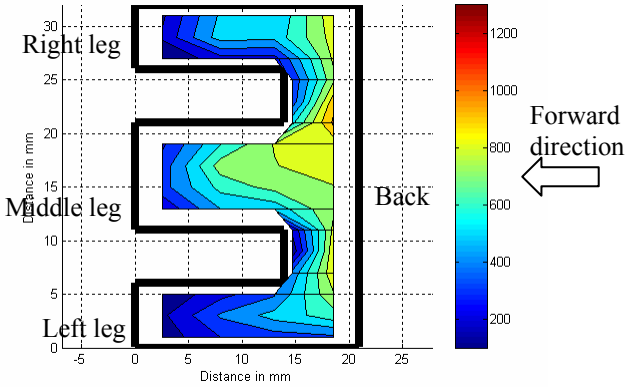

Figure 5.83 Contour plots of the average final pressure value (Pa) distribution in the right E-shaped die filled at feed shoe speed of 20 mm/s

5.3.3 Center vs. right dies

For E-shaped dies, the pressure sensor strip was placed at four locations, L1 to L4, to record pressure increase profile (Figure 5.84). For L1 location, the center and the right dies had similar final pressure values (Figure 5.85 (a)). For L2 location, the right die had higher average final pressure values, and some of the differences were significant ($P < 0.05$), such as pressure values at distances 13, 15, and 17 mm of the middle leg, and 27 and 29 mm of the right leg (Figure 5.84 and Figure 5.85 (b)). Most pressure values of L3 location were similar for the center and right dies (Figure 5.85 (c)). For L4 location, the center die had significantly higher ($P < 0.05$) final pressure values than the right die for almost all of the measured locations (Figure 5.85 (d)), except at distances 31 mm and 21 mm.

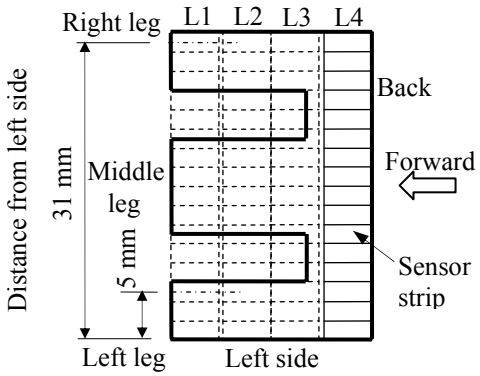

Figure 5.84 Locations of the pressure sensor strip in an E-shaped die (drawn to scale)

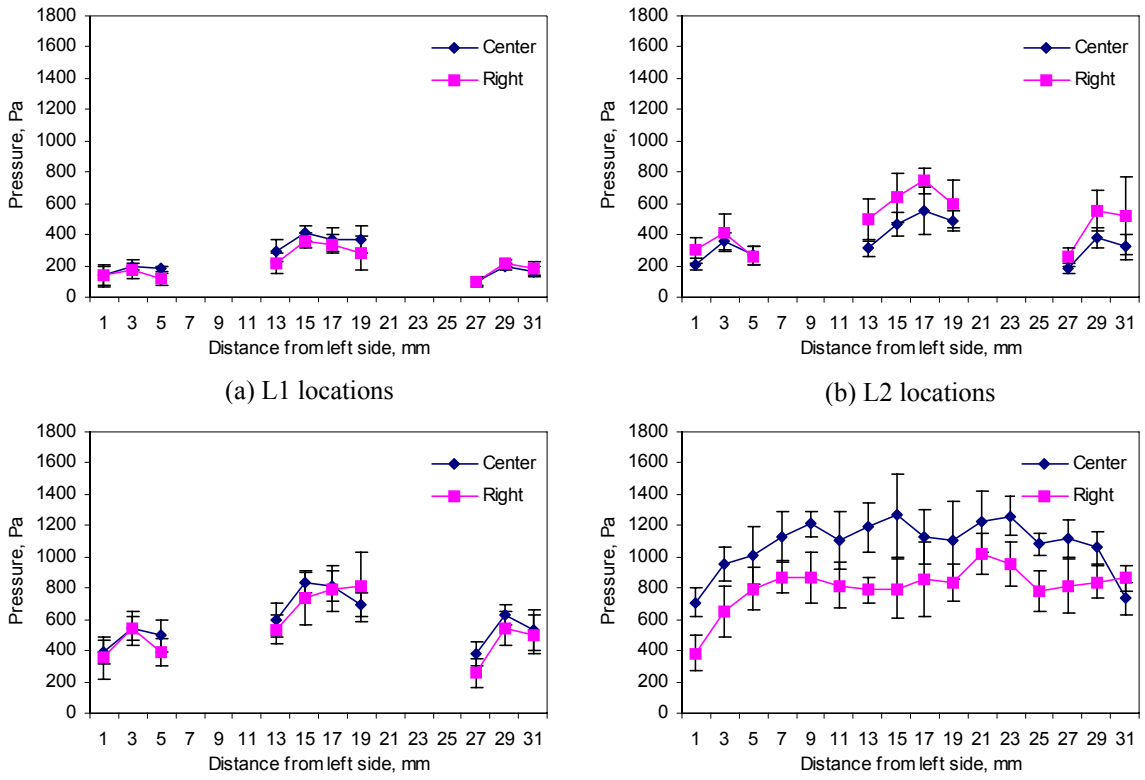

(a) L1 locations

(b) L2 locations

(c) L3 locations

(d) L4 locations

Figure 5.85 Comparison of center and right dies at 20 mm/s feed shoe speed

The elliptical shape of the feed shoe in contact with the table surface was partly responsible for the difference of L4 location. The inner long axis of the ellipse, which coincided with the center E-shaped die, was 224.5 mm; whereas, the inner dimension of the long axis direction that coincided with the right E-shaped die was only 193.9 mm. This difference benefited the center die from longer time of filling and pressure from the powder in the feed shoe. Longer time of filling was more important for the E-shaped dies than for the cylindrical and toroidal dies, since the volume of each E-shaped die (10.3 cm^3) was much larger than those of the cylindrical (5.5 cm^3) and toroidal (5.0 cm^3) dies. The difference of L2 location might be attributed to the

complex flow pattern within the feed shoe tube during simultaneous filling of the three dies. The reason discussed above for L4 location was also considered as one of the factors resulting in the difference of L2 location. Longer time of filling for the center die during the backward stoke also meant longer time for the drag effect. More particles in the center die were dragged from L2 location to L4 or L3 locations during the backward stroke than in the right die. This resulted in higher final pressure values at L2 location of the right die.

5.3.4 Summary

Based on above discussion, the following concluding remarks can be made for E-shaped dies filled with the battery powder mixture:

1. The final pressure values of the middle leg were higher than those of the left and the right legs. The average pressure of the middle leg ranged from 308.9 to 760.7 Pa, and the average pressures of the left and right legs ranged from 148.9 to 530.3 Pa.
2. The area along the back side had the highest final pressure value (1054.6 to 1303.8 Pa).
3. The pressure distribution was symmetrical about the center line parallel to the feed shoe movement direction.
4. Neither the center die, nor the right die always had higher pressure values than the other one.

5.4 Cylindrical vs. Toroidal Dies

5.4.1.1 Center cylindrical vs. center toroidal dies

20 mm/s feed shoe speed: For some of the measured locations, the toroidal die had significantly higher final pressure values ($P < 0.05$) than the cylindrical die, such as locations of 0° and 180° orientations (Figure 5.86). For some other locations, the cylindrical die had significantly higher final pressure values ($P < 0.05$), such as locations of 135° orientation, locations (4, 225°) and (6, 225°), and locations (4, 90°) and (6, 90°). While at the remaining locations, the two dies had similar final pressures. It seemed that neither of the two die shapes would result in consistently higher pressure values than the other.

100 mm/s feed shoe speed: Similar observations could be made when the feed shoe speed was 100 mm/s. At some locations, the toroidal die had significantly higher final pressure values ($P < 0.05$) than the cylindrical die (Figure 5.87). At some other locations, the cylindrical

die had significantly higher final pressure values ($P < 0.05$), such as locations of 225° and 270° orientations. Similar final pressure values were also observed at some locations.

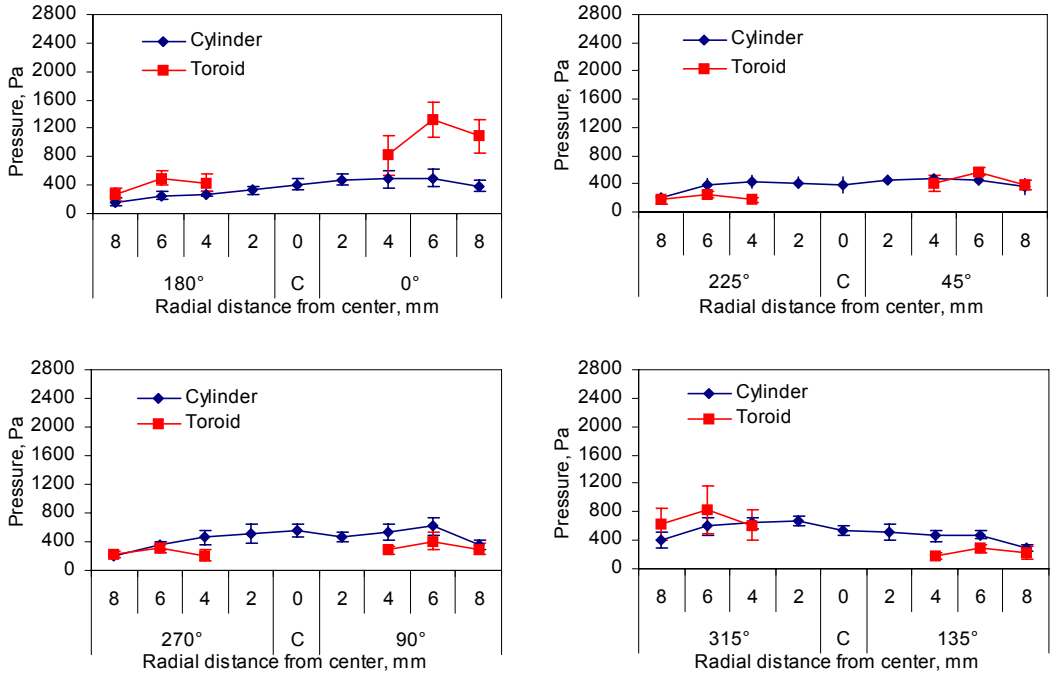

Figure 5.86 Comparison of the center cylindrical and the center toroidal dies at 20 mm/s feed shoe speed

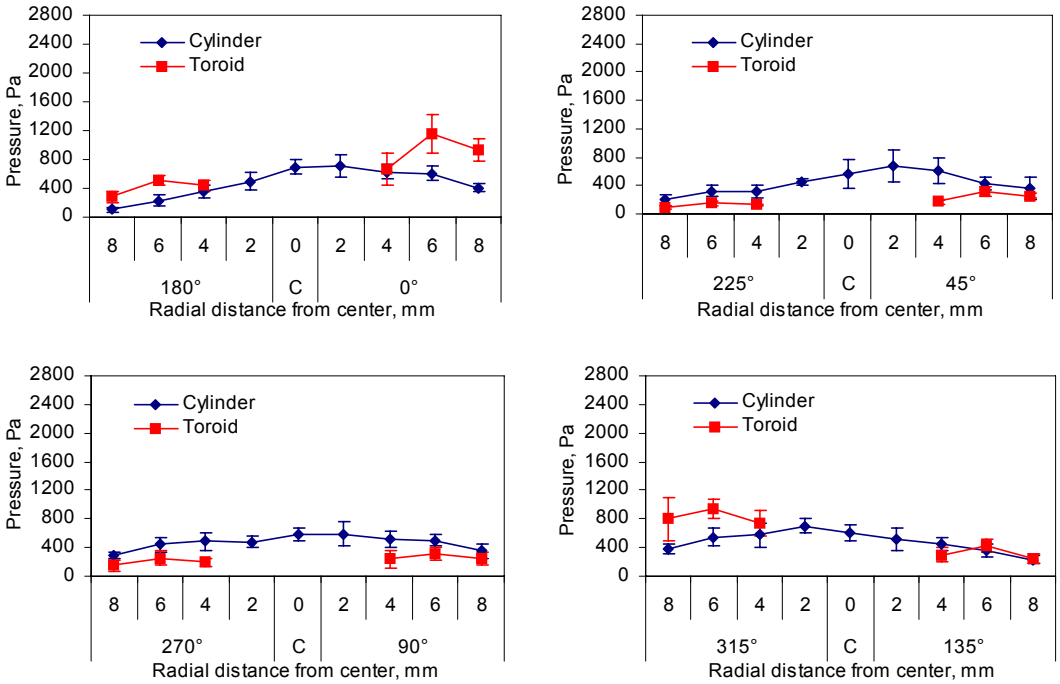

Figure 5.87 Comparison of the center cylindrical and the center toroidal dies at 100 mm/s feed shoe speed

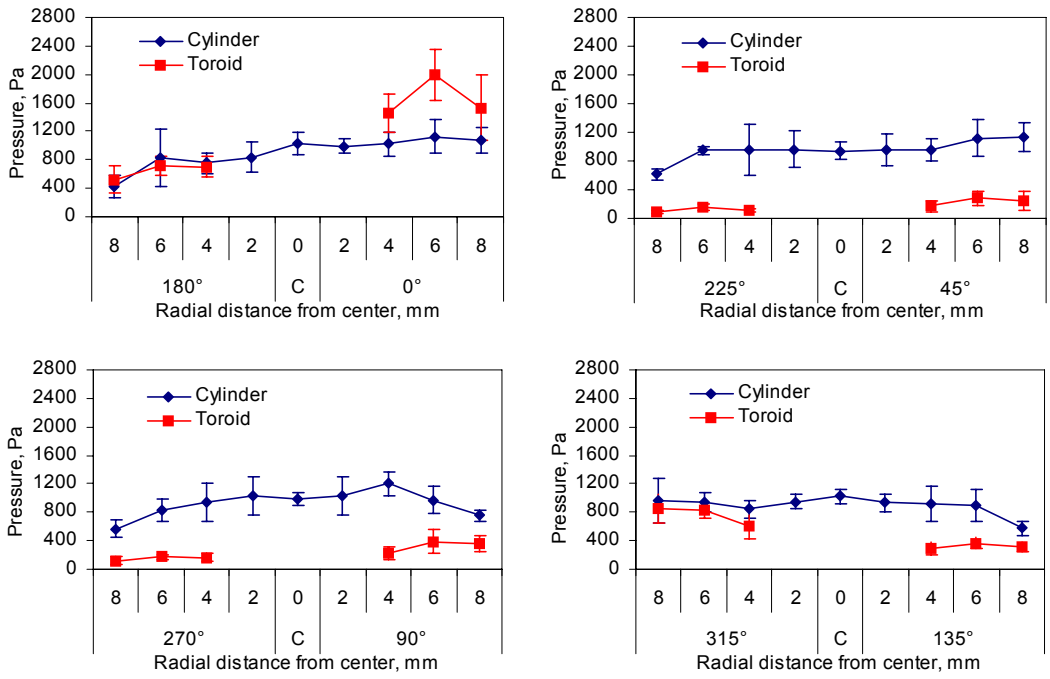

Figure 5.88 Comparison of the center cylindrical and the center toroidal dies at 500 mm/s feed shoe speed

500 mm/s feed shoe speed: At feed shoe speed of 500 mm/s, the cylindrical die had significantly higher final pressure values ($P < 0.05$), with the exception of 0°-180° orientation and locations (6, 315°) and (8, 315°) (Figure 5.88). At locations of 0° orientation, final pressure values of the toroidal die were significantly higher than those of the cylindrical die. As discussed previously, the highest feed shoe speed, 500 mm/s, resulted in significantly higher ($P < 0.05$) final pressure values than 20 and 100 mm/s for most of the measured locations in the cylindrical dies; whereas for the toroidal die, the presence of the center post negated the speed advantage. This contributed mostly to the significant differences observed between the center cylindrical and the center toroidal dies at feed shoe speed of 500 mm/s.

For all the three feed shoe speeds, the toroidal die had higher average final pressure values in 0° orientation. This was caused by the existence of the center post. During the forward stroke of the feed shoe motion, the center post blocked the particles from the feed shoe and bounced them back to the area near the trailing wall vicinity. The particles were packed more densely than the particles of similar location in the cylindrical die. The center post also acted as a lower punch for the particles around 0° orientation to be compressed by the upper punch, the feed shoe wall, in the forward and reverse strokes of the feed shoe motion.

5.4.1.2 Right cylindrical vs. right toroidal dies

20 mm/s feed shoe speed: The observations made for the comparison between the center cylindrical and toroidal dies were also generally true for the comparison of the right cylindrical and toroidal dies (Figure 5.89). Neither the two die shapes resulted in consistently higher pressure values than the other.

100 mm/s feed shoe speed: At some locations, the toroidal die had significantly higher final pressure values ($P < 0.05$) than the cylindrical die; i.e., locations (6, 0°), (8, 0°), (6, 90°), and (8, 90°) (Figure 5.90). For some other locations, the cylindrical die had significantly higher ($P < 0.05$) or similar final pressure values.

500 mm/s feed shoe speed: At 500 mm/s feed shoe speed, the observations were different from those of 20 and 100 mm/s in three major ways (Figure 5.91). One was that in the 90°-270° orientation, final pressure values of the cylindrical die increased substantially, and they were significantly higher ($P < 0.05$) than final pressure values of the toroidal die. The second was that final pressure values of the toroidal die along 0° orientation also increased considerably, and the average final pressure values were higher than those of the cylindrical die, with the differences of two locations being significant ($P < 0.05$). The third was that fewer locations of the toroidal die had higher average final pressure values than the cylindrical die.

For 0° orientation, the right toroidal die consistently had higher average final pressure values than the right cylindrical die for all the three feed shoe speeds. This observation was similar to that of the center cylindrical and the center toroidal dies. The rationale behind this was discussed in preceding sections.

5.4.2 Summary

Based on above comparison between cylindrical and toroidal dies, the following concluding remarks can be made:

1. Neither of the two die shapes (cylinder and toroid) led to consistently higher or lower final pressure values, when filled with the battery powder mixture.
2. For all the three feed shoe speeds, the toroidal die had higher average final pressure values in the 0° orientation.

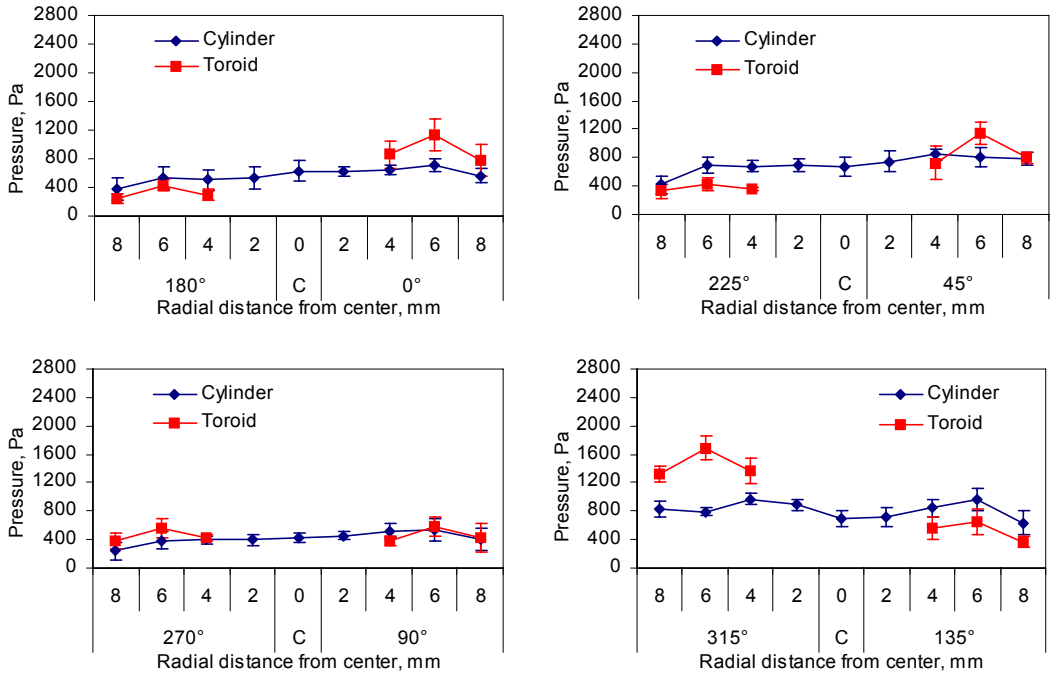

Figure 5.89 Comparison of the right cylindrical and the right toroidal dies at 20 mm/s feed shoe speed

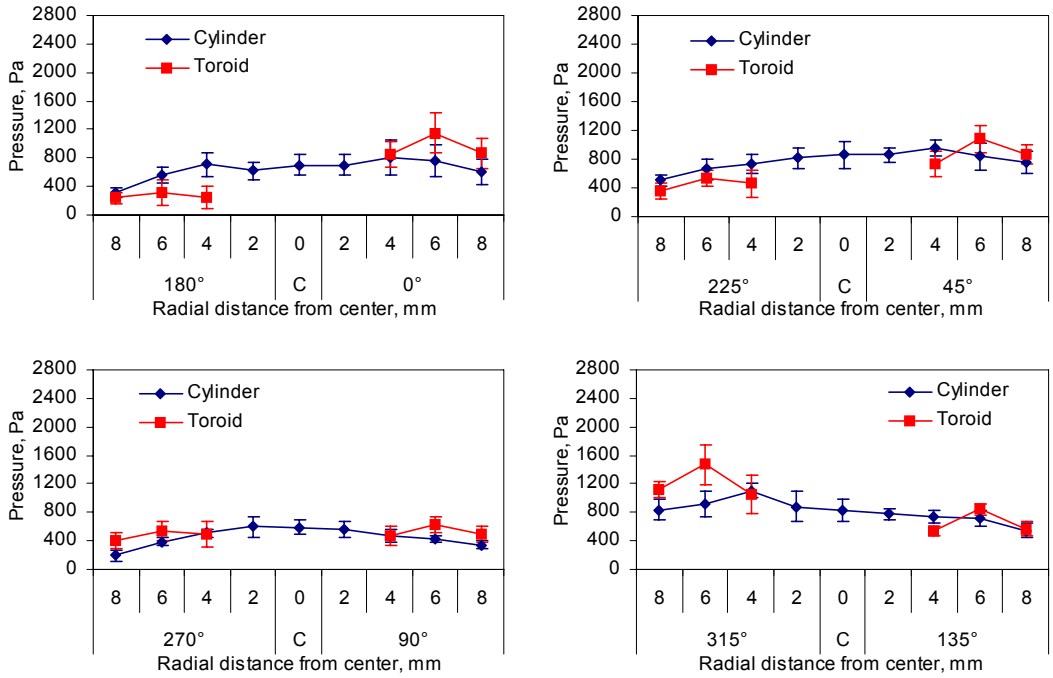

Figure 5.90 Comparison of the right cylindrical and the right toroidal dies at 100 mm/s feed shoe speed

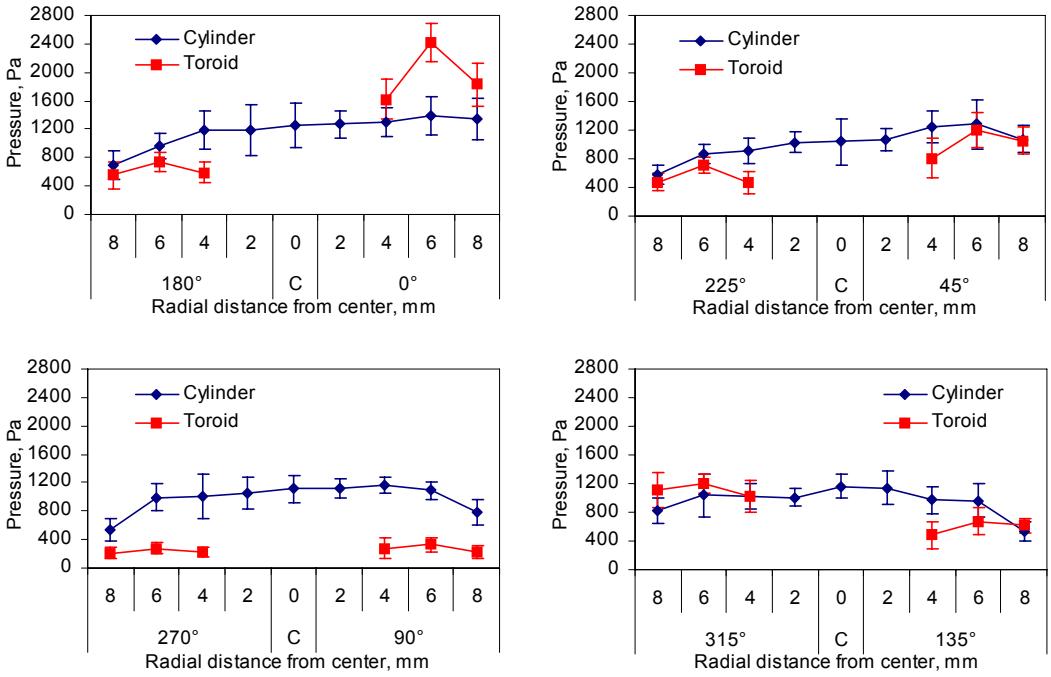

Figure 5.91 Comparison of the right cylindrical and the right toroidal dies at 500 mm/s feed shoe speed

CHAPTER 6 RESULTS OF PDT-II USING ALUMINA POWDER

6.1 Cylindrical Dies

Multiple cylindrical die configuration and dimensions and the dimension of the feed shoe are shown in Figure 5.1. As with the battery powder mixture, the feed shoe (158.7 mm I. D. inclined at 45°) cross-section in contact with the feed shoe table was an ellipse, and the movement direction of the feed shoe was parallel to the long axis of the ellipse. The three parallel cylindrical dies were configured symmetrically about the long axis of the ellipse.

6.1.1 Within-die comparison of the center die

In this section, data collected within each die are analyzed and compared. Prorated final pressure ratios of the center die in 0°-180°, 45°-225°, 90°-270°, and 135°-315° orientations and 20, 100, and 200 mm/s feed shoe speeds are discussed separately. Subsequently, contour plots obtained based on the data of all the four orientations are presented and discussed. The data measured were prorated in the same way as were the battery powder mixture data. Similar statistical analyses (paired t-test and modified Bonferroni procedure) were conducted for alumina powder as well (Chapter 5, section 5.1.1.2). The results of the statistical analysis for alumina powder are given in Appendix C.

6.1.1.1 0°-180° orientation

20 mm/s feed shoe speed: Figure 6.1 shows the average prorated final pressure ratios in the 0°-180° orientation of the center cylindrical die filled at feed shoe speed of 20 mm/s. As explained in the context of battery powder mixture, pressure ratios obtained at locations (8, 180°) and (8, 0°) are not included in the following discussion, especially in statistical analyses. Also, the locations right next to the die wall in other orientations, such as 45°-225°, 90°-270°, and 135°-315°, are not included in discussion below.

As shown in Figure 6.1, the final pressure ratio distribution was quite symmetrical, with pressure ratios decreasing with increasing radii. The highest pressure ratio was next to the center (at location (2, 180°)). Statistical analysis showed that final pressure ratio at location (6, 180°) was significantly lower than those of locations (4, 180°), (2, 180°), the center, and (2, 0°) ($P < 0.05$). Final pressure ratios of location (6, 0°) were significantly lower than those of locations (2,

180°), the center, and (2, 0°) ($P < 0.05$). Compared to location (2, 0°), the final pressure ratio at location (4, 0°) was significantly lower ($P < 0.05$).

100 mm/s feed shoe speed: Figure 6.2 shows the prorated final pressure ratios of 0°-180° orientation collected at feed shoe speed of 100 mm/s. The distribution was quite symmetrical, with pressure ratios decreasing with increasing radii. The highest pressure ratio occurred at the center. Statistical analysis showed that final pressure ratio at location (6, 180°) was significantly lower than those of locations (4, 180°), (2, 180°), the center, (2, 0°), and (4, 0°) ($P < 0.05$). Correspondingly, final pressure ratio at location (6, 0°) was also significantly lower ($P < 0.05$) than those of locations (4, 0°), (2, 0°), the center, and (2, 180°). At location (4, 180°), the final pressure ratio was significantly lower ($P < 0.05$) than those of locations (2, 180°) and the center. The center final pressure ratio was significantly higher ($P < 0.05$) than those of locations (2, 0°) and (4, 0°).

200 mm/s feed shoe speed: Compared with data of 20 and 100 mm/s feed shoe speeds, final pressure ratios of 200 mm/s feed shoe speed had two major differences (Figure 6.3). First, the standard deviations of final pressure ratios of 200 mm/s were obviously much larger than those of 20 and 100 mm/s. Second, the final pressure distribution of 200 mm/s was not as symmetrical as those of 20 and 100 mm/s. No significant difference was observed among final pressure ratios of different locations ($P > 0.05$). It seems that the highest feed shoe speed, 200 mm/s, resulted in larger variation among different replicates of the same treatment. This may be explained by the interaction between the air in the die and the incoming particles from the feed shoe. Compared with the battery powder mixture (d_{50} = 600 μm and bulk density = 1.65 g/cm^3), the alumina powder had finer granules (d_{50} = 95 μm) and lower bulk density (0.83 g/cm^3), both of which increased the potential for the air in the die and the air surrounding the particles to play a more important role during the deposition process. Because of the complex outflow pattern of the air, the deposition was more difficult to predict and mass of powder deposited at different locations was not as systematic as at lower feed shoe speeds, where the air effect was not nearly as pronounced.

6.1.1.2 90°-270° orientation

20 mm/s feed shoe speed: Pressure ratio distribution along 90°-270° direction was symmetrical as expected (Figure 6.4). Statistical analysis indicated that final pressure ratio at location (6, 270°) was significantly lower ($P < 0.05$) than those of locations (4, 270°), the center, and (2, 90°). The final pressure ratio at location (6, 90°) was significantly lower ($P < 0.05$) than those of locations (4, 90°), (2, 90°), and the center.

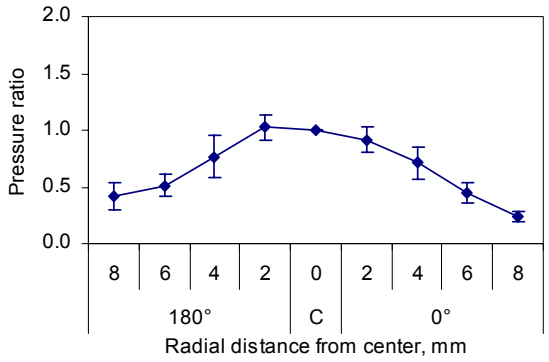

Figure 6.1 Prorated average final pressure ratios in **0°-180°** orientation of the center cylindrical die filled at feed shoe speed of **20 mm/s**

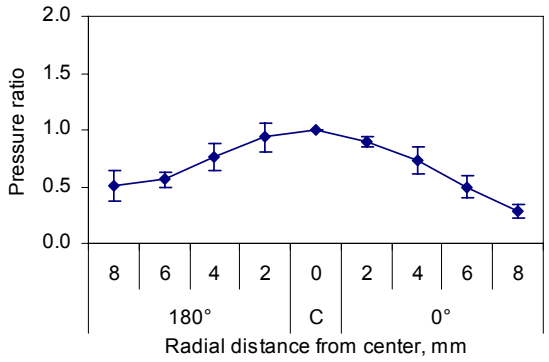

Figure 6.2 Prorated average final pressure ratios in **0°-180°** orientation of the center cylindrical die filled at feed shoe speed of **100 mm/s**

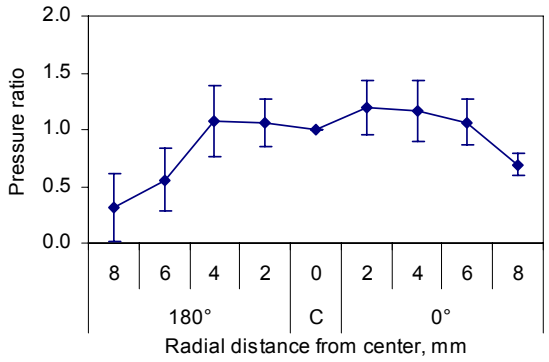

Figure 6.3 Prorated average final pressure ratios in **0°-180°** orientation of the center cylindrical die filled at feed shoe speed of **200 mm/s**

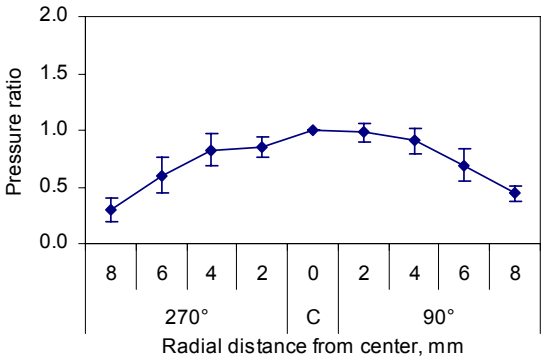

Figure 6.4 Prorated average final pressure ratios in **90°-270°** orientation of the center cylindrical die filled at feed shoe speed of **20 mm/s**

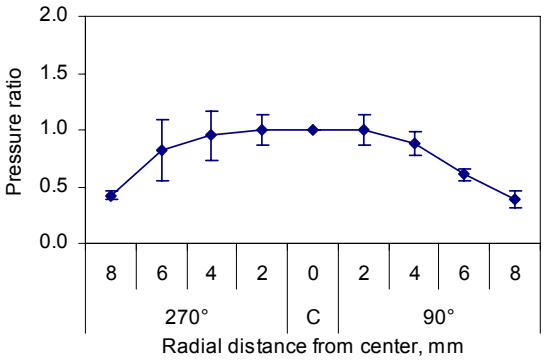

Figure 6.5 Prorated average final pressure ratios in **90°-270°** orientation of the center cylindrical die filled at feed shoe speed of **100 mm/s**

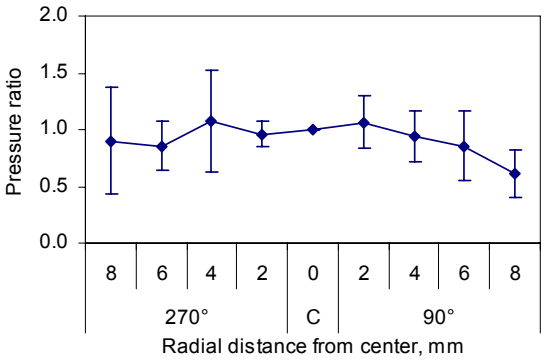

Figure 6.6 Prorated average final pressure ratios in **90°-270°** orientation of the center cylindrical die filled at feed shoe speed of **200 mm/s**

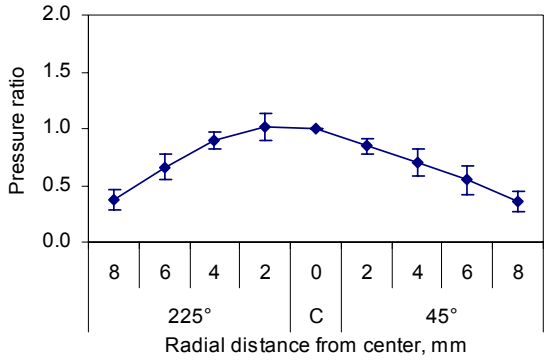

Figure 6.7 Prorated average final pressure ratios in **45°-225°** orientation of the center cylindrical die filled at feed shoe speed of **20 mm/s**

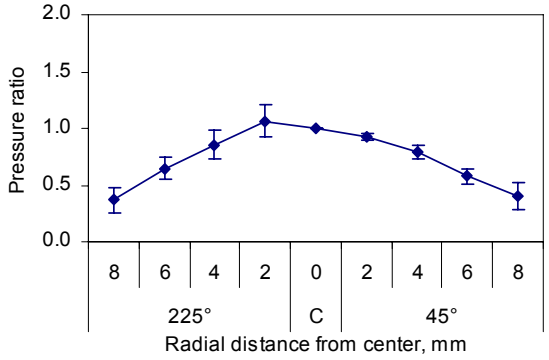

Figure 6.8 Prorated average final pressure ratios in **45°-225°** orientation of the center cylindrical die filled at feed shoe speed of **100 mm/s**

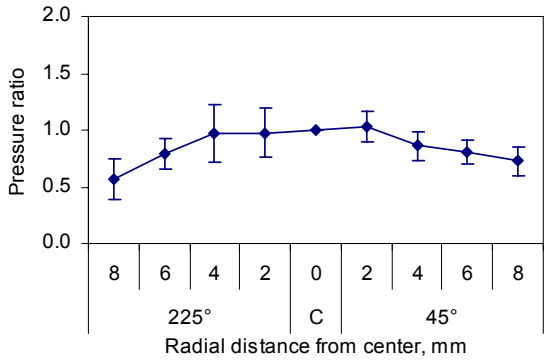

Figure 6.9 Prorated average final pressure ratios in **45°-225°** orientation of the center cylindrical die filled at feed shoe speed of **200 mm/s**

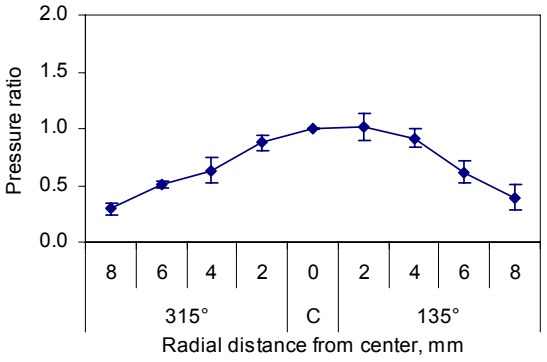

Figure 6.10 Prorated average final pressure ratios in **135°-315°** orientation of the center cylindrical die filled at feed shoe speed of **20 mm/s**

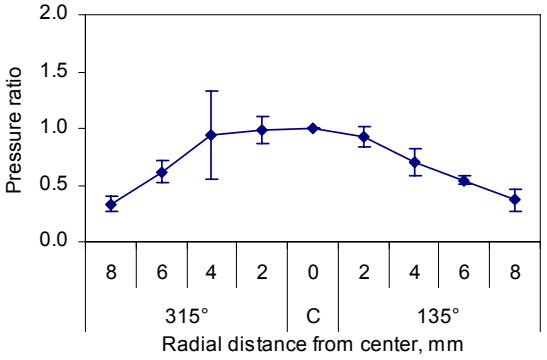

Figure 6.11 Prorated average final pressure ratios in **135°-315°** orientation of the center cylindrical die filled at feed shoe speed of **100 mm/s**

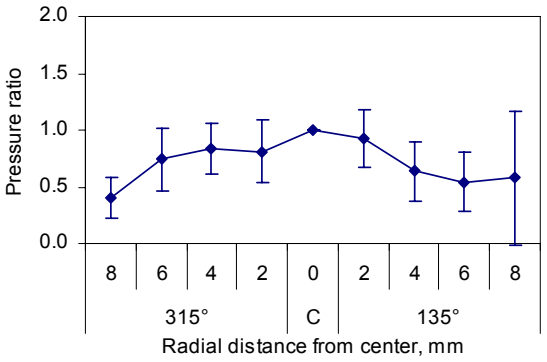

Figure 6.12 Prorated average final pressure ratios in **135°-315°** orientation of the center cylindrical die filled at feed shoe speed of **200 mm/s**

100 mm/s feed shoe speed: The distribution along 90°-270° orientation at feed shoe speed of 100 mm/s was symmetrical about the center as expected (Figure 6.5). Pressure ratios were almost uniformly distributed around the center, from location (6, 270°) to location (4, 90°). Only pressure ratio of location (6, 90°) was significantly lower than those of locations (4, 90°), (2, 90°), the center, and (2, 270°) ($P < 0.05$).

200 mm/s feed shoe speed: Similar to final pressure ratios of 0°-180° orientation at 200 mm/s, the final pressure ratios of 200 mm/s feed shoe speed of 90°-270° orientation also had two major features (Figure 6.6). The standard deviations of final pressure ratios of 200 mm/s were much larger than those of 20 and 100 mm/s, and the final pressure ratio distribution of 200 mm/s was not as symmetrical as those of 20 and 100 mm/s. There was no significant difference observed among final pressure ratios of different locations, except that pressure ratios of location (6, 270°) was significantly lower than that of location (2, 90°) ($P < 0.05$).

6.1.1.3 45°-225° orientation

20 mm/s feed shoe speed: Pressure distribution along 45°-225° orientation was quite symmetrical, with pressure ratios decreasing with increasing radii (Figure 6.7). The final pressure ratio at location (6, 225°) was significantly lower ($P < 0.05$) than those of locations (4, 225°), (2, 225°), and the center. At location (6, 45°), the final pressure ratio was significantly lower ($P < 0.05$) than those of locations (4, 225°), (2, 225°), and the center. Compared to locations (2, 225°) and (4, 225°), the final pressure ratio at the center was significantly higher.

100 mm/s feed shoe speed: Pressure distribution at 100 mm/s was quite symmetrical and very similar to that of 20 mm/s feed shoe speed (Figure 6.8). Location (6, 225°) had final pressure ratio that was significantly lower ($P < 0.05$) than those of locations (4, 225°), (2, 225°), the center, and (2, 45°). Consequently, the final pressure ratio at location (6, 45°) was significantly lower ($P < 0.05$) than those of locations (4, 45°), (2, 45°), the center, and (2, 225°). The final pressure ratio at the center was also significantly higher ($P < 0.05$) than those of locations (2, 45°) and (4, 45°).

200 mm/s feed shoe speed: At the highest feed shoe speed, 200 mm/s, final pressure ratios were more uniformly distributed along 45°-225° orientation (Figure 6.9) than those of 20 and 100 mm/s. Again, the standard deviations of final pressure ratios of 200 mm/s were larger than those of 20 and 100 mm/s. No significant difference ($P > 0.05$) was observed among final pressure ratios of different locations.

6.1.1.4 135°-315° orientation

20 mm/s feed shoe speed: Pressure ratio distribution along 135°-315° orientation was quite symmetrical, and pressure ratios decreased with increasing radii (Figure 6.10). The final pressure ratios at both locations (6, 315°) and (4, 315°) were significantly lower ($P < 0.05$) than those of locations (2, 315°), the center, (2, 135°), and (4, 135°). At location (6, 135°), the final pressure ratio was significantly lower ($P < 0.05$) than those of locations (4, 135°), (2, 135°), the center, and (2, 315°).

100 mm/s feed shoe speed: Pressure distribution at 100 mm/s was also quite symmetrical (Figure 6.11). The final pressure ratio at location (6, 315°) was significantly lower ($P < 0.05$) than those of locations (2, 315°), the center, and (2, 135°). Correspondingly, the final pressure ratio at location (6, 135°) was significantly lower ($P < 0.05$) than those of locations (2, 135°), the center, and (2, 315°). Location (4, 135°) final pressure ratio was significantly lower ($P < 0.05$) than those of location (2, 135°) and the center.

200 mm/s feed shoe speed: At feed shoe speed of 200 mm/s, the final pressure ratio pattern along 135°-315° orientation (Figure 6.12) was erratic. Again, the standard deviations of final pressure ratios of 200 mm/s were much larger than those of 20 and 100 mm/s. Except for one comparison, no significant differences were observed, i.e., final pressure ratio at location (6, 135°) was significantly lower than that of location (2, 135°) ($P < 0.05$).

6.1.1.5 Comparison of within-die pressure distribution using contour plots

To get a fuller appreciation of within-die pressure distribution, contour plots were drawn for the prorated final pressure ratios of all the four orientations. They are presented in the increasing order of the feed shoe speeds, i.e., 20, 100, and 200 mm/s.

20 mm/s feed shoe speed: Figure 6.13 shows contour plots of the center cylindrical die at feed shoe speed of 20 mm/s. Pressure distribution was symmetrical about the center line that was parallel to the feed shoe movement direction; i.e., 0°-180° orientation. The highest pressure ratios occurred close to the center zone, with the center of highest ratio region moved slightly away from the center of the die. In all of the orientations, final pressure ratios decreased monotonically with increasing radii.

100 mm/s feed shoe speed: Figure 6.14 shows the distribution of prorated average final pressure ratios in the center cylindrical die at feed shoe speed of 100 mm/s. Similar to 20 mm/s, the center region had the highest pressure ratios. Pressure ratio distribution was symmetrical about both 0°-180° and 90°-270° orientations. In all of the orientations, final pressure ratios decreased monotonically with increasing radii.

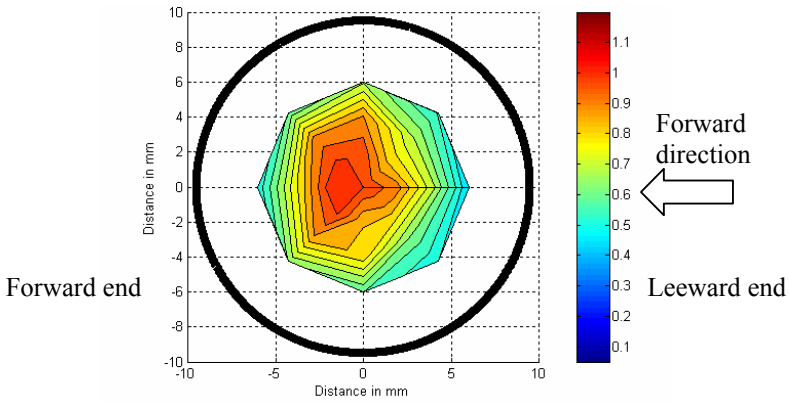

Figure 6.13 Contour plots of the distribution of prorated average final pressure ratios in the center cylindrical die filled at feed shoe speed of 20 mm/s

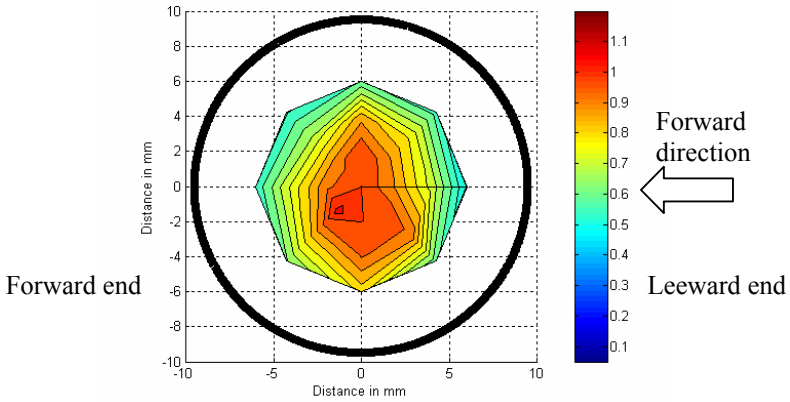

Figure 6.14 Contour plots of the distribution of prorated average final pressure ratios in the center cylindrical die filled at feed shoe speed of 100 mm/s

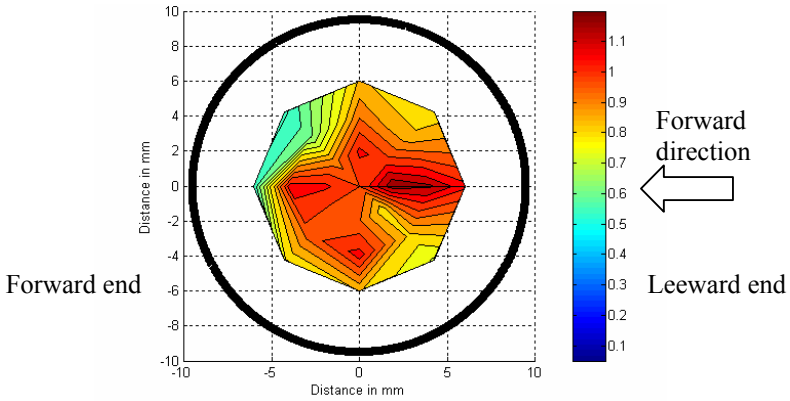

Figure 6.15 Contour plots of the distribution of prorated average final pressure ratios in the center cylindrical die filled at feed shoe speed of 200 mm/s

Different from the pressure ratio distributions of battery powder mixture, the half circle close to the leeward end did not have higher pressure ratios at either 20 or 100 mm/s feed shoe speeds. The backward stroke of the feed shoe movement did not contribute much to dragging of particles toward the leeward end. The most important reason for this might be that the particle

size of alumina powder was smaller than that of battery powder mixture, and the shape of alumina particles were also much more spherical. Both of these minimized the rolling, dragging, and sliding effects that contributed to pressure redistribution for the battery powder mixture during the backward stroke (Kondoh and Takemoto, 1996).

200 mm/s feed shoe speed: Figure 6.15 shows the distribution of prorated average final pressure ratios in the center cylindrical die filled at feed shoe speed of 200 mm/s. Unlike 20 and 100 mm/s feed shoe speeds, the highest pressure ratios were not located around the center area. The highest pressure ratios were near the 45° orientation. Orientations of 90°, 180°, and 270° also had relatively high final pressure ratios. Generally the pressure ratio distribution was very different from those of 20 and 100 mm/s feed shoe speeds. The major reason was that at the highest feed shoe speed (200 mm/s), the air in the die and the air surrounding the incoming particles played a more important role. Because of the undefined and random movement of the air currents, the deposition was not as systematic as at lower feed shoe speeds. The air currents at 200 mm/s feed shoe speed also prevented the formation of the heap of high pressure ratios around the center region, which was common for both 20 and 100 mm/s feed shoe speeds.

6.1.1.6 Comparison of uniformity among the three speeds

Table 6.1 shows some statistical parameters obtained for the center cylindrical die at the three feed shoe speeds (20, 100, and 200 mm/s) using the prorated final pressure ratios. Based on these parameters, it is not straightforward to predict which speed resulted in more uniform filling. The feed shoe speed of 200 mm/s had the lowest StDev (standard deviation) and COV, but its (Max-Min)/Mean and Max/Min were not the smallest.

Table 6.1 Comparison of key statistical parameters for the center cylindrical die at the three feed shoe speeds using prorated final pressure ratios

Feed shoe speed, mm/s	Max	Min	Mean	(Max-Min)/Mean	Max/Min	StDev	COV (StDev×100/Mean)
20	1.02	0.45	0.80	0.71	2.27	0.18	22.7
100	1.07	0.50	0.83	0.69	2.14	0.17	20.8
200	1.20	0.54	0.92	0.71	2.21	0.17	17.9

6.1.2 Within-die comparison of the right die

In this section, data collected for the right die are analyzed and compared to study and evaluate within die uniformity of filled dies. Prorated final pressure ratios of the right die in 0°-180°, 45°-225°, 90°-270°, and 135°-315° orientations and 20, 100, and 200 mm/s feed shoe

speeds are discussed separately. Subsequently, contour plots based on the data of all the four orientations are discussed. The results of statistical analysis are given in Appendix C.

6.1.2.1 0°-180° orientation

20 mm/s feed shoe speed: Figure 6.16 shows the average prorated final pressure ratios in the 0°-180° orientation of the right cylindrical die filled at feed shoe speed of 20 mm/s. The final pressure distribution was not very symmetrical, with the highest pressure ratio being next to the center at location (2, 180°). Generally, pressure ratios decreased with increasing radii, except there was a noticeable sharp rise at location (8, 180°). This may have been contributed by fine particles that got into the gap (0.23 mm) between the die plate and the pressure sensor. This made the die plate and even the feed shoe above the die plate contribute to the pressure ratios collected by the pressure sensor at location (6, 180°), which was close to the die wall. Statistical analysis showed that final pressure ratio at location (6, 0°) was significantly lower than those of locations (4, 0°), (2, 0°), the center, and (2, 180°) ($P < 0.05$). Final pressure ratio at location (4, 0°) was significantly lower ($P < 0.05$) than that of location (2, 180°). Location (4, 180°) had final pressure ratio that was significantly lower ($P < 0.05$) than those of locations (2, 180°) and the center. Compared to location (2, 180°), location (6, 180°) had significantly lower ($P < 0.05$) final pressure ratio.

100 mm/s feed shoe speed: Figure 6.17 shows the prorated final pressure ratios of 0°-180° orientation collected at feed shoe speed of 100 mm/s. Similar to 20 mm/s, pressure ratios decreased with increasing radii, but there was also a noticeable sharp rise at location (8, 180°). Not including location (8, 180°), the distribution was quite symmetrical, and the highest pressure ratio occurred at the center. Final pressure ratio at location (6, 180°) was significantly lower than those of locations (2, 180°), the center, (2, 0°), and (4, 0°) ($P < 0.05$). Correspondingly, final pressure ratio at location (6, 0°) was significantly lower ($P < 0.05$) than those of locations (4, 0°), (2, 0°), the center, and (2, 180°). At location (4, 180°), final pressure ratio was significantly lower ($P < 0.05$) than those of locations (2, 0°) and the center. Final pressure ratio at location (4, 0°) was also significantly lower ($P < 0.05$) than those of locations (2, 0°) and the center.

200 mm/s feed shoe speed: Final pressure ratio distribution of 200 mm/s feed shoe speed was not quite symmetrical (Figure 6.18). The pressure ratio distribution was more uniform than those of 20 and 100 mm/s. Final pressure ratio of location (6, 180°) was significantly lower than those of locations (2, 180°), the center, (2, 0°), (4, 0°), and (6, 0°) ($P < 0.05$). The highest feed shoe speed, 200 mm/s, did not result in larger variation among different replicates as was observed for the center die. Because of the relatively small standard deviations of final pressure

ratios, final pressure ratio of location (6, 0°) was significantly lower than that of location (2, 180°), even though their average final pressure ratios were close (0.903 and 1.029, respectively). Partly because of this reason, final pressure ratio of location (4, 180°) was significantly lower than that of location (2, 180°) ($P < 0.05$). The deposition of the right die at 200 mm/s was more repeatable than that of the center die at 200 mm/s. The effect of the interaction between the air in the die and the incoming particles from the feed shoe was not as pronounced for the right die as for the center die.

6.1.2.2 90°-270° orientation

20 mm/s feed shoe speed: Pressure ratio distribution along 90°-270° direction was quite symmetrical as expected (Figure 6.19). The highest final pressure ratio was at the center location, and pressure ratios decreased with increasing radii. The final pressure ratio at location (6, 270°) was significantly lower ($P < 0.05$) than those of locations (4, 270°), (2, 270°), the center, (2, 90°), and (4, 90°). Location (6, 90°) had final pressure ratio that was significantly lower ($P < 0.05$) than those of locations (2, 90°), the center, and (2, 270°). Compared to locations (2, 270°), the center, and (2, 90°), location (4, 270°) had significantly lower ($P < 0.05$) final pressure ratio. The final pressure ratio of location (2, 270°) was significantly lower ($P < 0.05$) than that of the center.

100 mm/s feed shoe speed: Final pressure ratio distribution along 90°-270° orientation at feed shoe speed of 100 mm/s was somewhat symmetrical about the center (Figure 6.20), except that final pressure ratio of location (6, 270°) was higher than expected. Location (4, 270°) had final pressure ratio that was significantly lower ($P < 0.05$) than that of location (2, 90°). At location (4, 90°), the final pressure ratio was significantly lower ($P < 0.05$) than that of locations (2, 90°).

200 mm/s feed shoe speed: Final pressure ratios at 200 mm/s feed shoe speed were symmetrical about the center, and more uniformly distributed than 20 and 100 mm/s (Figure 6.21). Similar to final pressure ratios of 0°-180° orientation at 200 mm/s, the standard deviations were close to those of 20 and 100 mm/s. The final pressure ratio of location (6, 270°) was significantly lower ($P < 0.05$) than those of locations (2, 270°), the center, and (2, 90°). Location (6, 90°) had final pressure ratio that was significantly lower ($P < 0.05$) than location (4, 90°).

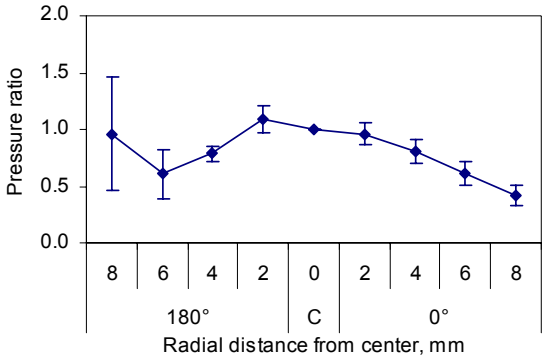

Figure 6.16 Prorated average final pressure ratios in **0°-180°** orientation of the right cylindrical die filled at feed shoe speed of **20 mm/s**

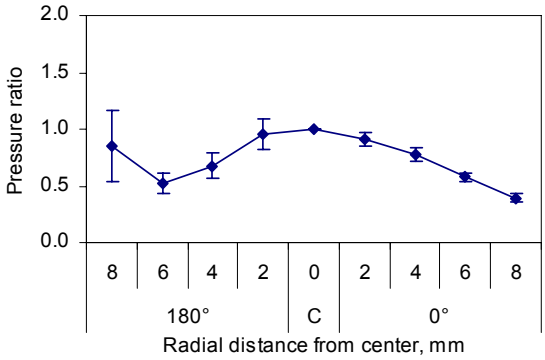

Figure 6.17 Prorated average final pressure ratios in **0°-180°** orientation of the right cylindrical die filled at feed shoe speed of **100 mm/s**

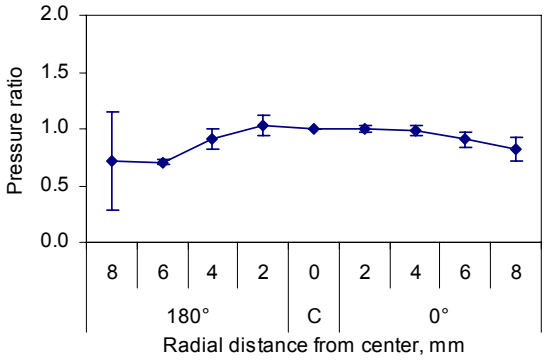

Figure 6.18 Prorated average final pressure ratios in **0°-180°** orientation of the right cylindrical die filled at feed shoe speed of **200 mm/s**

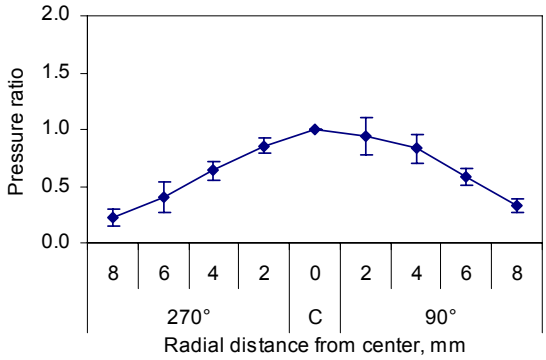

Figure 6.19 Prorated average final pressure ratios in **90°-270°** orientation of the right cylindrical die filled at feed shoe speed of **20 mm/s**

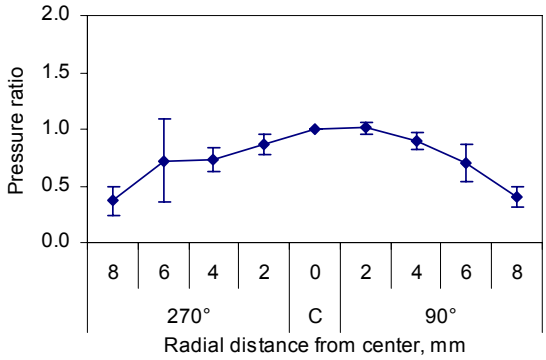

Figure 6.20 Prorated average final pressure ratios in **90°-270°** orientation of the right cylindrical die filled at feed shoe speed of **100 mm/s**

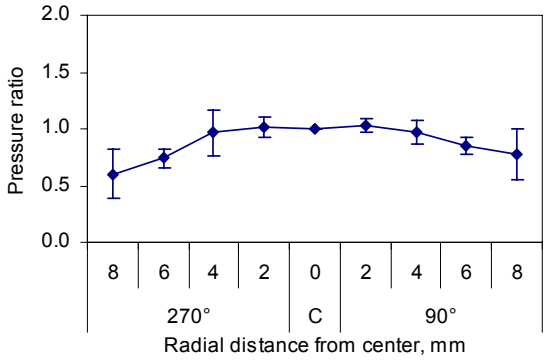

Figure 6.21 Prorated average final pressure ratios in **90°-270°** orientation of the right cylindrical die filled at feed shoe speed of **200 mm/s**

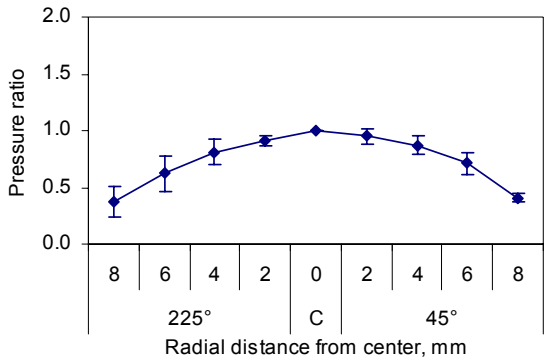

Figure 6.22 Prorated average final pressure ratios in **45°-225°** orientation of the right cylindrical die filled at feed shoe speed of **20 mm/s**

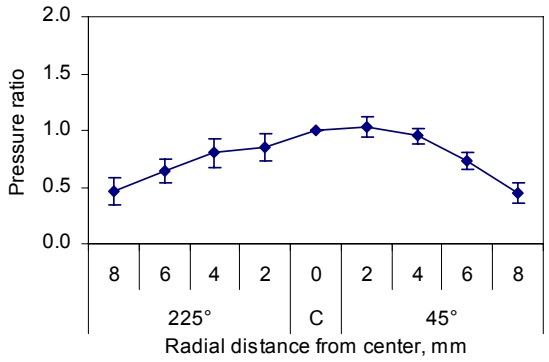

Figure 6.23 Prorated average final pressure ratios in **45°-225°** orientation of the right cylindrical die filled at feed shoe speed of **100 mm/s**

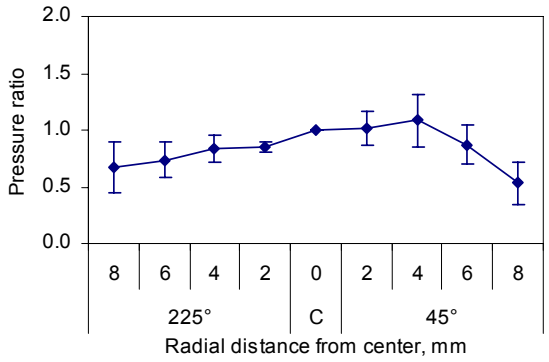

Figure 6.24 Prorated average final pressure ratios in **45°-225°** orientation of the right cylindrical die filled at feed shoe speed of **200 mm/s**

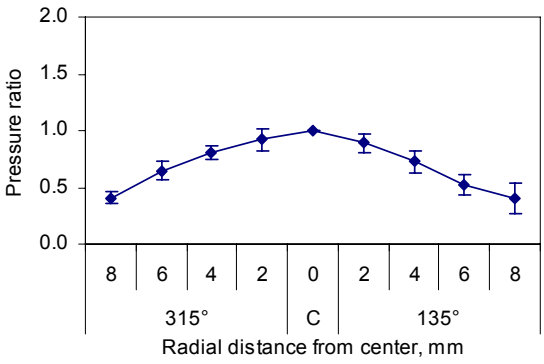

Figure 6.25 Prorated average final pressure ratios in **135°-315°** orientation of the right cylindrical die filled at feed shoe speed of **20 mm/s**

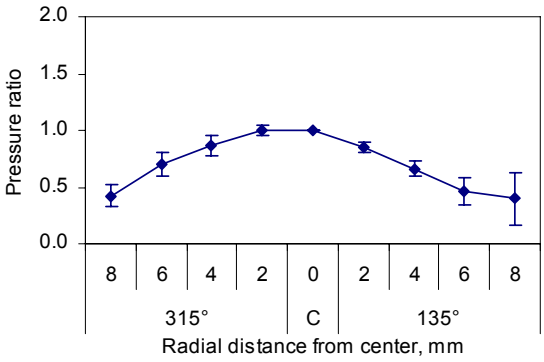

Figure 6.26 Prorated average final pressure ratios in **135°-315°** orientation of the right cylindrical die filled at feed shoe speed of **100 mm/s**

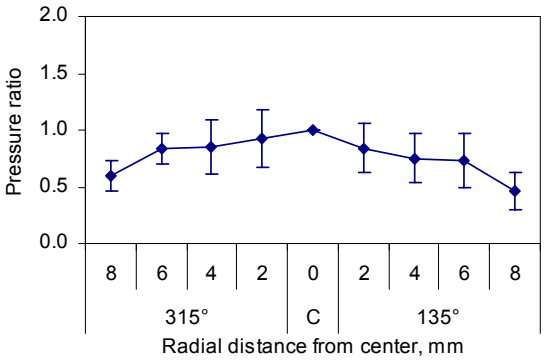

Figure 6.27 Prorated average final pressure ratios in **135°-315°** orientation of the right cylindrical die filled at feed shoe speed of **200 mm/s**

6.1.2.3 45°-225° orientation

20 mm/s feed shoe speed: Pressure ratio distribution along 45°-225° orientation at 20 mm/s feed shoe speed was very symmetrical, with the center having the highest final pressure ratio (Figure 6.22). Final pressure ratios decreased with increasing radii. Location (6, 45°) had final pressure ratio that was significantly lower ($P < 0.05$) than those of locations (4, 45°), (2, 45°), and the center. The final pressure ratio of location (6, 225°) was only significantly lower ($P < 0.05$) than that of the center.

100 mm/s feed shoe speed: Final pressure ratio distribution along 45°-225° orientation at 100 mm/s was quite symmetrical about location (2, 45°) (Figure 6.23). At location (6, 225°), the final pressure ratio was significantly lower ($P < 0.05$) than those of locations (2, 45°) and the center. The final pressure ratio of location (6, 45°) was significantly lower ($P < 0.05$) than those of locations (4, 45°), (2, 45°) and the center. As the location of the highest pressure ratio, location (2, 45°) had final pressure ratio that was significantly higher than those of locations (2, 225°) and (4, 225°).

200 mm/s feed shoe speed: At the highest feed shoe speed, 200 mm/s, final pressure ratio distribution was not symmetrical (Figure 6.24). The highest final pressure ratio was at location (4, 45°). The standard deviations were larger than those of 20 and 100 mm/s. The final pressure ratio of location (6, 225°) was significantly lower ($P < 0.05$) than those of locations (4, 225°), (2, 45°), and (4, 45°). At location (2, 225°), the final pressure ratio was significantly lower ($P < 0.05$) than that of the center.

6.1.2.4 135°-315° orientation

20 mm/s feed shoe speed: Pressure ratio distribution along 135°-315° orientation was very symmetrical about the center with pressure ratios decreasing with increasing radii (Figure 6.25). Location (6, 135°) had final pressure ratio that was significantly lower ($P < 0.05$) than almost all other locations except location (6, 315°). The final pressure ratio of location (6, 315°) was significantly lower ($P < 0.05$) than those of locations (4, 315°), (2, 315°), the center, and (2, 135°). At location (4, 135°), the final pressure ratio was significantly lower ($P < 0.05$) than those of locations (2, 135°) and the center. Compared with the center, location (4, 315°) had significantly lower ($P < 0.05$) final pressure ratio.

100 mm/s feed shoe speed: Pressure ratio distribution at 100 mm/s was quite symmetrical, and pressure ratios decreased with increasing radii (Figure 6.26). Location (6, 135°) had final pressure ratio that was significantly lower ($P < 0.05$) than those of all other locations. The final pressure ratio of location (4, 135°) was significantly lower ($P < 0.05$) than those of locations (2,

135°), the center, (2, 315°), and (4, 315°). At location (2, 135°), the final pressure ratio was also significantly lower ($P < 0.05$) than those of location (2, 315°) and the center. Compared with locations (4, 315°), (2, 315°), and the center, location (6, 315°) had significantly lower ($P < 0.05$) final pressure ratio. The final pressure ratio of location (4, 315°) was significantly lower ($P < 0.05$) than that of location (2, 315°).

200 mm/s feed shoe speed: At feed shoe speed of 200 mm/s, final pressure ratios were somewhat symmetrical about the center, but the variation increased substantially and final pressure ratios were more evenly distributed (Figure 6.27). No significant difference ($P > 0.05$) was observed among final pressure ratios of different locations.

6.1.2.5 Comparison of within-die pressure distribution using contour plots

20 mm/s feed shoe speed: Figure 6.28 displays contour plots of the right cylindrical die using the prorated final pressure ratios at feed shoe speed of 20 mm/s. Pressure distribution was symmetrical about the center line that was parallel to the feed shoe movement direction, i.e., 0°-180° orientation. The highest pressure ratios occurred close to the center area. In all of the orientations, final pressure ratios decreased monotonically with increasing radii.

100 mm/s feed shoe speed: Figure 6.29 shows the distribution of prorated average final pressure ratios in the right cylindrical die at feed shoe speed of 100 mm/s. The center region had the highest pressure ratios, with the center of highest value region moved a little bit away from the center of the die.

As discussed previously for the center cylindrical die, the backward stroke of the feed shoe movement did not contribute much to dragging particles toward the leeward end. This was different from the filling of the battery powder mixture. The reasons were discussed in section 6.1.1.5.

200 mm/s feed shoe speed: Figure 6.30 shows the distribution of prorated average final pressure ratios in the right cylindrical die filled at feed shoe speed of 200 mm/s. Unlike 20 and 100 mm/s feed shoe speeds, the highest pressure ratio values did not cluster around the center area. The highest pressure ratios were around 45° orientation. Orientations of 180° and 270° also had relatively high final pressure ratios. The overall pressure ratio distribution was different from those of 20 and 100 mm/s feed shoe speeds. The possible reasons discussed in section 6.1.1.5 are applicable here as well.

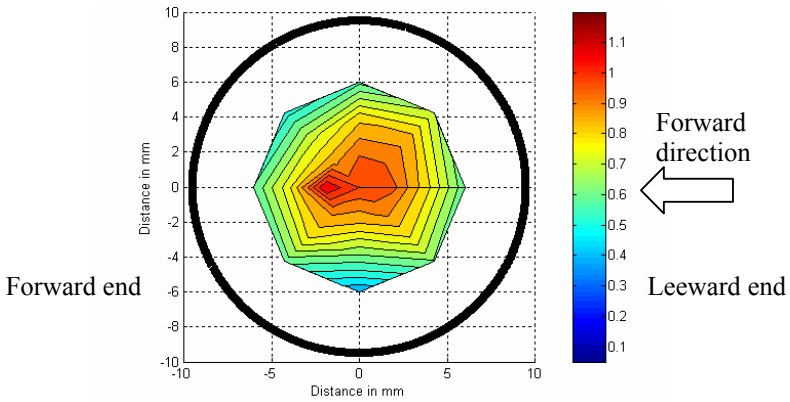

Figure 6.28 Contour plots of the distribution of prorated average final pressure ratios in the right cylindrical die filled at feed shoe speed of 20 mm/s

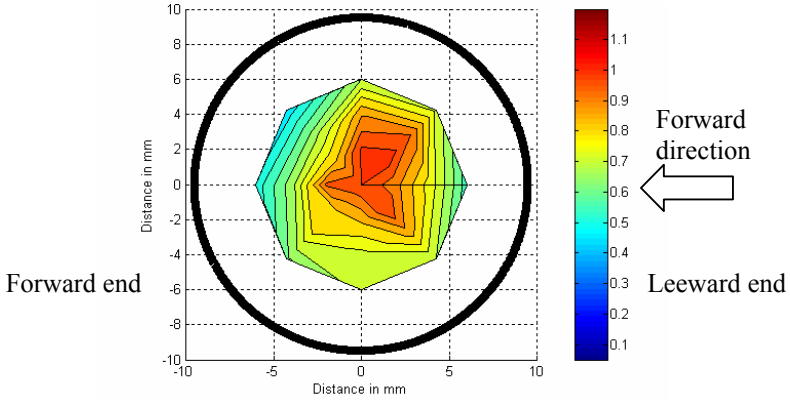

Figure 6.29 Contour plots of the distribution of prorated average final pressure ratios in the right cylindrical die filled at feed shoe speed of 100 mm/s

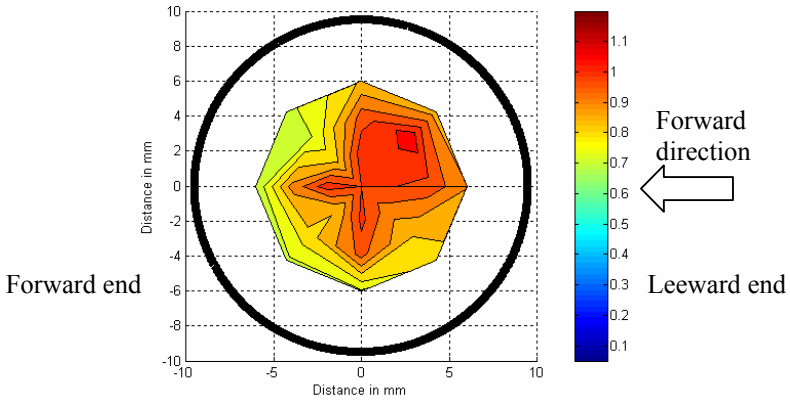

Figure 6.30 Contour plots of the distribution of prorated average final pressure ratios in the right cylindrical die filled at feed shoe speed of 200 mm/s

6.1.2.6 Comparison of uniformity among the three speeds

Table 6.2 shows some statistical parameters obtained for the right cylindrical die at the three feed shoe speeds (20, 100, and 200 mm/s) using the prorated final pressure ratios. Based on these values, 200 mm/s feed shoe speed, which had the lowest (Max-Min)/Mean, Max/Min,

StDev, and COV, resulted in the most uniform pressure distribution among the three speeds. The reason behind this might be that the higher momentum possessed by particles at higher feed shoe speed minimized arching and allowing particles to locally rearrange themselves. Another possible reason was that higher rate of die filling at 200 mm/s feed shoe speed decreased opportunity for particle segregation and promoted uniform filling.

As discussed in section 6.1.1.6, the highest feed shoe speed, 200 mm/s, did not result in the most uniform pressure distribution for the center cylindrical die. This again demonstrated the complexity of powder flow and deposition in the three parallel cylindrical dies. Also, the effects of die spacing and the distance of the shoe wall to the dies might have contributed to the difference between the center and the right dies. It indicated that 200 mm/s might be already close or over the highest feed shoe speed that is beneficial for the deposition of the alumina powder in the three cylindrical dies as well. Attempts to fill the dies at feed shoe speed of 250 mm/s demonstrated that the three parallel cylindrical dies could not be fully filled with the alumina powder (see section 4.5.2).

Table 6.2 Comparison of key statistical parameters for the right cylindrical die at the three feed shoe speeds using prorated final pressure ratios

Feed shoe speed, mm/s	Max	Min	Mean	(Max-Min)/Mean	Max/Min	StDev	COV (StDev×100/Mean)
20	1.10	0.40	0.80	0.86	2.72	0.17	21.6
100	1.03	0.46	0.82	0.69	2.22	0.16	19.8
200	1.08	0.71	0.91	0.41	1.53	0.11	11.9

6.1.3 Comparison of effects of the three feed shoe speeds

6.1.3.1 Center die

Figure 6.31 shows the comparison of average final pressure values measured at feed shoe speeds of 20 and 100 mm/s. For most of the locations, the final pressure values were similar for the two feed shoe speeds. One-way analysis of variance (ANOVA) (Tukey's method)) was used to do multiple comparisons for final pressure values of the same locations at the three different feed shoe speeds. No paired t-test was conducted here, so the previously used Bonferroni and modified Bonferroni procedures are not used here either. The results showed that there were almost no significant differences ($P > 0.05$) between 20 and 100 mm/s, except for locations (4, 45°), (6, 270°), (2, 270°), and (4, 135°).

Figure 6.32 was plotted based on the final pressure values at feed shoe speeds of 20 and 200 mm/s. Final pressure values at 200 mm/s feed shoe speed were significantly higher ($P < 0.05$) than 20 mm/s at all locations, except for locations (6, 180°), (2, 180°), the center along 0°-180° orientation, the center along 90°-270° orientation, and locations of 135°-315° orientation. Along

135°-315° orientation, 20 mm/s feed shoe speed had significantly higher ($P < 0.05$) final pressure values at many locations, including all locations of 135° orientation, the center, and location (2, 315°).

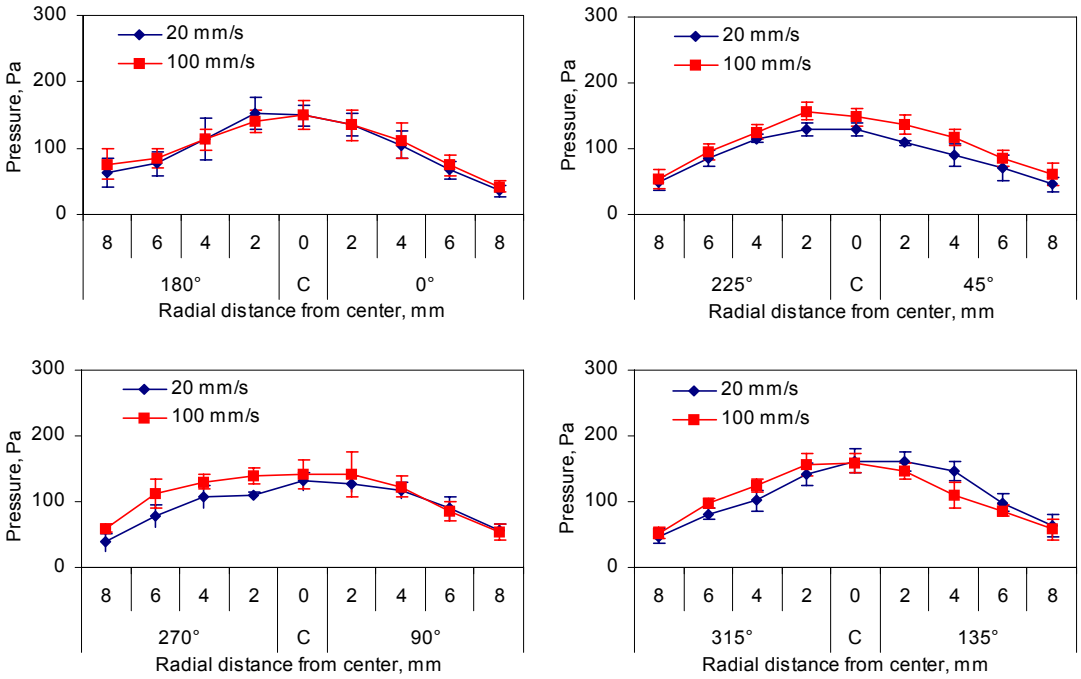

Figure 6.31 Comparison of 20 and 100 mm/s feed shoe speeds (center cylindrical die)

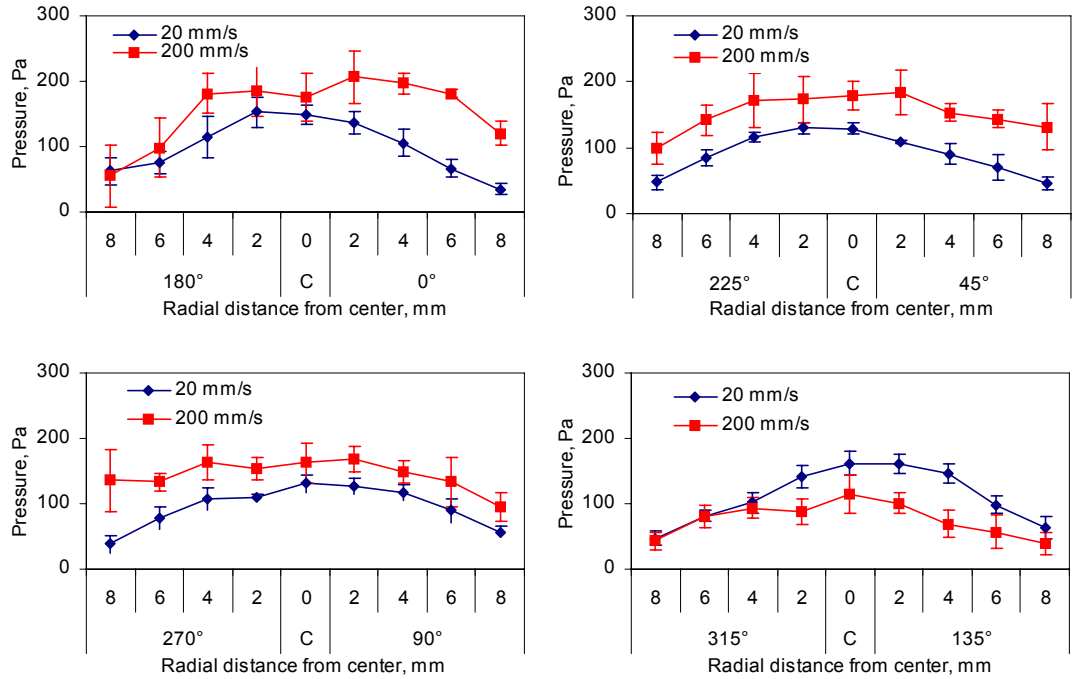

Figure 6.32 Comparison of 20 and 200 mm/s feed shoe speeds (center cylindrical die)

Figure 6.33 compares final pressure values of 100 and 200 mm/s feed shoe speeds. This comparison was very similar to that of 20 and 200 mm/s. 200 mm/s feed shoe speed had higher average final pressure values along 0°-180°, 45°-225°, and 90°-270° orientations, even though some of the differences were not significant ($P > 0.05$), such as at locations (6, 180°), the center along 0°-180° orientation, (2, 225°), (6, 270°), (2, 270°), (2, 90°), and the center along 90°-270° orientation. Along 135°-315° orientation, 100 mm/s feed shoe speed had significantly higher ($P < 0.05$) final pressure values at most locations, except for location (6, 315°).

A plausible explanation for 200 mm/s to result in higher final pressures is that the higher kinetic energy at higher feed shoe speed helped to densify the particles (by collapsing bridges and/or rearranging particles) in the die (Wu and Cocks, 2004). Compared to 20 and 100 mm/s, 200 mm/s had lower final pressures along 135°-315° orientation. The reason for this occurrence was that the final pressures at 200 mm/s along this orientation were much lower than other orientations of the same speed. This was attributed to the complexity of the flow and deposition process, especially at the highest feed shoe speed. The interaction between the air and the incoming particles from the feed shoe was the most pronounced at the highest feed shoe speed. In addition, the alumina powder had relatively fine particles and lower bulk density, which increased the potential for the air in the die and among the particles to play a more important role. Because of the complex and unknown movement of the air, the mass of filled powder were not as systematic as at lower feed shoe speeds, where the air current effect was not so pronounced.

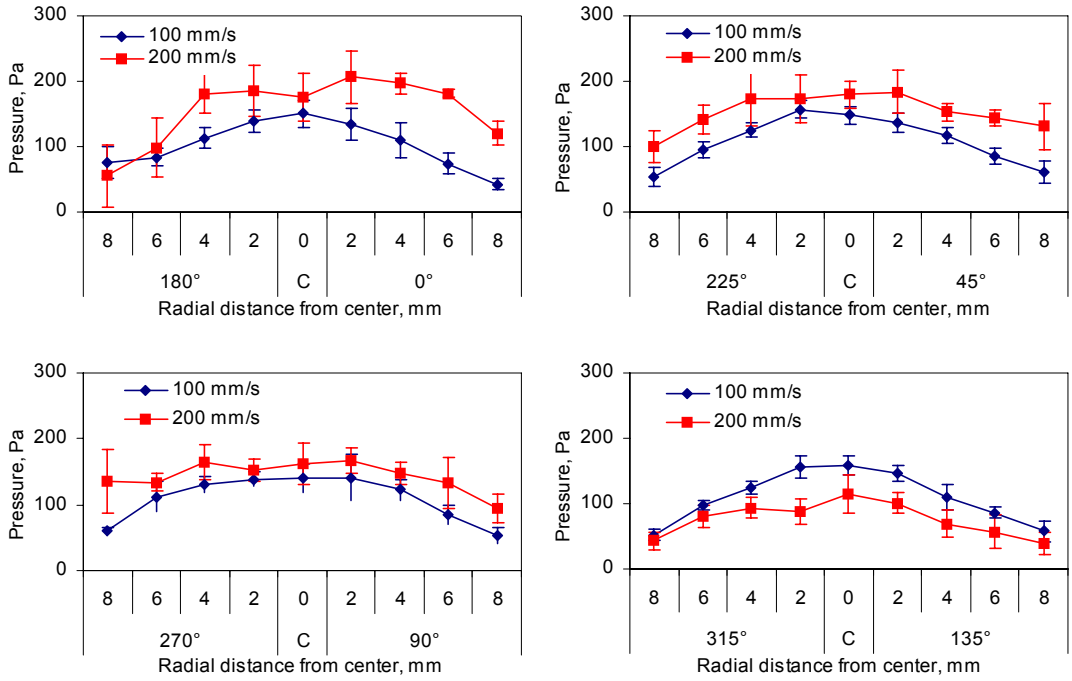

Figure 6.33 Comparison of 100 and 200 mm/s feed shoe speeds (center cylindrical die)

6.1.3.2 Right die

Figure 6.34 shows the comparison of average final pressure values measured at feed shoe speeds of 20 and 100 mm/s. For most of the locations along 90°-270° and 135°-315° orientations, the final pressure values were similar for the two feed shoe speeds. However, for locations along 0°-180° and 45°-225° orientations, 100 mm/s feed shoe speed had higher average final pressure values. Many of these differences were significant ($P < 0.05$), such as locations (2, 0°), (4, 0°), the center along 0°-180° orientation, and most of the locations along 45°-225° orientation except for (6, 225°).

Figure 6.35 compares final pressure values at feed shoe speeds of 20 and 200 mm/s. For most locations along 0°-180° orientation, the two speeds had similar final pressure values, except for location (6, 0°), where 200 mm/s had significantly higher ($P < 0.05$) pressure values. For locations of 45°-225° and 135°-315° orientations, 20 mm/s had higher final pressure values around the center area, and some differences were significant ($P < 0.05$), such as (2, 225°), (2, 45°), the center along 45°-225° orientation, and (2, 315°). This might be explained partly by the relatively more uniform distribution of final pressure values at 200 mm/s. For locations of 90°-270° orientation, 200 mm/s had significantly higher ($P < 0.05$) final pressure values. The main reason for this was that the pressure values of 20 mm/s along this orientation was especially low, compared to other orientations of the same speed. Additional reasons discussed in section 5.1.4 are applicable here as well.

Figure 6.36 was plotted based on the final pressure values of 100 and 200 mm/s feed shoe speeds. This comparison was very similar to that of 20 and 200 mm/s, except for the fact that the differences between 100 and 200 mm/s were larger than those of 20 and 200 mm/s. More significant differences ($P < 0.05$) were observed between 100 and 200 mm/s. It was possible that the right and the center dies had different optimum feed shoe speeds for their respective densest packing. Feed shoe speed of 100 mm/s might be closer to that optimum feed shoe speed for the right die. This could be a likely reason for the larger differences between 100 and 200 mm/s than those of 20 and 200 mm/s.

6.1.4 Center vs. right dies

20 mm/s feed shoe speed: For most of the tested locations, the right die had higher average final pressure values than the center die, except for locations of 90°-270° orientation, where the center die had higher average final pressure values (Figure 6.37). The difference between the center and the right dies were the least along 90°-270° orientation. Statistical analyses (two-sample *t*-test, assuming equal variances) showed that most of the differences were

significant ($P < 0.05$), except for locations (6, 180°), (2, 270°), and the center of 90°-270° orientation. The reasons discussed previously in section 5.1.4 are applicable here as well.

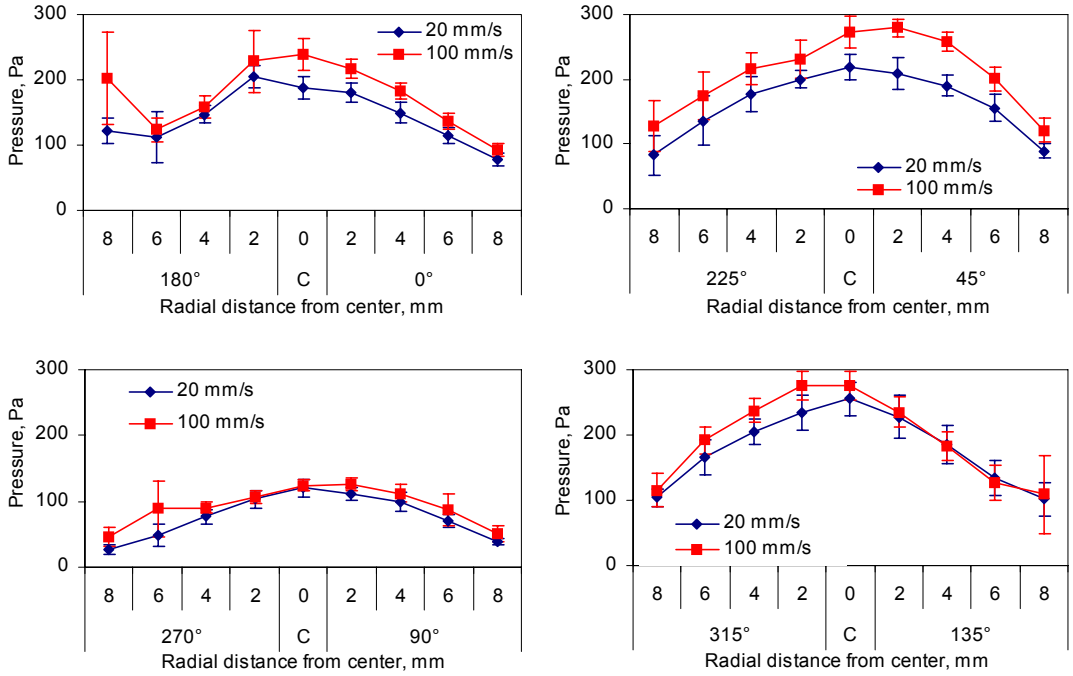

Figure 6.34 Comparison of 20 and 100 mm/s feed shoe speeds (right cylindrical die)

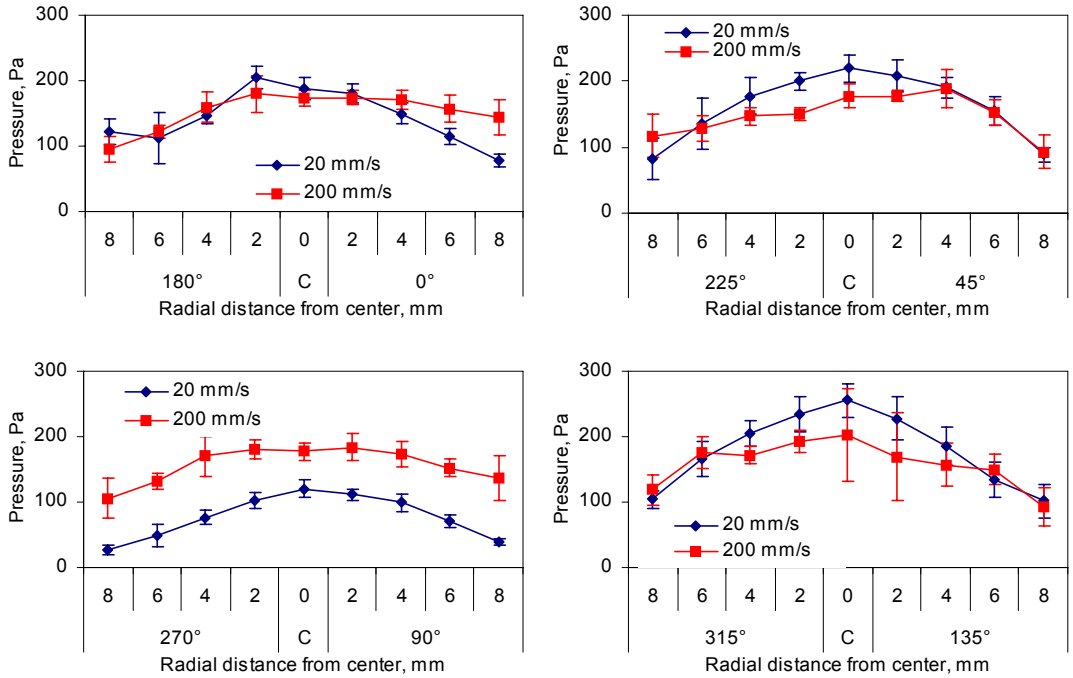

Figure 6.35 Comparison of 20 and 200 mm/s feed shoe speeds (right cylindrical die)

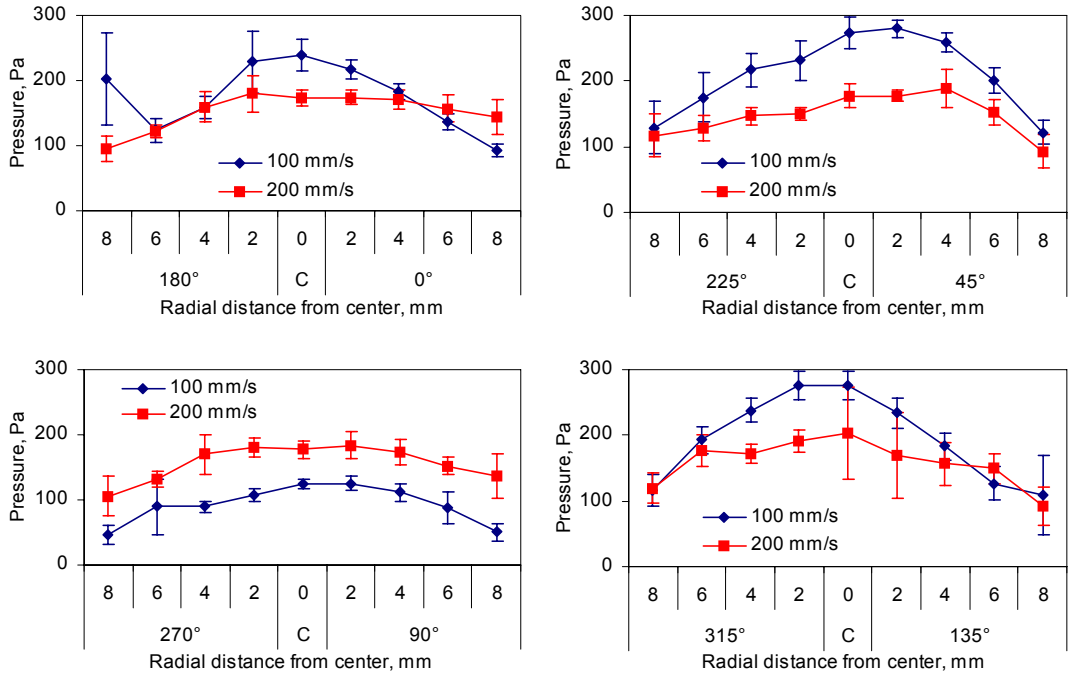

Figure 6.36 Comparison of 100 and 200 mm/s feed shoe speeds (right cylindrical die)

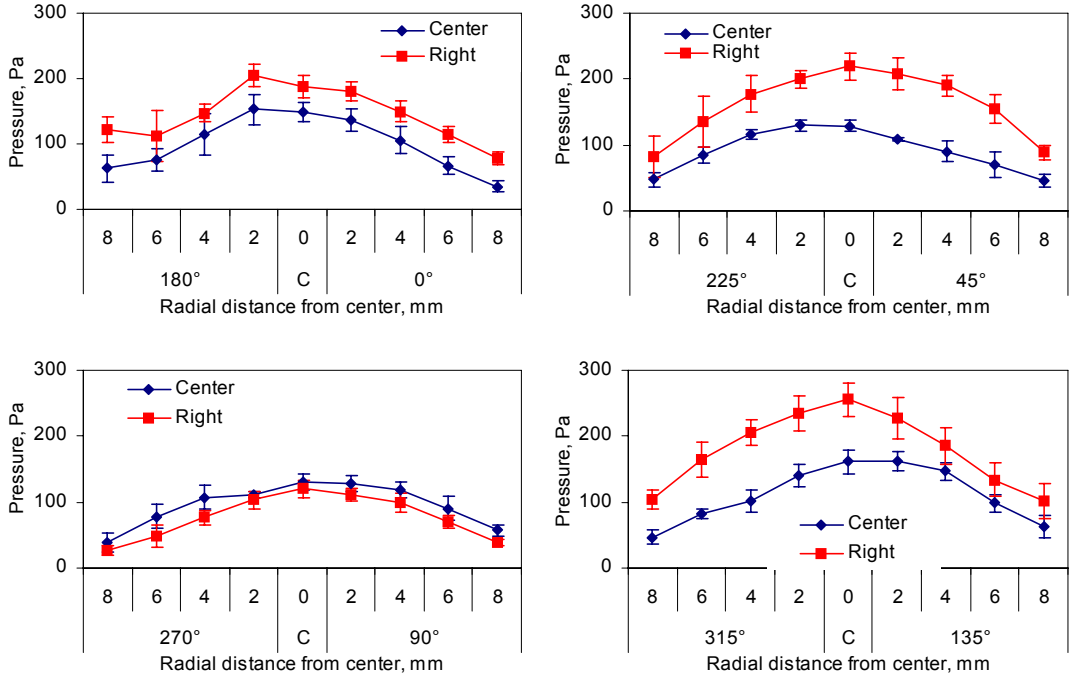

Figure 6.37 Comparison of center and right dies at 20 mm/s feed shoe speed

100 mm/s feed shoe speed: For all of the measured locations of 0°-180°, 45°-225°, and 135°-315° orientations, the right die had significantly higher ($P < 0.05$) final pressure values than the center die (Figure 6.38). For locations of 90°-270° orientation, the two dies had similar final

pressure values, except at locations (4, 270°) and (2, 270°), where the center die had significantly higher ($P < 0.05$) final pressure values. Generally, the difference between the center and the right dies were the least along 90°-270° orientation.

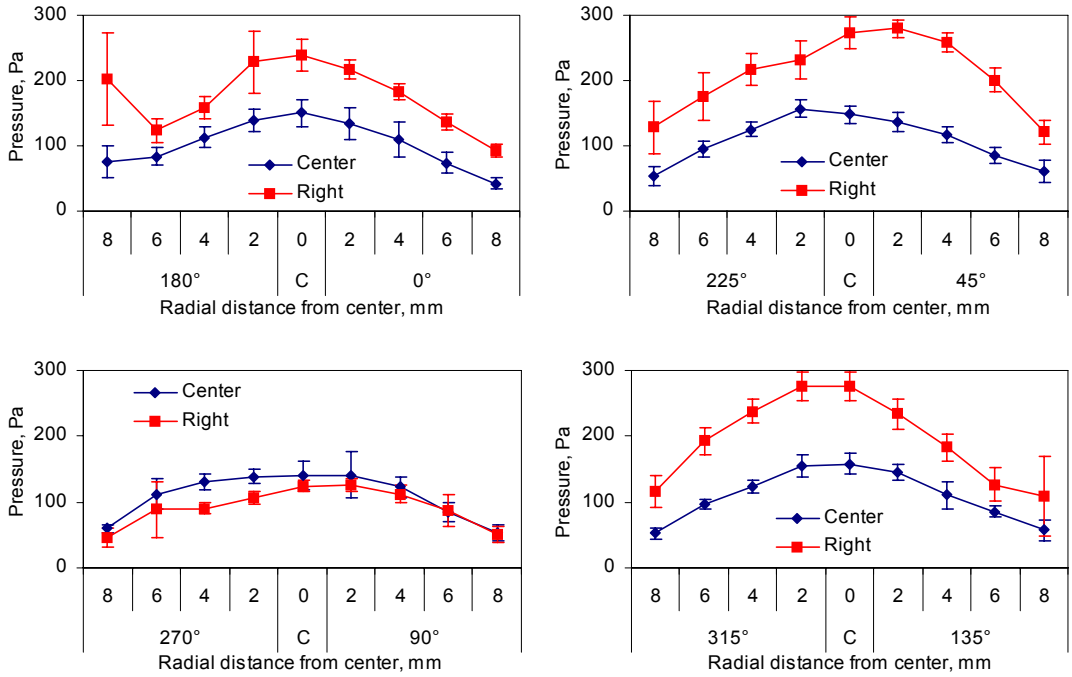

Figure 6.38 Comparison of center and right dies at 100 mm/s feed shoe speed

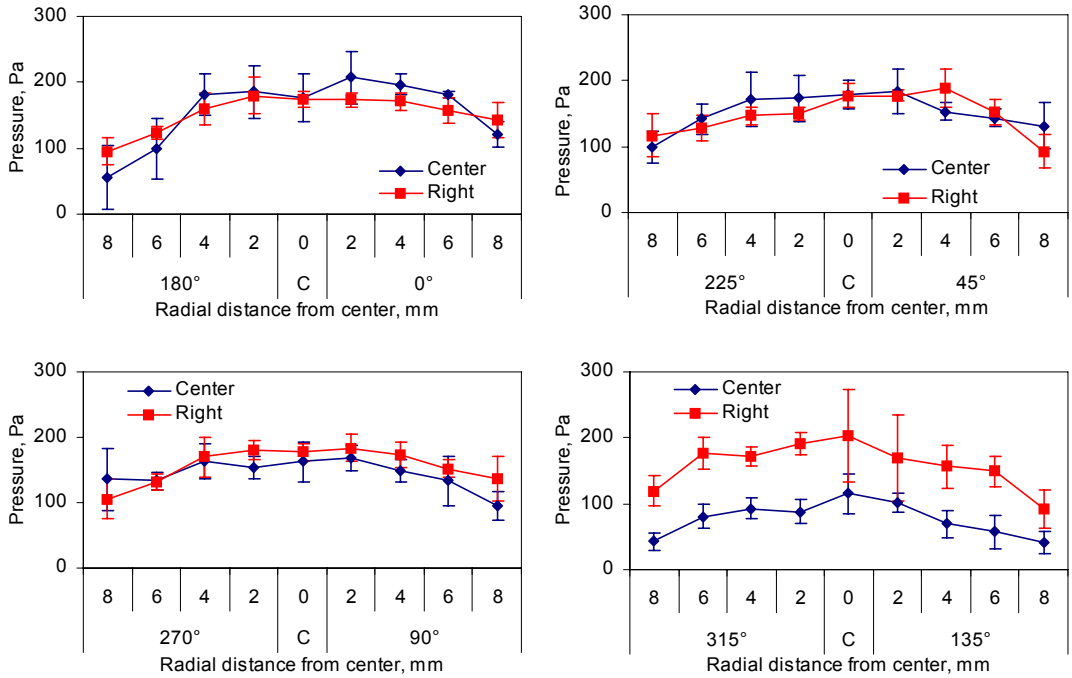

Figure 6.39 Comparison of center and right dies at 200 mm/s feed shoe speed

200 mm/s feed shoe speed: At most of the measured locations, the center and the right dies had similar final pressure values, except for locations of 135°-315° orientation (Figure 6.39). Only few significant differences ($P < 0.05$) were observed between the two dies for 0°-180°, 45°-225°, and 90°-270° orientation. They were locations (4, 0°) and (6, 0°), where the center die had the higher pressure values, and (4, 45°), (4, 90°), and (2, 270°), where the right die had higher pressure values. However, the right die had significantly higher ($P < 0.05$) final pressure values at all of the locations along 135°-315° orientation. The higher kinetic energy of particles at higher feed shoe speed densified particle packing in both dies and reduced the difference of the center and the right dies.

6.1.5 Summary

Based on above discussion, the following concluding remarks can be made for cylindrical dies filled with the alumina powder:

1. At lower feed shoe speed (20 and 100 mm/s), final pressure distribution was symmetrical about the center line that was parallel to the feed shoe movement direction. The center zone had the highest pressure values, and final pressures decreased monotonically with increasing radii.
2. At higher feed shoe speed (200 mm/s), final pressure distribution was irregular and varied more than at lower feed shoe speeds.
3. No consistent speed effect was discovered.
4. At low feed shoe speeds (20 and 100 mm/s), the right die tended to have higher final pressure values (49.5 to 288.8 Pa) than the center die (68.9 to 167.0 Pa). At the highest feed speed (500 mm/s), the center (58.7 to 213.6 Pa) and the right (126.7 to 208.9) dies had similar final pressure values.

6.2 Toroidal Dies

The alumina powder was also used to fill toroidal dies (Figure 5.41). However, many of the measured pressures were too close to the lower measurement limit of the P-1500 pressure sensor strip, which was 4.8 mg for individual pressure sensor element. For example, in one of the six replicates, the pressure values measured for the center toroidal die along 180° at 20 mm/s feed shoe speed was 5, 22, and 3 mg for the locations (8, 180°), (6, 180°), and (4, 180°), respectively. Similar pressure values were observed in other tests for both the center and the right toroidal die

along other orientations at all the three feed shoe speeds. Thus the data of alumina powder filled in the toroidal dies were not reliable, and are not included in this report.

6.3 E-shaped Dies

The E-shaped die configuration and dimensions and the dimension of the feed shoe are shown in Figure 4.11 and Figure 5.81. The feed shoe direction was parallel to the long axis of the ellipse. The three parallel E-shaped dies were symmetrical about the long axis of the ellipse. Due to time and resource constraints, only one feed shoe speed, 20 mm/s, was used for E-shaped dies.

6.3.1 Within-die comparison of the center die using contour plots

Figure 6.40 displays contour plots of the center E-shaped die made by using the average final pressure values. The pressure distribution was symmetrical about the center line parallel to the feed shoe movement direction. The final pressure values of the middle leg were much higher than those of the left and the right legs. This was attributed to the wider opening of the middle leg. Compared with the center die filled with the battery powder mixture (Figure 5.82), the area of the highest final pressure values of the alumina powder moved from the back side to the vicinity of the junction of the middle leg and the back (Figure 6.40). This observation was consistent with the pressure distribution of cylindrical and toroidal dies for the alumina powder. This could be explained by the relatively large opening of the middle leg and the less pronounced drag effect of the backward movement of the feed shoe for the alumina powder. As the alumina powder had smaller granule size with spherical shape, less granules in the top region were dragged backward by the movement of the feed shoe during the backstroke than the battery powder mixture.

6.3.2 Within-die comparison of the right die using contour plots

Figure 6.41 shows the average final pressure values of the right E-shaped die. The pressure distribution was very similar to that of the center die, except that the highest pressure value of the right die was lower than that of the center die. This is discussed in section 6.3.3.

6.3.3 Center vs. right dies

For E-shaped dies, the pressure sensor strip was placed at four locations, L1 to L4, to record pressure increase profile (Figure 6.42). For L1 and L2 locations, the center and the right dies had similar final pressure values (Figure 6.43 (a) and (b)). The center die had almost all of

the higher average final pressure values for L3 location (Figure 6.43 (c)), and some of the differences were significant ($P < 0.05$), such as at distances of 27, 29, and 31 mm, and distances of 3 and 19 mm. For L4 location, the center die had significantly higher ($P < 0.05$) final pressure values than the right die for most of the measured locations (Figure 6.43 (d)), except at distances 1 13, 15, and 23 mm. As discussed previously in section 5.3.3, the elliptical shape of the feed shoe in contact with the table surface was partly responsible for the difference of L4 location. The center die benefited from longer time of filling and pressure from the powder in the feed shoe.

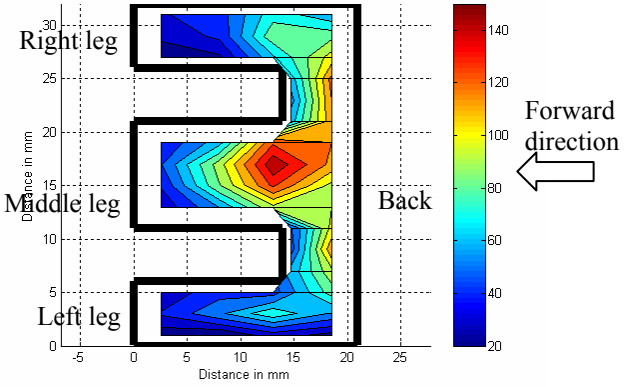

Figure 6.40 Contour plots of the average final pressure value distribution in the center E-shaped die filled at feed shoe speed of 20 mm/s

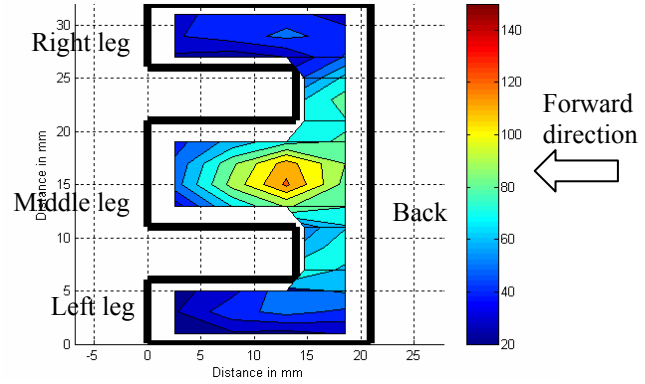

Figure 6.41 Contour plots of the average final pressure value distribution in the right E-shaped die filled at feed shoe speed of 20 mm/s

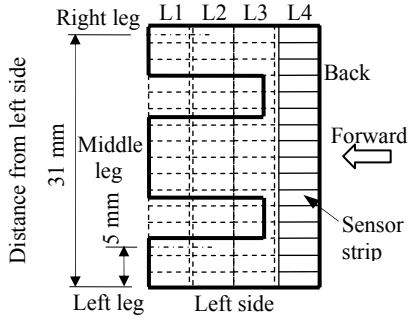

Figure 6.42 Locations of the pressure sensor strip in an E-shaped die (drawn to scale)

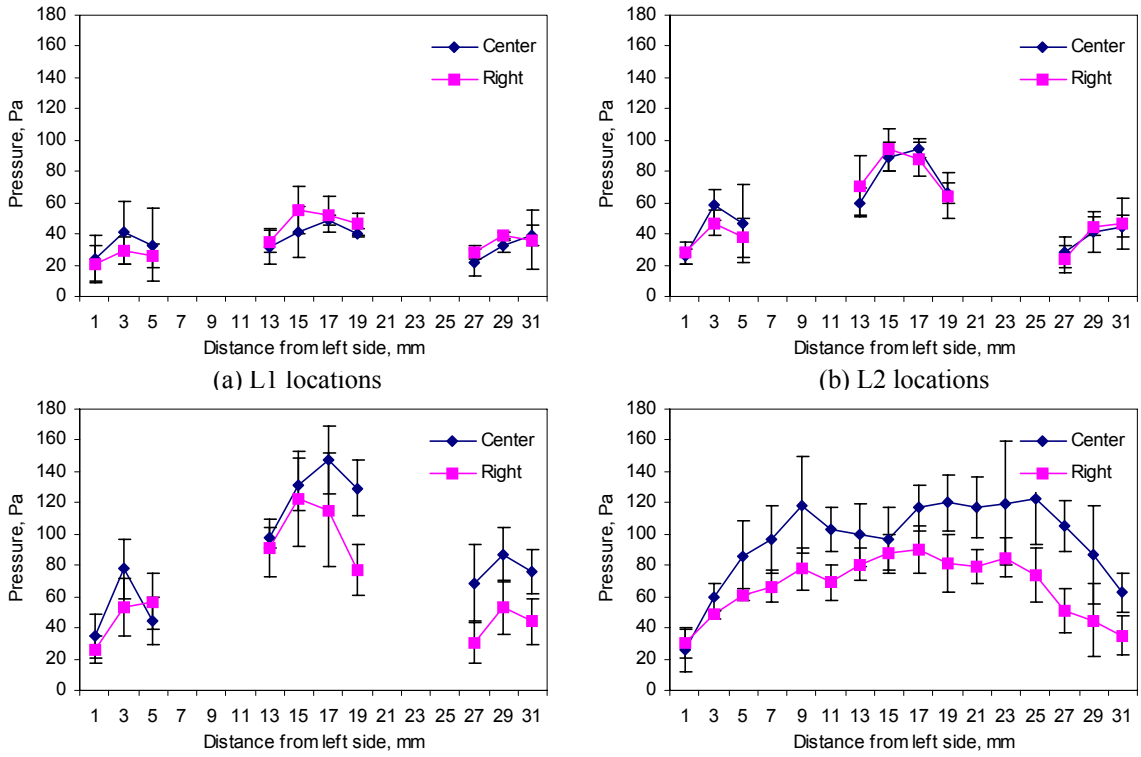

(a) L1 locations (b) L2 locations

(c) L3 locations (d) L4 locations

Figure 6.43 Comparison of center and right dies at 20 mm/s feed shoe speed

6.3.4 Summary

Based on above discussion, the following concluding remarks can be made for E-shaped dies filled with the alumina powder:

1. The final pressure values of the middle leg were higher than those of the left and the right legs. The average pressure of the middle leg ranged from 41.9 to 130.7 Pa, and the average pressures of the left and right legs ranged from 26.1 to 79.6 Pa.
2. The pressure distribution was symmetrical about the center line parallel to the feed shoe movement direction.
3. Neither the center die, nor the right die always had higher pressure values than the other one.
4. When filled with the alumina powder, unlike when filled with the battery powder mixture, the area of the highest final pressure value (126.4 to 152.3 Pa) of the alumina powder moved from the back side to the vicinity of the junction of the middle leg and the back.

CHAPTER 7 CT SCANNER RESULTS

7.1 Calibration of CT Numbers

7.1.1 Results of CT tests

As shown in Table 4.7, 16 tests were conducted by using the CT scanner. The tests included two die shapes (cylindrical and toroidal) and two feed shoe speeds (20 and 500 mm/s for the battery powder mixture, and 20 and 200 mm/s for the alumina powder). There were eight different combinations. For each combination, only two replicates were conducted due to cost considerations.

Each filled die was "cut" into 145 horizontal slices, and each slice had 201 × 201 pixels (including the data of filled powder within the circular die shape) (Figure 7.1). Each pixel was 0.1 × 0.1 mm in physical dimension. Each slice was 0.125 mm in thickness. Therefore, each voxel of CT image was: $\Delta x = \Delta y = 0.1$ mm, and $\Delta z = 0.125$ mm. The CT numbers of the 145 slices were "projected" along the vertical direction (parallel to the center line of the cylindrical or toroidal die) to the bottom, so as to get the hydro map of CT numbers. In other words, the hydro map of each filled die was the average of the CT numbers of the 145 horizontal slices along the vertical direction (parallel to the center line of the cylindrical or toroidal die). The CT numbers of these hydro maps were the final results of CT scanning that were used in this research.

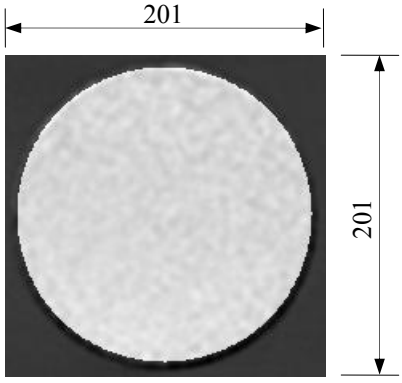

Figure 7.1 An image of a horizontal CT slice of a cylindrical die filled with the battery powder mixture

After the samples were scanned, they were weighed using a balance. The bulk density of the powder in each die was then calculated. Also, the average CT number of the powder in each die was obtained. For the battery powder mixture, eight tests of four combinations were conducted for two die shapes and two feed shoe speeds. Each test included three dies. In all 24 data points were obtained to correlate CT number with bulk density values of the filled battery

powder mixture. Similarly, 24 data points were also collected to get the correlation of CT numbers and bulk densities of the alumina powder.

Table 7.1 lists average CT number of each test and corresponding average bulk density value for battery powder mixture. Similar data for alumina powder are listed in Table 7.2. Figure 7.2 plots the 24 data points for the battery powder mixture and the linear relationship between the average CT numbers and the average bulk densities, together with 95% confidence interval (CI) and 95% prediction interval (PI) of the data. Confidence interval (CI) specified a range of values within which the mean may lie with 95% confidence. A 95% prediction interval (PI) indicated that, in general, 95% of the points would be contained within the band. Prediction interval (PI) can be used to predict the range of individual point with 95% confidence. Figure 7.3 plots the 24 data points for the alumina powder and confidence interval (CI) and prediction interval (PI) of the data.

The two variables, CT number and bulk density, were expected to have strong linear relationship. However, as the low R-squares (0.625 and 0.584 for the battery powder mixture and the alumina, respectively) indicated, the regression explained only 62.5% and 58.4% of the variation in the data, and therefore, predictions might be poor. Usually, R-square value of 0.8 is good. A value of 0.6 or above may be satisfactory in some applications, but in such cases errors in prediction may be relatively high (Aczel, 1995). Confidence intervals (CI) and prediction intervals (PI) of the two plots were quite large, and it was difficult to get accurate bulk density of a location from the CT number. For example, if the CT number of a location was known as 1630.6, with 95% confidence, its bulk density might range from 0.86 to 0.91 g/cm^3.

Several factors contributed toward this spread. These are:

1) Only two replicates were performed for each combination. The number of replicates was not large enough for each combination, although the overall sample size, 24, was quite large.

2) Some areas close to the die wall and the center post (only for toroidal die) were removed from the original CT images to eliminate the influence of the die plate. The physical radius of the cylindrical die was 9.5 mm. But the radius of the processed CT image of the cylindrical die was only 9.2 mm after removing a ring of 0.3 mm from the outer side. For the toroidal die, the physical outer and inner radii were 9.5 and 3.2 mm, respectively. After removal of an outer ring and an inner ring from the original CT image, the outer and inner radii of the processed CT image were 9.2 and 3.6 mm, respectively. The average of the CT numbers did not cover the entire space of each die as the bulk density.

3) The heterogeneous powder mixtures comprising of different chemical constituents of the two powders (manganese dioxide, graphite, potassium hydroxide, barium sulfate, niobium

titanium dioxide, and polytetrafluoroethylene for the battery powder mixture; aluminum oxide, silica, magnesium hydroxide, and calcium carbonate for the alumina) contributed to the error. For industrial CT systems with peak x-ray energy below a few MeV, there are predominantly two fundamental ways in which x-rays interact with matter: photoelectric absorption and Compton scattering (Jiang, 2003; ASTM E 1441-00, 2003). The photoelectric interaction is strongly dependent on the atomic number and density of the absorbing medium; the Compton scattering is predominantly a function of the electron density (i.e., the number of electrons per unit volume) of the material (ASTM E 1441-00, 2003). If the different chemical constituents were not homogeneously distributed within a die, the bulk density distribution pattern might be distorted, masked, or even reversed.

4) Partly due to the above mentioned heterogeneous nature of the powder mixtures, it is plausible that the CT scanner did not have sufficient resolution for the powder mixtures in this research.

Table 7.1 Average CT numbers of each test and corresponding average bulk densities for battery powder mixture

Test case			Average CT number			Average bulk density (g/cm^3)		
Die shape	Speed, mm/s		Left	Center	Right	Left	Center	Right
Cylinder	20	#1	4185	4272	4197	1.75	1.76	1.80
		#2	4221	4327	4237	1.78	1.79	1.80
	500	#1	4303	4360	4330	1.82	1.83	1.86
		#2	4305	4362	4306	1.83	1.83	1.85
Toroid	20	#1	4159	4245	4152	1.70	1.71	1.74
		#2	4159	4351	4151	1.71	1.75	1.77
	500	#1	4445	4461	4479	1.84	1.85	1.89
		#2	4397	4468	4467	1.84	1.84	1.87

Table 7.2 Average CT numbers of each test and corresponding average bulk densities for alumina

Test case			Average CT number			Average bulk density (g/cm^3)		
Die shape	Speed, mm/s		Left	Center	Right	Left	Center	Right
Cylinder	20	#1	1676	1657	1664	0.92	0.91	0.91
		#2	1672	1656	1665	0.91	0.91	0.91
	200	#1	1631	1623	1645	0.88	0.88	0.90
		#2	1627	1613	1626	0.88	0.88	0.89
Toroid	20	#1	1682	1685	1663	0.90	0.92	0.91
		#2	1677	1679	1664	0.88	0.91	0.90
	200	#1	1628	1635	1620	0.88	0.90	0.87
		#2	1632	1642	1620	0.87	0.87	0.87

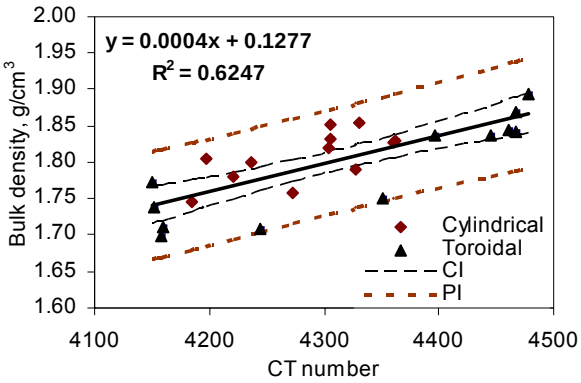

Figure 7.2 Regression of bulk densities vs. average CT numbers of all three dies of two different shapes filled with battery powder mixture at two speeds

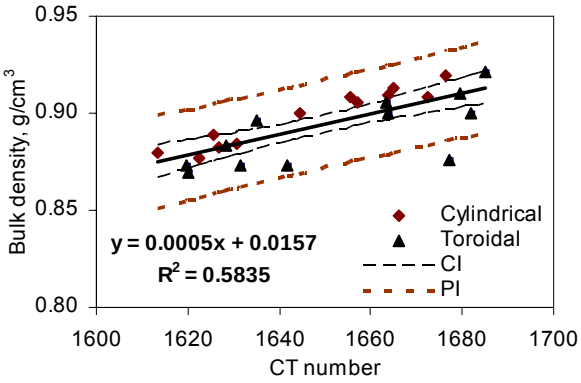

Figure 7.3 Regression of bulk densities vs. average CT numbers of all three dies of two different shapes filled with alumina powder at two speeds

7.1.2 Conversion of CT number to mass ratio

In order to compare the results of CT scans with those of PDT-II, the CT numbers need to be converted to mass values or mass ratios. For this purpose, ImageJ software (Wayne Rasband, National Institutes of Health, USA) was used. Each area covered by every pressure sensor element during PDT-II tests was selected and its average CT number was calculated from measured values. Then, by using the previously obtained linear relationship of bulk densities and the average CT numbers, the average CT number of each area was converted to corresponding bulk density. The bulk density was then multiplied by the volume of the powder above each area (1.9 × 5 × 19.25 mm) to get the mass value. Finally, prorated mass ratios of each orientation of the pressure sensor were obtained by dividing every mass value with the mass value corresponding to the center sensor element. Then the prorated mass ratios of CT tests were compared with the pressure ratios of PDT-II tests. Pressure ratios and mass ratios were the same, if the pressure was only generated by the powder filled in the dies.

7.2 CT Data of Cylindrical Dies Filled with Battery Powder Mixture

7.2.1 Results at feed shoe speed of 20 mm/s

In this subsection, the results obtained for feed shoe speed of 20 mm/s are discussed by using contour plots and statistical parameters. They are compared with the contour plots drawn by using the PDT-II data. Comparisons among the three dies are also performed.

7.2.1.1 Contour plots and comparison with PDT-II data

Figure 7.4 (a) shows contour plots of the prorated mass ratios of the center cylindrical die filled at 20 mm/s, which was obtained by using the average prorated mass ratios of two replicates. Figure 7.4 (b) is its counterpart obtained by using PDT-II data. The most significant difference of these two contour plots was their respective ranges of variations. Compared to the distribution of final pressure ratios obtained by using PDT-II, the distribution of final mass ratios obtained from CT scanning were considered as uniform. Table 7.3 compares some statistical parameters of prorated final mass (pressure) ratios between CT tests and PDT-II tests at feed shoe speed of 20 mm/s. Obviously, mass ratios of CT tests had much lower (Max-Min)/Mean, Max/Min, StDev, and COV values.

The major reason for this difference was that the two methods, CT scanning and PDT-II test, evaluated two distinct fill aspects. CT scanning assessed the distribution of bulk densities or mass values, while PDT-II measured the distribution of pressure values at the bottom of the filled dies. The contribution of mass values of the powder in the dies was only a part of the pressure measured by the pressure sensor of PDT-II. The rest of the measured pressure was generated by the powder in the feed shoe and the feed shoe wall during the filling process. The internal friction between the filled particles, the friction between the die wall and the particles, and residual stresses within the particles (some of the pressure from the powder in the feed shoe and feed shoe wall could not be released even after the filling process) contributed to PDT-II measured value. This was especially true for the battery powder mixture that had irregular and nonspherical particles.

Another difference was that the mass ratios of CT data distributed in a more systematic way. Along 0° orientation, the mass ratios increased monotonically from the center to the wall. But for PDT-II data, the pressure ratio distribution was more complex and irregular.

The third reason was that the uniform distribution of mass ratios obtained from CT numbers might be prone to variation. The R-square value (0.625) for the linear relationship between CT number and bulk density was quite low, and confidence interval (CI) and prediction

interval (PI) (Figure 7.2) were large. The bulk density values and mass ratios obtained from CT numbers are expected to have greater variation in practice.

Both of PDT-II and CT scanning have their own strengths and weaknesses. CT scanning is a mature technology and widely used in medical imaging and various industries. Its major strength for this research was expected to be that it could provide accurate and dependable data about absolute powder bulk density distribution in the dies. However, the weak linear correlation of CT number and bulk density revealed that CT technology also has its limitations. It cannot record real time bulk density distribution throughout the entire filling process. It is a time consuming and expensive method. More importantly, for the two powder mixtures used in this research, CT scanning failed to provide reliable information about bulk density distribution. Possible strategies to improve the quality and reliability of CT data include using chemically homogeneous powder and run more test replicates.

PDT-II can measure real time pressure distribution at multiple locations of the entire process. It is an efficient and effective tool for investigating the pressure change throughout the whole process. Its major weakness is that no direct mass distribution or bulk density distribution values can be collected. As there is no quantitative information available about friction within particles and friction between particles and the die wall, it is impossible to obtain mass distribution or bulk density distribution from the bottom pressure values collected by the PDT-II. Even though pressure distributions are very useful, bulk density or mass distribution knowledge is still desirable. Shallow dies are suggested for future research for PDT-II to collect pressure values that are more closely related to mass values.

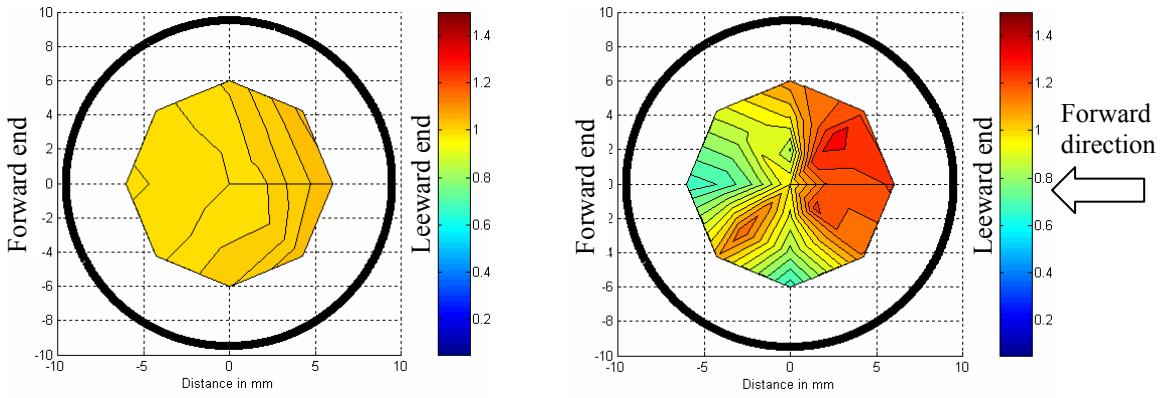

(a) CT mass ratio (b) PDT pressure ratio

Figure 7.4 Contour plots of the prorated average final mass (pressure) ratios in the center cylindrical die filled with battery powder mixture at feed shoe speed of 20 mm/s

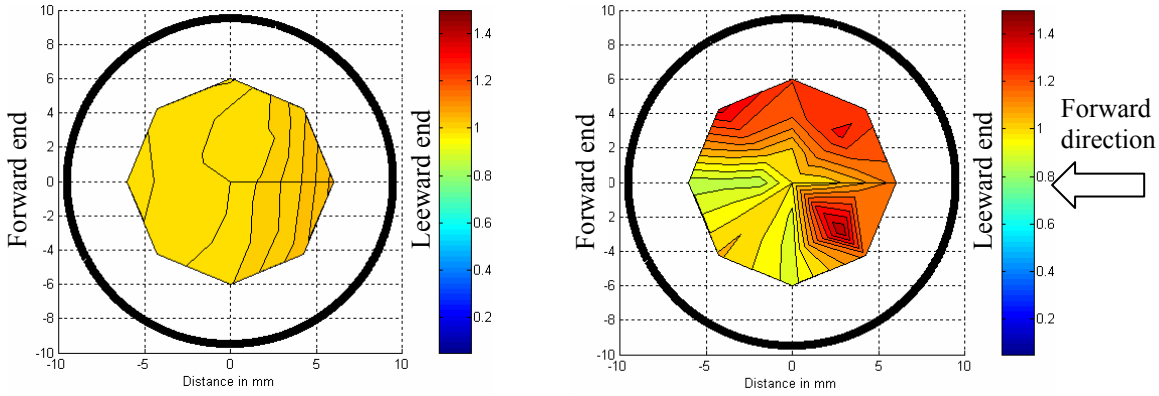

(a) CT mass ratio (b) PDT pressure ratio

Figure 7.5 Contour plots of the prorated average final mass (pressure) ratios in the right cylindrical die filled with battery powder mixture at feed shoe speed of 20 mm/s

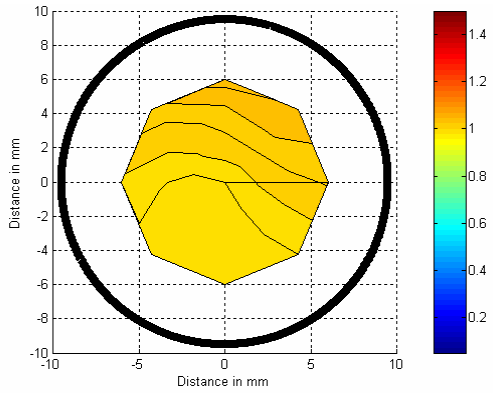

Figure 7.6 Contour plots of the prorated average final mass ratios in the left cylindrical die filled with battery powder mixture at feed shoe speed of 20 mm/s (CT data)

Table 7.3 Comparison of key statistical parameters of prorated final mass (pressure) ratios between CT tests and PDT-II tests at feed shoe speed of 20 mm/s for battery powder mixture

		Max	Min	Mean	(Max-Min)/Mean	Max/Min	StDev	COV (StDev×100/Mean)
Center die	CT	1.04	0.99	1.01	0.06	1.06	0.01	1.47
	PDT-II	1.34	0.66	1.03	0.65	2.01	0.19	18.7
Right die	CT	1.05	0.99	1.01	0.06	1.07	0.01	1.45
	PDT-II	1.45	0.87	1.10	0.54	1.68	0.16	14.7
Left die	CT	1.05	0.99	1.01	0.05	1.06	0.01	1.44

However, a similar trend was also observed for both contour plots of CT data and PDT-II data, i.e., the half circle close to the leeward end had higher final mass (pressure) ratios. Qualitatively, PDT-II could still provide useful information about the mass ratio distribution, even though it measured the pressure distribution.

Figure 7.5 (a) shows contour plots of the right cylindrical die at 20 mm/s feed shoe speed that was obtained by using the average prorated mass ratios of two CT test replicates. Figure 7.5

(b) is its counterpart of PDT-II data. Similar observations can be made as for the center die. As shown in Table 7.3, mass ratios of CT tests had much lower (Max-Min)/Mean, Max/Min, StDev, and COV values than pressure ratios of PDT-II data.

Figure 7.6 displays contour plots for the left die at the 20 mm/s feed shoe speed obtained by using CT data. It was different from the center and the right dies in that it did not show symmetry about the center line that was parallel to the feed shoe motion direction. Nonetheless, as the minimum mass ratio (0.99) and the maximum mass ratio (1.05) were sufficiently close, the seemingly nonsymmetrical distribution could also be viewed as not too far from being symmetrical. Previously, during experimental design process, powder deposition was assumed to be symmetrical about the feed shoe movement direction. The left die was expected to have the same powder distribution as the right die (section 4.4.2), and the powder distribution of the left die was not measured for all the three die shapes with PDT-II. It seemed that this assumption was, at least, not totally justified by the CT data.

7.2.1.2 Comparison among the three dies

It can be seen from Table 7.3 that the three dies had almost the same values for all the seven statistical parameters, i.e., Max, Min, Mean, (Max-Min)/Mean, Max/Min, StDev, and COV, according to the CT scanner results. This means that there were almost no differences among the three dies, with regard to the distribution uniformity. According to the contour plots of the three dies (Figure 7.4 (a), Figure 7.5 (a), and Figure 7.6), they had slight differences in the pattern of mass ratio distribution, especially the left die being different from those of the center and the right dies. But the absolute values of the differences were sufficiently low that the mass ratio distributions of the three dies could be considered as identical. However, as discussed in the last section, the R-square value (0.625) for the linear relationship between CT number and bulk density was low, and confidence interval and prediction interval (Figure 7.2) were large, the bulk density values and mass ratios obtained from CT numbers are likely to have greater variation in practice.

7.2.2 Results at feed shoe speed of 500 mm/s

In this subsection, the results obtained for feed shoe speed of 500 mm/s are discussed by using contour plots and some statistical parameters. They are compared with the contour plots drawn by using the PDT-II data. Comparisons among the three dies are also conducted.

7.2.2.1 Contour plots and comparison with PDT-II data

Figure 7.7 (a) shows contour plots of the prorated mass ratios of the center cylindrical die filled at 500 mm/s. It was obtained by using the average prorated mass ratios of two replicates of CT scanning. Figure 7.7 (b) is its counterpart obtained by using PDT-II data. Observations similar to feed shoe speed of 20 mm/s can be made for 500 mm/s. The most significant difference of these two contour plots was the difference in ranges of variations. Compared to the distribution of the data of PDT-II, the distributions of final mass ratios obtained from CT scanning were uniform. As shown in Table 7.4, mass ratios of CT tests had much lower (Max-Min)/Mean, Max/Min, StDev, and COV values than corresponding pressure ratios of PDT-II data. However, for reasons discussed in previous sections this high level of uniformity might not be completely reliable. As stated in section 7.1.2, all the mass ratios were converted from CT number values by using the linear regressions shown in Figure 7.2 and Figure 7.3. As discussed previously, the R-square values of the regression was quite low (0.625), the linear equations for the relationship between CT number and bulk density values may not accurately present the data. Also, as confidence interval and prediction interval (Figure 7.2) were large, the bulk density values and mass ratios obtained from CT numbers are expected to have greater variation in practice.

As at 20 mm/s, another difference between Figure 7.7 (a) and (b) was that the mass ratios of CT data distributed in a more systematic way. Higher values were observed close to the leeward half. For PDT-II data, the pressure ratio distribution was more complex and irregular.

Figure 7.8 (a) shows contour plots of the right cylindrical die at 500 mm/s feed shoe speed that was obtained by using the average prorated mass ratios of two CT test replicates. Figure 7.8 (b) is its counterpart of PDT-II data. Similar observations can be made as for the center die. As shown in Table 7.4, mass ratios of CT tests had much lower (Max-Min)/Mean, Max/Min, StDev, and COV values than pressure ratios of PDT-II data.

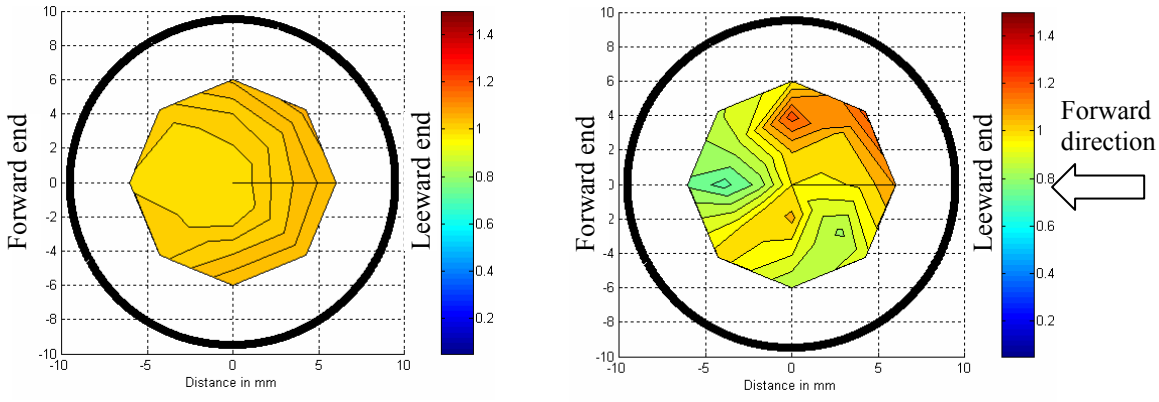

(a) CT mass ratio (b) PDT pressure ratio

Figure 7.7 Contour plots of the prorated average final mass (pressure) ratios in the center cylindrical die filled with battery powder mixture at feed shoe speed of 500 mm/s

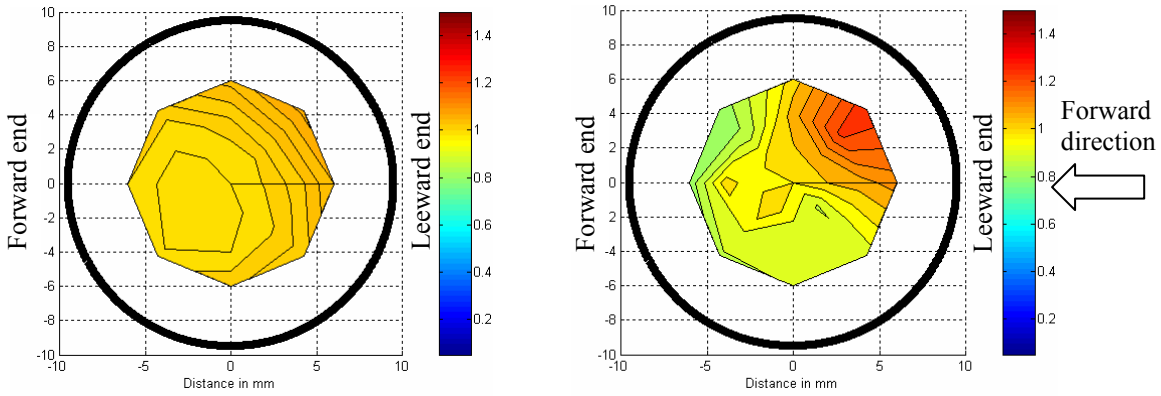

(a) CT mass ratio (b) PDT pressure ratio

Figure 7.8 Contour plots of the prorated average final mass (pressure) ratios in the right cylindrical die filled with battery powder mixture at feed shoe speed of 500 mm/s

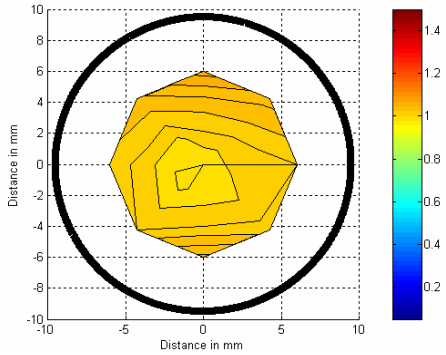

Figure 7.9 Contour plots of the prorated average final mass ratios in the left cylindrical die filled with battery powder mixture at feed shoe speed of 500 mm/s (CT data)

Table 7.4 Comparison of key statistical parameters of prorated final mass (pressure) ratios between CT tests and PDT-II tests at feed shoe speed of 500 mm/s for battery powder mixture

		Max	Min	Mean	(Max-Min)/Mean	Max/Min	StDev	COV (StDev×100/Mean)
Center die	CT	1.05	1.00	1.02	0.05	1.05	0.02	1.70
	PDT-II	1.23	0.73	0.98	0.51	1.69	0.11	11.6
Right die	CT	1.06	1.00	1.01	0.07	1.07	0.02	1.75
	PDT-II	1.29	0.81	1.00	0.48	1.59	0.11	11.3
Left die	CT	1.06	1.00	1.02	0.06	1.07	0.02	1.63

Figure 7.9 shows contour plots of the left die at the 500 mm/s feed shoe speed obtained by using CT data. It was different from the center and the right dies in the distribution pattern in that the center zone had the lowest mass ratios. No data were collected for the left die by using PDT-II, so there was no comparison between CT data and PDT-II data for the left die.

7.2.2.2 Comparison among the three dies

As shown in Table 7.4, the three dies had almost the same values for the seven statistical parameters. There were almost no differences among the three dies in the uniformity of the mass ratio distribution. The contour plots of the three dies (Figure 7.7 (a), Figure 7.8 (a), and Figure 7.9) showed that the left die had somewhat different distribution pattern from the center and the right dies. The lowest mass ratios of the left die were around the center zone, while the lowest mass ratios of the center and the right dies were somewhere close to the forward end.

7.3 CT Data of Alumina Powder

The alumina powder was also used for CT tests. However, the data manifested some abnormal features. Figure 7.10 shows the contour plots of CT number of the center toroidal die filled at 20 mm/s feed shoe speed. The distribution pattern, which was perfectly symmetrical, was considered to be implausible. Possible reasons for this unexpected pattern included insufficient replicate number, heterogeneous nature of the powder mixture, and low bulk density of the powder (compared to the density of the PVC die plates). Some distribution features might be masked or distorted by the higher density die plate. Similar problems were also noticed for the CT data of the alumina powder filled in the cylindrical dies. For instance, CT data of the alumina powder showed that the center cylindrical die had the highest final mass values. But measured densities indicated that the center die had the lowest bulk density values, even though the differences were not very large. Therefore, the CT data of the alumina powder are not discussed in this research.

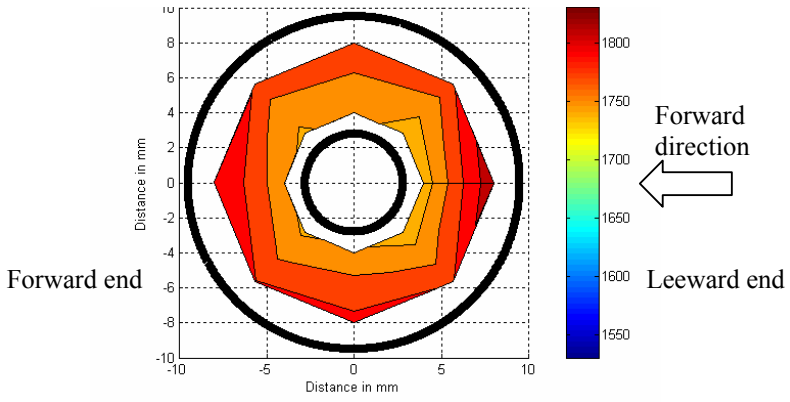

Figure 7.10 Contour plots of CT number of the center toroidal die filled with alumina powder at feed shoe speed of 20 mm/s

7.4 Summary

Based on above discussion, the following concluding remarks can be made:

1. CT number vs. bulk density did not have a strong linear correlation for the battery powder mixture and the alumina powder ($R^2 \leq 0.625$).
2. The final bulk density distribution obtained by CT scanning was uniform. However, this observation was based on the weak linear correlation ($R^2 \leq 0.625$) of CT number vs. bulk density.
3. CT data showed that there were almost no differences among the three dies, with regard to the distribution uniformity. However, this was based on the weak linear correlation ($R^2 \leq 0.625$) of CT number vs. bulk density.
4. CT scanner and PDT-II measured two different attributes. CT scanning assessed the distribution of bulk densities or mass values, while PDT-II measured the distribution of pressure values at the bottom of the filled dies. The distribution patterns of CT data and PDT-II data had similarities
5. Both CT data and PDT-II data revealed that the half circle close to the leeward had higher final mass (pressure) values. Qualitatively, PDT-II could provide useful information about the mass distribution, even though its basis is pressure distribution.

CHAPTER 8 MODEL DEVELOPMENT AND VERIFICATION

As stated previously in section 2.3.6, even though models have been developed and reported in the literature to simulate or investigate the die filling process, they had limitations. No models or methods published can be used to study or simulate the feed shoe filling process or pressure (mass) increase for real-world problems involving a large number of 3D particles of various shapes and sizes. In order to further the understanding of the die filling process, models were developed and verified to simulate the pressure ratio increase for the entire filling process of the battery powder mixtures filled in the cylindrical dies at 20 mm/s feed shoe speed. One of the reasons to select the data of 20 mm/s feed shoe speed was that the air pressure and buoyancy effects of the two phase flow could be minimized at this speed.

8.1 Analysis of the Filling Process

Figure 8.1 shows a typical pressure ratio increase profile obtained by the pressure sensor element at the center of the center cylindrical die (for configuration see Figure 4.19) filled with the battery powder mixture at feed shoe speed of 20 mm/s. The plot represents the average of six runs with the pressure sensor strip located along 0° orientation. This set of data is used to discuss analysis and model development for the filling process. The entire profile was quite complex and could not be simulated by a single physics-based mathematical formulation. Therefore, the whole filling process was divided into several phases and within each phase were stages. Every stage was modeled using a simple rate equation. There were three reasons for the selection of a simple rate equation to simulate each stage: 1) physics of the deposition process of each stage, 2) similarity of modeled data to measured data, and 3) model simplicity.

The relative positions of the feed shoe tube with reference to the center die were used to mark the start and end points of different phases. Here, the feed shoe tube position was represented by the position of the tube cross-section in contact with the table surface. These particular positions of the feed shoe tube were used to identify and demarcate filling phases as shown in Figure 8.2 and Figure 8.3. Corresponding to these positions, the particular times for the feed shoe tube to reach these positions are listed below and shown in Figure 8.2 and Figure 8.3:

T_0: when the feed shoe tube was starting to move from its original (start) position;

T_1: when the inner side of the front of the feed shoe tube reached the center die (Figure 8.4);

T_1': when the filling of powder into the middle die commenced (Figure 8.5);

T_2: when the inner side of the back wall of the feed shoe tube was leaving the middle die;

T_3: when the feed shoe tube reached the end of the forward stroke;

T_4: when the inner side of the back wall of the feed shoe tube reached the middle die;

T_5: when the inner side of the front wall of the feed shoe tube was leaving the middle die;

T_6: when the feed shoe returned to its original start position.

As Cocks et al. (2001) and Wu et al. (2003a) reported, during the forward stroke of feed shoe movement, the powder in the feed shoe was caused to move to the back of the feed shoe due to inertia when the feed shoe accelerated from rest. As the height of the powder in the feed shoe, about 40 mm, was not too high, a void was created at the front of the feed shoe, and the powder had a nose-shaped profile, as shown in Figure 8.4. The void volume increased with the advance of the feed shoe in the forward movement, from about 10 mm to 20 mm. On average, the empty space was about 15 mm in the feed shoe movement direction. As shown in Figure 8.5, T_1' denotes the onset time for the actual filling, at which time the inner side of the front wall of the feed shoe tube already passed over some (or most) of the die opening.

The feed shoe was driven by a computer controlled linear actuator. The linear actuator and the pressure sensor strip were controlled by two separate programs that were installed on two computers. The reason for having the two programs on separate computers was that if they were installed on the same computer, the data collected by the pressure sensor resulted in very high noise level. Both the programs needed to be started manually, and it was difficult to match the data (time and pressure values) collected by the pressure sensor strip with the exact positions of the feed shoe tube.

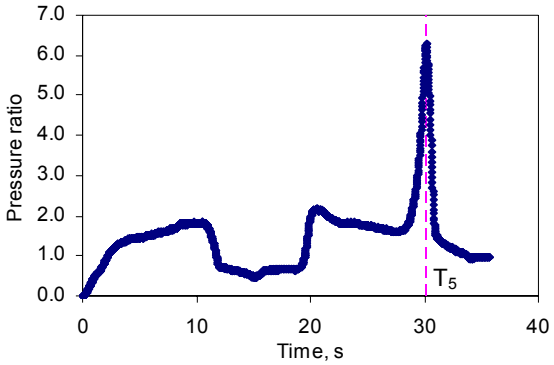

Figure 8.1 Average pressure ratio increase profile for the entire filling process at the center of 0° orientation of the center cylindrical die filled with the battery powder mixture at 20 mm/s feed shoe speed

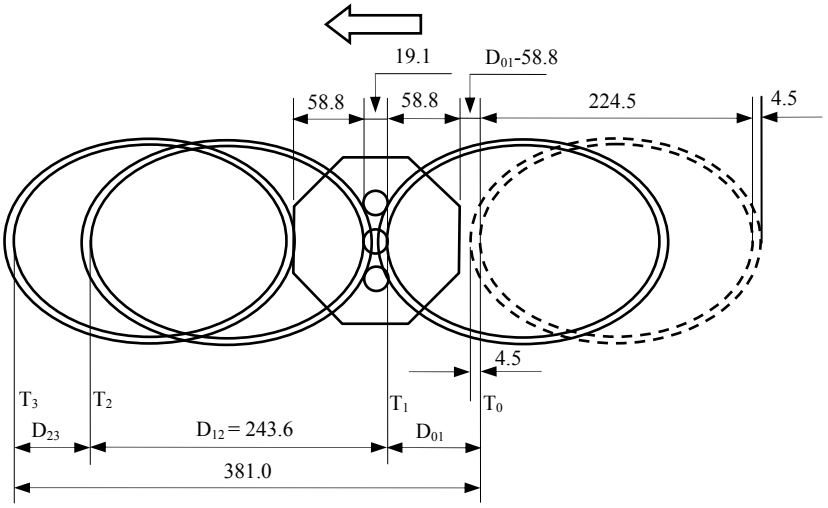

Figure 8.2 Filling phases during the forward stroke showing feed shoe travel distance (in mm) and onset of phases identified by T and its subscript. D_{01} = 73.3 mm, D_{23} = 64.1 mm.

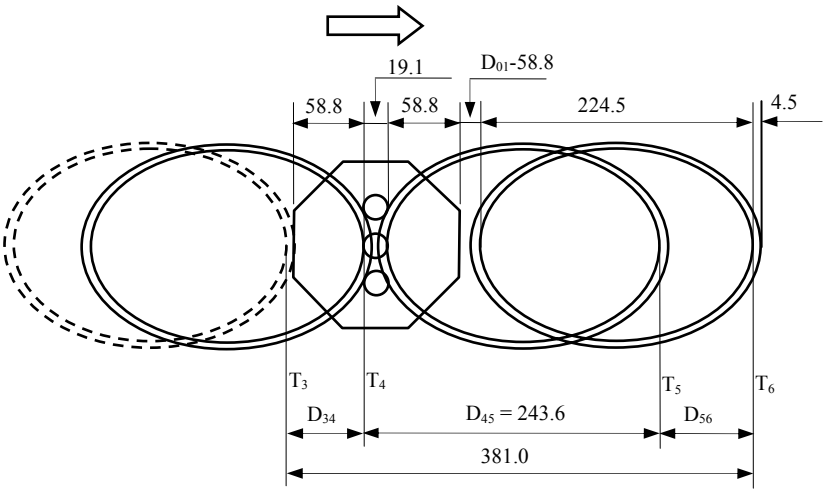

Figure 8.3 Filling phases during the backward stroke showing feed shoe travel distance (in mm) and onset of phases identified by T and its subscript. D_{34} = 64.1 mm, D_{56} = 73.3 mm.

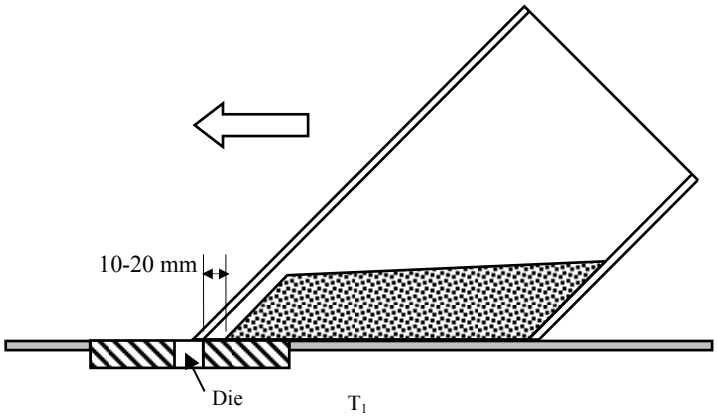

Figure 8.4 Nose-shaped profile formed at the front of the feed shoe

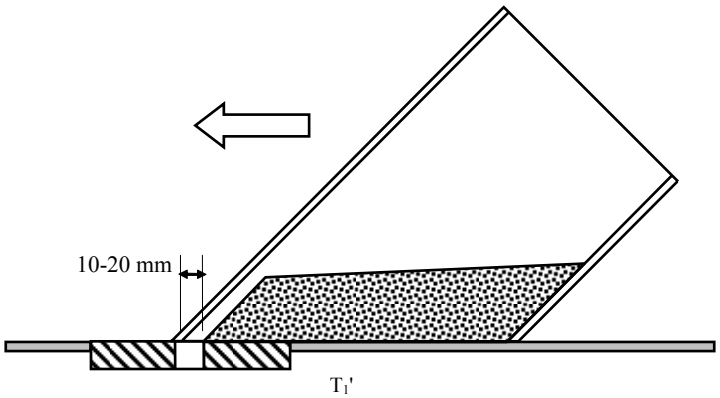

Figure 8.5 Filling started after the inner front wall passed over most of the die opening

Table 8.1 Particular positions and times of the feed shoe tube for the center die along 0° orientation at 20 mm/s feed shoe speed

Distance, mm		Time period, s		Cumulative time (T_1' = 0), s	
D_{01}	73.3	T_{01}	3.67	T_1	T_2-12.18
D_{12}	243.6	T_{12}	12.18	T_2	T_3-3.21
D_{23}	64.1	T_{23}	3.21	T_3	T_4-3.21
D_{34}	64.1	T_{34}	3.21	T_4	T_5-12.18
D_{45}	243.6	T_{45}	12.18	T_5	T_5
D_{56}	73.3	T_{56}	3.67	T_6	T_5+3.67

Table 8.2 Particular positions and times of the feed shoe tube for the center die along 0° orientation at 100 mm/s feed shoe speed

Distance, mm		Time period, s		Cumulative time (T_1' = 0), s	
D_{01}	73.3	T_{01}	0.76	T_1	T_2-2.44
D_{12}	243.6	T_{12}	2.44	T_2	T_3-0.67
D_{23}	64.1	T_{23}	0.67	T_3	T_4-0.67
D_{34}	64.1	T_{34}	0.67	T_4	T_5-2.44
D_{45}	243.6	T_{45}	2.44	T_5	T_5
D_{56}	73.3	T_{56}	0.76	T_6	T_5+0.76

Table 8.3 Particular positions and times of the feed shoe tube for the center die along 0° orientation at 500 mm/s feed shoe speed

Distance, mm		Time period, s		Cumulative time (T_1' = 0), s	
D_{01}	73.3	T_{01}	0.27	T_1	T_2-0.49
D_{12}	243.6	T_{12}	0.49	T_2	T_3-0.26
D_{23}	64.1	T_{23}	0.26	T_3	T_4-0.26
D_{34}	64.1	T_{34}	0.26	T_4	T_5-0.49
D_{45}	243.6	T_{45}	0.49	T_5	T_5
D_{56}	73.3	T_{56}	0.27	T_6	T_5+0.27

One of the possible methods to solve this problem was to find a common point that the time recorded by the pressure sensor and the position of the feed shoe tube coincided with each other. Another consideration was that this point could be identified without too much difficulty from the pressure profile recorded by the pressure sensor. Obviously, the point that was easiest to be identified from the pressure ratio profile in Figure 8.1 was the point of the maximum pressure ratio. The time corresponding to this point was denotes by T_5 (Figure 8.1). This was based on the assumption that T_5 was recorded when the inner side of the front wall of the feed shoe tube was just about to leave the middle die. The thickness of the forward end of the feed shoe tube was 4.5 mm. As an example, if the pressure sensor strip was in the 0°-180° orientation, the forward end of the feed shoe wall was right above the last two sensor elements at time T_5, and this produced the maximum pressure values of the filling process for the two sensor elements.

By using this method, first T_5 was determined from the pressure ratio increase profile, which was the time of the last maximum pressure ratio value(s) of the nine sensor elements along 0°-180° orientation. Once T_5 was determined, other points corresponding to the positions shown in Figure 8.2 and Figure 8.3 could be determined, since the distances between every two positions and the speeds of the feed shoe were known. For instance, the distance between T_4 and T_5 was 243.6 mm, so the time of T_4 was calculated to be 12.18 s earlier than the time of T_5 for the feed shoe speed of 20 mm/s.

The distances between every two consecutive particular positions and corresponding time periods needed to cover the distances for the feed shoe speed of 20 mm/s are listed in Table 8.1. The data of the pressure sensor strip along 0° orientation were used to mark the particular times and then the particular positions. Those key positions and corresponding times for 0° orientation at 100 and 500 mm/s feed shoe speeds are shown in Table 8.2 and Table 8.3, respectively. For distances D_{01}, D_{23}, D_{34}, and D_{56}, additional times (already included in the calculation of time periods of the tables) were needed for acceleration or deceleration of the feed shoe. When the pressure sensor strip was along other orientations, most of the distances and times were the same, except D_{45}, D_{56}, T_{45}, and T_{56}. For different orientations of the pressure sensor strip, the maximum pressure values (observed at time T_5) were recorded when the feed shoe was at different positions. This resulted in D_{45}, D_{56}, T_{45}, and T_{56} being different for different orientations of the pressure sensor strip, while the totals of (D_{45} + D_{56}) and (T_{45} + T_{56}) were the same.

8.1.1 Normalization of time

For different feed shoe speeds, it would take different times for the entire filling process. This made it difficult to compare the pressure ratio increase profiles of different feed shoe speeds.

This problem was resolved by normalizing time for the entire filling process. This was done by dividing the actual time recorded by the pressure sensor strip with the value of the time to finish the whole filling process, as shown in the following equation:

$$\tau = \frac{t}{T_6 - T_1'} \tag{8.1}$$

where τ = normalized time, and t = time values recorded by the pressure sensor strip (by setting 0 at T_1') , s. After time was normalized, the pressure ratio profile shown in Figure 8.1 was transformed into the plot shown in Figure 8.6.

8.1.2 Four phases of the filling process

By using the particular positions and times, considering the nature of the die filling process, the pressure ratio profile shown in Figure 8.1 was divided into four distinctive phases, as shown in Figure 8.6. Phase I was from time T_1' to time T_2, which corresponded to the actual filling of the die during forward stroke. Phase II represented the rest period, which started from time T_2, when the feed shoe tube was leaving the center die, and ended at time T_4, when the feed shoe tube was just approaching the center die during backward stroke. During phase II, no powder was filled into the dies. From time T_4 to T_5 was phase III, which represented the actual filling portion of the backward stroke. Phase IV started from time T_5, the end of the backward filling part. The end of this phase (T_6) was also the end of the entire filling process, where the feed shoe tube returned to its initial position.

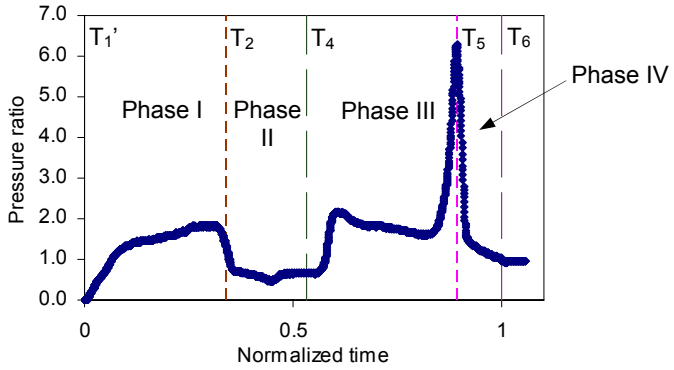

Figure 8.6 Average pressure ratio increase profile (with normalized time) at the center of 0° orientation of the center cylindrical die filled with the battery powder mixture at 20 mm/s feed shoe speed

8.1.3 Ten stages of the filling process

Based on the physics of the filling process and the feature of the pressure ratio profile, the entire pressure ratio profile divided into ten stages (Figure 8.7). Each stage is discussed and

modeled in the following sections. Start and end times of each stage are denoted continuously as $\tau^{a}_{b,c}$, where the superscript a designate the phase, subscript b denotes end of current stage and subscript c beginning of next stage. For example, the ending time of stage 1 is labeled as $\tau^{I}_{1,2}$, as it is in phase I, and it is the end of stage 1 and start of stage 2. Special cases are τ^{I}_{1} = T$_1$' (the start of stage 1, and also the start of the entire filling process), and τ^{IV}_{10} = T$_6$ (the end of stage 10, and also the end of the entire filling process), which have only one subscript. Figure 8.7 shows the start (or ending) times of all the nine stages, where $\tau^{III}_{8,9}$ = T$_5$ (please refer to Figure 8.6).

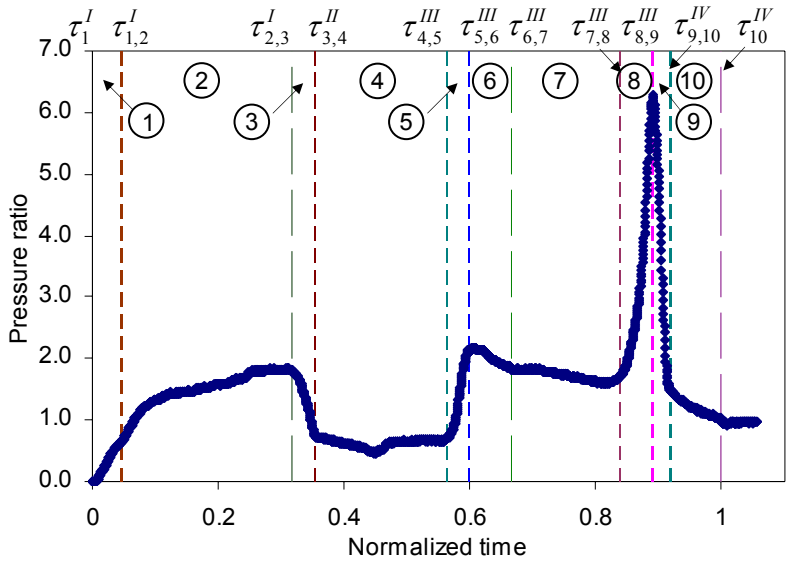

Figure 8.7 Ten stages of the average pressure ratio for modeling at the center of 0° orientation of the center cylindrical die filled with the battery powder mixture at 20 mm/s feed shoe speed

8.2 Phase I

Figure 8.8 shows the average pressure ratio profile during the forward stroke for the geometric center of the center cylindrical die (along 0° orientation) filled with the battery powder mixture at 20 mm/s feed shoe speed. The forward filling phase could again be divided into three stages. The first part, τ^{I}_{1} to $\tau^{I}_{1,2}$, was stage 1, which had almost constant deposition rate. The value of $\tau^{I}_{1,2}$ was determined by observation of the pressure ratio increase profile and performing numerical derivatives to the pressure ratio data. Usually, $\tau^{I}_{1,2}$ corresponded to the transitional point of a straight line and a curve, as shown in Figure 8.8. If numerical derivatives of the pressure ratio profile were taken, $\tau^{I}_{1,2}$ coincided with a rapid increase of the derivatives. For

example, the numerical derivative of the point before $\tau_{1,2}^{I}$ (Figure 8.8) was about 7.6, but the numerical derivative of the points after $\tau_{1,2}^{I}$ abruptly increased to 15.2. Central difference algorithm was used to get the numerical derivatives. The time interval was consistent throughout the process, and the error term had the order of square of the time interval (Pearson, 1986).

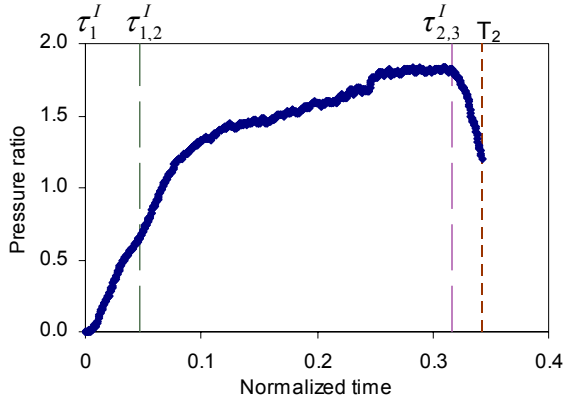

Figure 8.8 Average pressure ratio profile of phase I at the center of 0° orientation of the center cylindrical die filled with the battery powder mixture at 20 mm/s feed shoe speed

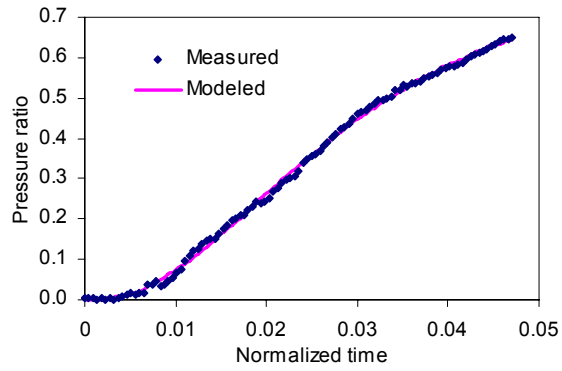

Figure 8.9 Model of stage 1 of the average pressure ratio at the center of 0° orientation of the center cylindrical die filled with the battery powder mixture at 20 mm/s feed shoe speed

8.2.1 Stage 1

As shown in Figure 8.9, stage 1 (τ_1^I to $\tau_{1,2}^I$) was a curve, which could again be divided into two parts for most locations around the forward end. The first part was concave up, and the powder filling rate (slope of the mass ratio curve) increased with time. The second part was concave down, and the powder filling rate decreased with time. The point of inflection was around normalized time of 0.02. This could be explained as follows. Actual die filling started right after time τ_1^I , and initially only a very small fraction of the powder in the front of the feed shoe was available for the die. Powder filling rate was very low at this time, especially for

locations at the forward end of the die, which was far from the feed shoe in stage 1. With the increase of time and the movement of the feed shoe, more powder in the front of the feed shoe could fill in the die, and so powder filling rate increased. This resulted in the concave-up curve of the first part. Around the end of the first part, powder filling rate increased to a certain degree, and the die was also filled to some extent. The distance between the top surface of the powder in the die and the bottom of the powder in the feed shoe became less and less. The upward pressure from the air above the filled powder became more pronounced and its effect reduced the powder filling rate. In the meanwhile, as indicated by previous researchers (Cocks et al., 2001; Wu et al., 2003a), nose flow (i.e., powder flowing from the tip of the powder mass) dominated the filling process. There must be a maximum filling rate for nose flow, which was reached at the end of the first part. These two reasons led to the decrease of the powder filling rate in the second part, when the data of the concave-down curve were collected.

All the ten stages of the filling profile could be mathematically represented by the following overall rate equation:

$$\frac{dP_p}{d\tau} = \alpha f(P_p, \tau) + \beta \tag{8.2}$$

where α, β are coefficients, and $f(P_p, \tau)$ is a function of pressure ratio and normalized time. It is expected that α, β, and $f(P_p, \tau)$ are location specific that are functions of powder characteristics. Furthermore, analysis of pressure rate profile showed that the nonlinear and complex Equation (8.2) can be simplified to

$$\frac{dP_p}{d\tau} = \alpha P_p F(\tau) + \beta \tag{8.3}$$

where $F(\tau)$ is a function of only normalized time.

Considering the sigmoidal shape of pressure ratio profile, the simplest choice for $F(\tau)$ that represented the data corresponded to the Chapman-Richards model. The functional form $F(\tau)$ is:

$$F(\tau) = \frac{1}{e^{b\tau} - 1} \tag{8.4}$$

where b is a deposition rate related coefficient. Integration of Equations (8.3) and (8.4) yielded the familiar Chapman-Richards model for the sigmoidal shape profile of stage 1 (τ_1^I to $\tau_{1,2}^I$), as shown below:

$$P_p = a(1 - e^{-b\tau})^c \tag{8.5}$$

where P_p = prorated pressure ratio,

a, b, and c are three coefficients (α of Equation (8.2) is the product of b and c).

In this model, coefficient *a* is the asymptote, the maximum pressure ratio value when time approaches ∞. Coefficients *b* and *c* together define the shape of the curve. For example, if *c* is kept constant, the larger *b* is, the faster the pressure ratio increases. If *b* is kept constant, the larger *c* is, the slower P_p increases. For the data shown in Figure 8.9 (pressure ratio at the center of the center cylindrical die filled with the battery powder mixture at feed shoe speed of 20 mm/s), $a = 0.79$, $b = 56.9$, and $c = 2.9$. The R-square value of this regression was 1.0.

The pressure ratio value at the end of this stage was close to that of the rest period. At 20 mm/s feed shoe speed, the average pressure ratio at the end of this stage for all of the measured locations (except two end locations close to the die wall) of the center cylindrical die was 0.56 (with a standard deviation of 0.10). The average pressure ratio of the last ten data points just before the end of the rest period, T_4, was 0.73 (with a standard deviation of 0.14). The pressure ratio at the end of the first stage was 78.3% (with a standard deviation of 11.3%) of the average pressure ratio before the end of the rest period. At 100 mm/s feed shoe speed, the average pressure ratio at the end of the stage of τ_1^I to $\tau_{1,2}^I$ for all of the measured locations (except two end locations close to the die wall) of the center cylindrical die was 0.45 (with a standard deviation of 0.05). The average pressure ratio of the last ten data points just before the end of the rest period, T_4, was 0.55 (with a standard deviation of 0.08). The pressure ratio at the end of the first stage was 84.1% (with a standard deviation of 13.1%) of the average pressure ratio before the end of the rest period.

The portion of deposition process from τ_1^I to $\tau_{1,2}^I$ was proposed to be responsible for most of the powder filling in the forward stroke. The following reasons supported this statement: (1) At 20 and 100 mm/s feed shoe speeds, the three dies were observed to be fully filled before or when the feed shoe arrived at the position corresponding to $\tau_{1,2}^I$, (2) In the portion of deposition process from τ_1^I to $\tau_{1,2}^I$, it was very likely that most pressures measured by the pressure sensor strip were exerted directly from the powder deposited into the dies. No pressure was from the feed shoe wall, and possibly very little pressure came from the powder in the feed shoe; (3) Nose flow prevailed in this stage, and according to Cocks et al. (2001) and Wu et al. (2003a), nose flow dominated the filling process. (4) The pattern of the filling pressure ratio profile from τ_1^I to $\tau_{1,2}^I$ was different from that of the following pressure ratio profile in the forward filling stage, which was obviously caused by the pressure of the powder in the feed shoe (Figure 8.8).

As stated in section 5.1.5, at 20 mm/s feed shoe speed, the forward stroke contributed 93.4% of the amount of powder filled in the dies during the entire filling process. At 100 mm/s

feed shoe speed, the forward stroke deposited 96.6% of the amount of powder filled in the dies during the entire filling process. Stage 1 also deposited most of the powder into the dies for the entire filling process.

For the center cylindrical die filled at 20 mm/s with the battery powder mixture, the average $\tau_{1,2}^{I}$ of all of the measured locations (except two end locations close to the die wall) was 0.038 (normalized time from τ_{1}^{I} to $\tau_{1,2}^{I}$) with a standard deviation of 0.006. The average total time from τ_{1}^{I} to τ_{10}^{IV} (T_6) for 20 mm/s feed shoe speed was 33.86 s. Therefore the actual time period between τ_{1}^{I} to $\tau_{1,2}^{I}$ was 1.29 s. At 20 mm/s feed shoe speed, the distance between τ_{1}^{I} to $\tau_{1,2}^{I}$ was 25.7 mm (somewhat larger than the diameter of the dies, 19.1 mm). This means that most of the powder filled into the dies just after the tip of the powder in the feed shoe passed over the die. As stated before, the average distance between T_1 and τ_{1}^{I} was 15 mm. So the average distance between T_1 and $\tau_{1,2}^{I}$ was 40.7 mm, as shown in Figure 8.10.

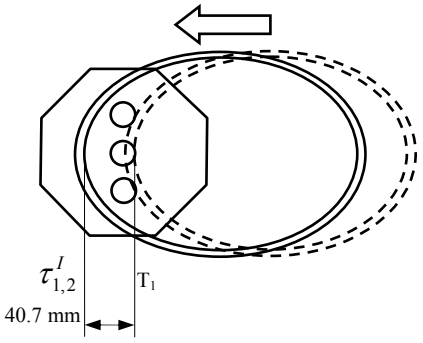

Figure 8.10 Position of the feed shoe at time $\tau_{1,2}^{I}$ for 20 mm/s feed shoe speed

To summarize above discussion about stage 1, most of the powder filled in the dies at a high filling rate within a very short time in the beginning of the forward stroke. This process (from τ_{1}^{I} to $\tau_{1,2}^{I}$) could be simulated as a sigmoidal curve. In the rest of the filling process, a very limited amount of powder was added to the dies.

8.2.2 Stage 2

Stage 2 ($\tau_{1,2}^{I}$ to $\tau_{2,3}^{I}$) was a curve, similar to that shown in Figure 8.8. It was caused by the pressure of the powder in the feed shoe, and could be simulated by a changing rate curve. The measured data points and the simulated curve of stage 2 are shown in Figure 8.11. Based on data analysis, the rate equation for the curve was:

$$\frac{dP_p}{d\tau} = \frac{q}{\tau - \tau_0} \tag{8.6}$$

where q and τ_o are two parameters. τ_o is the time lag or zero shift. It could be seen that the slope of the pressure ratio profile would decrease with time (or normalized time τ). The maximum slope, at the beginning of this stage τ_0, was determined by both q and τ_0. For the data shown in Figure 8.11 (pressure ratio at the center of the center cylindrical die filled with the battery powder mixture at feed shoe speed of 20 mm/s), q = 0.36, and τ_o = 0.04. The R-square value of this regression was 0.99. Upon integration, Equation (8.6) yielded the pressure ratio equation as follows:

$$P_p = P_{p0} + q\ln(\tau - \tau_0) \tag{8.7}$$

where P_{p0} is a parameter that is related to the pressure ratio at the end of stage 1. From Equation (8.7), q was obtained as:

$$q = \frac{P_p - P_{p0}}{\ln(\tau - \tau_0)} \tag{8.8}$$

This indicated that parameter q is the ratio of (P_p-P_{p0}) to ln(τ- τ_0), and (P_p-P_{p0}) is linearly proportional to ln(τ- τ_0).

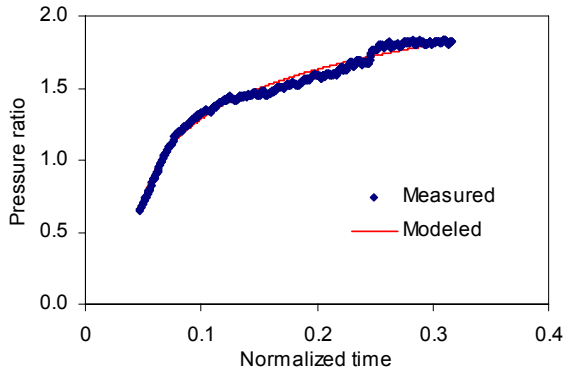

Figure 8.11 Model of stage 2 of the average pressure ratio at the center of 0° orientation of the center cylindrical die filled with the battery powder mixture at 20 mm/s feed shoe speed

The curve of stage 2 could be explained by the cumulative effect of two factors. First, the powder in the feed shoe had a nose-shaped profile at the front of the feed shoe, as shown in Figure 8.4. The powder in the feed shoe of this shape directly resulted in the pressure increase of stage 2. To a large extent, the shape of the powder in the feed shoe was similar to the curve shape of stage 2. Second, the particles in the dies were not completely tightly packed at this stage. Even though most of the powder mass in the feed shoe had an almost horizontal surface and generated the same pressure on the top surface of the dies, it took some time for the pressure sensor at the

bottom of the dies to experience the increased pressures. In other words, the pressure from the powder in the feed shoe compressed the powder in the dies incrementally, and in the meanwhile, the increasingly compacted powder in the dies transferred more and more pressure to the pressure sensor at the bottom of the die. Because of these two reasons, the pressure ratio increase profile was close to the curve shown in Figure 8.11.

8.2.3 First half of Stage 3

As shown in Figure 8.8, from $\tau_{2,3}^{I}$ to T_2 was the first half of stage 3. It was simulated by another constant negative rate. During this stage, the feed shoe started to leave the dies. The pressures applied by the powder in the feed shoe began to be released. The second half of stage 3 was in phase II, therefore the model for this stage is discussed in the following section.

8.3 Phase II

Phase II, the rest period, could be divided into two parts (Figure 8.12). The first part (T_2 to $\tau_{3,4}^{II}$) was the extension of the preceding stage (stage 3), i.e., constant declining rate. The existence of this stage meant that the pressure generated by the powder in the feed shoe could not be release immediately after the feed shoe left the dies, i.e., there was a time-dependent residual response. The time of the end of this stage was denoted as $\tau_{3,4}^{II}$. The second part, stage 4, started from time $\tau_{3,4}^{II}$, and ended at time T_4. During this stage, the powder gradually approached an equilibrium value. In other words, the approach to this steady state implied that $dP_p/d\tau$ was nearly zero as expected.

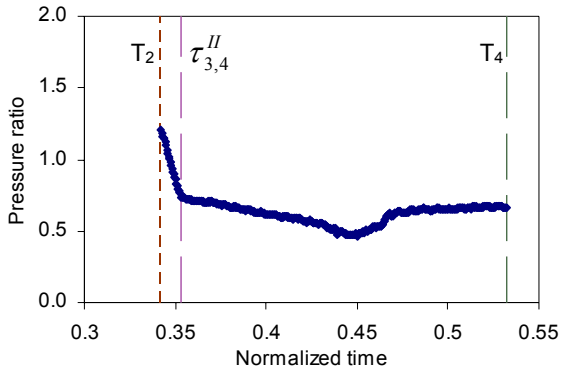

Figure 8.12 Average pressure ratio of phase II at the center of 0° orientation of the center cylindrical die filled with the battery powder mixture at 20 mm/s feed shoe speed

8.3.1 Stage 3

Figure 8.13 shows the measured data points and the simulated straight line of stage 3. The rate equation of this stage was:

$$\frac{dP_p}{d\tau} = m_3 \tag{8.9}$$

where m_3 = slope of the straight line. For the data shown in Figure 8.13 (pressure ratio at the center of the center cylindrical die filled with the battery powder mixture at feed shoe speed of 20 mm/s), the slope m_3 = -30.4. The R-square value of this regression was 0.96.

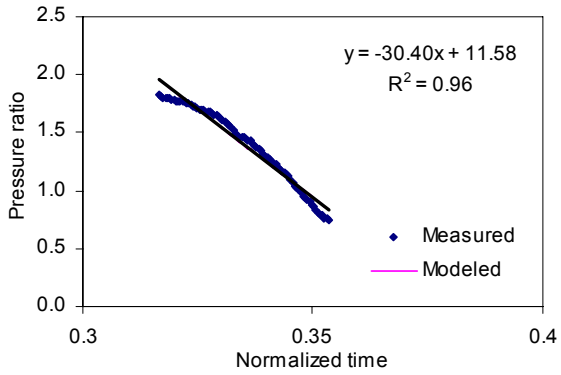

Figure 8.13 Model of stage 3 of the average pressure ratio at the center of 0° orientation of the center cylindrical die filled with the battery powder mixture at 20 mm/s feed shoe speed

8.3.2 Stage 4

The average of the ten data points before the end of the rest period (T_4) was taken as the pressure ratio (or pressure value) at the end of the forward stroke. The rationale was that right before T_4 the pressure reached an equilibrium state, and this state could best represent the pressure values of the rest period. Figure 8.14 compares the measured data points and the modeled horizontal line of stage 4. The measured pressure ratio decreased slowly in the first half of this stage, then there was a quick decline, after which the pressure ratio increased sharply back to normal. The rest of the profile was close to a horizontal line. The quick decline and sharp recovery occurred at about the end of the forward stroke. The motion of the feed shoe and the linear actuator at the end of the forward stroke seemed to be plausible reasons for this decline and recovery.

The pressure ratio during this stage should be constant, i.e., a horizontal line, since this stage represented the rest period. The pressure ratios that could really represent this stage were considered to be values right before the end of the rest period, i.e., time T_4. Pressure ratios in the first decreasing part were not stable since some of the pressures accumulated in the forward

stroke were slowly released. So this part was not selected to characterize the rest stage. The part of the quick decline was not representative of the rest stage, either. Because of these reasons, the simulated values of stage four were obtained by taking the average of the last ten data points right before the end of the rest period, time T_4, as shown in Figure 8.14. The simulated pressure ratio shown in Figure 8.14 was 0.67. The rate of pressure ratio in stage 4 is simply $dP_p/d\tau = 0$:

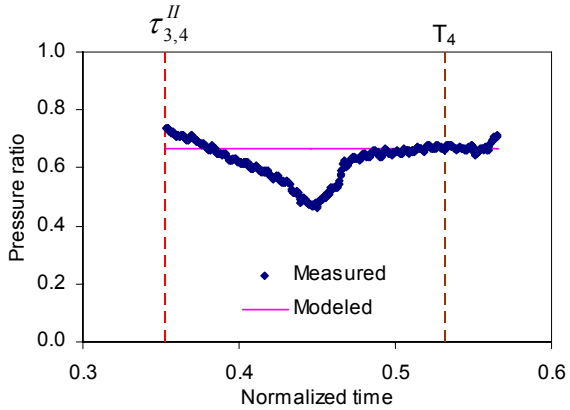

Figure 8.14 Model of stage 4 of the average pressure ratio at the center of 0° orientation of the center cylindrical die filled with the battery powder mixture at 20 mm/s feed shoe speed

8.4 Phase III

The backward filling stage could be divided into five parts, as shown in Figure 8.15. From T_4 to $\tau^{III}_{4,5}$ was a continuation of the stage 4. It took some time for the rear of the feed shoe wall to reach the pressure sensor element at the center of the die. A part of this time corresponded to the time from T_4 to $\tau^{III}_{4,5}$.

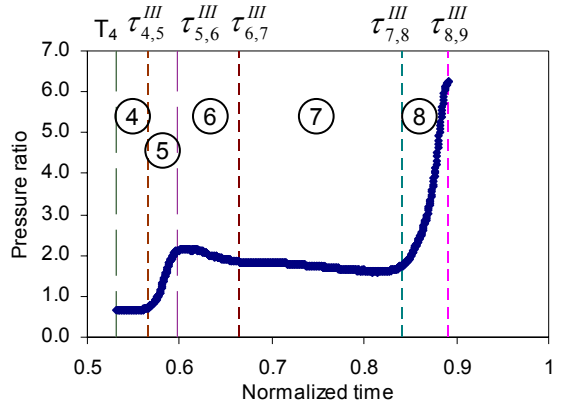

Figure 8.15 Average pressure ratio of phase III at the center of 0° orientation of the center cylindrical die filled with the battery powder mixture at 20 mm/s feed shoe speed

The second part ($\tau_{4,5}^{III}$ to $\tau_{5,6}^{III}$), stage 5, was the period when the rear of the feed shoe wall approached and passed over the location of the pressure sensor element. Because the powder in the dies was not tightly packed, the pressure increased by a relatively small amount. The pressure started to increase even before the rear of the feed shoe wall reached above the sensor element due to pressure transference and compression from the top to the bottom of the die. When the rear of the feed shoe wall reached right above the pressure sensor element, the pressure attained a maximum value at $\tau_{5,6}^{III}$. During this stage, the pressure profile can be represented by a constant rate equation.

The third part ($\tau_{5,6}^{III}$ to $\tau_{6,7}^{III}$), which was stage 6, covers the process when the rear of the feed shoe wall was moving away from the location of the pressure sensor element followed by the powder head in the feed shoe. As the rigid feed shoe wall gave way to flexible (compressible) powder head in feed shoe, the pressure decayed approaching a steady value.

The fourth part ($\tau_{6,7}^{III}$ to $\tau_{7,8}^{III}$), stage 7, began as the rear part of the feed shoe tube passed the location of the pressure sensor element. Much of the pressure during this part was generated by the powder head in the feed shoe. Theoretically, the pressure in this part should be constant, since the top surface of the powder in the feed shoe was almost horizontal. So the fourth part could be modelled by a horizontal line of constant pressure ratio.

The fifth part ($\tau_{7,8}^{III}$ to $\tau_{8,9}^{III}$), stage 8, occurred when the front of the feed shoe wall approached and passed over the location of the pressure sensor element. The pressure started to increase even before the front of the feed shoe wall reached above the sensor element due to pressure transference and compression from the top to the bottom of the die. As the front of the feed shoe wall reached just above the pressure sensor element, the pressure attained a maximum value at $\tau_{8,9}^{III}$. Because more powder was filled in the dies and the powder in the dies was more closely packed during the foregoing filling stages, the front of the feed shoe wall caused the maximum pressure ratio. The following subsection discusses mathematical representations for each of these stages.

8.4.1 Stage 5

The measured data points and the modeled straight line of stage 5 are shown in Figure 8.16. The rate equation of the straight line was:

$$\frac{dP_p}{d\tau} = m_5 \tag{8.10}$$

where m_5 = slope of the straight line. For the data shown in Figure 8.16 (pressure ratio at the center of the center cylindrical die filled with the battery powder mixture at feed shoe speed of 20 mm/s), the slope m_5 = 51.4. The R-square value of this regression was 0.98.

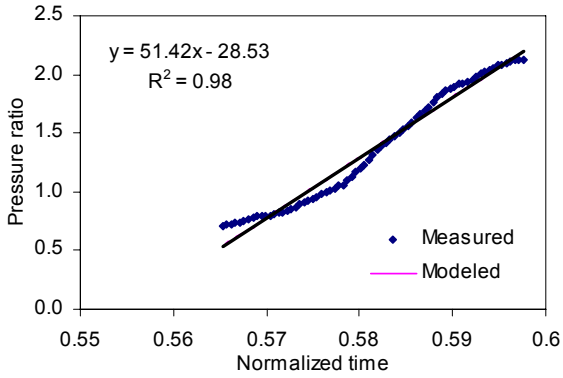

Figure 8.16 Model of stage 5 of the average pressure ratio at the center of 0° orientation of the center cylindrical die filled with the battery powder mixture at 20 mm/s feed shoe speed

8.4.2 Stage 6

Figure 8.17 shows the measured data points and the modeled straight line of stage 6. The rate equation of this stage was:

$$\frac{dP_p}{d\tau} = m_6 \tag{8.11}$$

where m_6 = slope of the straight line. For the data shown in Figure 8.17 (pressure ratio at the center of the center cylindrical die filled with the battery powder mixture at feed shoe speed of 20 mm/s), the slope m_6 = -5.5. The R-square value of this regression was 0.94.

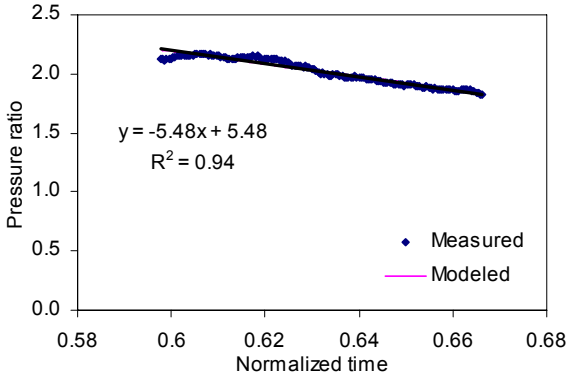

Figure 8.17 Model of stage 6 of the average pressure ratio at the center of 0° orientation of the center cylindrical die filled with the battery powder mixture at 20 mm/s feed shoe speed

8.4.3 Stage 7

Stage 7 was again simulated as a horizontal line (Figure 8.18). The simulated pressure ratio was 1.725, and it was obtained by taking the average of all the data points within this stage. The reason of using the average of all the data points, instead of select number of points (as for stage 4), was that the data were quite stable throughout the stage. The changing rate of pressure ratio in stage 7 was $dP_p/d\tau = 0$.

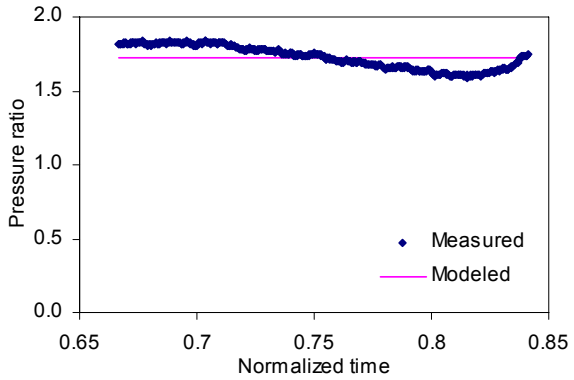

Figure 8.18 Model of stage 7 of the average pressure ratio at the center of 0° orientation of the center cylindrical die filled with the battery powder mixture at 20 mm/s feed shoe speed

8.4.4 Stage 8

The measured data points and the modeled straight line of stage 8 are shown in Figure 8.19. The rate equation of the profile was:

$$\frac{dP_p}{d\tau} = m_8 \tag{8.12}$$

where m_8 = slope of the straight line. For the data shown in Figure 8.19 (pressure ratio at the center of the center cylindrical die filled with the battery powder mixture at feed shoe speed of 20 mm/s), the slope m_8 = 95.3. The R-square value of this regression was 0.91.

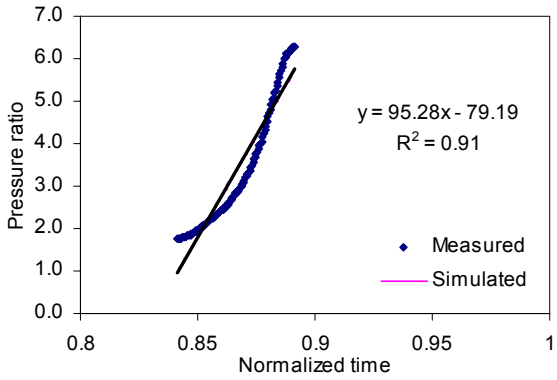

Figure 8.19 Model of stage 8 of the average pressure ratio at the center of 0° orientation of the center cylindrical die filled with the battery powder mixture at 20 mm/s feed shoe speed

8.5 Phase IV

Figure 8.20 shows the post-filling phase of the filling process. This phase comprised of two stages, stage 9 and stage 10. Stage 9, $\tau_{8,9}^{IV}$ to $\tau_{9,10}^{III}$, could be simulated by a rapid relaxation of pressure. During this stage, most of the pressure induced by the front side of the feed shoe wall and the powder in the feed shoe was released. Stage 10, $\tau_{9,10}^{IV}$ to τ_{10}^{IV}, was a process for the pressure to reach an equilibrium value. The pressure in this stage was produced by the powder in the dies and the residual pressure as a result of the feed shoe wall and the powder in the feed shoe. Stage 10 was represented by gradually declining pressure approaching an equilibrium value.

8.5.1 Stage 9

Figure 8.21 compares the measured data points and the modeled straight line of stage 9. The rate equation of the straight line was:

$$\frac{dP_p}{d\tau} = m_9 \tag{8.13}$$

where m_9 = slope of the straight line. For the data shown in Figure 8.21 (pressure ratio at the center of the center cylindrical die filled with the battery powder mixture at feed shoe speed of 20 mm/s), the slope m_9 = -200.8. The R-square value of this regression was 0.97.

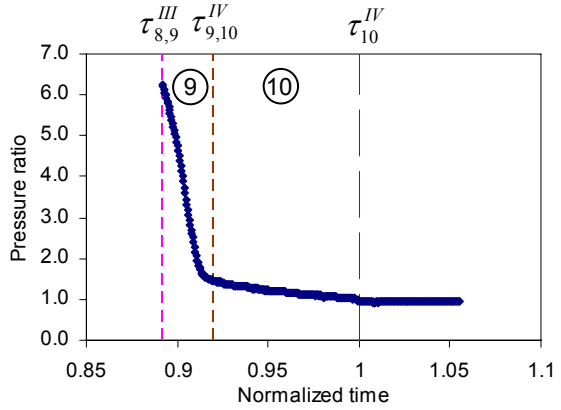

Figure 8.20 Average pressure ratio of phase IV at the center of 0° orientation of the center cylindrical die filled with the battery powder mixture at 20 mm/s feed shoe speed

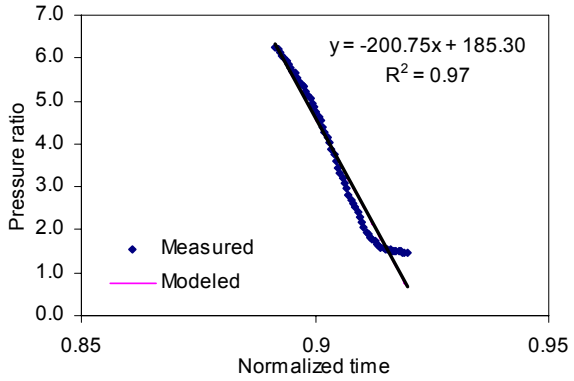

Figure 8.21 Model of stage 9 of the average pressure ratio at the center of 0° orientation of the center cylindrical die filled with the battery powder mixture at 20 mm/s feed shoe speed

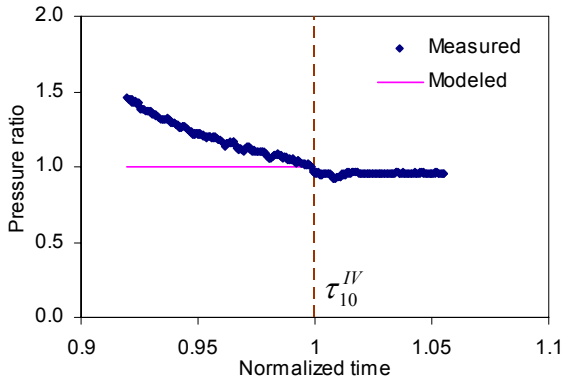

Figure 8.22 Model of stage 10 of the average pressure ratio at the center of 0° orientation of the center cylindrical die filled with the battery powder mixture at 20 mm/s feed shoe speed

8.5.2 Stage 10

Stage 10 was the last stage, where the pressure ratio became stable (Figure 8.22). The average of the last ten data was taken to represent the entire stage. The changing rate of pressure ratio in stage 10 was simplified as $dP_p/d\tau = 0$.

8.6 Overall Equation for All the Ten Stages

As shown in Equation (8.3), the rate of pressure ratio of all the ten stages can be mathematically represented by a single function represented by Equation (8.14).

$$\frac{dP_p}{d\tau} = \alpha P_p F(\tau) + \beta \qquad (8.14)$$

where α, β are coefficients, and $F(\tau)$ is a function of normalized time and function of locations and powder characteristics.

Table 8.4 shows the coefficients and specific forms of function $F(\tau)$, and the ranges of normalized time of the stages. The majority of the stages did not have the function $F(\tau)$ (their α

values were 0), since the changing rates of their pressure ratios were constant. Similarly, parameters for other locations can be obtained. As examples, Table 8.5 shows the parameters of location (r = 2 mm, θ = 180°) of the center cylindrical die filled at 20 mm/s feed shoe speed, and Table 8.6 shows the parameters of location (r = 2 mm, θ = 0°) of the center cylindrical die filled at 20 mm/s.

Figure 8.23 shows the measured data and simulated pressure ratios of the entire filling process. Some neighboring lines or curves did not intersect at the same starting or ending points as discussed above in separate stages. For instance, according to above division of stages, stage 7 and stage 8 intersected at $\tau = 0.841$. But the modeled lines of the two stages did not overlap at this point. Instead, they crossed at $\tau = 0.849$. However, most of the intersections of the modeled lines or curves were the same or quite close to the preceding end and proceeding start points of the stages. The root mean square error (RMSE) of the model for the data in Figure 8.23 was 0.13. The average relative difference (ARD) of the model for the data in Figure 8.23 was 0.06 (or 6%). RMSE and ARD were calculated according to the following equations.

$$RMSE = \sqrt{\frac{\sum (P_{p,\mathrm{mod}} - P_{p,mea})^2}{n}} \tag{8.15}$$

$$ARD = \frac{\sum \frac{\left| P_{p,\mathrm{mod}} - P_{p,mea} \right|}{P_{p,mea}}}{n} \tag{8.16}$$

where $P_{p,mod}$ = modeled pressure ratio,

$P_{p,mea}$ = measured pressure ratio,

n = the number of total data points.

Figure 8.24 and Figure 8.25 plot the pressure ratio profiles and the calculated profiles of the two cases. Figure 8.26 compares the measured pressure ratios of the three locations, (0, 0°), (2, 0°), and (2, 180°) of the center cylindrical die. The three profiles were very close to one another. Model parameters for other 14 locations in the vicinity of the center ($r \leq 4$ mm) of the center die are shown in Appendix D (Table A.162 to Table A.175). RMSE and ARD of the model for the data in Figure 8.24 were 0.11 and 0.06 (or 6%). RMSE and ARD of the model for the data in Figure 8.25 were 0.17 and 0.06 (or 6%). The average, maximum, and minimum values of RMSE for totally 17 locations in the vicinity of the center ($r \leq 4$ mm) of the center die were 0.13, 0.19, and 0.11. The average, maximum, and minimum values of ARD for totally 17 locations in the vicinity of the center ($r \leq 4$ mm) of the center die were 0.07, 0.09, and 0.06.

Most of the parameters of the model can not be determined quantitatively, as yet, through the physical properties of the powder, the size and shape of dies and the feed shoe, and other filling related parameters. Therefore, the model proposed in this research can only serve as a qualitative tool, instead of a quantitative prediction tool, for investigating the process.

Table 8.4 Model parameters for all the ten stages of the center (r = 0 mm, θ = 0°) of the center cylindrical die filled with the battery powder mixture at 20 mm/s feed shoe speed

Stage #	$P_pF(\tau)$	α	β	τ
1	$P_p/(e^{56.9\tau} -1)$	162.7	0	$0 \leq \tau \leq 0.05$
2	$1/(\tau-0.04)$	0.36	0	$0.05 \leq \tau \leq 0.32$
3	–	0	-30.4	$0.32 \leq \tau \leq 0.35$
4	–	0	0	$0.35 \leq \tau \leq 0.57$
5	–	0	51.4	$0.57 \leq \tau \leq 0.60$
6	–	0	-5.5	$0.60 \leq \tau \leq 0.67$
7	–	0	0	$0.67 \leq \tau \leq 0.84$
8	–	0	95.3	$0.84 \leq \tau \leq 0.89$
9	–	0	-200.8	$0.89 \leq \tau \leq 0.92$
10	–	0	0	$0.92 \leq \tau \leq 1.0$

Table 8.5 Model parameters for all the ten stages of location (r = 2 mm, θ = 180°) of the center cylindrical die filled with the battery powder mixture at 20 mm/s feed shoe speed

Stage #	$P_pF(\tau)$	α	β	τ
1	$P_p/(e^{75.6\tau} -1)$	393.5	0	$0 \leq \tau \leq 0.05$
2	$1/(\tau-0.04)$	0.35	0	$0.05 \leq \tau \leq 0.32$
3	–	0	-34.8	$0.32 \leq \tau \leq 0.36$
4	–	0	0	$0.36 \leq \tau \leq 0.57$
5	–	0	46.2	$0.57 \leq \tau \leq 0.60$
6	–	0	-4.9	$0.60 \leq \tau \leq 0.68$
7	–	0	0	$0.68 \leq \tau \leq 0.85$
8	–	0	78.8	$0.85 \leq \tau \leq 0.89$
9	–	0	-177.5	$0.89 \leq \tau \leq 0.92$
10	–	0	0	$0.92 \leq \tau \leq 1.0$

Table 8.6 Model parameters for all the ten stages of location (r = 2 mm, θ = 0°) of the center cylindrical die filled with the battery powder mixture at 20 mm/s feed shoe speed

Stage #	$P_pF(\tau)$	α	β	τ
1	$P_p/(e^{46.6\tau} -1)$	91.91	0	$0 \leq \tau \leq 0.05$
2	$1/(\tau-0.04)$	0.37	0	$0.05 \leq \tau \leq 0.32$
3	–	0	-33.1	$0.32 \leq \tau \leq 0.35$
4	–	0	0	$0.35 \leq \tau \leq 0.57$
5	–	0	51.4	$0.57 \leq \tau \leq 0.60$
6	–	0	-5.8	$0.60 \leq \tau \leq 0.69$
7	–	0	0	$0.69 \leq \tau \leq 0.85$
8	–	0	96.3	$0.85 \leq \tau \leq 0.90$
9	–	0	-239.6	$0.90 \leq \tau \leq 0.92$
10	–	0	0	$0.92 \leq \tau \leq 1.0$

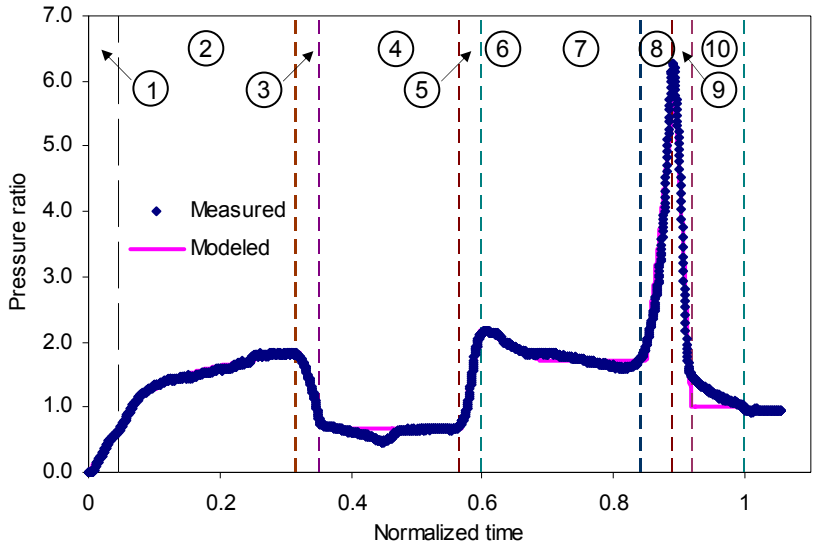

Figure 8.23 Comparison of the measured and modeled pressure ratios at the center of 0° orientation of the center cylindrical die filled with the battery powder mixture at 20 mm/s feed shoe speed

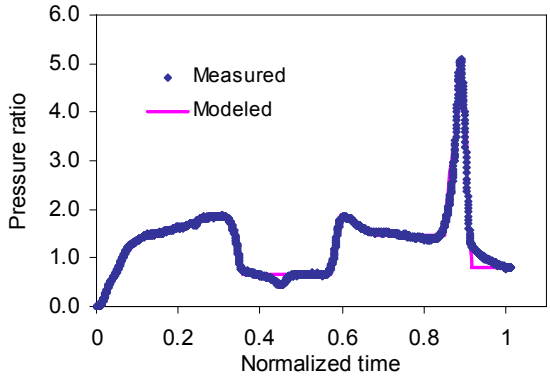

Figure 8.24 Comparison of the measured and modeled pressure ratios at location (2, 180°) of the center cylindrical die filled with the battery powder mixture at 20 mm/s feed shoe speed

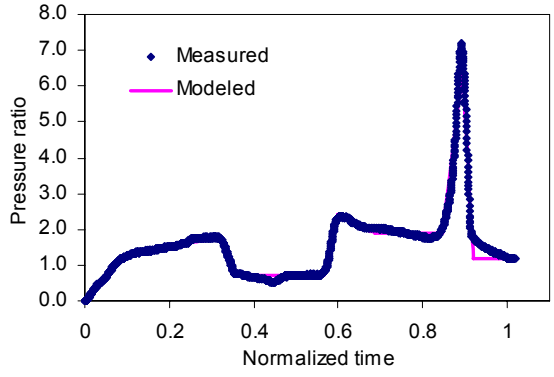

Figure 8.25 Comparison of the measured and modeled pressure ratios at location (2, 0°) of the center cylindrical die filled with the battery powder mixture at 20 mm/s feed shoe speed

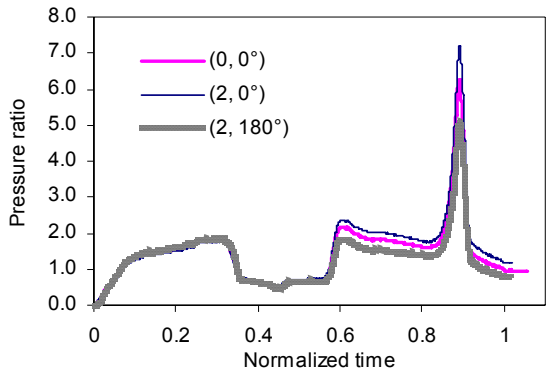

Figure 8.26 Comparison of the measured pressure ratios of locations (0, 0°), (2, 0°), and (2, 180°) of the center cylindrical die filled with the battery powder mixture at 20 mm/s feed shoe speed

8.7 Summary

Based on above discussion, the following concluding remarks can be made:

1. For cylindrical dies filled with the battery powder mixture, at lower feed shoe speeds (20 and 100 mm/s), the entire pressure increase profile could be divided into 10 stages. All the stages could be simulated by a rate equation, based on the data collected and the physics of the filling process.
2. The overall rate equation for all the ten stages was: $dP_p/d\tau = \alpha P_p F(\tau) + \beta$. The root mean square error (RMSE) of the model for the pressure ratio at the center of 0° orientation of the center cylindrical die filled with the battery powder mixture at 20 mm/s feed shoe speed was 0.13. The average relative difference (ARD) was 0.06 (or 6%). The average RMSE and ARD for totally 17 locations in the vicinity of the center ($r \leq 4$ mm) of the center die were 0.13 and 0.07 (or 7%), respectively.
3. For cylindrical dies filled with the battery powder mixture, stage 1, a very short period in the beginning of the forward stroke, deposited most of the total powder filled during the entire filling cycle. Rate equation for stage 1 was: $dP_p/d\tau = \alpha P_p/(e^{b\tau} - 1)$.

CHAPTER 9 CONCLUSIONS

Experimental data were collected for two powders (battery powder mixture and alumina powder) filled into three parallel-oriented dies of three shapes (cylinder, toroid, and E-shape) at three feed shoe speeds (20, 100, and 500 mm/s for the battery powder mixture; 20, 100, and 200 mm/s for the alumina powder; only 20 mm/s for E-shaped dies for both powders) by using PDT-II. Data were also collected for the two powders filled into three parallel-oriented dies of two shapes (cylinder and toroid) at two feed shoe speeds (20 and 500 mm/s for the battery powder mixture; 20 and 200 mm/s for the alumina powder) by CT scanning. Based on experimental data, data analysis, material properties, and model parameter determinations, as well as research objectives, the following key observations or conclusions are summarized:

1. PDT-II met the design requirements, such as precise and automatic control of feed shoe speed and acceleration rate, flexibility and ease of accommodating different combinations of various deposition-related parameters, and high precision and sensitivity of measurement system. It worked satisfactorily in terms of measurement of pressure change and pressure distribution at the bottom of dies during the powder filling process. PDT-II can generate real-time deposition profile throughout the entire process, in addition to final pressure values at multiple locations.
2. Data collected by PDT-II can be used to study the effects of various filling related parameters, such as die shape, powder flowability, and feed shoe speed, on the deposition process and final pressure distribution. The quantitative information can be used to optimize the deposition process to obtain a better filling.
3. Cylindrical dies filled with the battery powder mixture:
    a. At low feed shoe speeds (20 and 100 mm/s), the half circle close to the leeward end had higher final pressure values than the forward half circle. The backward stroke of feed shoe movement contributed to this distribution pattern.
    b. At high feed shoe speed (500 mm/s), the final pressure distribution was more uniform than at lower feed shoe speeds. Higher momentum of particles at higher feed shoe speed contributed to this trend by minimizing arching and allowing particles to locally rearrange. Another possible reason was that higher rate of die filling decreased opportunity for particle segregation and promoted uniform filling.

c. The final within-die pressure distribution at the bottom of the dies was not always symmetrical about the center line of the feed shoe movement direction. The overall trend was that pressure decreased with increasing radial distance for lower feed shoe speeds. The distribution was not always regular for higher feed shoe speed.
d. The three parallel dies did not always have similar and symmetrical pressure distributions. This phenomenon could be attributed to the complex flow pattern within the feed shoe tube during simultaneous filling of the three dies.
e. Higher feed shoe speed (500 mm/s) resulted in higher final pressure values (774.5 to 1424.5 Pa) than lower feed shoe speeds (20 and 100 mm/s) (235.2 to 1136.0 Pa) at most of the locations. The experimental data suggested there is an upper limit, beyond which fill density will decrease with increasing feed shoe speed.
f. At lower feed shoe speeds (20 and 100 mm/s), the right die tended to have higher final pressure values (393.8 to 1136.0 Pa) than the center die (235.2 to 726.0 Pa). At higher feed shoe speed (500 mm/s), the quantitative differences between center (774.5 to 1246.1 Pa) and right dies (897.3 to 1424.5 Pa) were reduced.
g. Most of the filled powder was deposited in the forward stroke (about 93% at 20 mm/s, 97% at 100 mm/s, and 90% at 500 mm/s).

4. Toroidal dies filled with the battery powder mixture:
   a. The area around 0° orientation (close to the leeward end) had the highest pressure values (1186.7 to 2498.0 Pa). The average pressure values of the remaining area were 353.7 to 648.0 Pa.
   b. The pressure distribution was symmetrical about the center line parallel to the feed shoe movement direction.
   c. Based on PDT-II data, the highest feed shoe speed (500 mm/s) led to the most nonuniform and the densest filling among the three speeds.
   d. Higher feed shoe speed did not always result in higher final pressure values.
   e. The right die tended to have higher final pressure values (215.0 to 2498.0 Pa) than the center die (95.4 to 2052.5 Pa). The possible reasons for this trend were the complex powder flow pattern, the oval cross-section shape of the feed shoe, and the relative positions of the two dies to the feed shoe wall.
5. E-shaped dies filled with the battery powder mixture and the alumina powders:

a. The final pressure values of the middle leg were higher than those of the left and the right legs. For the battery powder mixture, the average pressure of the middle leg was from 308.9 to 760.7 Pa, and the average pressures of the left and right legs were from 148.9 to 530.3 Pa. For the alumina powder, the average pressure of the middle leg was from 41.9 to 130.7 Pa, and the average pressures of the left and right legs were from 26.1 to 79.6 Pa. This was attributed to the wider opening of the middle leg.
b. For the battery powder mixture, the area along the back side had the highest final pressure values (1054.6 to 1303.8 Pa). This could be explained by the larger opening of the back and the drag effect of the backward movement of the feed shoe.
c. The pressure distribution was symmetrical about the center line parallel to the feed shoe movement direction.
d. Neither the center die, nor the right die always had higher pressure values than the other one. Because of the complexity of the E-shape, the pattern of powder flow and deposition into E-shaped dies was much more complex than the cylindrical and toroidal dies.
e. When filled with the alumina powder, unlike the battery powder mixture, the area of the highest final pressure value (126.4 to 152.3 Pa) of the alumina powder moved from the back side to the vicinity of the junction of the middle leg and the back.

6. Cylindrical dies filled with the alumina powder:
   a. At lower feed shoe speed (20 and 100 mm/s), the final pressure distribution was symmetrical about the center line that was parallel to the feed shoe movement direction. The center zone had the highest pressure values, and final pressures decreased monotonically with increasing radii.
   b. At higher feed shoe speed (200 mm/s), the final pressure distribution was irregular and varied more than at lower feed shoe speeds. This was attributed to the indefinable movement of the air currents, which had more influence on the alumina powder of finer granules and lower bulk density.
   c. No consistent speed effect was discovered.
   d. At low feed shoe speeds (20 and 100 mm/s), the right die tended to have higher final pressure values (49.5 to 288.8 Pa) than the center die (68.9 to 167.0 Pa). At the highest feed speed (500 mm/s), the center (58.7 to 213.6 Pa) and the right

(126.7 to 208.9) dies had similar final pressure values. The higher kinetic energy of particles at higher feed shoe speed densified particle packing in both dies and reduced the difference of the center and the right dies.

7. Effect of die shape (cylindrical vs. toroidal):
    a. Neither of the two die shapes (cylinder and toroid) led to consistently higher or lower final pressure values, when filled with the battery powder mixture.
    b. For alumina powder, no consistent trend and no large differences were observed between cylindrical and toroidal dies.
8. CT data of cylindrical dies filled with battery powder mixture and its comparison with PDT-II data:
    a. CT number vs. bulk density did not have a strong linear correlation for the battery powder mixture and the alumina powder ($R^2 \leq 0.625$). There were a couple of reasons, including the heterogeneity of the powder mixtures of different chemical constituents.
    b. The final bulk density distribution obtained by CT scanning was considered as uniform. However, this was based on the weak linear correlation ($R^2 \leq 0.625$) of CT number vs. bulk density.
    c. CT data showed that there were almost no differences among the three dies, with regard to the distribution uniformity. However, this was based on the weak linear correlation ($R^2 \leq 0.625$) of CT number vs. bulk density.
    d. CT scanner and PDT-II measured two different attributes. CT scanning assessed the distribution of bulk densities or mass values, while PDT-II measured the distribution of pressure values at the bottom of the filled dies. The distribution patterns of CT data and PDT-II data had similarities.
    e. Both CT data and PDT-II data revealed that the half circle close to the leeward had higher final mass (pressure) values. Qualitatively, PDT-II could provide useful information about the mass distribution, even though its basis is pressure distribution.
9. Model:
    a. For cylindrical dies filled with the battery powder mixture at 20 mm/s feed shoe speed, the entire pressure increase profile could be divided into 10 stages. All the stages could be simulated by a rate equation, based on the data collected and the physics of the filling process.

b. The overall rate equation for all the ten stages was: $dP_p/d\tau = \alpha P_p F(\tau) + \beta$. The root mean square error (RMSE) of the model for the pressure ratio at the center of 0° orientation of the center cylindrical die filled with the battery powder mixture at 20 mm/s feed shoe speed was 0.13. The average relative difference (ARD) was 0.06 (or 6%). The average RMSE and ARD for totally 17 locations in the vicinity of the center ($r \leq 4$ mm) of the center die were 0.13 and 0.07 (or 7%), respectively.

c. Stage 1, a very short period in the beginning of the forward stroke, deposited most of the total powder filled during the entire filling cycle. Rate equation for stage 1 was: $dP_p/d\tau = \alpha P_p/(e^{b\tau} -1)$.

d. The model proposed in this research can only serve as a qualitative tool, instead of a quantitative prediction tool, for investigating the process.

CHAPTER 10 RECOMMENDATIONS FOR FUTURE WORK

Based on the experience gained from this study, the following recommendations can be made for future research:

1. PDT-II tester:
    a. *Pressure sensor*: If it is possible, smaller and square sensor elements are preferred to the current sensor elements. Compared to the size of the dies used in this research, the sensor elements were not sufficiently small. Rectangular element shape made comparison of pressure values at the same location along different orientations difficult, since the overlapped area is only a small fraction of the total area of a sensor element. Also, sensor elements arranged in a matrix, instead of a strip, can make data comparison of multiple locations easier. Higher sensitivity of the pressure sensor is also necessary for better data.
    b. *Feed shoe*: For the reason that is similar to using dies of simpler shapes, the feed shoe tube of square cross section is suggested to be used. Also, feed shoe angle is suggested to be a factor influencing the die filling process, especially in the first part of the forward stroke and the last part of the backward stroke. For example, a feed shoe tube perpendicular to the table surface may exert less pressure to the powder in the dies during the backward stroke than a feed shoe of 45° angle. The major reason is that the tilted feed shoe wall (inner side) may produce downward pressure to the powder in the dies, while the vertical feed shoe wall (inner side) cannot. Because of limited time and resources, only the angle of 45° was used for this research, since it is the most common feed shoe angle in industrial practices.
    c. *Transparent components of the tester*: If the upper parts of the tester, such as feed shoe, feed shoe table, and dies, are fabricated of transparent materials, it will make direct observation and recording of the filling process by video cameras possible or more convenient.
    d. *High speed video camera*: It is better to have one or a couple of high speed video cameras to record the entire filling process, especially the short initial period of the forward stroke. At least, qualitative information about the filling process, such as the behavior of the filling powder and the extent of the filling at certain filling stage, can be obtained from the recorded videos.

2. Testing dies:
    a. *Shape*: Dies of simpler geometrical shapes (such as cubic shape) can be used to study the feed shoe die filling process, especially for model purpose. Considering the fact that the deposition process is very complex, simpler die shape may help make the process less complicated and relatively easier to be investigated.
    b. *Horizontal dimension*: Dies of relative larger size are also preferred because it can make pressure or mass distribution pattern more evident. It provides larger area around the center of the dies far from the die wall and less affected. Also, larger dies can make the filling process longer, so that more data can be collected and probably more details or features can be observed from the data.
    c. *Depth*: Not all of the pressure recorded by the pressure sensor strip was generated by the powder filled in dies. The measured pressure value was a mixture of effects of filled powder, powder in the feed shoe, feed shoe wall, bridging, powder internal friction, and friction between particles and the die wall. The pressure values could not be used directly for evaluation of bulk density distribution or mass distribution of powder deposition, especially for deep dies. To overcome this limitation and minimize effects other than filled powder, shallower dies should be used. As long as pressure to be measured is above the minimum sensitivity, the shallower, the better.
    d. *Space between dies*: Dies of different interval spaces might result in different filling features if other factors kept the same.
    e. *Layout of dies*: Locations of dies relative to the feed shoe wall were suspected to influence die filling. Also, dies arranged in different ways (e.g., three dies in a row or three dies in a triangle) could be investigated.
3. Testing powder samples: More powder samples of different physical properties (size, size distribution, and bulk density, etc.) are necessary to verify and improve the conclusions and the model proposed in this study.
4. Testing parameters:
    a. *Feed shoe speed*: The current lowest feed speed, 20 mm/s, is relatively slow; however, it is recommended that even lower feed shoe speeds be used to extend the filling process, so as to get more data and more features about the filling.
    b. *Height of powder in the feed shoe*: Less powder in the feed shoe will generate less pressure in the dies. This will make the pressures generated directly by the filled powder more notable.

5. CT scanning:
    a. *Powder of uniform chemical components*: If it is possible, powder samples of single chemical constituent are preferred for CT scanning test. At least, different chemical constituents of a sample should be homogeneously distributed.
    b. *Replicates*: More replicates should be conducted to get reliable and repeatable results.
6. Model improvement: More attention should be directed to the very short period in the beginning of the forward stroke, when the cylindrical dies were 80-90% filled (at 20-100 mm/s feed shoe speed with the battery powder mixture). Also, the model needs to be expanded to other die shapes, powders, and feed shoe speeds.

REFERENCES

1. Abdullah, E. C. and D. Geldart. 1999. The use of density measurements as flowability indicators. *Powder Technology* 102 (2): 151-165.
2. Aczel, Amir D. 1995. *Statistics: Concepts and Applications*. Chicago: Richard D. Irwin, Inc.
3. ASAE D274.1 Feb03. 2003. Flow of Grain and Seeds through Orifices. American Society of Agricultural Engineers.
4. ASTM B212-99. Standard test method for apparent density of free-flowing metal powders using the hall flowmeter funnel. ASTM International.
5. ASTM B213-03. Standard test method for flow rate of metal powders. ASTM International.
6. ASTM B 855-94 (Reapproved 1999). Standard test method for volumetric flow rate of metal powders using Arnold Meter and Hall Funnel. ASTM International.
7. ASTM E 1441-00. 2003. Standard guide for computed tomography (CT) imaging. ASTM International.
8. Bell, T. A. 1993. Measurement of powder flowability. *Advances in Powder Metallurgy & Particulate Materials* 1: 169-180.
9. Benenati, R. F. and C. B. Brosilow. 1962. Void fraction distribution in beds of spheres. *American Institute of Chemical Engineers Journal* 8(3): 359-361.
10. Beverloo, W. A., H. A. Leniger, and Van de Velde J. 1961. The flow of granular materials through orifices. *Chem. Engng. Sci.* 15: 260-269.
11. Bishop, A. W. and D. J. Henkel. 1957. *The Measurement of Soil Properties in the Triaxial Test*. E. Arnold, London.
12. Bocchini, G. F. 1987. Influence of small die width on filing and compacting densities. *Powder Metallurgy* 30(4): 261-266.
13. Brown, R. L. and J. C. Richards. 1959. Exploratory study of the flow of granules through apertures. *Trans. Instn. Chem. Engrs.* 37: 108-119.
14. Brown, R. L. and J. C. Richards. 1960. Profile of flow of granules through apertures. *Trans. Instn. Chem. Engrs.* 38: 243-256.
15. Brown, R. L. and J. C. Richards. 1965. Kinematics of the flow of dry powders and bulk solids. *Rheologica. Acta.* 4(3): 153-165.
16. Bruff, W. and A. W. Jenike. 1967. A silo for ground anthracite. *Powder Technology* 1: 252-256.
17. Carman, P. C. 1937. Fluid flow through granular beds. *Trans. Inst. Chem. Eng.* 15: 150-166.
18. Carstensen, J. T. 1984. Tableting and pelletization in the pharmaceutical industry. In *Handbook of Powder Science and Technology*, ed. M. E. Fayed and L. Otten, ch. 7, 252-269. New York: Van Nostrand Reinhold Company.
19. Chang, C. S. and H. H. Converse. 1988. Flow rates of wheat and sorghum through horizontal orifices. *Transactions of the ASAE* 31(1): 300-304.
20. Chang, C. S., H. H. Converse, and F. S. Lai. 1984. Flow rate of corn through orifices as affected by moisture content. *Transactions of the ASAE* 27(5): 1586-1589.
21. Chang, C. S., H. H. Converse, and J. L. Steele. 1991. Flow rates of grain through various shapes of vertical and horizontal orifices. *Transactions of the ASAE* 34(4): 1789-1796.
22. Chen, J. F., S. K. Yu, J. Y. Ooi, and J. M. Rotter. 2001. Finite element modeling of filling pressures in a full-scale silo. *Journal of Engineering Mechanics* 1058-1066.
23. Chen, W. F. and G. Y. Baladi. 1985. *Soil Plasticity: Theory and Implementation*. Amsterdam, Netherlands: Elsevier.
24. Cocks, A. C. F., L. Dihoru, and T. Lawrence. 2001. A fundamental study of die filling. In *PM 2001 Proceedings*, 255-260. Acropolis Convention Center, Nice, France. 22-24 October.
25. Copley, D. C., J. W. Eberhard, and G. A. Mohr. 1994. Computed tomography part I: introduction and industrial applications. *JOM* 46(1): 14-26.
26. Crewdson, B. J., A. L. Ormond, and R. M. Nedderman. 1977. Air-impeded discharge of fine particles from a hopper. *Powder Technology* 16(2): 197-207.
27. Cumberland, D. J. and R. J. Crawford. 1987. *The Packing of Particles*. Amsterdam: Elsevier.

28. Davidson, J. F. and R. M. Nedderman. 1973. The hour-glass theory of hopper flow. *Trans. Instn. Chem. Engrs.* 51: 29.
29. Davies, R. 2001. Particle science and technology-a view at the millennium. *Powder Technology* 119: 45-57.
30. Demetry, C., F. S. Souto, B. C. Ryden, and J. M. Roy. 1998. Tactile sensing of density uniformity in powder beds after die filing. *Powder Technology* 99: 119-124.
31. Dhanoa, P. S. and V. M. Puri. 1997. Experimental analysis of deposition of particulate materials into confined spaces. ASAE Paper No. 974106. ASAE, St Joseph, MI.
32. Dhanoa, P. S. and V. M. Puri. 1998. Deposition of particulate materials confined spaces-new tester development and experimental results. *KONA Powder and Particle* 16:152-159.
33. Duffy, S. P. and V. M. Puri. 2002. Primary segregation shear cell for size-segregation analysis of binary mixtures. *KONA Powder and Particle* 20:196-207.
34. Duffy, S. P. and V. M. Puri. 2003. Development and validation of a constitutive model for size-segregation during percolation. *KONA Powder and Particle* 21:151-162.
35. Faikin, V. I., V. P. Levin, and Y. N. Gribenyuk. 1976. Influence of the rate of die filling on the density of the powder. *Soviet Powder Metallurgy and Metal Ceramics* 15(8):590-592.
36. Farber, L, G. Tardos, & J. N. Michaels. 2003. Use of x-ray tomography to study the porosity and morphology of granules. *Powder Technology* 132: 57-63.
37. Fickie, K. E., R. Mehrabi, and R. Jackson. 1989. Density variations in a granular material flowing from a wedge-shaped hopper. *A. I. Che. J.* 35:853.
38. Fowler, R. T. and J. R. Glastonbury. 1959. The flow of granular solids through orifices. *Chemical Engineering Science* 10: 150-156.
39. Franklin, F. L. and L. N. Johanson. 1955. Flow of granular material through a circular orifice. *Chemical Engineering Science* 4: 119-129.
40. Fraser, H. J. 1935. Experimental study of porosity and permeability of clastic sediments. *Journal of Geology* 43(8): 910-1010.
41. Freeman, R. 2001. An insight into the flowability and characterization of powders. *American Laboratory* 33(16): 13-14+16.
42. Geldart, D. 1990. Powder processing-the overall view. In *Principles of Powder Technology*, ed. M. Rhodes, 1-7. England: John Wiley & Sons.
43. German, R. M. 1989. *Particle Packing Characteristics*. Princeton, New Jersey: Metal Powder Industries Federation.
44. Graton, L. C. and H. J. Fraser. 1935. Systematic packing of spheres–with particular relation to porosity and permeability. *Journal of Geology* 43(8): 785-909.
45. Gray, W. A. 1959. A study of the packing of large, solid, spherical particles. Ph. D. Thesis. University of Leeds.
46. Gray, W. A. 1968. *The Packing of Solid Particles*. London: Chapman and Hall Ltd.
47. Guillot, M., M. Pesant, H. Chtourou, D. Boies, and P. Carrier. 2002. Study and improvement of die filling systems for reducing density variations. *Advances in Powder Metallurgy & Particulate Materials* 4: 237-251.
48. Harmens, A. 1963. Flow of granular material through horizontal apertures. *Chemical Engineering Science* 18: 297-306.
49. Hashimoto, Y., M. Murakami, and Y. Seki. 2002. Improvement of die filling by “agitating-shoe”. *Advances in Powder Metallurgy & Particulate Materials* 4: 252-257.
50. Haskins. J. J. and W. F. Jandeska. 1998. Powder flow and die filling studies using computed tomography. *Advances in Powder Metallurgy & Particulate Materials* 3(10): 77-87.
51. Hinchley, J. W. 1926. *Chemical Engineering*. Encylopaedia Bratannica.
52. Hjortsberg, E. 2000. Density variations in iron powder caused by die filling. In *Proceedings of 2000 Powder Metallurgy World Congress*, 617-620. Japan, 12-16 November.
53. Hjortsberg, E. and B. Bergquist. 2002. Filling induced density variations in metal powder. *Powder Metallurgy* 45(2): 146-153.
54. Holst, J. M. F. G., J. Y. Ooi, J. M. Rotter, and G. H. Rong. 1999. Numerical modeling of silo filling. I: continuum analyses. *Journal of Engineering Mechanics* 94-103.
55. Huntington, A. P. and N. M. Rooney. 1971. Discharge of granular materials from hoppers. Project Report, Department of Chemical Engineering, University of Cambridge.

56. Jaccard, J. and C. K. Wan. 1996. LISREL approaches to interaction effects in multiple regression. Thousand Oaks, CA: Sage Publications.
57. Jenike, A. W. 1961. Gravity flow of bulk solids. Utah Engineering Experimental Station, University of Utah, Bulletin 108.
58. Jiang, H. 2003. *Computed Tomography: Principles, Design, Artifacts, and Recent Advances*. Bellingham, Washington: Spie Press.
59. Jofriet, J. C., B. LeLievre, and T. F. Fwa. 1977. Friction model for finite element analyses of silos. *Transactions of the ASAE* 20(4): 735-739.
60. Kamath, S and V. M. Puri. 1990. Measurement of powder flow constitutive model parameters using a cubical triaxial tester. *Powder Technology* 90: 59-70.
61. Kamath, S. and V. M. Puri. 1999. Finite element model development and validation for incipient flow analysis of cohesive powder from hopper bins. *Powder Technology* 102: 184-193.
62. Katalymov, A. V. and P. I. Lukyanov. 1976. *Theor. Found. Chem. Engng.* (USSR). 10: 153.
63. Kestenbaum, D. 1997. Sand castles and cocktail nuts. *New Scientist* 2083: 25-28.
64. Ketchum, M. S. 1929. *The Design of Walls, Bins and Grain Elevators*. New York: McGraw-Hill.
65. Kolbuszewski, J. 1950. Notes on the deposition of sands. *Research* 3: 478-483.
66. Kondoh, M. and S. Takemoto. 1996. Visualization of powder behavior for gravity filling. *Advances in Powder Metallurgy & Particulate Materials* 2(7): 117-129.
67. Kondoh, M., S. Takemoto, and I. Urata. 1998. Development of uniform powder filling method − aeration powder filling. In *Proceedings of the 1998 Powder Metallurgy World Congress & Exhibition*, 85-90. Granada, Spain, 18-22 October.
68. Kotchanova, I. I. 1970. Experimental and theoretical investigations on the discharge of granular materials from bins. *Powder Technology* 4(1): 32.
69. Ladipo, D. D. and V. M. Puri. 1997. Computer controlled shear cell for measurement of flow properties of particulate materials. *Powder Technology* 92: 135-146.
70. Langston, P. A., U. Tuzun, and D. M. Heyes. 1995. Discrete element simulation of granular flow in 2D and 3D hoppers: dependence of discharge rate and wall stress on particle interactions. *Chemical Engineering Science* 50(6): 967-987.
71. Larsson M. and H. Vidarsson. 2000. Efficient bonding for dimensional stability. *Advances in Powder Metallurgy & Particulate Materials* 2: 41-53.
72. Lawrence, L. R. and J. K. Beddow. 1968. Some effects of vibration upon powder segregation during die filling. *Powder Technology* 2(2): 125-130.
73. Lawrence, L. R. and J. K. Beddow. 1969. Powder segregation during die filling. *Powder Technology* 2(5): 253-259.
74. Levy, A. and H. Kalman. 2001. *Handbook of Conveying and Handling of Particulate Solids*. New York: Elsevier.
75. Macleod, H. M. 1983. Compaction of ceramics. In *Enlargement and Compaction of Particulate Solids*, ed. N. G. Stanley-Wood, ch. 11, 241-276. London: Butterworths.
76. Macrae, J. C. and W. A. Gray. 1961. Significance of the properties of materials in the packing of real spherical particles. *British Journal of Applied Physics* 12 (4): 164-172.
77. Martz, H. E. J., C. M. Logan, and P. J. Shull. 2002. Radiology. In *Nondestructive Evaluation: Theory, Techniques, and Applications*, ed. P. J. Shull, ch. 7, 447-595. New York: Marcel Dekker, Inc.
78. Matuttis, H. G., S. Luding, and H. J. Herrmann. 2000. Discrete element simulations of dense packings and heaps made of spherical and non-spherical particles. *Powder Technology* 109: 278-292.
79. McGeary, R. K. 1961. Mechanical packing of spherical particles. *Journal of American Ceramic Society* 44(10): 513-522.
80. Mittal, B. and V. M. Puri. 1999a. Correlation between powder deposition methods and green compact quality: part I mechanical properties of powders. *Particulate Science and Technology* 17: 283-299.
81. Mittal, B. and V. M. Puri. 1999b. Correlation between powder deposition methods and green compact quality: part II compact quality and correlations. *Particulate Science and Technology* 17: 301-315.
82. Mittal, B. and V. M. Puri. 2001. A real-time mass deposition tester for bulk solids deposition profiles in non-simple shape storage containers. ASAE Paper. No. 014023. ASAE, St. Joseph, MI.
83. Mittal, B., V. M. Puri, and W. Shaffer. 2001a. Analysis of feed shoe powder deposition method using a real-time cumulative mass deposition tester. *KONA Powder and Particle* 19: 144-154.

84. Mittal, B., H. Yi, V. M. Puri, A. S. McNitt, and C. F. Mancino. 2001b. Measurement of bulk mechanical properties and modeling the load-response of rootzone sands. Part 2: Effect of moisture on continuous sand mixtures. *Particulate Science and Technology* 19: 369-386.
85. Molenda, M., J. Horabik, and I. J. Ross. 1993. Loads in model grain bins as affected by filling methods. *Transactions of ASAE* 36(3): 915-919.
86. Molenda, M., J. Horabik and I. J. Ross. 1996. Effect of filling method on load distribution in model grain bins. *Transactions of ASAE* 39(1): 219-224.
87. Montgomery, D. C. 2005. *Design and Analysis of Experiments*. New York: John Wiley & Sons, Inc.
88. Morrison, H. L. 1978. One-dimensional analysis of granular flow in bunkers. *Chemical Engineering Science* 33(2): 241-251.
89. Morrison, H. L. and O. Richmond. 1976. Application of spencer's ideal soil model to granular materials flow. Journal of Applied Mechanics, *Transactions ASME* 43(1): 49-53.
90. Moysey, E. B. 1984. The effect of grain spreaders on grain friction and bin wall pressures. *J. agri. Engng Res.* 30(2): 149-156.
91. Mroz, Z. and C. Z. Szymanski. 1971. Gravity flow of a granular material in a converging channel. *Archives of Mechanics* 23(6): 897-917.
92. Myers, M. E. and M. Sellers. 1978. Rate of discharge from wedge-shaped hoppers. Project Report, Department of Chemical Engineering, University of Cambridge.
93. Nakatani, K., S. Takemoto, and I. Urata. 1999. A study of aeration powder filling method for high performance P/M parts. *Advances in Powder Metallurgy & Particulate Materials* 2(7): 299-306.
94. Nedderman R. M., U. Tüzün, S. B. Savage, and G. T. Houlsby. 1982. The flow of granular materials-1: discharge rates from hoppers. *Chemical Engineering Science* 37(11): 1597-1609.
95. Newton, R. H., G. S. Dunham, and T. P. Simpson. 1945. TCC catalytic cracking process for motor gasoline production. *Transactions of the American Institute of Chemical Engineers* 41(2): 215-232.
96. Obrist, A. F., A. Flisch, and J. Hofmann. 2004. Point cloud reconstruction with sub-pixel accuracy by slice-adaptive thresholding of X-ray computed tomography images. *NDT and E International* 37(5): 373-380.
97. Oman, A. O. and K. M. Watson. 1944. Pressure drops in granular beds. *National Petroleum News* 36(44): R795-R796 + R798-R802.
98. Pearson, C. E. 1986. *Numerical Methods in Engineering and Science*. New York: Van Nostrand Reinhold Company.
99. Peterson, J. E. and A. M. Small. 1994. Evaluation of metal powders using Arnold density meter and Hall flowmeter. *Powder Metallurgy* 37(1): 37-41.
100. Pietsch, W. 1997. Size enlargement by agglomeration. In *Handbook of Powder Science and Technology*, ed. M. E. Fayed and L. Otten, ch. 6, 202-377. New York: Chapman & Hall.
101. Puri, V. M. and P. S. Dhanoa. 2000. Real-time spatial particulate mass deposition testers. United States Patent. Patent number: 6,089,100.
102. Readey, M. J. and F. M. Mahoney. 1995. Compaction of spray-dried ceramic powders: an experimental study of the factors that control green density. 27th International SAMPE Technical Conference. Oct. 9-12.
103. Reed, J. S. 1995. *Principles of Ceramics Processing*. New York: John Wiley & Sons, Inc.
104. Rice, E. R. and J. Tengzelius. 1986. Die filling characteristics of metal powders. *Powder Metallurgy* 29(3): 183-194.
105. Richards, J. C. 1966. *The Storage and Recovery of Particulate Solids*. London: Inst. Chem. Engrs.
106. Ridgway, K. and K. J. Tarbuck. 1966. Radial voidage variation in randomly-packed beds of spheres of different sizes. *J. Pharm. Pharmac.* 18: 1685-1755.
107. Rose, H. F. and T. Tanaka. 1959. Rate of discharge of granular materials from bins and hoppers. *The Engineer* (London) 208: 465.
108. Savage, S. B. 1965. The mass flow of granular materials derived from coupled velocity-stress fields. *British Journal of Applied Physics* 16: 1885-1888.
109. Sawayama, T. and Y. Seki. 1999. The effect of filling conditions on die filling. *Advances in Powder Metallurgy & Particulate Materials* 1(2): 61-72.
110. Schiff, D. and R. B. D'Agostino. 1996. *Practical Engineering Statistics*. New York: John Wiley & Sons, Inc.
111. Schulze, D. 1998. Measurement of the flowability of bulk solids. In *Silos: Fundamental of Theory, Behavior and Design*, ed. C. J. Brown, 18-52. London: E & Fn Spon.

112. Seville, J. P. K., U. Tüzün, and R. Clift. 1997. *Processing of Particulate Solids*. London: Blackie Academic & Professional.
113. Shergold, F. A. 1953. Percentage voids in compacted gravel as measure of its angularity. *Magazine of Concrete Research* 13: 3-10
114. Smid, J., P. V. Xuan, and Jiri Thyn. 1993. Effect of filling method on the packing distribution of a catalyst bed. *Chem. Eng. Technol.* 16: 114-118.
115. Sohn, H. Y. and C. Moreland. 1968. The effect of particle size distribution on packing density. *Canadian Journal of Chemical Engineering* 46(3): 162-167
116. Sullivan, W. N. 1973. Heat transfer to flowing granular media. Ph. D. Thesis, California Institute of Technology.
117. Sundaresan, S. 2001. Some outstanding questions in handling of cohesionless particles. *Powder Technology* 115: 2-7.
118. Suzuki, H., M. Lutheran, T. Sawayama, and Y. Seki. 1997. Die flowability test and weight variation. *Advances in Powder Metallurgy & Particulate Materials* 1(2): 3-11.
119. Tang, P. and V. M. Puri. 2004. Methods for minimizing segregation, a review. *Particulate Science and Technology* 22(4): 321 - 337
120. Tejchman, J. 1998. Numerical simulation of filling in silos with a polar hypoplastic constitutive model. *Powder Technology* 96: 227-239.
121. Thomson, F. M. 1984. Storage of particulate solids. In *Handbook of Powder Science and Technology*, ed. M. E. Fayed and L. Otten, ch. 9, 365-463. New York: Van Nostrand Reinhold Company.
122. Thomson, F. M. 1997. Storage and flow of particulate solids. In *Handbook of Powder Science and Technology*, ed. M. E. Fayed and L. Otten, ch. 8, 389-486. New York: Chapman & Hall.
123. Urata, I., S. Takemoto, and M. Kondoh. 1998. Improvement of dimensional tolerance for automotive PM parts by aeration powder filling method. In *Proceedings of the 1998 Powder Metallurgy World Congress & Exhibition*, 91-96. Granada, Spain, 18-22 October.
124. Verghese, T. M. and R. M. Nedderman. 1995. The discharge of fine sands from conical hoppers. *Chemical Engineering Science* 50(9): 3143-3153.
125. Vidarsson H. and J. Arvidsson. 2000. Die filling capability of powder mixes. In *Proceedings of 2000 Powder Metallurgy World Congress*, 413-416. Japan, 12-16 November.
126. Wadsworth, J. 1960. Experimental examination of local processes in packed beds of homogeneous spheres. Nat. Res. Council of Canada, *Mech. Eng. Report.* MT-41. NRC No. 5895.
127. Wakeman, R. J. 1975. Packing densities of particles with log-normal size distributions. *Powder Technology* 11(3): 297-299.
128. Walker, D. M. 1967. Basis for bunker design. *Powder Technology* 1(4): 228-236.
129. White, D. G. 2002. State of the North American P/M industry-2002. *Advances in Powder Metallurgy & Particulate Materials* 1: 1-12.
130. Wieghardt, V. K. 1952. Über einige versuche an strömungen in sand. *Ingenieur-Archiv* 20: 109-115.
131. Williams, J. C. 1976. The segregation of particulate materials. A review. Powder Technology. 15(2): 245-251
132. Wu, C. and A. C. F. Cocks. 2004. Flow behavior of powders during die filling. *Powder Metallurgy* 47(2): 127-136.
133. Wu, C., A. C. F. Cocks, and O. T. Gillia. 2002. Experimental and numerical investigations of die filling and powder transfer. *Advances in Powder Metallurgy and Particulate Materials* 4: 258-272.
134. Wu, C., A. C. F. Cocks, and O. T. Gillia. 2003a. Die filling and powder transfer. *The International Journal of Powder Metallurgy* 39(4): 51-64.
135. Wu, C., L. Dihoru, and A. C. F. Cocks. 2003b. The flow of powder into simple and stepped dies. *Powder technology* 134: 24-39.
136. Zahrah, T. F. and R. Rowland. 2002. Use of fluidization for die filling applications. *P/M Science & Technology Briefs* 4(2): 13-17.
137. Zahrah, T. F., R. Rowland, and G. Gasbarre Jr. 2001. Fluidized fill shoe for uniform die filling. *Key Engineering Materials* 189-191: 288-294.
138. Zhang, J. Y. and V. Rudolph. 1991. Effect of shear friction on solid flow through an orifice. *Ind. Eng. Chem. Res.* 30: 1977-1981.
139. Zhang, Q., V. M. Puri, and H. B. Manbeck. 1986. Finite element modeling of thermally induced pressures in grain bins filled with cohesionless granular materials. *Transactions of the ASAE* 29(1): 248-256.

APPENDICES

Appendix A Programs to Run the Linear Actuator

The following prorams were used to control the motion of the linear actuator and the feed shoe. The only parameters to be changed to achieve the desired accelerations, velocities, and travel distances are those starting with A (acceleration), AD (deceleration), V (velocity), and D (distance). As an example, V20A2G.PRG was a program to run the feed shoe at 20 mm with 0.2g acceleration. In this program, A77.2 represents that the acceleration is 77.2 in/s^2 (1.96 m/s^2 or 0.2g), while AD77.2 shows that the deceleration is also 77.2 in/s^2 (1.96 m/s^2 or 0.2g). V0.787 stands for velocity of 0.787 in/s (20 mm/s). D15 indicates that the travel distance of the forward stroke is 15 in (381 mm), while D-15 signifies that the travel distance of the backward stroke is also 15 in (381 mm). V100A2G.PRG, V200A2G.PRG, and V500A2G.PRG were programs to run the linear actuator at 100, 200, and 500 mm/s, respectively, with an acceleration of 0.2g (1.96 m/s^2).

V20A2G.PRG

```
MC0
MA0
LH3
SCALE1
DRES25000
SCLV25000
SCLD25000
SCLA25000
A77.2
AD77.2
V0.787
D15
GO
D-15
GO
END
```

V100A2G.PRG

```
MC0
MA0
LH3
SCALE1
DRES25000
SCLV25000
SCLD25000
SCLA25000
A77.2
AD77.2
V3.937
D15
GO
D-15
GO
END
```

V200A2G.PRG

```
MC0
MA0
LH3
SCALE1
DRES25000
SCLV25000
SCLD25000
SCLA25000
A77.2
AD77.2
V7.874
D15
GO
D-15
GO
END
```

V500A2G.PRG

```
MC0
MA0
LH3
SCALE1
DRES25000
SCLV25000
SCLD25000
SCLA25000
A77.2
AD77.2
V19.685
D15
GO
D-15
GO
END
```

Appendix B Selected PDT-II Data of Battery powder mixture

Center Cylindrical Die

Table A.1 Prorated final pressure ratios in 0°-180° orientation of the center cylindrical die filled at feed shoe speed of 20 mm/s

Orientation	180°				Center	0°			
Radius, mm	8	6	4	2	0	2	4	6	8
Run #1	0.208	0.683	0.848	0.814	1.000	1.540	1.019	1.021	1.241
Run #2	0.666	1.085	0.887	1.029	1.000	1.539	1.476	1.533	1.415
Run #3	0.418	0.535	0.562	0.909	1.000	0.778	1.007	1.099	0.682
Run #4	0.491	0.601	0.662	0.703	1.000	1.228	1.318	1.490	0.719
Run #5	0.323	0.461	0.549	0.656	1.000	0.890	1.429	1.349	1.095
Run #6	0.386	0.624	0.723	0.764	1.000	1.218	0.997	1.095	1.073
Mean	0.415	0.665	0.705	0.813	1.000	1.199	1.208	1.264	1.037
StDev	0.155	0.220	0.142	0.138	–	0.318	0.225	0.222	0.289
COV	37.4	33.0	20.1	17.0	–	26.5	18.7	17.5	27.8

Table A.2 P-values of paired t-test after modified Bonferroni procedure for prorated final pressure ratios in 0°-180° orientation of the center cylindrical die filled at feed shoe speed of 20 mm/s

	Orientation	180°				Center	0°			
	Radius, mm	8	6	4	2	0	2	4	6	8
180°	8	–	–	–	–	–	–	–	–	–
	6	–	–							–
	4	–	9.848							–
	2	–	1.026	2.165						–
Center	0	–	0.283	0.079	0.440					–
0°	2	–	**0.030**	**0.026**	0.520	3.909				–
	4	–	0.065	0.109	0.300	1.541	20.043			–
	6	–	**0.029**	0.053	0.149	0.691	14.122	3.644	–	–
	8	–	–	–	–	–	–	–	–	–

*Entries in bold are significantly different (P < 0.05)

Table A.3 Prorated final pressure ratios in 0°-180° orientation of the center cylindrical die filled at feed shoe speed of 100 mm/s

Orientation	180°				Center	0°			
Radius, mm	8	6	4	2	0	2	4	6	8
Run #1	0.215	0.451	0.543	0.745	1.000	1.264	1.215	1.267	0.901
Run #2	0.187	0.517	0.715	1.032	1.000	0.913	1.184	1.110	0.667
Run #3	0.090	0.212	0.437	0.602	1.000	1.199	0.899	0.657	0.512
Run #4	0.134	0.257	0.493	0.737	1.000	1.313	1.108	0.782	0.804
Run #5	0.234	0.456	0.691	0.849	1.000	0.751	0.718	0.893	0.673
Run #6	0.107	0.197	0.337	0.416	1.000	0.793	0.625	0.902	0.456
Mean	0.161	0.348	0.536	0.730	1.000	1.039	0.958	0.935	0.669
StDev	0.059	0.142	0.146	0.210	–	0.249	0.249	0.221	0.168
COV	36.7	40.6	27.3	28.8	–	24.0	26.0	23.7	25.2

Table A.4 P-values of paired t-test after modified Bonferroni procedure for prorated final pressure ratios in 0°-180° orientation of the center cylindrical die filled at feed shoe speed of 100 mm/s

	Orientation	180°				Center	0°			
	Radius, mm	8	6	4	2	0	2	4	6	8
180°	8	–	–	–	–	–	–	–	–	–
	6	–	–							–
	4	–	**0.010**							–
	2	–	**0.007**	**0.031**						–
Center	0	–	**0.002**	**0.010**	0.535					–
0°	2	–	**0.041**	0.247	1.510	15.092				–
	4	–	**0.017**	0.149	0.932	14.652	7.675			–
	6	–	**0.004**	0.069	1.745	10.601	10.296	17.237	–	–
	8	–	–	–	–	–	–	–	–	–

*Entries in bold are significantly different (P < 0.05)

Table A.5 Prorated final pressure ratios in 0°-180° orientation of center cylindrical die filled at feed shoe speed of 500 mm/s

Orientation	180°				Center	0°			
Radius, mm	8	6	4	2	0	2	4	6	8
Run #1	0.176	0.291	0.634	0.534	1.000	0.932	1.037	0.940	1.105
Run #2	0.442	0.639	0.708	0.929	1.000	1.200	1.165	1.316	0.955
Run #3	0.362	0.707	0.647	0.881	1.000	1.012	0.977	1.095	1.334
Run #4	0.531	1.089	0.805	0.726	1.000	1.098	1.324	1.421	0.988
Run #5	0.599	0.955	0.905	0.960	1.000	0.878	0.847	0.855	0.926
Run #6	0.369	1.060	0.674	0.843	1.000	0.780	0.717	0.990	1.030
Mean	0.413	0.790	0.729	0.812	1.000	0.983	1.011	1.103	1.056
StDev	0.148	0.306	0.106	0.159	–	0.152	0.218	0.222	0.150
COV	35.9	38.7	14.5	19.5	–	15.5	21.5	20.2	14.2

Table A.6 P-values of paired t-test after modified Bonferroni procedure for prorated final pressure ratios in 0°-180° orientation of the center cylindrical die filled at feed shoe speed of 500 mm/s

	Orientation	180°				Center	0°			
	Radius, mm	8	6	4	2	0	2	4	6	8
180°	8	–	–	–	–	–	–	–	–	–
	6	–	–							–
	4	–	12.300							–
	2	–	17.816	4.750						–
Center	0	–	3.236	**0.031**	0.708					–
0°	2	–	5.360	0.423	2.158	16.819				–
	4	–	4.901	0.673	3.586	18.992	12.099			–
	6	–	1.521	0.279	0.983	6.478	1.529	2.840	–	–
	8	–	–	–	–	–	–	–	–	–

*Entries in bold are significantly different ($P < 0.05$)

Table A.7 Prorated final pressure ratios in 90°-270° orientation of the center cylindrical die filled at feed shoe speed of 20 mm/s

Orientation	270°				Center	90°			
Radius, mm	8	6	4	2	0	2	4	6	8
Run #1	0.383	0.510	0.720	0.768	1.000	0.608	0.690	0.982	0.647
Run #2	0.337	0.749	0.956	0.969	1.000	0.678	0.798	1.033	0.517
Run #3	0.486	0.981	0.740	1.056	1.000	1.006	1.751	1.902	0.933
Run #4	0.364	0.629	0.817	0.712	1.000	0.714	0.698	0.924	0.576
Run #5	0.411	0.594	0.955	1.348	1.000	0.974	1.037	0.912	0.581
Run #6	0.326	0.520	0.793	0.754	1.000	1.077	1.091	1.036	0.675
Mean	0.385	0.664	0.830	0.934	1.000	0.843	1.011	1.131	0.655
StDev	0.059	0.178	0.103	0.244	–	0.199	0.400	0.381	0.147
COV	15.2	26.8	12.4	26.1	–	23.6	39.6	33.7	22.5

Table A.8 P-values of paired t-test after modified Bonferroni procedure for prorated final pressure ratios in 90°-270° orientation of the center cylindrical die filled at feed shoe speed of 20 mm/s

	Orientation	270°				Center	90°			
	Radius, mm	8	6	4	2	0	2	4	6	8
270°	8	–	–	–	–	–	–	–	–	–
	6	–	–							–
	4	–	2.292							–
	2	–	0.947	5.518						–
Center	0	–	0.120	0.209	11.300					–
90°	2	–	2.640	18.794	8.545	2.322				–
	4	–	0.720	7.551	13.364	19.954	4.434			–
	6	–	0.110	3.190	6.174	9.188	2.119	3.035	–	–
	8	–	–	–	–	–	–	–	–	–

Table A.9 Prorated final pressure ratios in 90°-270° orientation of the center cylindrical die filled at feed shoe speed of 100 mm/s

Orientation	270°				Center	90°			
Radius, mm	8	6	4	2	0	2	4	6	8
Run #1	0.518	0.717	0.667	0.584	1.000	1.227	0.905	0.612	0.645
Run #2	0.495	0.844	1.149	1.047	1.000	0.972	1.099	0.891	0.357
Run #3	0.465	0.737	0.500	0.675	1.000	1.069	1.047	0.763	0.584
Run #4	0.489	0.920	0.947	0.792	1.000	0.963	0.695	0.903	0.493
Run #5	0.507	0.510	0.826	0.963	1.000	0.919	0.685	0.966	0.716
Run #6	0.725	1.132	1.091	1.039	1.000	0.837	0.943	1.264	0.979
Mean	0.533	0.810	0.863	0.850	1.000	0.998	0.896	0.900	0.629
StDev	0.096	0.210	0.250	0.196	–	0.135	0.174	0.219	0.212
COV	18.0	26.0	29.0	23.1	–	13.6	19.4	24.3	33.7

Table A.10 P-values of paired t-test after modified Bonferroni procedure for prorated final pressure ratios in 90°-270° orientation of the center cylindrical die filled at feed shoe speed of 100 mm/s

	Orientation	270°				Center	90°			
	Radius, mm	8	6	4	2	0	2	4	6	8
270°	8	–	–	–	–	–	–	–	–	–
	6	–	–							–
	4	–	12.060							–
	2	–	14.635	17.246						–
Center	0	–	1.625	4.985	2.512					–
90°	2	–	3.727	8.322	6.516	20.395				–
	4	–	8.534	16.854	14.276	4.232	5.501			–
	6	–	6.529	13.810	7.988	6.555	10.957	20.454	–	–
	8	–	–	–	–	–	–	–	–	–

Table A.11 Prorated final pressure ratios in 90°-270° orientation of center cylindrical die filled at feed shoe speed of 500 mm/s

Orientation	270°				Center	90°			
Radius, mm	8	6	4	2	0	2	4	6	8
Run #1	0.826	0.928	1.043	1.803	1.000	1.352	1.325	0.938	0.899
Run #2	0.593	0.650	0.675	0.860	1.000	1.247	1.435	0.838	0.622
Run #3	0.663	1.145	1.028	1.073	1.000	0.881	1.105	1.237	0.869
Run #4	0.527	0.937	1.348	0.965	1.000	0.610	1.316	1.231	0.737
Run #5	0.314	0.654	0.668	0.822	1.000	1.012	1.080	0.852	0.776
Run #6	0.639	0.791	0.969	0.865	1.000	1.227	1.116	0.846	0.753
Mean	0.594	0.851	0.955	1.065	1.000	1.055	1.229	0.990	0.776
StDev	0.169	0.191	0.256	0.373	–	0.277	0.148	0.192	0.100
COV	28.5	22.5	26.8	35.0	–	26.3	12.1	19.4	12.8

Table A.12 P-values of paired t-test after modified Bonferroni procedure for prorated final pressure ratios in 90°-270° orientation of the center cylindrical die filled at feed shoe speed of 500 mm/s

	Orientation	270°				Center	90°			
	Radius, mm	8	6	4	2	0	2	4	6	8
270°	8	–	–	–	–	–	–	–	–	–
	6	–	–							–
	4	–	4.557							–
	2	–	3.844	10.746						–
Center	0	–	2.401	14.407	14.452					–
90°	2	–	5.499	13.164	19.954	13.615				–
	4	–	0.355	1.356	6.604	0.269	4.200			–
	6	–	0.495	13.152	14.063	19.002	15.476	1.388	–	–
	8	–	–	–	–	–	–	–	–	–

Table A.13 Prorated final pressure ratios in 45°-225° orientation of the center cylindrical die filled at feed shoe speed of 20 mm/s

Orientation	225°				Center	45°			
Radius, mm	8	6	4	2	0	2	4	6	8
Run #1	0.854	1.251	1.099	1.250	1.000	1.344	1.526	1.264	0.690
Run #2	0.716	1.513	1.560	1.163	1.000	1.751	1.856	1.458	1.074
Run #3	0.451	0.784	1.195	1.272	1.000	1.095	1.240	1.392	0.987
Run #4	0.594	1.123	1.397	1.135	1.000	1.250	1.231	1.285	1.338
Run #5	0.368	0.921	0.884	0.798	1.000	0.919	0.798	0.850	0.704
Run #6	0.571	0.934	0.988	1.182	1.000	1.331	1.368	1.146	0.999
Mean	0.592	1.088	1.187	1.133	1.000	1.282	1.337	1.233	0.966
StDev	0.176	0.265	0.254	0.172	–	0.281	0.351	0.216	0.244
COV	29.7	24.4	21.4	15.2	–	21.9	26.3	17.5	25.2

Table A.14 P-values of paired t-test after modified Bonferroni procedure for prorated final pressure ratios in 45°-225° orientation of the center cylindrical die filled at feed shoe speed of 20 mm/s

	Orientation	225°				Center	45°			
	Radius, mm	8	6	4	2	0	2	4	6	8
225°	8	–	–	–	–	–	–	–	–	–
	6	–	–							–
	4	–	6.157							–
	2	–	15.038	12.686						–
Center	0	–	9.574	2.760	2.454					–
45°	2	–	0.501	6.120	4.204	1.206				–
	4	–	0.844	4.329	2.518	1.385	6.029			–
	6	–	4.648	9.906	1.949	0.969	12.168	6.254	–	–
	8	–	–	–	–	–	–	–	–	–

Table A.15 Prorated final pressure ratios in 45°-225° orientation of the center cylindrical die filled at feed shoe speed of 100 mm/s

Orientation	225°				Center	45°			
Radius, mm	8	6	4	2	0	2	4	6	8
Run #1	0.211	0.821	0.810	0.742	1.000	1.011	0.887	0.842	0.876
Run #2	0.485	0.706	0.553	1.002	1.000	1.303	1.377	0.860	0.814
Run #3	0.187	0.418	0.547	0.960	1.000	1.061	0.990	0.589	0.280
Run #4	0.823	0.844	0.874	1.129	1.000	1.212	1.360	1.127	0.522
Run #5	0.201	0.353	0.229	0.448	1.000	0.888	0.640	0.453	0.626
Run #6	0.441	0.599	0.664	0.861	1.000	1.854	1.706	1.047	0.660
Mean	0.391	0.623	0.613	0.857	1.000	1.221	1.160	0.820	0.630
StDev	0.248	0.205	0.230	0.239	–	0.343	0.390	0.259	0.214
COV	63.4	33.0	37.6	27.9	–	28.1	33.6	31.6	34.0

Table A.16 P-values of paired t-test after modified Bonferroni procedure for prorated final pressure ratios in 45°-225° orientation of the center cylindrical die filled at feed shoe speed of 100 mm/s

	Orientation	225°				Center	45°			
	Radius, mm	8	6	4	2	0	2	4	6	8
225°	8	–	–	–	–	–	–	–	–	–
	6	–	–							–
	4	–	17.317							–
	2	–	0.868	0.485						–
Center	0	–	0.136	0.194	4.274					–
45°	2	–	0.209	0.167	0.943	3.669				–
	4	–	0.293	0.228	1.048	7.570	7.445			–
	6	–	0.505	0.341	13.911	3.134	0.254	0.307	–	–
	8	–	–	–	–	–	–	–	–	–

Table A.17 Prorated final pressure ratios in 45°-225° orientation of center cylindrical die filled at feed shoe speed of 500 mm/s

Orientation	225°				Center	45°			
Radius, mm	8	6	4	2	0	2	4	6	8
Run #1	0.523	0.973	0.775	1.293	1.000	1.269	1.004	1.134	1.138
Run #2	0.906	1.152	0.868	0.866	1.000	1.021	1.472	1.866	1.741
Run #3	0.740	1.056	1.684	0.820	1.000	0.819	0.838	1.221	1.247
Run #4	0.636	0.841	0.945	0.825	1.000	1.133	1.007	0.926	0.819
Run #5	0.656	1.247	1.258	1.144	1.000	1.136	1.128	1.437	1.324
Run #6	0.561	0.911	0.676	1.135	1.000	0.738	0.713	0.726	1.090
Mean	0.670	1.030	1.034	1.014	1.000	1.019	1.027	1.218	1.227
StDev	0.138	0.152	0.375	0.202	–	0.204	0.262	0.401	0.306
COV	20.6	14.7	36.3	19.9	–	20.0	25.5	32.9	24.9

Table A.18 P-values of paired t-test after modified Bonferroni procedure for prorated final pressure ratios in 45°-225° orientation of the center cylindrical die filled at feed shoe speed of 500 mm/s

	Orientation	225°				Center	45°			
	Radius, mm	8	6	4	2	0	2	4	6	8
225°	8	–	–	–	–	–	–	–	–	–
	6	–	–							–
	4	–	20.517							–
	2	–	18.423	19.407						–
Center	0	–	13.618	17.468	18.344					–
45°	2	–	19.251	19.736	20.093	17.342				–
	4	–	20.445	20.409	19.588	17.028	19.754			–
	6	–	3.690	8.276	7.419	5.030	5.767	1.405	–	–
	8	–	–	–	–	–	–	–	–	–

Table A.19 Prorated final pressure ratios in 135°-315° orientation of the center cylindrical die filled at feed shoe speed of 20 mm/s

Orientation	315°				Center	135°			
Radius, mm	8	6	4	2	0	2	4	6	8
Run #1	0.573	0.971	1.220	1.271	1.000	0.813	0.801	0.960	0.589
Run #2	0.642	1.082	1.183	1.283	1.000	0.761	0.758	1.031	0.452
Run #3	0.653	0.866	1.284	1.491	1.000	0.963	0.916	1.065	0.771
Run #4	0.759	1.043	1.047	1.101	1.000	1.099	1.001	0.735	0.450
Run #5	0.668	1.160	1.338	1.274	1.000	0.800	0.741	0.836	0.623
Run #6	1.415	1.738	1.078	1.190	1.000	1.345	1.072	0.926	0.699
Mean	0.785	1.143	1.192	1.268	1.000	0.963	0.882	0.926	0.597
StDev	0.315	0.308	0.114	0.130	–	0.226	0.137	0.123	0.130
COV	40.1	26.9	9.5	10.2	–	23.4	15.5	13.3	21.7

Table A.20 P-values of paired t-test after modified Bonferroni procedure for prorated final pressure ratios in 135°-315° orientation of the center cylindrical die filled at feed shoe speed of 20 mm/s

	Orientation	315°				Center	135°			
	Radius, mm	8	6	4	2	0	2	4	6	8
315°	8	–	–	–	–	–	–	–	–	–
	6	–	–							–
	4	–	16.044							–
	2	–	9.712	1.890						–
Center	0	–	6.427	0.191	0.077					–
135°	2	–	2.005	2.871	1.167	14.856				–
	4	–	1.239	0.477	0.155	1.827	2.107			–
	6	–	3.975	0.088	**0.003**	4.179	15.918	13.079	–	–
	8	–	–	–	–	–	–	–	–	–

*Entries in bold are significantly different ($P < 0.05$)

Table A.21 Prorated final pressure ratios in 135°-315° orientation of the center cylindrical die filled at feed shoe speed of 100 mm/s

Orientation	315°				Center	135°			
Radius, mm	8	6	4	2	0	2	4	6	8
Run #1	0.466	0.631	0.912	0.747	1.000	1.907	1.199	1.151	0.895
Run #2	0.373	0.755	0.874	1.009	1.000	0.860	0.428	0.627	0.634
Run #3	0.449	0.603	0.747	1.086	1.000	1.087	0.922	0.783	0.445
Run #4	0.341	0.535	0.737	0.592	1.000	1.247	1.216	1.323	0.681
Run #5	0.201	0.376	0.571	0.777	1.000	1.044	0.792	0.584	0.469
Run #6	0.570	0.692	0.675	0.939	1.000	1.178	1.465	1.258	0.825
Mean	0.400	0.599	0.753	0.858	1.000	1.220	1.003	0.954	0.658
StDev	0.126	0.132	0.126	0.185	–	0.361	0.368	0.329	0.183
COV	31.5	22.1	16.8	21.5	–	29.6	36.7	34.5	27.8

Table A.22 P-values of paired t-test after modified Bonferroni procedure for prorated final pressure ratios in 135°-315° orientation of the center cylindrical die filled at feed shoe speed of 100 mm/s

	Orientation	315°				Center	135°			
	Radius, mm	8	6	4	2	0	2	4	6	8
315°	8	–	–	–	–	–	–	–	–	–
	6	–	–							–
	4	–	10.730							–
	2	–	2.070	3.764						–
Center	0	–	15.711	20.633	4.101					–
135°	2	–	13.114	10.166	2.564	2.503				–
	4	–	4.191	4.059	0.355	0.098	5.840			–
	6	–	0.964	1.129	0.227	**0.015**	0.233	0.278	–	–
	8	–	–	–	–	–	–	–	–	–

*Entries in bold are significantly different (P < 0.05)

Table A.23 Prorated final pressure ratios in 135°-315° orientation of center cylindrical die filled at feed shoe speed of 500 mm/s

Orientation	315°				Center	135°			
Radius, mm	8	6	4	2	0	2	4	6	8
Run #1	0.953	1.117	1.089	0.937	1.000	1.085	1.478	1.186	0.669
Run #2	1.429	0.941	0.672	0.836	1.000	0.650	0.592	1.183	0.534
Run #3	0.966	0.988	0.988	0.963	1.000	0.976	1.122	0.771	0.481
Run #4	0.543	0.683	0.866	1.004	1.000	0.935	0.876	0.855	0.593
Run #5	0.980	0.848	0.697	0.937	1.000	1.004	0.898	0.726	0.720
Run #6	0.844	1.019	0.707	0.880	1.000	0.886	0.605	0.623	0.434
Mean	0.953	0.933	0.836	0.926	1.000	0.923	0.928	0.891	0.572
StDev	0.286	0.151	0.174	0.060	–	0.149	0.335	0.239	0.110
COV	30.0	16.2	20.8	6.5	–	16.2	36.1	26.9	19.2

Table A.24 P-values of paired t-test after modified Bonferroni procedure for prorated final pressure ratios in 135°-315° orientation of the center cylindrical die filled at feed shoe speed of 500 mm/s

	Orientation	315°				Center	135°			
	Radius, mm	8	6	4	2	0	2	4	6	8
315°	8	–	–	–	–	–	–	–	–	–
	6	–	–							–
	4	–	5.450							–
	2	–	19.658	4.150						–
Center	0	–	6.795	1.458	0.614					–
135°	2	–	19.026	3.584	19.820	5.466				–
	4	–	20.490	5.940	20.698	13.090	20.023			–
	6	–	14.547	12.935	15.830	6.595	17.028	16.722	–	–
	8	–	–	–	–	–	–	–	–	–

Right Cylindrical Die

Table A.25 Prorated final pressure ratios in 0°-180° orientation of the right cylindrical die filled at feed shoe speed of 20 mm/s

Orientation	180°				Center	0°			
Radius, mm	8	6	4	2	0	2	4	6	8
Run #1	0.487	0.540	0.442	0.562	1.000	0.889	0.929	0.964	0.679
Run #2	0.681	1.216	1.630	0.956	1.000	1.330	1.537	1.697	1.523
Run #3	0.760	0.822	0.505	0.824	1.000	0.897	0.812	0.984	0.627
Run #4	0.713	1.183	0.880	1.213	1.000	0.908	0.824	1.059	1.027
Run #5	0.436	0.853	0.944	0.734	1.000	1.104	1.225	1.282	1.062
Run #6	0.372	0.581	0.848	0.900	1.000	0.988	1.207	1.040	0.811
Mean	0.575	0.866	0.875	0.865	1.000	1.019	1.089	1.171	0.955
StDev	0.163	0.287	0.424	0.220	–	0.173	0.285	0.282	0.330
COV	28.3	33.2	48.5	25.4	–	16.9	26.2	24.0	34.6

Table A.26 P-values of paired t-test after modified Bonferroni procedure for prorated final pressure ratios in 0°-180° orientation of the right cylindrical die filled at feed shoe speed of 20 mm/s

	Orientation	180°				Center	0°			
	Radius, mm	8	6	4	2	0	2	4	6	8
180°	8	–	–	–	–	–	–	–	–	–
	6	–	–							–
	4	–	19.865							–
	2	–	20.796	20.002						–
Center	0	–	6.406	10.542	4.044					–
0°	2	–	3.940	5.174	4.417	16.683				–
	4	–	3.783	1.586	4.008	10.056	5.572			–
	6	–	0.557	0.214	1.411	4.132	0.498	4.601	–	–
	8	–	–	–	–	–	–	–	–	–

Table A.27 Prorated final pressure ratios in 0°-180° orientation of the right cylindrical die filled at feed shoe speed of 100 mm/s

Orientation	180°				Center	0°			
Radius, mm	8	6	4	2	0	2	4	6	8
Run #1	0.422	0.670	0.460	0.641	1.000	0.956	1.297	1.023	0.869
Run #2	0.584	1.241	1.132	0.874	1.000	1.453	1.704	1.293	1.143
Run #3	0.563	1.039	1.461	1.022	1.000	1.164	1.232	1.446	1.245
Run #4	0.351	0.711	1.169	0.757	1.000	0.980	1.107	1.097	0.675
Run #5	0.374	0.644	1.111	1.150	1.000	0.663	0.674	1.185	0.924
Run #6	0.341	0.659	0.967	0.925	1.000	0.952	1.008	0.509	0.423
Mean	0.439	0.827	1.050	0.895	1.000	1.028	1.170	1.092	0.880
StDev	0.108	0.251	0.331	0.182	0.000	0.263	0.341	0.322	0.302
COV	24.6	30.4	31.5	20.4	0.0	25.6	29.1	29.5	34.3

Table A.28 P-values of paired t-test after modified Bonferroni procedure for prorated final pressure ratios in 0°-180° orientation of the right cylindrical die filled at feed shoe speed of 100 mm/s

	Orientation	180°				Center	0°			
	Radius, mm	8	6	4	2	0	2	4	6	8
180°	8	–	–	–	–	–	–	–	–	–
	6	–	–							–
	4	–	2.753							–
	2	–	12.599	4.042						–
Center	0	–	3.210	15.243	4.527					–
0°	2	–	0.132	18.640	8.438	16.911				–
	4	–	0.212	12.016	4.260	5.782	0.864			–
	6	–	1.139	16.151	4.347	10.811	13.853	13.541	–	–
	8	–	–	–	–	–	–	–	–	–

Table A.29 Prorated final pressure ratios in 0°-180° orientation of right cylindrical die filled at feed shoe speed of 500 mm/s

Orientation	180°				Center	0°			
Radius, mm	8	6	4	2	0	2	4	6	8
Run #1	0.716	1.399	1.624	0.983	1.000	1.212	1.493	1.291	1.636
Run #2	0.434	0.731	1.438	1.159	1.000	1.193	1.063	1.304	1.761
Run #3	0.513	0.683	0.557	0.585	1.000	0.832	0.899	1.186	0.825
Run #4	0.619	0.473	0.755	1.143	1.000	0.691	0.899	0.876	0.848
Run #5	0.537	0.805	0.710	1.162	1.000	1.231	1.326	1.172	1.164
Run #6	0.552	0.791	1.029	0.792	1.000	1.141	0.794	0.913	0.653
Mean	0.562	0.814	1.019	0.971	1.000	1.050	1.079	1.124	1.148
StDev	0.096	0.311	0.429	0.238	–	0.230	0.275	0.186	0.459
COV	17.2	38.2	42.1	24.5	–	21.9	25.5	16.5	40.0

Table A.30 P-values of paired t-test after modified Bonferroni procedure for prorated final pressure ratios in 0°-180° orientation of the right cylindrical die filled at feed shoe speed of 500 mm/s

	Orientation	180°				Center	0°			
	Radius, mm	8	6	4	2	0	2	4	6	8
180°	8	–	–	–	–	–	–	–	–	–
	6	–	–							–
	4	–	3.328							–
	2	–	7.956	16.621						–
Center	0	–	4.243	19.305	16.270					–
0°	2	–	1.261	17.455	11.040	12.938				–
	4	–	0.459	14.930	8.036	10.783	16.207			–
	6	–	0.660	10.970	5.332	3.439	8.599	12.909	–	–
	8	–	–	–	–	–	–	–	–	–

Table A.31 Prorated final pressure ratios in 90°-270° orientation of the right cylindrical die filled at feed shoe speed of 20 mm/s

Orientation	270°				Center	90°			
Radius, mm	8	6	4	2	0	2	4	6	8
Run #1	1.037	1.278	0.936	0.913	1.000	0.945	1.097	1.173	1.166
Run #2	0.472	0.897	0.916	0.792	1.000	0.999	1.120	1.471	1.135
Run #3	0.692	0.858	0.922	1.034	1.000	1.094	1.627	1.326	1.014
Run #4	0.344	0.785	1.041	1.213	1.000	1.136	1.494	1.588	0.819
Run #5	0.322	0.607	0.783	0.728	1.000	1.024	1.015	1.200	0.834
Run #6	0.645	1.150	0.928	0.916	1.000	1.109	0.980	0.759	0.448
Mean	0.585	0.929	0.921	0.933	1.000	1.051	1.222	1.253	0.902
StDev	0.268	0.246	0.082	0.174	0.000	0.074	0.270	0.289	0.266
COV	45.8	26.4	8.9	18.7	0.0	7.0	22.1	23.1	29.5

Table A.32 P-values of paired t-test after modified Bonferroni procedure for prorated final pressure ratios in 90°-270° orientation of the right cylindrical die filled at feed shoe speed of 20 mm/s

	Orientation	270°				Center	90°			
	Radius, mm	8	6	4	2	0	2	4	6	8
270°	8	–	–	–	–	–	–	–	–	–
	6	–	–							–
	4	–	19.610							–
	2	–	20.539	16.898						–
Center	0	–	10.740	1.363	8.122					–
90°	2	–	6.948	0.254	1.842	3.112				–
	4	–	3.013	0.557	0.213	2.104	3.009			–
	6	–	3.125	0.635	0.780	1.787	3.314	16.226	–	–
	8	–	–	–	–	–	–	–	–	–

Table A.33 Prorated final pressure ratios in 90°-270° orientation of the right cylindrical die filled at feed shoe speed of 100 mm/s

Orientation	270°				Center	90°			
Radius, mm	8	6	4	2	0	2	4	6	8
Run #1	0.182	0.646	0.683	0.990	1.000	0.925	0.655	0.661	0.528
Run #2	0.262	0.672	0.905	1.011	1.000	1.146	1.015	0.597	0.400
Run #3	0.375	0.763	0.877	0.935	1.000	0.850	0.869	0.903	0.769
Run #4	0.335	0.593	0.771	1.169	1.000	0.564	0.480	0.593	0.520
Run #5	0.703	0.607	0.955	0.996	1.000	1.269	0.872	0.777	0.742
Run #6	0.327	0.690	1.203	0.980	1.000	1.006	0.961	0.866	0.630
Mean	0.364	0.662	0.899	1.013	1.000	0.960	0.809	0.733	0.598
StDev	0.179	0.062	0.178	0.081	0.000	0.246	0.202	0.135	0.142
COV	49.3	9.4	19.8	7.9	0.0	25.6	25.0	18.5	23.8

Table A.34 P-values of paired t-test after modified Bonferroni procedure for prorated final pressure ratios in 90°-270° orientation of the right cylindrical die filled at feed shoe speed of 100 mm/s

	Orientation	270°				Center	90°			
	Radius, mm	8	6	4	2	0	2	4	6	8
270°	8	–	–	–	–	–	–	–	–	–
	6	–	–							–
	4	–	0.412							–
	2	–	**0.028**	5.382						–
Center	0	–	**0.001**	4.696	14.685					–
90°	2	–	0.706	11.573	14.341	14.868				–
	4	–	2.044	4.283	2.495	1.441	1.305			–
	6	–	3.326	0.820	0.391	0.090	1.710	7.588	–	–
	8	–	–	–	–	–	–	–	–	–

Table A.35 Prorated final pressure ratios in 90°-270° orientation of right cylindrical die filled at feed shoe speed of 500 mm/s

Orientation	270°				Center	90°			
Radius, mm	8	6	4	2	0	2	4	6	8
Run #1	0.584	1.045	0.709	1.062	1.000	1.455	1.315	1.421	0.957
Run #2	0.295	1.009	0.958	1.032	1.000	0.779	0.878	0.761	0.426
Run #3	0.431	0.930	1.128	0.971	1.000	1.186	1.076	0.970	0.721
Run #4	0.459	0.862	1.257	1.148	1.000	0.956	1.196	1.117	1.038
Run #5	0.443	0.710	0.681	0.789	1.000	0.793	0.852	0.739	0.582
Run #6	0.749	0.863	0.734	0.728	1.000	1.103	1.145	1.141	0.732
Mean	0.493	0.903	0.911	0.955	1.000	1.046	1.077	1.025	0.743
StDev	0.155	0.121	0.242	0.164	–	0.258	0.182	0.258	0.228
COV	31.5	13.4	26.6	17.2	–	24.7	16.9	25.2	30.7

Table A.36 P-values of paired t-test after modified Bonferroni procedure for prorated final pressure ratios in 90°-270° orientation of the right cylindrical die filled at feed shoe speed of 500 mm/s

	Orientation	270°				Center	90°			
	Radius, mm	8	6	4	2	0	2	4	6	8
270°	8	–	–	–	–	–	–	–	–	–
	6	–	–							–
	4	–	19.798							–
	2	–	8.282	12.214						–
Center	0	–	2.239	8.604	11.147					–
90°	2	–	3.606	8.951	9.774	14.366				–
	4	–	1.106	4.554	3.913	7.317	12.762			–
	6	–	5.194	10.172	11.441	17.282	14.676	4.358	–	–
	8	–	–	–	–	–	–	–	–	–

Table A.37 Prorated final pressure ratios in 45°-225° orientation of the right cylindrical die filled at feed shoe speed of 20 mm/s

Orientation	225°				Center	45°			
Radius, mm	8	6	4	2	0	2	4	6	8
Run #1	0.587	0.973	1.078	1.026	1.000	0.965	1.343	1.667	1.354
Run #2	0.503	0.836	0.698	0.774	1.000	0.812	0.877	0.880	1.066
Run #3	0.450	0.997	0.915	1.034	1.000	1.215	1.227	1.072	1.138
Run #4	0.649	1.056	1.253	1.098	1.000	1.516	1.223	1.165	1.326
Run #5	0.902	1.236	0.945	1.091	1.000	0.902	1.296	1.273	1.078
Run #6	1.051	1.253	1.404	1.257	1.000	1.477	1.948	1.589	1.491
Mean	0.690	1.058	1.049	1.047	1.000	1.148	1.319	1.274	1.242
StDev	0.237	0.161	0.253	0.158	–	0.302	0.349	0.304	0.173
COV	34.3	15.2	24.1	15.0	–	26.3	26.5	23.8	14.0

Table A.38 P-values of paired t-test after modified Bonferroni procedure for prorated final pressure ratios in 45°-225° orientation of the right cylindrical die filled at feed shoe speed of 20 mm/s

	Orientation	225°				Center	45°			
	Radius, mm	8	6	4	2	0	2	4	6	8
225°	8	–	–	–	–	–	–	–	–	–
	6	–	–							–
	4	–	19.021							–
	2	–	15.310	20.452						–
Center	0	–	8.727	13.802	10.483					–
45°	2	–	9.650	4.153	6.424	5.965				–
	4	–	1.004	0.375	0.597	1.588	4.509			–
	6	–	2.033	1.176	1.228	1.637	9.321	13.565	–	–
	8	–	–	–	–	–	–	–	–	–

Table A.39 Prorated final pressure ratios in 45°-225° orientation of the right cylindrical die filled at feed shoe speed of 100 mm/s

Orientation	225°				Center	45°			
Radius, mm	8	6	4	2	0	2	4	6	8
Run #1	0.800	0.960	1.396	1.081	1.000	1.378	1.576	1.313	1.233
Run #2	0.545	0.628	0.665	0.922	1.000	0.841	0.856	0.601	0.569
Run #3	0.888	1.325	0.950	0.938	1.000	1.101	1.036	1.020	0.704
Run #4	0.619	0.600	0.601	0.871	1.000	0.924	1.049	0.723	0.929
Run #5	0.544	0.687	0.785	0.960	1.000	0.993	1.054	1.252	1.013
Run #6	0.569	0.867	1.013	0.988	1.000	0.968	1.321	1.215	1.137
Mean	0.661	0.844	0.902	0.960	1.000	1.034	1.149	1.021	0.931
StDev	0.147	0.274	0.289	0.071	–	0.188	0.257	0.297	0.254
COV	22.3	32.5	32.1	7.4	–	18.2	22.4	29.1	27.3

Table A.40 P-values of paired t-test after modified Bonferroni procedure for prorated final pressure ratios in 45°-225° orientation of the right cylindrical die filled at feed shoe speed of 100 mm/s

	Orientation	225°				Center	45°			
	Radius, mm	8	6	4	2	0	2	4	6	8
225°	8	–	–	–	–	–	–	–	–	–
	6	–	–							–
	4	–	12.921							–
	2	–	6.782	11.562						–
Center	0	–	4.693	9.312	4.767					–
45°	2	–	2.062	1.436	4.955	14.150				–
	4	–	1.376	0.100	1.411	4.530	2.448			–
	6	–	4.724	4.386	11.952	18.287	18.560	3.608	–	–
	8	–	–	–	–	–	–	–	–	–

Table A.41 Prorated final pressure ratios in 45°-225° orientation of right cylindrical die filled at feed shoe speed of 500 mm/s

Orientation	225°				Center	45°			
Radius, mm	8	6	4	2	0	2	4	6	8
Run #1	0.977	0.907	0.841	1.132	1.000	1.244	1.533	1.025	1.362
Run #2	0.526	1.052	1.249	1.096	1.000	1.267	1.670	2.047	1.474
Run #3	0.575	1.112	1.475	1.297	1.000	1.104	1.610	1.439	1.218
Run #4	0.482	0.662	0.778	0.814	1.000	0.897	1.018	1.214	0.993
Run #5	0.584	1.055	0.926	1.246	1.000	1.091	0.819	1.189	1.116
Run #6	0.378	0.557	0.435	0.703	1.000	0.813	0.947	0.833	0.533
Mean	0.587	0.891	0.951	1.048	1.000	1.070	1.266	1.291	1.116
StDev	0.205	0.231	0.367	0.238	–	0.183	0.378	0.422	0.333
COV	35.0	25.9	38.6	22.8	–	17.1	29.9	32.7	29.8

Table A.42 P-values of paired t-test after modified Bonferroni procedure for prorated final pressure ratios in 45°-225° orientation of the right cylindrical die filled at feed shoe speed of 500 mm/s

	Orientation	225°				Center	45°			
	Radius, mm	8	6	4	2	0	2	4	6	8
225°	8	–	–	–	–	–	–	–	–	–
	6	–	–							–
	4	–	10.356							–
	2	–	**0.035**	7.192						–
Center	0	–	6.267	15.867	13.500					–
45°	2	–	0.453	7.373	15.681	8.267				–
	4	–	0.728	0.895	3.764	3.054	2.930			–
	6	–	0.658	0.655	3.937	3.185	3.636	18.231	–	–
	8	–	–	–	–	–	–	–	–	–

*Entries in bold are significantly different ($P < 0.05$)

Table A.43 Prorated final pressure ratios in 135°-315° orientation of the right cylindrical die filled at feed shoe speed of 20 mm/s

Orientation	315°				Center	135°			
Radius, mm	8	6	4	2	0	2	4	6	8
Run #1	1.177	1.343	1.438	1.326	1.000	1.314	1.464	1.191	1.106
Run #2	0.762	1.910	1.802	1.343	1.000	1.792	2.209	1.590	1.624
Run #3	0.824	0.964	1.077	1.181	1.000	1.327	1.430	0.956	1.188
Run #4	1.098	1.320	0.933	0.775	1.000	1.070	1.177	1.079	0.944
Run #5	0.678	1.359	0.967	0.728	1.000	1.379	1.286	1.154	1.300
Run #6	0.700	1.312	1.138	0.843	1.000	0.985	1.141	1.045	1.200
Mean	0.873	1.368	1.226	1.033	1.000	1.311	1.451	1.169	1.227
StDev	0.212	0.304	0.335	0.282	0.000	0.283	0.393	0.222	0.228
COV	24.3	22.3	27.3	27.4	0.0	21.6	27.1	19.0	18.6

Table A.44 P-values of paired t-test after modified Bonferroni procedure for prorated final pressure ratios in 135°-315° orientation of the right cylindrical die filled at feed shoe speed of 20 mm/s

	Orientation	315°				Center	135°			
	Radius, mm	8	6	4	2	0	2	4	6	8
315°	8	–	–	–	–	–	–	–	–	–
	6	–	–							–
	4	–	0.538							–
	2	–	1.702	1.897						–
Center	0	–	2.537	0.788	0.905					–
135°	2	–	5.277	0.236	0.762	16.529				–
	4	–	10.160	0.493	8.132	3.348	1.156			–
	6	–	0.141	9.774	12.493	0.662	1.376	3.717	–	–
	8	–	–	–	–	–	–	–	–	–

Table A.45 Prorated final pressure ratios in 135°-315° orientation of the right cylindrical die filled at feed shoe speed of 100 mm/s

Orientation	315°				Center	135°			
Radius, mm	8	6	4	2	0	2	4	6	8
Run #1	1.080	1.206	1.373	1.013	1.000	1.060	0.843	0.765	0.476
Run #2	1.139	1.000	1.568	0.995	1.000	1.104	0.892	0.799	0.946
Run #3	1.133	1.265	1.231	1.270	1.000	0.712	0.723	0.753	0.429
Run #4	1.257	1.149	1.332	0.912	1.000	1.196	1.192	0.915	0.871
Run #5	0.716	0.913	1.059	0.983	1.000	0.744	0.745	0.615	0.378
Run #6	0.919	1.209	1.691	1.286	1.000	0.925	0.974	1.194	0.794
Mean	1.041	1.124	1.376	1.076	1.000	0.957	0.895	0.840	0.649
StDev	0.193	0.137	0.228	0.160	–	0.198	0.173	0.198	0.249
COV	18.6	12.2	16.6	14.9	–	20.7	19.3	23.6	38.4

Table A.46 P-values of paired t-test after modified Bonferroni procedure for prorated final pressure ratios in 135°-315° orientation of the right cylindrical die filled at feed shoe speed of 100 mm/s

	Orientation	315°				Center	135°			
	Radius, mm	8	6	4	2	0	2	4	6	8
315°	8	–	–	–	–	–	–	–	–	–
	6	–	–							–
	4	–	0.879							–
	2	–	9.016	0.525						–
Center	0	–	1.652	0.210	6.185					–
135°	2	–	3.075	0.109	8.407	12.943				–
	4	–	0.849	0.061	3.444	4.110	5.450			–
	6	–	0.239	**0.004**	0.572	2.205	5.703	9.653	–	–
	8	–	–	–	–	–	–	–	–	–

*Entries in bold are significantly different ($P < 0.05$)

Table A.47 Prorated final pressure ratios in 135°-315° orientation of right cylindrical die filled at feed shoe speed of 500 mm/s

Orientation	315°				Center	135°			
Radius, mm	8	6	4	2	0	2	4	6	8
Run #1	0.732	1.283	1.404	1.215	1.000	1.688	1.365	0.713	0.631
Run #2	0.846	1.238	0.847	0.638	1.000	0.790	0.707	1.042	0.547
Run #3	0.593	1.071	1.052	1.013	1.000	1.081	0.911	0.780	0.469
Run #4	0.598	0.709	0.657	0.887	1.000	0.792	0.564	0.709	0.374
Run #5	0.734	0.701	0.838	0.794	1.000	0.745	0.751	0.869	0.515
Run #6	0.726	0.522	0.642	0.819	1.000	1.020	0.849	0.793	0.243
Mean	0.705	0.921	0.907	0.894	1.000	1.019	0.858	0.818	0.463
StDev	0.096	0.319	0.286	0.199	–	0.355	0.276	0.124	0.137
COV	13.6	34.6	31.6	22.3	–	34.8	32.2	15.2	29.6

Table A.48 P-values of paired t-test after modified Bonferroni procedure for prorated final pressure ratios in 135°-315° orientation of the right cylindrical die filled at feed shoe speed of 500 mm/s

	Orientation	315°				Center	135°			
	Radius, mm	8	6	4	2	0	2	4	6	8
315°	8	–	–	–	–	–	–	–	–	–
	6	–	–							–
	4	–	18.278							–
	2	–	17.724	18.347						–
Center	0	–	11.941	9.665	5.242					–
135°	2	–	10.580	4.278	4.086	18.883				–
	4	–	12.993	8.494	12.900	5.523	0.370			–
	6	–	9.569	11.487	11.952	0.331	6.405	16.495	–	–
	8	–	–	–	–	–	–	–	–	–

Center vs. Right Cylindrical Dies

Table A.49 P-values of t-test (two-sample assuming equal variances) between final pressure values of the center and right cylindrical dies at feed shoe speed of 20 mm/s

Orientation	180°, 270°, 225, or 315°				Center	0°, 90, 45°, or 135°			
Radius, mm	8	6	4	2	0	2	4	6	8
0°-180°	**0.017**	**0.004**	**0.005**	**0.012**	**0.010**	**0.027**	**0.028**	**0.019**	**0.022**
90°-270°	0.636	0.853	0.120	**0.049**	**0.015**	0.403	0.478	0.257	0.736
45°-225°	**0.002**	**0.001**	**<0.001**	**<0.001**	**0.002**	**0.001**	**<0.001**	**<0.001**	**<0.001**
135°-315°	**<0.001**	**0.005**	**<0.001**	**<0.001**	**0.010**	**0.023**	**<0.001**	**<0.001**	**0.002**

Table A.50 P-values of t-test (two-sample assuming equal variances) between final pressure values of the center and right cylindrical dies at feed shoe speed of 100 mm/s

Orientation	180°, 270°, 225, or 315°				Center	0°, 90, 45°, or 135°			
Radius, mm	8	6	4	2	0	2	4	6	8
0°-180°	**<0.001**	**<0.001**	**0.003**	0.238	0.652	0.607	0.276	0.417	0.130
90°-270°	**0.012**	0.083	0.852	0.161	0.873	0.520	0.244	**0.014**	0.610
45°-225°	**<0.001**	**<0.001**	**<0.001**	**<0.001**	**0.026**	0.084	**0.003**	**0.001**	**0.002**
135°-315°	**<0.001**	**0.001**	**<0.001**	0.058	**0.007**	**0.006**	**<0.001**	**<0.001**	**0.001**

Table A.51 P-values of t-test (two-sample assuming equal variances) between final pressure values of the center and right cylindrical dies at feed shoe speed of 500 mm/s

Orientation	180°, 270°, 225, or 315°				Center	0°, 90, 45°, or 135°			
Radius, mm	8	6	4	2	0	2	4	6	8
0°-180°	**0.021**	0.488	**0.006**	0.056	0.119	**0.013**	**0.025**	0.099	0.070
90°-270°	0.646	0.135	0.680	0.877	0.195	0.457	0.615	0.226	0.683
45°-225°	0.474	0.173	0.712	0.549	0.506	0.331	**0.028**	0.362	0.615
135°-315°	0.315	0.501	0.083	0.346	0.110	0.091	0.739	0.664	0.434

Center Toroidal Die

Table A.52 Final pressure values in 0°-180° orientation of the center toroidal die filled at feed shoe speed of 20 mm/s (Pa)

Orientation	180°						Center	0°		
Radius, mm	8	6	4					4	6	8
Run #1	407.7	628.4	517.9					1096.1	1750.6	1540.8
Run #2	306.2	444.5	295.6					1037.5	1413.9	963.7
Run #3	350.5	456.3	318.8					337.2	981.1	916.5
Run #4	177.6	386.8	427.3					1028.0	1263.7	1172.7
Run #5	232.0	653.1	481.0					878.0	1338.2	949.5
Run #6	220.1	525.3	648.5					723.9	1485.1	1184.3
Mean	282.4	515.7	448.2					850.1	1372.1	1121.3
StDev	87.5	106.7	131.6					285.3	254.4	236.1
COV	31.0	20.7	29.4					33.6	18.5	21.1

Table A.53 P-values of paired t-test after modified Bonferroni procedure for final pressure values in 0°-180° orientation of the center toroidal die filled at feed shoe speed of 20 mm/s

	Orientation	180°			0°		
	Radius, mm	8	6	4	4	6	8
180°	8	–	–	–	–	–	–
	6	**0.034**					–
	4	1.049	3.410				–
0°	4	**0.043**	0.542	0.315			–
	6	**0.002**	**0.003**	**0.002**	**0.020**		–
	8	**0.004**	**0.018**	**0.006**	0.757	0.067	–

*Entries in bold are significantly different ($P < 0.05$)

Table A.54 Final pressure values in 0°-180° orientation of the center toroidal die filled at feed shoe speed of 100 mm/s (Pa)

Orientation	180°				Center		0°		
Radius, mm	8	6	4				4	6	8
Run #1	405.8	591.4	534.5				622.4	1434.7	1106.0
Run #2	337.8	548.9	516.0				508.7	923.7	1145.2
Run #3	206.3	402.5	324.9				502.9	960.4	800.0
Run #4	347.0	548.6	529.2				588.1	1491.1	995.1
Run #5	187.4	527.6	370.2				759.0	924.3	748.6
Run #6	264.4	570.2	411.7				1107.5	1385.8	991.7
Mean	291.4	531.6	447.7				681.4	1186.7	964.5
StDev	86.2	66.9	90.8				228.7	276.8	160.1
COV	29.6	12.6	20.3				33.6	23.3	16.6

Table A.55 P-values of paired t-test after modified Bonferroni procedure for final pressure values in 0°-180° orientation of the center toroidal die filled at feed shoe speed of 100 mm/s

	Orientation	180°			0°		
	Radius, mm	8	6	4	4	6	8
180°	8	–	–	–	–	–	–
	6	**0.004**					–
	4	**0.001**	0.297				–
0°	4	0.227	2.126	1.246			–
	6	**0.003**	**0.018**	**0.010**	0.058		–
	8	**<0.001**	**0.006**	**0.001**	0.953	1.254	–

*Entries in bold are significantly different (P < 0.05)

Table A.56 Final pressure values in 0°-180° orientation of center toroidal die filled at feed shoe speed of 500 mm/s (Pa)

Orientation	180°				Center		0°		
Radius, mm	8	6	4				4	6	8
Run #1	783.9	763.5	790.4				1695.3	2533.7	2150.3
Run #2	337.4	588.5	530.4				1781.5	2198.9	1183.4
Run #3	449.1	881.8	764.8				1548.3	2179.4	2182.9
Run #4	625.9	843.2	755.6				1078.7	2188.1	1466.2
Run #5	360.3	565.7	929.9				1669.3	1558.8	1316.0
Run #6	699.3	841.2	570.3				1273.2	1655.9	1174.5
Mean	542.6	747.4	723.6				1507.7	2052.5	1578.8
StDev	186.5	137.5	148.7				274.6	371.1	467.6
COV	34.4	18.4	20.6				18.2	18.1	29.6

Table A.57 P-values of paired t-test after modified Bonferroni procedure for final pressure values in 0°-180° orientation of the center toroidal die filled at feed shoe speed of 500 mm/s

	Orientation	180°			0°		
	Radius, mm	8	6	4	4	6	8
180°	8	–	–	–	–	–	–
	6	0.116					–
	4	1.941	11.945				–
0°	4	**0.028**	**0.036**	**0.021**			–
	6	**0.002**	**0.005**	**0.008**	0.371		–
	8	**0.035**	**0.033**	**0.040**	11.083	0.347	–

*Entries in bold are significantly different (P < 0.05)

Table A.58 Final pressure values in 90°-270° orientation of the center toroidal die filled at feed shoe speed of 20 mm/s (Pa)

Orientation	270°				Center		90°		
Radius, mm	8	6	4				4	6	8
Run #1	252.3	360.5	173.1				201.9	367.5	354.9
Run #2	316.1	402.5	321.4				302.4	285.9	169.5
Run #3	246.3	319.6	303.0				308.3	369.1	391.2
Run #4	184.7	316.1	176.0				387.4	571.3	300.5
Run #5	166.7	215.0	160.8				270.0	573.7	339.4
Run #6	218.3	304.2	149.4				265.3	320.4	270.8
Mean	230.8	319.6	213.9				289.2	414.7	304.3
StDev	53.7	62.8	76.9				61.2	126.1	78.3
COV	23.2	19.7	36.0				21.2	30.4	25.7

Table A.59 P-values of paired t-test after modified Bonferroni procedure for final pressure values in 90°-270° orientation of the center toroidal die filled at feed shoe speed of 20 mm/s

	Orientation	270°			90°		
	Radius, mm	8	6	4	4	6	8
270°	8	–	–	–	–	–	–
	6	**0.009**					–
	4	6.757	0.152				–
90°	4	2.556	6.583	1.288			–
	6	0.737	3.671	0.591	0.662		–
	8	2.677	11.583	2.013	11.190	1.111	–

*Entries in bold are significantly different ($P < 0.05$)

Table A.60 Final pressure values in 90°-270° orientation of the center toroidal die filled at feed shoe speed of 100 mm/s (Pa)

Orientation	270°				Center		90°		
Radius, mm	8	6	4				4	6	8
Run #1	320.3	468.2	282.6				248.3	363.4	397.9
Run #2	128.8	267.6	249.5				220.1	312.6	211.5
Run #3	137.6	260.2	180.0				215.4	391.3	309.5
Run #4	129.3	205.5	171.7				489.2	442.2	296.4
Run #5	98.1	175.5	156.1				160.9	191.2	127.2
Run #6	129.1	213.6	141.2				135.9	236.8	223.3
Mean	157.2	265.1	196.8				245.0	322.9	261.0
StDev	81.1	105.4	56.2				126.6	95.3	93.9
COV	51.6	39.7	28.6				51.7	29.5	36.0

Table A.61 P-values of paired t-test after modified Bonferroni procedure for final pressure values in 90°-270° orientation of the center toroidal die filled at feed shoe speed of 100 mm/s

	Orientation	270°			90°		
	Radius, mm	8	6	4	4	6	8
270°	8	–	–	–	–	–	–
	6	**0.007**					–
	4	1.842	0.688				–
90°	4	3.023	11.661	6.307			–
	6	0.167	4.136	0.316	0.835		–
	8	0.084	13.231	1.474	11.441	0.969	–

*Entries in bold are significantly different ($P < 0.05$)

Table A.62 Final pressure values in 90°-270° orientation of center toroidal die filled at feed shoe speed of 500 mm/s (Pa)

Orientation	270°				Center		90°		
Radius, mm	8	6	4				4	6	8
Run #1	119.5	189.2	134.7				155.9	340.2	352.6
Run #2	103.9	237.8	194.9				189.7	302.8	342.4
Run #3	224.1	167.0	130.2				290.6	388.6	282.6
Run #4	130.4	185.8	101.8				217.5	541.7	414.0
Run #5	101.0	170.6	266.5				368.6	652.6	570.0
Run #6	71.3	137.0	154.8				124.1	184.7	246.1
Mean	125.1	181.2	163.8				224.5	401.9	368.0
StDev	52.5	33.3	59.0				90.7	169.3	114.9
COV	42.0	18.4	36.0				40.4	42.2	31.2

Table A.63 P-values of paired t-test after modified Bonferroni procedure for final pressure values in 90°-270° orientation of the center toroidal die filled at feed shoe speed of 500 mm/s

	Orientation	270°			90°		
	Radius, mm	8	6	4	4	6	8
270°	8	–	–	–	–	–	–
	6	1.168					–
	4	5.332	8.080				–
90°	4	0.522	4.934	1.627			–
	6	0.152	0.374	0.211	0.145		–
	8	0.099	0.155	**0.039**	0.109	5.318	–

*Entries in bold are significantly different (P < 0.05)

Table A.64 Final pressure values in 45°-225° orientation of the center toroidal die filled at feed shoe speed of 20 mm/s (Pa)

Orientation	225°				Center		45°		
Radius, mm	8	6	4				4	6	8
Run #1	243.9	319.5	175.4				385.8	655.4	383.6
Run #2	152.5	208.5	247.4				283.8	524.8	306.0
Run #3	139.6	300.1	197.3				441.2	547.2	322.1
Run #4	105.3	184.8	130.8				360.0	552.2	442.9
Run #5	198.0	250.3	165.8				414.1	574.6	462.1
Run #6	238.2	287.3	161.3				613.8	655.4	455.7
Mean	179.6	258.4	179.7				416.4	584.9	395.4
StDev	56.1	53.5	39.6				110.7	56.9	69.1
COV	31.3	20.7	22.0				26.6	9.7	17.5

Table A.65 P-values of paired t-test after modified Bonferroni procedure for final pressure values in 45°-225° orientation of the center toroidal die filled at feed shoe speed of 20 mm/s

	Orientation	225°			45°		
	Radius, mm	8	6	4	4	6	8
225°	8	–	–	–	–	–	–
	6	**0.041**					–
	4	14.956	0.486				–
45°	4	**0.025**	**0.046**	**0.043**			–
	6	**<0.001**	**<0.001**	**0.001**	**0.037**		–
	8	**0.013**	0.057	**0.036**	9.226	**0.013**	–

*Entries in bold are significantly different (P < 0.05)

Table A.66 Final pressure values in 45°-225° orientation of the center toroidal die filled at feed shoe speed of 100 mm/s (Pa)

Orientation	225°				Center		45°		
Radius, mm	8	6	4				4	6	8
Run #1	88.6	130.5	124.4				167.5	293.2	281.4
Run #2	123.2	183.3	104.9				150.1	300.5	224.7
Run #3	90.7	168.8	117.9				188.0	313.6	236.1
Run #4	68.7	119.7	114.4				115.7	261.6	226.1
Run #5	101.2	205.0	156.4				241.1	310.3	285.7
Run #6	100.1	146.7	152.4				192.8	470.8	325.2
Mean	95.5	159.0	128.4				175.9	325.0	263.2
StDev	18.0	32.6	21.2				42.5	73.8	40.7
COV	18.8	20.5	16.5				24.2	22.7	15.5

Table A.67 P-values of paired t-test after modified Bonferroni procedure for final pressure values in 45°-225° orientation of the center toroidal die filled at feed shoe speed of 100 mm/s

	Orientation	225°			45°		
	Radius, mm	8	6	4	4	6	8
225°	8	–	–	–	–	–	–
	6	**0.018**					–
	4	0.473	1.120				–
45°	4	**0.030**	3.476	**0.049**			–
	6	**0.008**	**0.031**	**0.009**	**0.049**		–
	8	**0.003**	**0.027**	**0.001**	**0.032**	0.109	–

*Entries in bold are significantly different ($P < 0.05$)

Table A.68 Final pressure values in 45°-225° orientation of center toroidal die filled at feed shoe speed of 500 mm/s (Pa)

Orientation	225°				Center		45°		
Radius, mm	8	6	4				4	6	8
Run #1	112.6	249.1	125.9				176.2	411.8	405.4
Run #2	88.5	161.7	126.2				97.0	138.7	137.4
Run #3	73.9	118.4	132.4				124.8	265.3	127.3
Run #4	95.0	106.0	66.0				251.2	412.5	463.1
Run #5	91.8	135.2	133.3				268.3	270.7	170.4
Run #6	126.9	159.2	103.9				115.8	280.0	238.3
Mean	98.1	154.9	114.7				172.2	296.5	257.0
StDev	18.8	51.1	26.1				72.9	103.5	143.9
COV	19.2	33.0	22.8				42.3	34.9	56.0

Table A.69 P-values of paired t-test after modified Bonferroni procedure for final pressure values in 45°-225° orientation of the center toroidal die filled at feed shoe speed of 500 mm/s

	Orientation	225°			45°		
	Radius, mm	8	6	4	4	6	8
225°	8	–	–	–	–	–	–
	6	0.374					–
	4	4.708	1.427				–
45°	4	0.965	10.278	2.373			–
	6	0.066	0.322	0.202	0.253		–
	8	0.541	2.005	1.294	2.443	3.321	–

Table A.70 Final pressure values in 135°-315° orientation of the center toroidal die filled at feed shoe speed of 20 mm/s (Pa)

Orientation	315°				Center		135°		
Radius, mm	8	6	4				4	6	8
Run #1	871.7	1460.6	837.5				181.4	345.6	352.2
Run #2	522.5	697.2	578.0				164.3	205.0	144.7
Run #3	455.3	622.6	453.8				213.1	337.4	238.8
Run #4	386.4	521.6	375.2				189.4	223.5	151.3
Run #5	686.0	745.1	571.8				124.9	305.6	315.7
Run #6	972.2	1099.0	943.2				229.8	317.8	195.5
Mean	649.0	857.7	626.6				183.8	289.2	233.0
StDev	235.8	354.5	220.5				37.0	60.0	86.0
COV	36.3	41.3	35.2				20.2	20.7	36.9

Table A.71 P-values of paired t-test after modified Bonferroni procedure for final pressure values in 135°-315° orientation of the center toroidal die filled at feed shoe speed of 20 mm/s

	Orientation	315°			135°		
	Radius, mm	8	6	4	4	6	8
315°	8	–	–	–	–	–	–
	6	0.658					–
	4	5.487	0.488				–
135°	4	0.067	0.079	0.057			–
	6	0.120	0.114	0.131	0.130		–
	8	0.068	0.064	0.084	4.520	0.791	–

Table A.72 Final pressure values in 135°-315° orientation of the center toroidal die filled at feed shoe speed of 100 mm/s (Pa)

Orientation	315°				Center		135°		
Radius, mm	8	6	4				4	6	8
Run #1	961.9	1143.9	915.7				355.7	580.6	213.4
Run #2	874.7	830.3	667.4				171.6	305.6	237.9
Run #3	605.6	930.5	662.5				370.4	354.3	293.6
Run #4	1357.8	1078.0	988.4				430.3	490.2	389.1
Run #5	692.2	1016.8	817.2				186.0	436.4	255.1
Run #6	451.3	823.7	508.2				323.6	448.8	199.0
Mean	823.9	970.6	759.9				306.3	436.0	264.7
StDev	319.5	131.6	179.6				104.7	97.6	69.3
COV	38.8	13.6	23.6				34.2	22.4	26.2

Table A.73 P-values of paired t-test after modified Bonferroni procedure for final pressure values in 135°-315° orientation of the center toroidal die filled at feed shoe speed of 100 mm/s

	Orientation	315°			135°		
	Radius, mm	8	6	4	4	6	8
315°	8	–	–	–	–	–	–
	6	3.351					–
	4	6.675	**0.019**				–
135°	4	0.056	**0.001**	**0.022**			–
	6	0.370	**<0.001**	**0.042**	0.367		–
	8	**0.034**	**0.001**	**0.007**	4.765	0.264	–

*Entries in bold are significantly different ($P < 0.05$)

Table A.74 Final pressure values in 135°-315° orientation of center toroidal die filled at feed shoe speed of 500 mm/s (Pa)

Orientation	315°				Center		135°		
Radius, mm	8	6	4				4	6	8
Run #1	864.6	955.8	510.7				333.2	450.2	429.9
Run #2	1142.2	1074.3	463.7				394.5	323.8	281.0
Run #3	618.8	690.1	923.0				186.7	299.2	277.9
Run #4	987.0	803.0	454.8				204.2	363.6	328.6
Run #5	643.4	854.0	615.6				330.7	342.4	226.5
Run #6	974.3	815.0	717.2				353.3	489.6	332.9
Mean	871.7	865.3	614.1				300.4	378.1	312.8
StDev	206.4	133.4	181.5				84.6	75.2	69.3
COV	23.7	15.4	29.6				28.2	19.9	22.2

Table A.75 P-values of paired t-test after modified Bonferroni procedure for final pressure values in 135°-315° orientation of the center toroidal die filled at feed shoe speed of 500 mm/s

	Orientation	315°			135°		
	Radius, mm	8	6	4	4	6	8
315°	8	–	–	–	–	–	–
	6	13.862					–
	4	2.035	1.367				–
135°	4	**0.009**	**<0.001**	0.308			–
	6	**0.026**	**0.007**	0.568	1.266		–
	8	**0.014**	**0.003**	0.161	11.800	0.568	–

*Entries in bold are significantly different (P < 0.05)

Right Toroidal Die

Table A.76 Final pressure values in 0°-180° orientation of the right toroidal die filled at feed shoe speed of 20 mm/s (Pa)

Orientation	180°				Center		0°		
Radius, mm	8	6	4				4	6	8
Run #1	201.8	364.5	183.7				809.8	1061.8	756.3
Run #2	230.1	450.9	245.3				768.0	1074.7	642.1
Run #3	289.1	453.5	347.7				698.3	932.4	793.5
Run #4	379.2	523.6	358.3				1186.4	1197.2	718.5
Run #5	162.1	335.0	362.8				758.6	1179.7	643.6
Run #6	262.6	514.6	357.5				1085.1	1591.3	1256.2
Mean	254.2	440.4	309.2				884.4	1172.9	801.7
StDev	75.7	77.0	76.1				200.5	226.0	230.8
COV	29.8	17.5	24.6				22.7	19.3	28.8

Table A.77 P-values of paired t-test after modified Bonferroni procedure for final pressure values in 0°-180° orientation of the right toroidal die filled at feed shoe speed of 20 mm/s

	Orientation	180°			0°		
	Radius, mm	8	6	4	4	6	8
180°	8	–	–	–	–	–	–
	6	**0.002**					–
	4	0.341	**0.038**				–
0°	4	**0.003**	**0.014**	**0.010**			–
	6	**0.003**	**0.005**	**0.002**	**0.036**		–
	8	**0.032**	**0.036**	**0.042**	6.074	**0.021**	–

*Entries in bold are significantly different (P < 0.05)

Table A.78 Final pressure values in 0°-180° orientation of the right toroidal die filled at feed shoe speed of 100 mm/s (Pa)

Orientation	180°				Center		0°		
Radius, mm	8	6	4				4	6	8
Run #1	374.4	689.6	506.4				1231.4	1523.1	1140.7
Run #2	229.7	323.8	187.7				865.4	1387.2	900.4
Run #3	307.1	240.1	324.5				774.4	1247.4	1103.5
Run #4	167.5	254.5	132.4				912.9	921.7	868.0
Run #5	196.2	167.3	92.1				680.1	1313.6	852.2
Run #6	210.7	253.0	278.3				823.2	744.0	512.5
Mean	247.6	321.4	253.6				881.2	1189.5	896.2
StDev	77.9	187.1	151.4				189.3	296.5	224.9
COV	31.5	58.2	59.7				21.5	24.9	25.1

Table A.79 P-values of paired t-test after modified Bonferroni procedure for final pressure values in 0°-180° orientation of the right toroidal die filled at feed shoe speed of 100 mm/s

	Orientation	180°			0°		
	Radius, mm	8	6	4	4	6	8
180°	8	–	–	–	–	–	–
	6	3.545					–
	4	13.044	2.503				–
0°	4	**0.002**	**<0.001**	**0.001**			–
	6	**0.004**	**0.006**	**0.007**	0.716		–
	8	**0.004**	**0.015**	**0.009**	13.122	0.059	–

*Entries in bold are significantly different (P < 0.05)

Table A.80 Final pressure values in 0°-180° orientation of right toroidal die filled at feed shoe speed of 500 mm/s (Pa)

Orientation	180°				Center		0°		
Radius, mm	8	6	4				4	6	8
Run #1	872.8	713.0	887.2				2234.0	2247.3	2269.6
Run #2	375.7	850.9	424.1				1413.7	2110.0	1642.7
Run #3	738.7	786.7	611.4				1483.4	2464.9	1670.6
Run #4	366.0	590.3	573.5				1688.2	2576.2	1751.7
Run #5	460.5	631.7	629.6				1702.5	2788.3	1654.2
Run #6	588.9	953.1	535.6				1526.7	2801.3	2315.7
Mean	567.1	754.3	610.2				1674.7	2498.0	1884.1
StDev	205.8	136.7	154.1				296.8	281.7	319.1
COV	36.3	18.1	25.2				17.7	11.3	16.9

Table A.81 P-values of paired t-test after modified Bonferroni procedure for final pressure values in 0°-180° orientation of the right toroidal die filled at feed shoe speed of 500 mm/s

	Orientation	180°			0°		
	Radius, mm	8	6	4	4	6	8
180°	8	–	–	–	–	–	–
	6	1.476					–
	4	6.703	3.075				–
0°	4	**0.001**	**0.028**	**<0.001**			–
	6	**0.001**	**0.001**	**0.001**	**0.036**		–
	8	**0.001**	**0.003**	**0.001**	2.248	0.064	–

*Entries in bold are significantly different (P < 0.05)

Table A.82 Final pressure values in 90°-270° orientation of the right toroidal die filled at feed shoe speed of 20 mm/s (Pa)

Orientation	270°				Center		90°		
Radius, mm	8	6	4				4	6	8
Run #1	497.0	587.4	365.9				348.3	437.9	343.3
Run #2	222.1	372.1	422.4				262.8	472.2	304.0
Run #3	298.5	538.5	460.7				474.5	573.1	267.7
Run #4	464.4	534.8	392.7				420.8	770.8	515.3
Run #5	490.3	694.0	500.4				409.7	771.9	828.4
Run #6	347.9	763.6	493.7				446.6	594.3	424.3
Mean	386.7	581.7	439.3				393.8	603.4	447.2
StDev	114.3	136.8	54.8				76.8	142.8	206.8
COV	29.6	23.5	12.5				19.5	23.7	46.3

Table A.83 P-values of paired t-test after modified Bonferroni procedure for final pressure values in 90°-270° orientation of the right toroidal die filled at feed shoe speed of 20 mm/s

	Orientation	270°			90°		
	Radius, mm	8	6	4	4	6	8
270°	8	–	–	–	–	–	–
	6	0.191					–
	4	5.841	0.437				–
90°	4	13.355	0.109	2.616			–
	6	0.175	11.208	0.416	0.124		–
	8	6.057	1.905	13.841	8.307	0.453	–

Table A.84 Final pressure values in 90°-270° orientation of the right toroidal die filled at feed shoe speed of 100 mm/s (Pa)

Orientation	270°				Center		90°		
Radius, mm	8	6	4				4	6	8
Run #1	466.7	530.8	734.1				589.3	779.1	564.8
Run #2	549.6	527.1	357.5				416.1	520.7	367.2
Run #3	462.1	836.9	595.9				359.2	536.9	459.2
Run #4	210.0	445.6	367.1				288.2	674.1	465.7
Run #5	383.8	439.9	306.8				589.7	769.8	690.7
Run #6	476.1	561.3	696.4				610.4	620.1	480.3
Mean	424.8	557.0	509.6				475.4	650.2	504.7
StDev	117.6	145.7	188.3				138.8	111.4	110.7
COV	27.7	26.2	37.0				29.2	17.1	21.9

Table A.85 P-values of paired t-test after modified Bonferroni procedure for final pressure values in 90°-270° orientation of the right toroidal die filled at feed shoe speed of 100 mm/s

	Orientation	270°			90°		
	Radius, mm	8	6	4	4	6	8
270°	8	–	–	–	–	–	–
	6	1.153					–
	4	4.508	8.125				–
90°	4	6.109	6.244	9.999			–
	6	0.522	5.494	2.520	0.256		–
	8	4.937	8.563	14.390	8.433	**0.028**	–

*Entries in bold are significantly different ($P < 0.05$)

Table A.86 Final pressure values in 90°-270° orientation of right toroidal die filled at feed shoe speed of 500 mm/s (Pa)

Orientation	270°				Center		90°		
Radius, mm	8	6	4				4	6	8
Run #1	202.7	376.9	232.4				437.5	469.8	318.0
Run #2	330.3	392.1	223.2				137.4	216.0	231.1
Run #3	196.5	302.1	348.4				155.9	392.8	340.8
Run #4	103.9	168.2	173.5				280.9	313.7	129.1
Run #5	276.8	261.1	246.4				481.6	432.2	240.9
Run #6	179.6	225.4	178.6				172.9	218.3	128.9
Mean	215.0	287.6	233.7				277.7	340.5	231.5
StDev	78.9	87.1	63.4				150.1	108.7	90.0
COV	36.7	30.3	27.1				54.1	31.9	38.9

Table A.87 P-values of paired t-test after modified Bonferroni procedure for final pressure values in 90°-270° orientation of the right toroidal die filled at feed shoe speed of 500 mm/s

	Orientation	270°			90°		
	Radius, mm	8	6	4	4	6	8
270°	8	–	–	–	–	–	–
	6	0.565					–
	4	9.367	2.753				–
90°	4	6.096	13.422	8.266			–
	6	1.195	5.363	0.619	2.505		–
	8	10.409	1.490	13.670	7.643	0.333	–

Table A.88 Final pressure values in 45°-225° orientation of the right toroidal die filled at feed shoe speed of 20 mm/s (Pa)

Orientation	225°				Center		45°		
Radius, mm	8	6	4				4	6	8
Run #1	329.8	403.6	359.1				588.6	1076.2	766.3
Run #2	264.8	408.8	364.6				1154.4	923.9	776.2
Run #3	460.7	552.2	369.2				524.8	1281.8	839.8
Run #4	436.6	394.3	415.4				631.9	1312.5	802.9
Run #5	196.3	347.0	344.1				700.1	1155.6	794.0
Run #6	330.8	573.9	390.7				889.8	1301.2	976.3
Mean	336.5	446.6	373.9				748.3	1175.2	825.9
StDev	100.3	93.1	25.4				235.1	154.6	78.0
COV	29.8	20.8	6.8				31.4	13.2	9.4

Table A.89 P-values of paired t-test after modified Bonferroni procedure for final pressure values in 45°-225° orientation of the right toroidal die filled at feed shoe speed of 20 mm/s

	Orientation	225°			45°		
	Radius, mm	8	6	4	4	6	8
225°	8	–	–	–	–	–	–
	6	0.549					–
	4	5.012	1.524				–
45°	4	0.300	0.511	0.095			–
	6	**<0.001**	**0.001**	**0.001**	0.455		–
	8	**0.002**	**<0.001**	**<0.001**	6.908	**0.015**	–

*Entries in bold are significantly different ($P < 0.05$)

Table A.90 Final pressure values in 45°-225° orientation of the right toroidal die filled at feed shoe speed of 100 mm/s (Pa)

Orientation	225°				Center		45°		
Radius, mm	8	6	4				4	6	8
Run #1	451.7	713.8	802.2				891.0	1028.7	1068.8
Run #2	356.0	614.2	584.9				920.9	1076.6	984.5
Run #3	283.5	463.1	333.6				919.2	1333.5	784.3
Run #4	333.2	426.8	329.5				740.9	1316.3	1010.9
Run #5	205.6	486.4	351.9				515.3	1156.2	787.8
Run #6	530.7	587.9	442.0				548.8	793.6	735.4
Mean	360.1	548.7	474.1				756.0	1117.5	895.3
StDev	116.6	108.8	187.9				186.1	201.1	142.0
COV	32.4	19.8	39.6				24.6	18.0	15.9

Table A.91 P-values of paired t-test after modified Bonferroni procedure for final pressure values in 45°-225° orientation of the right toroidal die filled at feed shoe speed of 100 mm/s

	Orientation	225°			45°		
	Radius, mm	8	6	4	4	6	8
225°	8	–	–	–	–	–	–
	6	0.051					–
	4	2.146	1.482				–
45°	4	0.101	0.640	0.257			–
	6	**0.024**	0.070	0.077	0.140		–
	8	**0.009**	**0.027**	**0.014**	1.176	0.875	–

*Entries in bold are significantly different ($P < 0.05$)

Table A.92 Final pressure values in 45°-225° orientation of right toroidal die filled at feed shoe speed of 500 mm/s (Pa)

Orientation	225°				Center		45°		
Radius, mm	8	6	4				4	6	8
Run #1	457.4	729.7	367.9				482.1	1051.2	1018.6
Run #2	654.4	819.6	378.5				707.2	1397.1	1320.1
Run #3	417.2	625.7	515.7				1197.0	1095.1	1086.7
Run #4	542.2	918.8	787.9				1164.9	1628.1	1173.4
Run #5	289.8	608.6	493.2				771.2	988.4	1162.0
Run #6	536.1	669.8	334.8				668.3	1272.7	744.4
Mean	482.9	728.7	479.7				831.8	1238.8	1084.2
StDev	125.0	120.7	167.5				287.2	243.4	194.6
COV	25.9	16.6	34.9				34.5	19.6	18.0

Table A.93 P-values of paired t-test after modified Bonferroni procedure for final pressure values in 45°-225° orientation of the right toroidal die filled at feed shoe speed of 500 mm/s

	Orientation	225°			45°		
	Radius, mm	8	6	4	4	6	8
225°	8	–	–	–	–	–	–
	6	**0.020**					–
	4	14.590	0.063				–
45°	4	0.677	6.376	**0.045**			–
	6	**0.002**	**0.005**	**0.004**	0.306		–
	8	**0.016**	**0.044**	**0.011**	1.423	3.417	–

*Entries in bold are significantly different ($P < 0.05$)

Table A.94 Final pressure values in 135°-315° orientation of the right toroidal die filled at feed shoe speed of 20 mm/s (Pa)

Orientation	315°				Center		135°		
Radius, mm	8	6	4				4	6	8
Run #1	1530.9	1926.3	1587.0				367.9	662.5	441.7
Run #2	1474.5	1676.4	1671.0				686.4	1036.1	472.5
Run #3	1285.8	1864.5	1287.5				700.3	664.9	431.8
Run #4	1247.2	1578.6	1342.6				389.5	514.7	324.0
Run #5	1295.6	1868.4	1371.0				662.2	636.8	325.3
Run #6	1308.7	1520.4	1173.9				720.8	510.8	267.8
Mean	1357.1	1739.1	1405.5				587.8	671.0	377.2
StDev	116.0	170.3	187.7				163.3	192.2	82.1
COV	8.5	9.8	13.4				27.8	28.6	21.8

Table A.95 P-values of paired t-test after modified Bonferroni procedure for final pressure values in 135°-315° orientation of the right toroidal die filled at feed shoe speed of 20 mm/s

	Orientation	315°			135°		
	Radius, mm	8	6	4	4	6	8
315°	8	–	–	–	–	–	–
	6	**0.037**					–
	4	4.965	**0.039**				–
135°	4	**0.006**	**0.002**	**0.013**			–
	6	**0.002**	**0.001**	**<0.001**	5.779		–
	8	**<0.001**	**<0.001**	**<0.001**	0.125	**0.017**	–

*Entries in bold are significantly different ($P < 0.05$)

Table A.96 Final pressure values in 135°-315° orientation of the right toroidal die filled at feed shoe speed of 100 mm/s (Pa)

Orientation	315°				Center		135°		
Radius, mm	8	6	4				4	6	8
Run #1	1054.1	1830.1	1300.3				518.9	826.6	440.5
Run #2	1044.4	1548.9	1357.5				618.5	787.4	548.7
Run #3	1081.8	1712.7	1135.7				438.2	991.8	710.7
Run #4	1208.7	1118.6	913.9				584.2	878.4	683.3
Run #5	1242.0	1230.1	629.9				555.4	802.2	520.6
Run #6	1300.4	1659.3	1168.6				587.4	938.7	619.6
Mean	1155.2	1516.6	1084.3				550.5	870.9	587.2
StDev	109.0	282.4	270.7				64.4	81.2	103.0
COV	9.4	18.6	25.0				11.7	9.3	17.5

Table A.97 P-values of paired t-test after modified Bonferroni procedure for final pressure values in 135°-315° orientation of the right toroidal die filled at feed shoe speed of 100 mm/s

	Orientation	315°			135°		
	Radius, mm	8	6	4	4	6	8
315°	8	–	–	–	–	–	–
	6	0.208					–
	4	9.605	**0.035**				–
135°	4	**0.001**	**0.010**	**0.032**			–
	6	**0.034**	**0.031**	1.747	**0.027**		–
	8	**0.002**	**0.014**	**0.050**	7.950	**0.002**	–

*Entries in bold are significantly different ($P < 0.05$)

Table A.98 Final pressure values in 135°-315° orientation of right toroidal die filled at feed shoe speed of 500 mm/s (Pa)

Orientation	315°				Center		135°		
Radius, mm	8	6	4				4	6	8
Run #1	853.7	995.4	783.8				418.5	645.7	601.9
Run #2	1110.5	1259.5	948.2				447.3	751.7	574.3
Run #3	1267.4	1216.2	904.4				828.8	1031.8	645.8
Run #4	1536.0	1248.0	1149.5				584.9	675.7	486.4
Run #5	889.6	1426.7	1449.5				435.8	443.4	673.1
Run #6	1190.7	1272.3	1067.3				247.2	593.5	806.6
Mean	1141.3	1236.4	1050.5				493.7	690.3	631.4
StDev	253.5	139.1	233.3				196.3	196.4	107.5
COV	22.2	11.2	22.2				39.7	28.4	17.0

Table A.99 P-values of paired t-test after modified Bonferroni procedure for final pressure values in 135°-315° orientation of the right toroidal die filled at feed shoe speed of 500 mm/s

	Orientation	315°			135°		
	Radius, mm	8	6	4	4	6	8
315°	8	–	–	–	–	–	–
	6	6.456					–
	4	8.193	0.254				–
135°	4	**0.021**	**0.011**	0.138			–
	6	0.097	0.056	1.090	0.197		–
	8	0.146	**0.003**	0.125	3.868	8.673	–

*Entries in bold are significantly different ($P < 0.05$)

Center vs. Right Toroidal Dies

Table A.100 P-values of t-test (two-sample assuming equal variances) between final pressure values of the center and right toroidal dies at feed shoe speed of 20 mm/s

Orientation	180°, 270°, 225, or 315°				Center		0°, 90, 45°, or 135°		
Radius, mm	8	6	4				4	6	8
0°-180°	0.564	0.191	**0.049**				0.815	0.182	**0.039**
90°-270°	**0.013**	**0.002**	**<0.001**				**0.026**	**0.036**	0.145
45°-225°	**0.007**	**0.002**	**<0.001**				**0.011**	**<0.001**	**<0.001**
135°-315°	**<0.001**	**<0.001**	**<0.001**				**<0.001**	**0.001**	**0.014**

Table A.101 P-values of t-test (two-sample assuming equal variances) between final pressure values of the center and right toroidal dies at feed shoe speed of 100 mm/s

Orientation	180°, 270°, 225, or 315°				Center		0°, 90, 45°, or 135°		
Radius, mm	8	6	4				4	6	8
0°-180°	0.377	**0.027**	**0.023**				0.130	0.987	0.558
90°-270°	**0.001**	**0.003**	**0.003**				**0.013**	**<0.001**	**0.002**
45°-225°	**<0.001**	**<0.001**	**0.001**				**<0.001**	**<0.001**	**<0.001**
135°-315°	**0.037**	**0.002**	**0.034**				**0.001**	**<0.001**	**<0.001**

Table A.102 P-values of t-test (two-sample assuming equal variances) between final pressure values of the center and right toroidal dies at feed shoe speed of 500 mm/s

Orientation	180°, 270°, 225, or 315°				Center		0°, 90, 45°, or 135°		
Radius, mm	8	6	4				4	6	8
0°-180°	0.834	0.932	0.224				0.335	**0.041**	0.216
90°-270°	**0.043**	**0.019**	0.076				0.474	0.472	**0.045**
45°-225°	**<0.001**	**<0.001**	**<0.001**				**<0.001**	**<0.001**	**<0.001**
135°-315°	0.071	**0.001**	**0.005**				0.051	**0.005**	**<0.001**

Center vs. Right E-shaped Dies

Table A.103 P-values of t-test (two-sample assuming equal variances) between final pressure values of the center and right E-shaped dies at feed shoe speed of 20 mm/s

Distance, mm	1	3	5	7	9	11	13	15	17	19	21	23	25	27	29	31
L1	0.972	0.536	**0.005**	-	-	-	0.067	0.151	0.490	0.142	-	-	-	0.666	0.113	0.438
L2	**0.039**	0.283	0.891	-	-	-	**0.007**	**0.037**	**0.020**	0.144	-	-	-	**0.030**	**0.013**	0.089
L3	0.577	0.887	0.078	-	-	-	0.269	0.223	0.746	0.263	-	-	-	**0.031**	0.111	0.697
L4	**<0.001**	**0.004**	**0.047**	**0.009**	**0.001**	**0.014**	**<0.001**	**0.006**	**0.048**	**0.037**	0.060	**0.002**	**0.001**	**0.005**	**0.004**	**0.037**

Center Cylindrical vs. Center Toroidal Dies

Table A.104 P-values of t-test (two-sample assuming equal variances) between final pressure values of the center cylindrical and the center toroidal dies at feed shoe speed of 20 mm/s

Orientation	180°, 270°, 225, or 315°				Center		0°, 90, 45°, or 135°		
Radius, mm	8	6	4				4	6	8
0°-180°	**0.043**	**0.001**	**0.026**				**0.029**	**<0.001**	**<0.001**
90°-270°	0.931	0.159	**0.001**				**<0.001**	**0.008**	0.054
45°-225°	0.214	**0.006**	**<0.001**				0.165	**0.009**	0.644
135°-315°	0.069	0.159	0.764				**<0.001**	**<0.001**	**0.045**

Table A.105 P-values of t-test (two-sample assuming equal variances) between final pressure values of the center cylindrical and the center toroidal dies at feed shoe speed of 100 mm/s

Orientation	180°, 270°, 225, or 315°				Center		0°, 90, 45°, or 135°		
Radius, mm	8	6	4				4	6	8
0°-180°	**0.001**	**<0.001**	0.384				0.850	**0.002**	**<0.001**
90°-270°	**0.001**	**0.003**	**<0.001**				**0.001**	**0.001**	0.068
45°-225°	**0.013**	**<0.001**	**<0.001**				**<0.001**	**0.037**	0.176
135°-315°	**0.008**	**<0.001**	0.118				**0.023**	0.215	0.467

Table A.106 P-values of t-test (two-sample assuming equal variances) between final pressure values of the center cylindrical and the center toroidal dies at feed shoe speed of 500 mm/s

Orientation	180°, 270°, 225, or 315°				Center		0°, 90, 45°, or 135°		
Radius, mm	8	6	4				4	6	8
0°-180°	0.349	0.530	0.570				**0.008**	**0.001**	**0.047**
90°-270°	**<0.001**	**<0.001**	**<0.001**				**<0.001**	**<0.001**	**<0.001**
45°-225°	**<0.001**	**<0.001**	**<0.001**				**<0.001**	**<0.001**	**<0.001**
135°-315°	0.379	0.140	**0.014**				**<0.001**	**<0.001**	**<0.001**

Right Cylindrical vs. Right Toroidal Dies

Table A.107 P-values of t-test (two-sample assuming equal variances) between final pressure values of the right cylindrical and the right toroidal dies at feed shoe speed of 20 mm/s

Orientation	180°, 270°, 225, or 315°				Center		0°, 90, 45°, or 135°		
Radius, mm	8	6	4				4	6	8
0°-180°	0.112	0.183	**0.010**				**0.040**	**0.001**	0.062
90°-270°	0.091	**0.039**	0.296				**0.020**	0.603	0.685
45°-225°	0.161	**0.002**	**<0.001**				0.251	**0.003**	0.779
135°-315°	**<0.001**	**<0.001**	**0.001**				**0.008**	**0.011**	**0.010**

Table A.108 P-values of t-test (two-sample assuming equal variances) between final pressure values of the right cylindrical and the right toroidal dies at feed shoe speed of 100 mm/s

Orientation	180°, 270°, 225, or 315°				Center		0°, 90, 45°, or 135°		
Radius, mm	8	6	4				4	6	8
0°-180°	0.150	**0.016**	**0.001**				0.701	**0.021**	**0.041**
90°-270°	**0.004**	**0.035**	0.768				0.981	**0.002**	**0.016**
45°-225°	**0.025**	0.109	**0.016**				**0.029**	0.054	0.192
135°-315°	**0.005**	**0.002**	0.559				**<0.001**	**0.012**	0.430

Table A.109 P-values of t-test (two-sample assuming equal variances) between final pressure values of the right cylindrical and the right toroidal dies at feed shoe speed of 500 mm/s

Orientation	180°, 270°, 225, or 315°						Center	0°, 90, 45°, or 135°	
Radius, mm	8	6	4				4	6	8
0°-180°	0.186	**0.028**	**0.001**				0.057	**<0.001**	**0.021**
90°-270°	**0.001**	**<0.001**	**<0.001**				**<0.001**	**<0.001**	**<0.001**
45°-225°	0.153	**0.035**	**0.001**				**0.012**	0.591	0.714
135°-315°	**0.049**	0.298	0.908				**0.001**	**0.034**	0.278

Appendix C Selected PDT-II Data of Alumina Powder

Center Cylindrical Die

Table A.110 Prorated final pressure ratios in 0°-180° orientation of the center cylindrical die filled at feed shoe speed of 20 mm/s

Orientation	180°				Center	0°			
Radius, mm	8	6	4	2	0	2	4	6	8
Run #1	0.619	0.688	1.150	1.147	1.000	0.839	0.485	0.492	0.297
Run #2	0.361	0.432	0.684	0.952	1.000	0.838	0.634	0.299	0.195
Run #3	0.429	0.566	0.712	1.141	1.000	0.998	0.773	0.469	0.194
Run #4	0.279	0.499	0.654	1.030	1.000	0.770	0.674	0.451	0.257
Run #5	0.324	0.420	0.709	0.847	1.000	0.982	0.787	0.417	0.192
Run #6	0.501	0.466	0.700	1.022	1.000	1.070	0.912	0.579	0.286
Mean	0.419	0.512	0.768	1.023	1.000	0.916	0.711	0.451	0.237
StDev	0.126	0.101	0.188	0.114	–	0.117	0.147	0.092	0.049
COV	30.0	19.7	24.5	11.2	–	12.7	20.7	20.5	20.7

Table A.111 P-values of paired t-test after modified Bonferroni procedure for prorated final pressure ratios in 0°-180° orientation of the center cylindrical die filled at feed shoe speed of 20 mm/s

	Orientation	180°				Center	0°			
	Radius, mm	8	6	4	2	0	2	4	6	8
180°	8	–	–	–	–	–	–	–	–	–
	6	–	–							–
	4	–	**0.039**							–
	2	–	**<0.001**	0.243						–
Center	0	–	**0.001**	0.618	13.411					–
0°	2	–	**0.035**	4.127	3.924	2.904				–
	4	–	1.722	14.053	0.343	0.063	**0.031**			–
	6	–	4.761	0.193	**0.001**	**0.001**	**0.002**	0.129	–	–
	8	–	–	–	–	–	–	–	–	–

*Entries in bold are significantly different (P < 0.05)

Table A.112 Prorated final pressure ratios in 0°-180° orientation of the center cylindrical die filled at feed shoe speed of 100 mm/s

Orientation	180°				Center	0°			
Radius, mm	8	6	4	2	0	2	4	6	8
Run #1	0.700	0.589	0.737	0.962	1.000	0.936	0.846	0.454	0.317
Run #2	0.590	0.509	0.740	0.962	1.000	0.884	0.626	0.529	0.296
Run #3	0.375	0.533	0.766	0.774	1.000	0.903	0.609	0.346	0.208
Run #4	0.558	0.690	0.945	1.104	1.000	0.921	0.878	0.637	0.368
Run #5	0.418	0.534	0.799	1.025	1.000	0.804	0.658	0.454	0.271
Run #6	0.394	0.512	0.570	0.805	1.000	0.907	0.768	0.571	0.242
Mean	0.506	0.561	0.759	0.939	1.000	0.892	0.731	0.499	0.284
StDev	0.130	0.069	0.121	0.127	–	0.047	0.116	0.102	0.056
COV	25.8	12.4	15.9	13.6	–	5.2	15.9	20.5	19.9

Table A.113 P-values of paired t-test after modified Bonferroni procedure for prorated final pressure ratios in 0°-180° orientation of the center cylindrical die filled at feed shoe speed of 100 mm/s

	Orientation	180°				Center	0°			
	Radius, mm	8	6	4	2	0	2	4	6	8
180°	8	–	–	–	–	–	–	–	–	–
	6	–	–							–
	4	–	**0.027**							–
	2	–	**0.004**	**0.042**						–
Center	0	–	**<0.001**	**0.041**	6.120					–
0°	2	–	**0.001**	1.185	9.810	**0.029**				–
	4	–	**0.031**	13.814	0.220	**0.031**	0.198			–
	6	–	3.350	0.057	**0.004**	**0.001**	**0.004**	**0.028**	–	–
	8	–	–	–	–	–	–	–	–	–

*Entries in bold are significantly different (P < 0.05)

Table A.114 Prorated final pressure ratios in 0°-180° orientation of center cylindrical die filled at feed shoe speed of 200 mm/s

Orientation	180°				Center	0°			
Radius, mm	8	6	4	2	0	2	4	6	8
Run #1	0.025	0.584	1.122	0.898	1.000	1.490	1.448	1.196	0.773
Run #2	0.015	0.104	1.421	1.418	1.000	1.443	1.281	1.299	0.648
Run #3	0.216	0.402	0.596	0.904	1.000	1.167	0.721	0.743	0.630
Run #4	0.812	0.852	1.238	1.006	1.000	1.211	1.353	1.196	0.836
Run #5	0.430	0.706	0.822	1.189	1.000	0.918	0.973	0.930	0.599
Run #6	0.378	0.707	1.263	0.954	1.000	0.952	1.189	1.023	0.678
Mean	0.313	0.559	1.077	1.062	1.000	1.197	1.161	1.065	0.694
StDev	0.300	0.269	0.309	0.205	–	0.239	0.269	0.206	0.092
COV	95.8	48.1	28.7	19.3	–	19.9	23.2	19.4	13.2

Table A.115 P-values of paired t-test after modified Bonferroni procedure for prorated final pressure ratios in 0°-180° orientation of the center cylindrical die filled at feed shoe speed of 200 mm/s

	Orientation	180°				Center	0°			
	Radius, mm	8	6	4	2	0	2	4	6	8
180°	8	–	–	–	–	–	–	–	–	–
	6	–	–							–
	4	–	0.671							–
	2	–	0.686	18.982						–
Center	0	–	0.214	11.949	10.364					–
0°	2	–	0.361	8.130	6.449	2.082				–
	4	–	0.179	5.784	10.181	4.278	15.350			–
	6	–	0.396	17.806	20.496	10.032	3.240	1.874	–	–
	8	–	–	–	–	–	–	–	–	–

Table A.116 Prorated final pressure ratios in 45°-225° orientation of the center cylindrical die filled at feed shoe speed of 20 mm/s

Orientation	225°				Center	45°			
Radius, mm	8	6	4	2	0	2	4	6	8
Run #1	0.457	0.805	0.963	1.176	1.000	0.943	0.602	0.385	0.335
Run #2	0.284	0.606	0.883	1.054	1.000	0.878	0.711	0.479	0.413
Run #3	0.432	0.793	0.968	1.028	1.000	0.826	0.849	0.764	0.502
Run #4	0.326	0.540	0.925	1.008	1.000	0.870	0.831	0.554	0.336
Run #5	0.271	0.593	0.782	0.810	1.000	0.816	0.691	0.605	0.294
Run #6	0.451	0.646	0.867	0.981	1.000	0.746	0.528	0.482	0.264
Mean	0.370	0.664	0.898	1.010	1.000	0.846	0.702	0.545	0.357
StDev	0.086	0.110	0.070	0.119	–	0.067	0.126	0.131	0.087
COV	23.2	16.6	7.8	11.8	–	7.9	17.9	24.0	24.3

Table A.117 P-values of paired t-test after modified Bonferroni procedure for prorated final pressure ratios in 45°-225° orientation of the center cylindrical die filled at feed shoe speed of 20 mm/s

	Orientation	225°				Center	45°			
	Radius, mm	8	6	4	2	0	2	4	6	8
225°	8	–	–	–	–	–	–	–	–	–
	6	–	–							–
	4	–	**0.020**							–
	2	–	**0.009**	0.237						–
Center	0	–	**0.013**	0.336	17.846					–
45°	2	–	0.218	2.617	0.089	**0.037**				–
	4	–	12.996	0.238	0.183	**0.034**	0.875			–
	6	–	2.876	**0.034**	**0.043**	**0.008**	0.152	0.215	–	–
	8	–	–	–	–	–	–	–	–	–

*Entries in bold are significantly different ($P < 0.05$)

Table A.118 Prorated final pressure ratios in 45°-225° orientation of the center cylindrical die filled at feed shoe speed of 100 mm/s

Orientation	225°				Center	45°			
Radius, mm	8	6	4	2	0	2	4	6	8
Run #1	0.214	0.533	0.831	1.217	1.000	0.874	0.879	0.716	0.489
Run #2	0.368	0.665	0.988	1.194	1.000	0.933	0.759	0.569	0.542
Run #3	0.480	0.627	0.767	0.941	1.000	0.917	0.740	0.561	0.270
Run #4	0.323	0.663	0.773	0.958	1.000	0.928	0.733	0.549	0.297
Run #5	0.313	0.575	0.730	0.902	1.000	0.966	0.851	0.540	0.508
Run #6	0.497	0.820	1.036	1.185	1.000	0.922	0.770	0.530	0.327
Mean	0.366	0.647	0.854	1.066	1.000	0.923	0.789	0.578	0.406
StDev	0.108	0.099	0.127	0.147	–	0.030	0.061	0.069	0.120
COV	29.5	15.3	14.9	13.8	–	3.2	7.8	12.0	29.7

Table A.119 P-values of paired t-test after modified Bonferroni procedure for prorated final pressure ratios in 45°-225° orientation of the center cylindrical die filled at feed shoe speed of 100 mm/s

	Orientation	225°				Center	45°			
	Radius, mm	8	6	4	2	0	2	4	6	8
225°	8	–	–	–	–	–	–	–	–	–
	6	–	–							–
	4	–	**0.024**							–
	2	–	**0.017**	**0.023**						–
Center	0	–	**0.006**	0.795	6.709					–
45°	2	–	**0.015**	5.563	1.868	**0.019**				–
	4	–	1.300	7.192	0.056	**0.006**	0.138			–
	6	–	6.615	0.137	**0.005**	**0.001**	**0.005**	**0.005**	–	–
	8	–	–	–	–	–	–	–	–	–

*Entries in bold are significantly different ($P < 0.05$)

Table A.120 Prorated final pressure ratios in 45°-225° orientation of center cylindrical die filled at feed shoe speed of 200 mm/s

Orientation	225°				Center	45°			
Radius, mm	8	6	4	2	0	2	4	6	8
Run #1	0.501	0.740	0.825	0.969	1.000	1.197	0.715	0.633	0.939
Run #2	0.731	0.926	1.340	1.240	1.000	1.109	0.875	0.861	0.663
Run #3	0.323	0.628	0.612	0.594	1.000	0.875	0.717	0.875	0.767
Run #4	0.804	0.828	0.970	1.076	1.000	1.105	1.020	0.925	0.753
Run #5	0.621	0.959	1.142	1.038	1.000	0.990	0.973	0.775	0.557
Run #6	0.428	0.692	0.952	0.929	1.000	0.884	0.884	0.792	0.674
Mean	0.568	0.795	0.974	0.975	1.000	1.027	0.864	0.810	0.726
StDev	0.184	0.132	0.251	0.215	–	0.131	0.127	0.103	0.129
COV	32.4	16.5	25.8	22.1	–	12.8	14.7	12.7	17.7

Table A.121 P-values of paired t-test after modified Bonferroni procedure for prorated final pressure ratios in 45°-225° orientation of the center cylindrical die filled at feed shoe speed of 200 mm/s

	Orientation	225°				Center	45°			
	Radius, mm	8	6	4	2	0	2	4	6	8
225°	8	–	–	–	–	–	–	–	–	–
	6	–	–							–
	4	–	0.673							–
	2	–	0.413	20.690						–
Center	0	–	0.262	16.972	16.462					–
45°	2	–	0.201	12.864	9.968	13.422				–
	4	–	3.721	5.027	3.729	0.979	1.604			–
	6	–	17.422	3.864	3.206	0.133	0.841	6.747	–	–
	8	–	–	–	–	–	–	–	–	–

Table A.122 Prorated final pressure ratios in 90°-270° orientation of the center cylindrical die filled at feed shoe speed of 20 mm/s

Orientation	270°				Center	90°			
Radius, mm	8	6	4	2	0	2	4	6	8
Run #1	0.348	0.874	1.045	0.946	1.000	1.035	0.987	0.732	0.474
Run #2	0.148	0.458	0.732	0.749	1.000	0.874	0.817	0.584	0.335
Run #3	0.449	0.549	0.890	0.810	1.000	0.990	0.935	0.845	0.472
Run #4	0.324	0.692	0.865	0.776	1.000	0.988	0.840	0.693	0.443
Run #5	0.292	0.488	0.795	0.884	1.000	0.895	0.780	0.480	0.396
Run #6	0.227	0.556	0.628	0.959	1.000	1.098	1.078	0.810	0.524
Mean	0.298	0.603	0.826	0.854	1.000	0.980	0.906	0.691	0.441
StDev	0.104	0.155	0.143	0.089	–	0.084	0.114	0.138	0.067
COV	34.7	25.8	17.3	10.4	–	8.6	12.6	20.0	15.1

Table A.123 P-values of paired t-test after modified Bonferroni procedure for prorated final pressure ratios in 90°-270° orientation of the center cylindrical die filled at feed shoe speed of 20 mm/s

	Orientation	270°				Center	90°			
	Radius, mm	8	6	4	2	0	2	4	6	8
270°	8	–	–	–	–	–	–	–	–	–
	6	–	–							–
	4	–	**0.048**							–
	2	–	0.174	14.624						–
Center	0	–	**0.028**	0.650	0.213					–
90°	2	–	**0.018**	1.459	0.154	12.263				–
	4	–	0.072	7.261	3.907	2.104	0.269			–
	6	–	5.431	2.863	0.857	**0.047**	**0.009**	**0.023**	–	–
	8	–	–	–	–	–	–	–	–	–

*Entries in bold are significantly different (P < 0.05)

Table A.124 Prorated final pressure ratios in 90°-270° orientation of the center cylindrical die filled at feed shoe speed of 100 mm/s

Orientation	270°				Center	90°			
Radius, mm	8	6	4	2	0	2	4	6	8
Run #1	0.400	0.638	0.804	0.869	1.000	1.016	0.955	0.676	0.404
Run #2	0.381	0.867	0.968	0.905	1.000	0.767	0.740	0.543	0.334
Run #3	0.464	0.768	0.952	1.039	1.000	0.927	0.939	0.565	0.314
Run #4	0.387	0.527	0.649	0.902	1.000	1.142	0.751	0.571	0.354
Run #5	0.462	0.817	1.066	1.097	1.000	1.049	0.918	0.660	0.534
Run #6	0.452	1.316	1.276	1.195	1.000	1.074	0.966	0.634	0.373
Mean	0.424	0.822	0.953	1.001	1.000	0.996	0.878	0.608	0.386
StDev	0.039	0.272	0.215	0.130	–	0.132	0.104	0.055	0.079
COV	9.1	33.1	22.6	13.0	–	13.3	11.9	9.1	20.5

Table A.125 P-values of paired t-test after modified Bonferroni procedure for prorated final pressure ratios in 90°-270° orientation of the center cylindrical die filled at feed shoe speed of 100 mm/s

	Orientation	270°				Center	90°			
	Radius, mm	8	6	4	2	0	2	4	6	8
270°	8	–	–	–	–	–	–	–	–	–
	6	–	–							–
	4	–	0.386							–
	2	–	1.329	7.833						–
Center	0	–	3.578	12.877	20.702					–
90°	2	–	4.859	14.894	19.732	19.766				–
	4	–	12.699	7.747	0.883	0.742	2.126			–
	6	–	2.306	0.210	**0.012**	**<0.001**	**0.008**	**0.006**	–	–
	8	–	–	–	–	–	–	–	–	–

*Entries in bold are significantly different (P < 0.05)

Table A.126 Prorated final pressure ratios in 90°-270° orientation of center cylindrical die filled at feed shoe speed of 200 mm/s

Orientation	270°				Center	90°			
Radius, mm	8	6	4	2	0	2	4	6	8
Run #1	0.712	0.729	0.897	0.946	1.000	0.980	0.941	0.591	0.469
Run #2	1.634	1.268	1.971	1.152	1.000	1.496	1.318	1.156	0.919
Run #3	0.507	0.909	1.036	0.901	1.000	1.149	0.895	1.027	0.805
Run #4	0.525	0.780	0.978	0.916	1.000	0.959	0.683	0.594	0.521
Run #5	1.326	0.705	0.811	1.006	1.000	0.860	1.045	1.201	0.587
Run #6	0.683	0.732	0.746	0.835	1.000	0.931	0.773	0.570	0.365
Mean	0.898	0.854	1.073	0.959	1.000	1.063	0.942	0.857	0.611
StDev	0.468	0.215	0.453	0.110	–	0.233	0.224	0.303	0.211
COV	52.2	25.2	42.2	11.4	–	21.9	23.7	35.4	34.5

Table A.127 P-values of paired t-test after modified Bonferroni procedure for prorated final pressure ratios in 90°-270° orientation of the center cylindrical die filled at feed shoe speed of 200 mm/s

	Orientation	270°				Center	90°			
	Radius, mm	8	6	4	2	0	2	4	6	8
270°	8	–	–	–	–	–	–	–	–	–
	6	–	–							–
	4	–	1.690							–
	2	–	3.080	10.063						–
Center	0	–	3.315	14.881	8.541					–
90°	2	–	**0.001**	19.294	4.262	11.306				–
	4	–	4.876	7.415	16.040	11.682	3.073			–
	6	–	20.621	5.118	7.214	6.274	2.876	7.048	–	–
	8	–	–	–	–	–	–	–	–	–

*Entries in bold are significantly different (P < 0.05)

Table A.128 Prorated final pressure ratios in 135°-315° orientation of the center cylindrical die filled at feed shoe speed of 20 mm/s

Orientation	315°				Center	135°			
Radius, mm	8	6	4	2	0	2	4	6	8
Run #1	0.337	0.469	0.742	1.009	1.000	1.076	0.883	0.661	0.353
Run #2	0.384	0.510	0.643	0.845	1.000	0.908	0.798	0.596	0.417
Run #3	0.265	0.557	0.737	0.877	1.000	1.189	1.057	0.698	0.469
Run #4	0.257	0.517	0.691	0.870	1.000	0.915	0.929	0.443	0.194
Run #5	0.229	0.489	0.486	0.823	1.000	1.064	0.919	0.589	0.442
Run #6	0.284	0.500	0.502	0.842	1.000	0.912	0.896	0.705	0.493
Mean	0.293	0.507	0.634	0.878	1.000	1.011	0.913	0.615	0.395
StDev	0.057	0.030	0.114	0.067	–	0.117	0.084	0.098	0.109
COV	19.6	5.9	18.0	7.6	–	11.6	9.2	15.9	27.7

Table A.129 P-values of paired t-test after modified Bonferroni procedure for prorated final pressure ratios in 135°-315° orientation of the center cylindrical die filled at feed shoe speed of 20 mm/s

	Orientation	315°				Center	135°			
	Radius, mm	8	6	4	2	0	2	4	6	8
315°	8	–	–	–	–	–	–	–	–	–
	6	–	–							–
	4	–	0.740							–
	2	–	**0.002**	**0.012**						–
Center	0	–	**<0.001**	**0.008**	0.060					–
135°	2	–	**0.002**	**0.011**	0.744	17.514				–
	4	–	**0.001**	**0.025**	9.539	1.116	0.636			–
	6	–	0.975	16.506	**0.021**	**0.003**	**0.006**	**0.017**	–	–
	8	–	–	–	–	–	–	–	–	–

*Entries in bold are significantly different (P < 0.05)

Table A.130 Prorated final pressure ratios in 135°-315° orientation of the center cylindrical die filled at feed shoe speed of 100 mm/s

Orientation	315°				Center	135°			
Radius, mm	8	6	4	2	0	2	4	6	8
Run #1	0.446	0.591	0.705	0.908	1.000	0.941	0.850	0.529	0.462
Run #2	0.311	0.703	1.714	1.176	1.000	0.865	0.527	0.526	0.201
Run #3	0.356	0.762	0.860	1.034	1.000	0.980	0.686	0.567	0.385
Run #4	0.325	0.573	0.848	0.898	1.000	1.053	0.799	0.599	0.474
Run #5	0.265	0.564	0.775	1.026	1.000	0.926	0.729	0.499	0.334
Run #6	0.298	0.513	0.717	0.877	1.000	0.784	0.597	0.545	0.349
Mean	0.333	0.618	0.936	0.986	1.000	0.925	0.698	0.544	0.367
StDev	0.063	0.095	0.387	0.115	–	0.093	0.121	0.035	0.100
COV	18.9	15.3	41.3	11.6	–	10.0	17.4	6.4	27.2

Table A.131 P-values of paired t-test after modified Bonferroni procedure for prorated final pressure ratios in 135°-315° orientation of the center cylindrical die filled at feed shoe speed of 100 mm/s

	Orientation	315°				Center	135°			
	Radius, mm	8	6	4	2	0	2	4	6	8
315°	8	–	–	–	–	–	–	–	–	–
	6	–	–							–
	4	–	1.538							–
	2	–	**0.002**	14.602						–
Center	0	–	**0.003**	14.772	16.475					–
135°	2	–	**0.019**	19.929	7.920	2.194				–
	4	–	6.440	5.801	0.266	**0.024**	**0.022**			–
	6	–	2.557	1.226	**0.008**	**<0.001**	**0.002**	0.520	–	–
	8	–	–	–	–	–	–	–	–	–

*Entries in bold are significantly different (P < 0.05)

Table A.132 Prorated final pressure ratios in 135°-315° orientation of center cylindrical die filled at feed shoe speed of 200 mm/s

Orientation	315°				Center	135°			
Radius, mm	8	6	4	2	0	2	4	6	8
Run #1	0.661	0.795	1.192	1.128	1.000	0.965	0.768	0.596	0.424
Run #2	0.444	0.764	0.812	0.593	1.000	1.111	0.792	0.543	0.336
Run #3	0.290	0.789	0.832	0.762	1.000	0.897	0.599	0.470	0.197
Run #4	0.272	0.547	0.660	1.022	1.000	1.006	0.289	0.900	1.773
Run #5	0.188	0.369	0.571	0.406	1.000	0.452	0.380	0.091	0.395
Run #6	0.562	1.193	0.957	0.952	1.000	1.125	0.983	0.646	0.347
Mean	0.403	0.743	0.837	0.810	1.000	0.926	0.635	0.541	0.579
StDev	0.184	0.278	0.221	0.275	–	0.248	0.264	0.265	0.590
COV	45.7	37.4	26.4	34.0	–	26.8	41.7	48.9	102.0

Table A.133 P-values of paired t-test after modified Bonferroni procedure for prorated final pressure ratios in 135°-315° orientation of the center cylindrical die filled at feed shoe speed of 200 mm/s

	Orientation	315°				Center	135°			
	Radius, mm	8	6	4	2	0	2	4	6	8
315°	8	–	–	–	–	–	–	–	–	–
	6	–	–							–
	4	–	6.678							–
	2	–	12.221	16.014						–
Center	0	–	1.526	2.745	3.201					–
135°	2	–	1.368	8.077	5.743	10.443				–
	4	–	1.891	0.864	5.284	0.413	0.552			–
	6	–	3.346	1.127	0.237	0.163	**0.038**	11.430	–	–
	8	–	–	–	–	–	–	–	–	–

*Entries in bold are significantly different (P < 0.05)

Right Cylindrical Die

Table A.134 Prorated final pressure ratios in 0°-180° orientation of the right cylindrical die filled at feed shoe speed of 20 mm/s

Orientation	180°				Center	0°			
Radius, mm	8	6	4	2	0	2	4	6	8
Run #1	0.602	0.330	0.721	1.208	1.000	1.072	1.011	0.811	0.561
Run #2	0.796	0.918	0.836	1.241	1.000	1.069	0.733	0.592	0.420
Run #3	1.775	0.807	0.878	1.106	1.000	0.952	0.749	0.631	0.449
Run #4	0.599	0.600	0.795	1.057	1.000	0.908	0.807	0.568	0.429
Run #5	1.382	0.535	0.720	0.912	1.000	0.942	0.758	0.571	0.308
Run #6	0.599	0.441	0.766	1.051	1.000	0.828	0.754	0.501	0.350
Mean	0.959	0.605	0.786	1.096	1.000	0.962	0.802	0.613	0.419
StDev	0.502	0.222	0.063	0.119	–	0.095	0.105	0.106	0.088
COV	52.3	36.7	8.1	10.9	–	9.9	13.1	17.3	20.9

Table A.135 P-values of paired t-test after modified Bonferroni procedure for prorated final pressure ratios in 0°-180° orientation of the right cylindrical die filled at feed shoe speed of 20 mm/s

	Orientation	180°				Center	0°			
	Radius, mm	8	6	4	2	0	2	4	6	8
180°	8	–	–	–	–	–	–	–	–	–
	6	–	–							–
	4	–	1.030							–
	2	–	**0.040**	**0.018**						–
Center	0	–	0.153	**0.007**	2.241					–
0°	2	–	0.222	0.258	0.261	7.749				–
	4	–	3.626	16.803	**0.036**	0.076	0.278			–
	6	–	19.943	0.544	**0.002**	**0.006**	**0.002**	**0.006**	–	–
	8	–	–	–	–	–	–	–	–	–

*Entries in bold are significantly different (P < 0.05)

Table A.136 Prorated final pressure ratios in 0°-180° orientation of the right cylindrical die filled at feed shoe speed of 100 mm/s

Orientation	180°				Center	0°			
Radius, mm	8	6	4	2	0	2	4	6	8
Run #1	0.695	0.458	0.724	0.960	1.000	0.887	0.753	0.620	0.397
Run #2	0.903	0.471	0.550	0.776	1.000	0.858	0.720	0.588	0.422
Run #3	0.393	0.480	0.796	0.965	1.000	0.996	0.861	0.604	0.388
Run #4	1.099	0.697	0.792	0.989	1.000	0.987	0.824	0.531	0.413
Run #5	0.737	0.460	0.583	1.173	1.000	0.865	0.708	0.511	0.316
Run #6	1.278	0.564	0.595	0.865	1.000	0.892	0.762	0.595	0.408
Mean	0.851	0.522	0.673	0.955	1.000	0.914	0.771	0.575	0.391
StDev	0.314	0.094	0.111	0.133	–	0.061	0.060	0.043	0.038
COV	36.9	18.1	16.4	14.0	–	6.7	7.8	7.6	9.8

Table A.137 P-values of paired t-test after modified Bonferroni procedure for prorated final pressure ratios in 0°-180° orientation of the right cylindrical die filled at feed shoe speed of 100 mm/s

	Orientation	180°				Center	0°			
	Radius, mm	8	6	4	2	0	2	4	6	8
180°	8	–	–	–	–	–	–	–	–	–
	6	–	–							–
	4	–	0.455							–
	2	–	**0.016**	0.061						–
Center	0	–	**0.001**	**0.010**	9.302					–
0°	2	–	**0.001**	**0.004**	10.736	0.391				–
	4	–	**0.010**	0.291	0.604	**0.004**	**<0.001**			–
	6	–	6.715	1.808	**0.024**	**<0.001**	**0.002**	**0.011**	–	–
	8	–	–	–	–	–	–	–	–	–

*Entries in bold are significantly different (P < 0.05)

Table A.138 Prorated final pressure ratios in 0°-180° orientation of right cylindrical die filled at feed shoe speed of 200 mm/s

Orientation	180°				Center	0°			
Radius, mm	8	6	4	2	0	2	4	6	8
Run #1	0.631	0.685	0.889	0.947	1.000	0.978	0.972	0.844	0.669
Run #2	0.543	0.689	0.886	1.009	1.000	1.010	1.023	0.868	0.873
Run #3	0.583	0.698	1.018	1.143	1.000	0.998	1.010	0.968	0.788
Run #4	1.589	0.750	0.753	0.917	1.000	0.992	0.924	0.825	0.818
Run #5	0.368	0.693	0.978	1.030	1.000	1.061	1.018	0.955	0.812
Run #6	0.578	0.727	0.957	1.128	1.000	0.963	0.946	0.959	0.980
Mean	0.716	0.707	0.913	1.029	1.000	1.000	0.982	0.903	0.823
StDev	0.437	0.026	0.094	0.092	–	0.034	0.041	0.065	0.102
COV	61.1	3.7	10.3	9.0	–	3.4	4.2	7.1	12.4

Table A.139 P-values of paired t-test after modified Bonferroni procedure for prorated final pressure ratios in 0°-180° orientation of the right cylindrical die filled at feed shoe speed of 200 mm/s

	Orientation	180°				Center	0°			
	Radius, mm	8	6	4	2	0	2	4	6	8
180°	8	–	–	–	–	–	–	–	–	–
	6	–	–							–
	4	–	0.084							–
	2	–	**0.009**	**0.039**						–
Center	0	–	**<0.001**	1.540	9.970					–
0°	2	–	**0.001**	1.442	10.822	20.646				–
	4	–	**0.003**	1.607	5.219	7.060	4.685			–
	6	–	**0.021**	12.491	**0.012**	0.300	0.315	0.536	–	–
	8	–	–	–	–	–	–	–	–	–

*Entries in bold are significantly different (P < 0.05)

Table A.140 Prorated final pressure ratios in 45°-225° orientation of the right cylindrical die filled at feed shoe speed of 20 mm/s

Orientation	225°				Center	45°			
Radius, mm	8	6	4	2	0	2	4	6	8
Run #1	0.459	0.629	0.866	0.983	1.000	0.863	0.913	0.710	0.398
Run #2	0.235	0.425	0.954	0.896	1.000	0.994	0.883	0.788	0.457
Run #3	0.400	0.707	0.811	0.914	1.000	1.003	0.994	0.847	0.448
Run #4	0.238	0.560	0.781	0.934	1.000	1.007	0.872	0.729	0.400
Run #5	0.354	0.523	0.836	0.920	1.000	0.933	0.774	0.602	0.374
Run #6	0.582	0.875	0.619	0.839	1.000	0.895	0.799	0.598	0.361
Mean	0.378	0.620	0.811	0.914	1.000	0.949	0.873	0.712	0.406
StDev	0.134	0.157	0.111	0.047	–	0.061	0.079	0.100	0.039
COV	35.3	25.4	13.7	5.2	–	6.5	9.1	14.0	9.5

Table A.141 P-values of paired t-test after modified Bonferroni procedure for prorated final pressure ratios in 45°-225° orientation of the right cylindrical die filled at feed shoe speed of 20 mm/s

	Orientation	225°				Center	45°			
	Radius, mm	8	6	4	2	0	2	4	6	8
225°	8	–	–	–	–	–	–	–	–	–
	6	–	–							–
	4	–	2.768							–
	2	–	0.231	0.864						–
Center	0	–	**0.035**	0.186	0.142					–
45°	2	–	0.176	0.584	7.189	2.077				–
	4	–	0.358	4.974	4.766	0.230	1.388			–
	6	–	6.878	1.363	0.065	**0.017**	**0.012**	**0.005**	–	–
	8	–	–	–	–	–	–	–	–	–

*Entries in bold are significantly different (P < 0.05)

Table A.142 Prorated final pressure ratios in 45°-225° orientation of the right cylindrical die filled at feed shoe speed of 100 mm/s

Orientation	225°				Center	45°			
Radius, mm	8	6	4	2	0	2	4	6	8
Run #1	0.518	0.644	0.790	0.893	1.000	1.106	0.979	0.808	0.554
Run #2	0.373	0.592	0.988	1.006	1.000	1.162	1.059	0.755	0.463
Run #3	0.626	0.747	0.679	0.777	1.000	0.940	0.857	0.700	0.414
Run #4	0.395	0.493	0.701	0.871	1.000	0.976	0.931	0.738	0.426
Run #5	0.324	0.589	0.916	0.917	1.000	1.065	0.958	0.814	0.520
Run #6	0.567	0.773	0.724	0.643	1.000	0.937	0.920	0.613	0.310
Mean	0.467	0.640	0.800	0.851	1.000	1.031	0.951	0.738	0.448
StDev	0.120	0.106	0.126	0.126	–	0.094	0.068	0.075	0.086
COV	25.7	16.5	15.7	14.8	–	9.1	7.1	10.2	19.3

Table A.143 P-values of paired t-test after modified Bonferroni procedure for prorated final pressure ratios in 45°-225° orientation of the right cylindrical die filled at feed shoe speed of 100 mm/s

	Orientation	225°				Center	45°			
	Radius, mm	8	6	4	2	0	2	4	6	8
225°	8	–	–	–	–	–	–	–	–	–
	6	–	–							–
	4	–	1.989							–
	2	–	1.292	4.559						–
Center	0	–	**0.007**	0.239	0.713					–
45°	2	–	**0.036**	**0.006**	**0.018**	9.603				–
	4	–	0.053	0.094	0.835	2.811	0.108			–
	6	–	4.225	4.509	0.302	**0.007**	**0.002**	**0.015**	–	–
	8	–	–	–	–	–	–	–	–	–

*Entries in bold are significantly different (P < 0.05)

Table A.144 Prorated final pressure ratios in 45°-225° orientation of right cylindrical die filled at feed shoe speed of 200 mm/s

Orientation	225°				Center	45°			
Radius, mm	8	6	4	2	0	2	4	6	8
Run #1	0.867	0.783	0.907	0.915	1.000	1.200	1.319	1.063	0.910
Run #2	0.920	0.905	0.960	0.867	1.000	0.998	1.169	1.028	0.415
Run #3	0.772	0.887	0.949	0.882	1.000	1.151	1.164	0.948	0.531
Run #4	0.620	0.744	0.836	0.830	1.000	1.047	1.268	0.835	0.468
Run #5	0.337	0.558	0.678	0.803	1.000	0.807	0.771	0.657	0.444
Run #6	0.521	0.555	0.694	0.823	1.000	0.891	0.807	0.693	0.440
Mean	0.673	0.739	0.837	0.853	1.000	1.016	1.083	0.871	0.535
StDev	0.222	0.154	0.125	0.042	–	0.150	0.236	0.171	0.188
COV	33.0	20.8	14.9	4.9	–	14.8	21.7	19.6	35.1

Table A.145 P-values of paired t-test after modified Bonferroni procedure for prorated final pressure ratios in 45°-225° orientation of the right cylindrical die filled at feed shoe speed of 200 mm/s

	Orientation	225°				Center	45°			
	Radius, mm	8	6	4	2	0	2	4	6	8
225°	8	–	–	–	–	–	–	–	–	–
	6	–	–							–
	4	–	**0.019**							–
	2	–	1.595	14.559						–
Center	0	–	0.184	0.510	**0.007**					–
45°	2	–	**0.029**	0.066	0.362	16.958				–
	4	–	**0.038**	0.187	0.854	8.968	4.881			–
	6	–	0.181	5.788	15.903	2.598	0.241	0.171	–	–
	8	–	–	–	–	–	–	–	–	–

*Entries in bold are significantly different (P < 0.05)

Table A.146 Prorated final pressure ratios in 90°-270° orientation of the right cylindrical die filled at feed shoe speed of 20 mm/s

Orientation	270°				Center	90°			
Radius, mm	8	6	4	2	0	2	4	6	8
Run #1	0.307	0.488	0.717	0.764	1.000	1.101	0.873	0.594	0.294
Run #2	0.170	0.435	0.603	0.866	1.000	0.983	0.671	0.687	0.350
Run #3	0.268	0.428	0.703	0.959	1.000	1.108	0.838	0.647	0.433
Run #4	0.229	0.459	0.682	0.828	1.000	0.696	0.729	0.538	0.248
Run #5	0.104	0.126	0.512	0.873	1.000	0.786	0.847	0.551	0.319
Run #6	0.278	0.481	0.606	0.855	1.000	0.983	1.019	0.488	0.329
Mean	0.226	0.403	0.637	0.857	1.000	0.943	0.830	0.584	0.329
StDev	0.076	0.138	0.078	0.064	–	0.168	0.121	0.074	0.062
COV	33.8	34.2	12.2	7.4	–	17.8	14.6	12.6	18.9

Table A.147 P-values of paired t-test after modified Bonferroni procedure for prorated final pressure ratios in 90°-270° orientation of the right cylindrical die filled at feed shoe speed of 20 mm/s

	Orientation	270°				Center	90°			
	Radius, mm	8	6	4	2	0	2	4	6	8
270°	8	–	–	–	–	–	–	–	–	–
	6	–	–							–
	4	–	**0.022**							–
	2	–	**0.018**	**0.043**						–
Center	0	–	**0.002**	**0.002**	**0.033**					–
90°	2	–	**0.008**	**0.045**	5.803	9.290				–
	4	–	**0.028**	0.513	13.522	0.382	3.579			–
	6	–	0.651	4.844	**0.008**	**0.001**	**0.028**	0.180	–	–
	8	–	–	–	–	–	–	–	–	–

*Entries in bold are significantly different (P < 0.05)

Table A.148 Prorated final pressure ratios in 90°-270° orientation of the right cylindrical die filled at feed shoe speed of 100 mm/s

Orientation	270°				Center	90°			
Radius, mm	8	6	4	2	0	2	4	6	8
Run #1	0.213	0.434	0.819	0.856	1.000	0.955	0.873	0.650	0.428
Run #2	0.270	0.544	0.666	0.713	1.000	0.970	0.869	0.941	0.399
Run #3	0.395	0.605	0.745	0.982	1.000	1.078	0.941	0.617	0.385
Run #4	0.557	1.444	0.849	0.882	1.000	0.973	0.773	0.455	0.259
Run #5	0.325	0.608	0.572	0.833	1.000	1.044	0.967	0.710	0.407
Run #6	0.435	0.702	0.724	0.915	1.000	1.027	0.943	0.830	0.551
Mean	0.366	0.723	0.729	0.863	1.000	1.008	0.894	0.701	0.405
StDev	0.124	0.364	0.101	0.090	–	0.049	0.071	0.170	0.093
COV	33.8	50.4	13.9	10.5	–	4.9	8.0	24.2	23.1

Table A.149 P-values of paired t-test after modified Bonferroni procedure for prorated final pressure ratios in 90°-270° orientation of the right cylindrical die filled at feed shoe speed of 100 mm/s

	Orientation	270°				Center	90°			
	Radius, mm	8	6	4	2	0	2	4	6	8
270°	8	–	–	–	–	–	–	–	–	–
	6	–	–							–
	4	–	20.281							–
	2	–	8.010	0.579						–
Center	0	–	2.550	**0.026**	0.292					–
90°	2	–	2.579	0.065	0.089	15.064				–
	4	–	7.578	1.102	10.215	0.318	**0.042**			–
	6	–	19.233	16.561	3.119	0.159	0.173	0.539	–	–
	8	–	–	–	–	–	–	–	–	–

*Entries in bold are significantly different (P < 0.05)

Table A.150 Prorated final pressure ratios in 90°-270° orientation of right cylindrical die filled at feed shoe speed of 200 mm/s

Orientation	270°				Center	90°			
Radius, mm	8	6	4	2	0	2	4	6	8
Run #1	0.981	0.904	1.113	1.169	1.000	1.014	1.028	0.902	1.121
Run #2	0.596	0.737	0.879	1.051	1.000	1.107	0.858	0.772	0.585
Run #3	0.425	0.702	0.732	0.927	1.000	1.057	1.014	0.891	0.809
Run #4	0.480	0.715	0.848	1.001	1.000	0.950	0.831	0.758	0.551
Run #5	0.432	0.742	0.928	1.008	1.000	0.981	1.023	0.879	0.927
Run #6	0.689	0.641	1.288	0.941	1.000	1.091	1.088	0.936	0.647
Mean	0.600	0.740	0.965	1.016	1.000	1.033	0.973	0.856	0.773
StDev	0.213	0.088	0.202	0.088	–	0.062	0.104	0.073	0.222
COV	35.5	11.9	20.9	8.7	–	6.0	10.7	8.5	28.7

Table A.151 P-values of paired t-test after modified Bonferroni procedure for prorated final pressure ratios in 90°-270° orientation of the right cylindrical die filled at feed shoe speed of 200 mm/s

	Orientation	270°				Center	90°			
	Radius, mm	8	6	4	2	0	2	4	6	8
270°	8	–	–	–	–	–	–	–	–	–
	6	–	–							–
	4	–	1.086							–
	2	–	**<0.001**	11.763						–
Center	0	–	**0.015**	14.377	14.089					–
90°	2	–	**0.036**	9.028	15.488	5.244				–
	4	–	0.177	18.894	10.545	11.724	4.933			–
	6	–	1.112	3.791	0.480	0.101	0.062	**0.006**	–	–
	8	–	–	–	–	–	–	–	–	–

*Entries in bold are significantly different (P < 0.05)

Table A.152 Prorated final pressure ratios in 135°-315° orientation of the right cylindrical die filled at feed shoe speed of 20 mm/s

Orientation	315°				Center	135°			
Radius, mm	8	6	4	2	0	2	4	6	8
Run #1	0.366	0.577	0.782	0.987	1.000	0.784	0.682	0.537	0.515
Run #2	0.378	0.551	0.748	0.847	1.000	0.808	0.557	0.443	0.299
Run #3	0.445	0.647	0.752	0.755	1.000	0.881	0.734	0.427	0.241
Run #4	0.340	0.646	0.804	0.920	1.000	0.995	0.799	0.595	0.381
Run #5	0.464	0.798	0.893	1.009	1.000	0.985	0.826	0.646	0.405
Run #6	0.459	0.655	0.848	0.992	1.000	0.880	0.751	0.497	0.597
Mean	0.408	0.646	0.805	0.918	1.000	0.889	0.725	0.524	0.406
StDev	0.054	0.086	0.057	0.100	–	0.087	0.096	0.086	0.133
COV	13.2	13.3	7.0	10.9	–	9.8	13.3	16.4	32.7

Table A.153 P-values of paired t-test after modified Bonferroni procedure for prorated final pressure ratios in 135°-315° orientation of the right cylindrical die filled at feed shoe speed of 20 mm/s

	Orientation	315°				Center	135°			
	Radius, mm	8	6	4	2	0	2	4	6	8
315°	8	–	–	–	–	–	–	–	–	–
	6	–	–							–
	4	–	**0.007**							–
	2	–	**0.014**	0.174						–
Center	0	–	**0.003**	**0.006**	2.154					–
135°	2	–	**0.002**	0.632	11.993	0.550				–
	4	–	0.318	0.710	0.066	**0.011**	**0.008**			–
	6	–	0.158	**0.001**	**0.001**	**0.001**	**0.001**	**0.010**	–	–
	8	–	–	–	–	–	–	–	–	–

*Entries in bold are significantly different (P < 0.05)

Table A.154 Prorated final pressure ratios in 135°-315° orientation of the right cylindrical die filled at feed shoe speed of 100 mm/s

Orientation	315°				Center	135°			
Radius, mm	8	6	4	2	0	2	4	6	8
Run #1	0.382	0.661	0.855	0.947	1.000	0.890	0.753	0.562	0.313
Run #2	0.346	0.655	0.863	1.008	1.000	0.805	0.558	0.419	0.252
Run #3	0.292	0.594	0.762	0.996	1.000	0.845	0.657	0.387	0.522
Run #4	0.465	0.682	0.917	1.014	1.000	0.903	0.630	0.313	0.209
Run #5	0.508	0.738	0.774	0.945	1.000	0.813	0.644	0.468	0.270
Run #6	0.534	0.882	1.020	1.082	1.000	0.835	0.734	0.632	0.813
Mean	0.421	0.702	0.865	0.999	1.000	0.849	0.663	0.463	0.397
StDev	0.096	0.100	0.096	0.051	–	0.040	0.072	0.117	0.232
COV	22.8	14.2	11.1	5.1	–	4.7	10.8	25.3	58.4

Table A.155 P-values of paired t-test after modified Bonferroni procedure for prorated final pressure ratios in 135°-315° orientation of the right cylindrical die filled at feed shoe speed of 100 mm/s

	Orientation	315°				Center	135°			
	Radius, mm	8	6	4	2	0	2	4	6	8
315°	8	–	–	–	–	–	–	–	–	–
	6	–	–							–
	4	–	**0.021**							–
	2	–	**0.005**	**0.028**						–
Center	0	–	**0.010**	0.091	19.998					–
135°	2	–	0.542	14.507	**0.020**	**0.004**				–
	4	–	7.658	**0.025**	**0.004**	**0.002**	**0.011**			–
	6	–	**0.013**	**0.005**	**0.002**	**0.002**	**0.010**	**0.018**	–	–
	8	–	–	–	–	–	–	–	–	–

*Entries in bold are significantly different ($P < 0.05$)

Table A.156 Prorated final pressure ratios in 135°-315° orientation of right cylindrical die filled at feed shoe speed of 200 mm/s

Orientation	315°				Center	135°			
Radius, mm	8	6	4	2	0	2	4	6	8
Run #1	0.458	0.650	0.437	0.527	1.000	0.781	0.481	0.330	0.280
Run #2	0.580	0.888	0.929	1.023	1.000	0.988	0.952	0.909	0.483
Run #3	0.634	0.893	0.949	0.887	1.000	1.020	0.916	0.741	0.502
Run #4	0.813	0.993	1.048	1.210	1.000	0.503	0.561	0.887	0.352
Run #5	0.515	0.743	0.891	0.977	1.000	0.918	0.835	0.805	0.714
Run #6	0.686	1.418	3.469	1.628	1.000	0.782	1.211	1.234	0.547
Mean	0.600	0.833	0.851	0.925	1.000	0.842	0.749	0.734	0.466
StDev	0.136	0.136	0.239	0.251	–	0.211	0.214	0.236	0.167
COV	22.7	16.3	28.0	27.2	–	25.0	28.6	32.1	35.7

Table A.157 P-values of paired t-test after modified Bonferroni procedure for prorated final pressure ratios in 135°-315° orientation of the right cylindrical die filled at feed shoe speed of 200 mm/s

	Orientation	315°				Center	135°			
	Radius, mm	8	6	4	2	0	2	4	6	8
315°	8	–	–	–	–	–	–	–	–	–
	6	–	–							–
	4	–	16.525							–
	2	–	5.283	2.403						–
Center	0	–	1.090	4.934	11.361					–
135°	2	–	19.955	20.004	13.502	3.534				–
	4	–	9.193	7.479	4.628	1.235	3.970			–
	6	–	4.560	0.464	0.126	1.368	10.158	18.451	–	–
	8	–	–	–	–	–	–	–	–	–

Center vs. Right Cylindrical Dies

Table A.158 P-values of t-test (two-sample assuming equal variances) between final pressure values of the center and right cylindrical dies at feed shoe speed of 20 mm/s

Orientation	180°, 270°, 225, or 315°				Center	0°, 90, 45°, or 135°			
Radius, mm	8	6	4	2	0	2	4	6	8
0°-180°	**0.012**	0.060	**0.042**	**0.001**	**0.002**	**0.001**	**0.002**	**<0.001**	**<0.001**
90°-270°	0.092	**0.013**	**0.004**	0.202	0.214	**0.028**	**0.034**	**0.040**	**0.001**
45°-225°	**0.026**	**0.012**	**<0.001**	**<0.001**	**<0.001**	**<0.001**	**<0.001**	**<0.001**	**<0.001**
135°-315°	**<0.001**	**<0.001**	**<0.001**	**<0.001**	**<0.001**	**0.001**	**0.015**	**0.013**	**0.012**

Table A.159 P-values of t-test (two-sample assuming equal variances) between final pressure values of the center and right cylindrical dies at feed shoe speed of 100 mm/s

Orientation	180°, 270°, 225, or 315°				Center	0°, 90, 45°, or 135°			
Radius, mm	8	6	4	2	0	2	4	6	8
0°-180°	**0.002**	**0.002**	**0.001**	**0.001**	**<0.001**	**<0.001**	**<0.001**	**<0.001**	**<0.001**
90°-270°	0.055	0.281	**<0.001**	**<0.001**	0.114	0.317	0.224	0.846	0.638
45°-225°	**0.002**	**0.001**	**<0.001**	**<0.001**	**<0.001**	**<0.001**	**<0.001**	**<0.001**	**<0.001**
135°-315°	**<0.001**	**<0.001**	**0.003**	**<0.001**	**<0.001**	**<0.001**	**<0.001**	**0.004**	0.074

Table A.160 P-values of t-test (two-sample assuming equal variances) between final pressure values of the center and right cylindrical dies at feed shoe speed of 200 mm/s

Orientation	180°, 270°, 225, or 315°				Center	0°, 90, 45°, or 135°			
Radius, mm	8	6	4	2	0	2	4	6	8
0°-180°	0.078	0.235	0.195	0.781	0.872	0.079	**0.013**	**0.017**	0.114
90°-270°	0.215	0.731	0.686	**0.014**	0.286	0.193	**0.037**	0.295	**0.029**
45°-225°	0.330	0.322	0.170	0.166	0.840	0.659	**0.019**	0.422	0.056
135°-315°	**<0.001**	**<0.001**	**0.024**	**<0.001**	**0.019**	**0.034**	**<0.001**	**<0.001**	0.338

Center vs. Right E-shaped Dies

Table A.161 P-values of t-test (two-sample assuming equal variances) between final pressure values of the center and right E-shaped dies at feed shoe speed of 20 mm/s

Distance, mm	1	3	5	7	9	11	13	15	17	19	21	23	25	27	29	31
L1	0.754	0.223	0.478				0.544	0.145	0.524	0.108				0.150	**0.016**	0.726
L2	0.648	0.052	0.441				0.248	0.515	0.206	0.778				0.407	0.620	0.841
L3	0.211	**0.045**	0.236				0.389	0.535	0.088	**<0.001**				**0.007**	**0.007**	**0.003**
L4	0.483	**0.014**	**0.033**	**0.013**	**0.014**	**0.001**	0.066	0.348	**0.011**	**0.004**	**0.002**	0.064	**0.005**	**<0.001**	**0.026**	**0.004**

Appendix D Model Parameters of the Center Die

Table A.162 Model parameters for all the ten stages of location (r = 4 mm, θ = 180°) of the center cylindrical die filled with the battery powder mixture at 20 mm/s feed shoe speed

Stage #	$P_pF(\tau)$	α	β	τ
1	$P_p/(e^{85.1\tau}-1)$	737.1	0	$0\leq\tau\leq0.05$
2	$1/(\tau-0.04)$	0.50	0	$0.05\leq\tau\leq0.33$
3	–	0	-53.6	$0.33\leq\tau\leq0.36$
4	–	0	0	$0.36\leq\tau\leq0.57$
5	–	0	33.3	$0.57\leq\tau\leq0.60$
6	–	0	-5.5	$0.60\leq\tau\leq0.69$
7	–	0	0	$0.69\leq\tau\leq0.85$
8	–	0	65.6	$0.85\leq\tau\leq0.89$
9	–	0	-131.3	$0.89\leq\tau\leq0.92$
10	–	0	0	$0.92\leq\tau\leq1.0$

Table A.163 Model parameters for all the ten stages of location (r = 4 mm, θ = 225°) of the center cylindrical die filled with the battery powder mixture at 20 mm/s feed shoe speed

Stage #	$P_pF(\tau)$	α	β	τ
1	$P_p/(e^{81.2\tau}-1)$	301.2	0	$0\leq\tau\leq0.04$
2	$1/(\tau-0.03)$	0.51	0	$0.04\leq\tau\leq0.32$
3	–	0	-54.8	$0.32\leq\tau\leq0.35$
4	–	0	0	$0.35\leq\tau\leq0.56$
5	–	0	45.4	$0.56\leq\tau\leq0.60$
6	–	0	-13.9	$0.60\leq\tau\leq0.62$
7	–	0	0	$0.62\leq\tau\leq0.85$
8	–	0	72.7	$0.85\leq\tau\leq0.89$
9	–	0	-140.7	$0.89\leq\tau\leq0.91$
10	–	0	0	$0.91\leq\tau\leq1.0$

Table A.164 Model parameters for all the ten stages of location (r = 4 mm, θ = 270°) of the center cylindrical die filled with the battery powder mixture at 20 mm/s feed shoe speed

Stage #	$P_pF(\tau)$	α	β	τ
1	$P_p/(e^{9.0\tau}-1)$	6.8	0	$0\leq\tau\leq0.04$
2	$1/(\tau-0.01)$	0.44	0	$0.04\leq\tau\leq0.31$
3	–	0	-33.5	$0.31\leq\tau\leq0.35$
4	–	0	0	$0.35\leq\tau\leq0.55$
5	–	0	34.2	$0.55\leq\tau\leq0.59$
6	–	0	-8.5	$0.59\leq\tau\leq0.64$
7	–	0	0	$0.64\leq\tau\leq0.84$
8	–	0	74.7	$0.84\leq\tau\leq0.88$
9	–	0	-137.6	$0.88\leq\tau\leq0.91$
10	–	0	0	$0.91\leq\tau\leq1.0$

Table A.165 Model parameters for all the ten stages of location (r = 4 mm, θ = 135°) of the center cylindrical die filled with the battery powder mixture at 20 mm/s feed shoe speed

Stage #	$P_pF(\tau)$	α	β	τ
1	$P_p/(e^{87.8\tau}-1)$	443.3	0	$0\leq\tau\leq0.04$
2	$1/(\tau-0.04)$	0.44	0	$0.04\leq\tau\leq0.32$
3	–	0	-38.1	$0.32\leq\tau\leq0.36$
4	–	0	0	$0.36\leq\tau\leq0.56$
5	–	0	33.7	$0.56\leq\tau\leq0.60$
6	–	0	-8.5	$0.60\leq\tau\leq0.65$
7	–	0	0	$0.65\leq\tau\leq0.85$
8	–	0	79.6	$0.85\leq\tau\leq0.89$
9	–	0	-129.0	$0.89\leq\tau\leq0.91$
10	–	0	0	$0.91\leq\tau\leq1.0$

Table A.166 Model parameters for all the ten stages of location (r = 2 mm, θ = 225°) of the center cylindrical die filled with the battery powder mixture at 20 mm/s feed shoe speed

Stage #	$P_pF(\tau)$	α	β	τ
1	$P_p/(e^{-51.1\tau} -1)$	94.1	0	$0 \leq \tau \leq 0.04$
2	$1/(\tau - 0.03)$	0.42	0	$0.04 \leq \tau \leq 0.32$
3	–	0	-38.2	$0.32 \leq \tau \leq 0.35$
4	–	0	0	$0.35 \leq \tau \leq 0.56$
5	–	0	47.2	$0.56 \leq \tau \leq 0.60$
6	–	0	-11.0	$0.60 \leq \tau \leq 0.62$
7	–	0	0	$0.62 \leq \tau \leq 0.85$
8	–	0	86.3	$0.85 \leq \tau \leq 0.89$
9	–	0	-154.5	$0.89 \leq \tau \leq 0.91$
10	–	0	0	$0.91 \leq \tau \leq 1.0$

Table A.167 Model parameters for all the ten stages of location (r = 2 mm, θ = 270°) of the center cylindrical die filled with the battery powder mixture at 20 mm/s feed shoe speed

Stage #	$P_pF(\tau)$	α	β	τ
1	$P_p/(e^{6.7\tau} -1)$	4.8	0	$0 \leq \tau \leq 0.05$
2	$1/(\tau - 0.01)$	0.45	0	$0.05 \leq \tau \leq 0.32$
3	–	0	-39.8	$0.32 \leq \tau \leq 0.35$
4	–	0	0	$0.35 \leq \tau \leq 0.56$
5	–	0	48.4	$0.56 \leq \tau \leq 0.59$
6	–	0	-8.2	$0.59 \leq \tau \leq 0.65$
7	–	0	0	$0.65 \leq \tau \leq 0.84$
8	–	0	90.9	$0.84 \leq \tau \leq 0.88$
9	–	0	-210.4	$0.88 \leq \tau \leq 0.91$
10	–	0	0	$0.91 \leq \tau \leq 1.0$

Table A.168 Model parameters for all the ten stages of location (r = 2 mm, θ = 135°) of the center cylindrical die filled with the battery powder mixture at 20 mm/s feed shoe speed

Stage #	$P_pF(\tau)$	α	β	τ
1	$P_p/(e^{74.9\tau} -1)$	253.6	0	$0 \leq \tau \leq 0.04$
2	$1/(\tau - 0.04)$	0.39	0	$0.04 \leq \tau \leq 0.31$
3	–	0	-34.8	$0.31 \leq \tau \leq 0.36$
4	–	0	0	$0.36 \leq \tau \leq 0.56$
5	–	0	41.0	$0.56 \leq \tau \leq 0.60$
6	–	0	-8.1	$0.60 \leq \tau \leq 0.66$
7	–	0	0	$0.66 \leq \tau \leq 0.85$
8	–	0	91.9	$0.85 \leq \tau \leq 0.89$
9	–	0	-166.3	$0.89 \leq \tau \leq 0.91$
10	–	0	0	$0.91 \leq \tau \leq 1.0$

Table A.169 Model parameters for all the ten stages of location (r = 2 mm, θ = 45°) of the center cylindrical die filled with the battery powder mixture at 20 mm/s feed shoe speed

Stage #	$P_pF(\tau)$	α	β	τ
1	$P_p/(e^{7.1\tau} -1)$	6.1	0	$0 \leq \tau \leq 0.05$
2	$1/(\tau - 0.03)$	0.36	0	$0.05 \leq \tau \leq 0.31$
3	–	0	-26.3	$0.31 \leq \tau \leq 0.36$
4	–	0	0	$0.36 \leq \tau \leq 0.56$
5	–	0	48.4	$0.56 \leq \tau \leq 0.59$
6	–	0	-9.4	$0.59 \leq \tau \leq 0.63$
7	–	0	0	$0.63 \leq \tau \leq 0.85$
8	–	0	88.3	$0.85 \leq \tau \leq 0.89$
9	–	0	-187.1	$0.89 \leq \tau \leq 0.91$
10	–	0	0	$0.91 \leq \tau \leq 1.0$

Table A.170 Model parameters for all the ten stages of location (r = 2 mm, θ = 90°) of the center cylindrical die filled with the battery powder mixture at 20 mm/s feed shoe speed

Stage #	$P_pF(\tau)$	α	β	τ
1	$P_p/(e^{4.0\tau} -1)$	2.7	0	$0 \leq \tau \leq 0.03$
2	$1/(\tau - 0.02)$	0.37	0	$0.03 \leq \tau \leq 0.31$
3	–	0	-36.1	$0.31 \leq \tau \leq 0.34$
4	–	0	0	$0.34 \leq \tau \leq 0.55$
5	–	0	37.9	$0.55 \leq \tau \leq 0.59$
6	–	0	-7.8	$0.59 \leq \tau \leq 0.65$
7	–	0	0	$0.65 \leq \tau \leq 0.84$
8	–	0	81.6	$0.84 \leq \tau \leq 0.88$
9	–	0	-179.7	$0.88 \leq \tau \leq 0.91$
10	–	0	0	$0.91 \leq \tau \leq 1.0$

Table A.171 Model parameters for all the ten stages of location (r = 2 mm, θ = 315°) of the center cylindrical die filled with the battery powder mixture at 20 mm/s feed shoe speed

Stage #	$P_pF(\tau)$	α	β	τ
1	$P_p/(e^{37.8\tau} -1)$	51.0	0	$0 \leq \tau \leq 0.05$
2	$1/(\tau - 0.03)$	0.33	0	$0.05 \leq \tau \leq 0.31$
3	–	0	-27.9	$0.31 \leq \tau \leq 0.36$
4	–	0	0	$0.36 \leq \tau \leq 0.56$
5	–	0	43.8	$0.56 \leq \tau \leq 0.60$
6	–	0	-7.0	$0.60 \leq \tau \leq 0.66$
7	–	0	0	$0.66 \leq \tau \leq 0.85$
8	–	0	100.0	$0.85 \leq \tau \leq 0.89$
9	–	0	-189.5	$0.89 \leq \tau \leq 0.91$
10	–	0	0	$0.91 \leq \tau \leq 1.0$

Table A.172 Model parameters for all the ten stages of location (r = 4 mm, θ = 0°) of the center cylindrical die filled with the battery powder mixture at 20 mm/s feed shoe speed

Stage #	$P_pF(\tau)$	α	β	τ
1	$P_p/(e^{28.5\tau} -1)$	39.2	0	$0 \leq \tau \leq 0.05$
2	$1/(\tau - 0.02)$	0.39	0	$0.05 \leq \tau \leq 0.32$
3	–	0	-26.8	$0.32 \leq \tau \leq 0.35$
4	–	0	0	$0.35 \leq \tau \leq 0.57$
5	–	0	46.4	$0.57 \leq \tau \leq 0.60$
6	–	0	-6.0	$0.60 \leq \tau \leq 0.69$
7	–	0	0	$0.69 \leq \tau \leq 0.85$
8	–	0	99.4	$0.85 \leq \tau \leq 0.90$
9	–	0	-242.5	$0.90 \leq \tau \leq 0.92$
10	–	0	0	$0.92 \leq \tau \leq 1.0$

Table A.173 Model parameters for all the ten stages of location (r = 4 mm, θ = 45°) of the center cylindrical die filled with the battery powder mixture at 20 mm/s feed shoe speed

Stage #	$P_pF(\tau)$	α	β	τ
1	$P_p/(e^{8.1\tau} -1)$	7.4	0	$0 \leq \tau \leq 0.05$
2	$1/(\tau - 0.03)$	0.38	0	$0.05 \leq \tau \leq 0.32$
3	–	0	-29.5	$0.32 \leq \tau \leq 0.35$
4	–	0	0	$0.35 \leq \tau \leq 0.56$
5	–	0	46.1	$0.56 \leq \tau \leq 0.60$
6	–	0	-9.6	$0.60 \leq \tau \leq 0.63$
7	–	0	0	$0.63 \leq \tau \leq 0.85$
8	–	0	100.5	$0.85 \leq \tau \leq 0.89$
9	–	0	-187.4	$0.89 \leq \tau \leq 0.91$
10	–	0	0	$0.91 \leq \tau \leq 1.0$

Table A.174 Model parameters for all the ten stages of location (r = 4 mm, θ = 90°) of the center cylindrical die filled with the battery powder mixture at 20 mm/s feed shoe speed

Stage #	$P_pF(\tau)$	α	β	τ
1	$P_p/(e^{14.9}-1)$	12.4	0	$0 \leq \tau \leq 0.04$
2	$1/(\tau - 0.02)$	0.43	0	$0.04 \leq \tau \leq 0.32$
3	–	0	-36.3	$0.32 \leq \tau \leq 0.35$
4	–	0	0	$0.35 \leq \tau \leq 0.55$
5	–	0	38.0	$0.55 \leq \tau \leq 0.59$
6	–	0	-7.8	$0.59 \leq \tau \leq 0.65$
7	–	0	0	$0.65 \leq \tau \leq 0.84$
8	–	0	82.1	$0.84 \leq \tau \leq 0.88$
9	–	0	-172.4	$0.88 \leq \tau \leq 0.91$
10	–	0	0	$0.91 \leq \tau \leq 1.0$

Table A.175 Model parameters for all the ten stages of location (r = 4 mm, θ = 315°) of the center cylindrical die filled with the battery powder mixture at 20 mm/s feed shoe speed

Stage #	$P_pF(\tau)$	α	β	τ
1	$P_p/(e^{14.2}-1)$	15.7	0	$0 \leq \tau \leq 0.04$
2	$1/(\tau - 0.04)$	0.32	0	$0.04 \leq \tau \leq 0.31$
3	–	0	-26.3	$0.31 \leq \tau \leq 0.35$
4	–	0	0	$0.35 \leq \tau \leq 0.56$
5	–	0	47.6	$0.56 \leq \tau \leq 0.60$
6	–	0	-6.9	$0.60 \leq \tau \leq 0.66$
7	–	0	0	$0.66 \leq \tau \leq 0.85$
8	–	0	107.0	$0.85 \leq \tau \leq 0.89$
9	–	0	-207.2	$0.89 \leq \tau \leq 0.91$
10	–	0	0	$0.91 \leq \tau \leq 1.0$

VITA

XINSHENG XIE

The Pennsylvania State University, University Park, PA, USA

Ph. D. Agricultural and Biological Engineering, May 2006

Dissertation Title:

Uniformity of Simultaneous Deposition of Powder in Multiple Dies: Measurements and Modeling

Zhejiang University, Hangzhou, Zhejiang, China

M. Sc. Agrobiological Environment Engineering, July 1999

Thesis Title:

An Algorithm and Program for Environment Control in Domestic Animal Houses

Northwest Agricultural University, Yangling, China

B. Sc. Agricultural Architecture and Environment Engineering, July, 1992